arXiv:0907.3877v1 [hep-ph] 22 Jul 2009

UNIVERSITÀ DEL SALENTO

DIPARTIMENTO DI FISICA

Stückelberg Axions and Anomalous Abelian Extensions of the Standard Model

Advisor
Claudio Corianò

Candidate
Simone Morelli

Tesi di Dottorato di Ricerca in Fisica – XXI Ciclo

Truth is one,
but the wise call it by different names.
(Rig Veda; section 1, hymn 164, verse 64.)

Contents

Acknowledgements **7**

List of publications **9**

Introduction **11**

1 Stückelberg Axions and the Effective Action of Anomalous Abelian Models 1. A unitarity analysis of the Higgs-axion mixing **13**

1.1 Introduction to the chapter 13
  1.1.1 The quantization of anomalous Abelian models and the axion 14
  1.1.2 The Case of String/Branes Inspired Models 15
  1.1.3 The content of this chapter 15
  1.1.4 The role of the Chern-Simons interactions 16
1.2 Massive $U(1)$'s *à la* Stückelberg 16
  1.2.1 The Stückelberg action from a field-enlarging transformation 17
  1.2.2 Implications at the LHC 19
1.3 The Effective Action in the A-B Model 19
  1.3.1 The anomalous effective action of the A-B Model 23
1.4 Higgs-Axion Mixing in $U(1)$ Models: massless axi-Higgs 24
  1.4.1 Higgs-Axion Mixing in $U(1)$ Models: massive axi-Higgs 25
1.5 Unitarity issues in the A-B Model in the exact phase 27
  1.5.1 Unitarity and CS interactions in the A-B Model 27
1.6 Gauge independence of the A self-energy to higher orders and the loop counting 29
1.7 Unitarity Analysis of the A-B Model in the broken phase 31
  1.7.1 A-B Model: $BB \to BB$ mediated by a B gauge boson in the broken phase 33
1.8 The Effective Action in the Y-B Model 35
1.9 The fermion sector 37
1.10 The Effective Action in configuration space 38
1.11 Conclusions 40
1.12 Appendix. The triangle diagrams and their ambiguities 42
1.13 Appendix. Chern-Simons cancellations 45
  1.13.1 Cancellation of gauge dependences in the broken Higgs phase 47
  1.13.2 Cancellations in the A-B Model: $BB \to BB$ mediated by a B gauge boson 47
  1.13.3 Gauge cancellations in the self-energy diagrams 49
1.14 Appendix. Ward Identities on the tetragon 49
1.15 Appendix. DR-HVBM 52

1.15.1 The vanishing of a massive **AAV/VVV** 55
1.15.2 **AVV** and shifts 55
1.15.3 DR-HVBM scheme 56
1.15.3.1 The **AVV** diagram 56
1.15.3.2 The **AAA** diagram 58
1.15.4 Equivalence of the shift-based (CVC) and of DR-HVBM schemes 60
1.16 Appendix. The Chern-Simons and Wess-Zumino vertices 61
1.17 Appendix. Computation of the Effective Action 61
1.18 Appendix. Decay of the axi-Higgs: the pseudoscalar triangle χBB 62

2 Stückelberg Axions and the Effective Action of Anomalous Abelian Models 2. A $SU(3)_C \times SU(2)_W \times U(1)_Y \times U(1)_B$ Model and its signature at the LHC 65
2.1 Introduction to the chapter 65
2.2 Effective models at low energy: the $SU(3)_C \times SU(2)_W \times U(1)_Y \times U(1)_B$ case 67
2.3 The Effective Action of the mLSOM with a single anomalous $U(1)$ 68
2.4 Three gauge boson amplitudes and gauge-fixing 69
2.4.1 The non-Abelian sector before symmetry breaking 69
2.4.2 The Abelian sector before symmetry breaking 71
2.5 Ward Identities, Green-Schwarz and Chern-Simons counterterms in the Stückelberg phase 73
2.6 The neutral currents sector in the mLSOM 81
2.7 The $Z\gamma\gamma$ vertex in the Standard Model 82
2.7.1 The $Z\gamma\gamma$ vertex in anomalous Abelian models: the Higgs-Stückelberg phase 84
2.7.2 $q\bar{q} \to \gamma\gamma$ with an intermediate Z 89
2.7.3 Isolation of the massless limit: the $Z^* \to \gamma^*\gamma^*$ amplitude 91
2.7.4 Extension to $Z \to \gamma^*\gamma$ 92
2.8 Conclusions 94
2.9 Appendix. A Summary on the single anomalous $U(1)$ Model. 95
2.9.1 The neutral gauge sector 97
2.9.2 Rotation matrix O^χ on the axi-Higgs 99
2.9.3 Appendix. Vanishing of $\Delta^{\lambda\mu\nu}$ for on-shell external physical states 101
2.10 Appendix. Anomalous traces 102
2.11 Appendix. CS and GS terms rotated 103

3 Unitarity Bounds for Gauged Axionic Interactions and the Green-Schwarz Mechanism 105
3.1 Introduction to the chapter 105
3.1.1 WZ and GS counterterms 106
3.2 Anomaly cancellation and gauge dependences: the GS and the WZ mechanisms in field theory 106
3.2.1 The Lagrangian 107
3.3 Local and non-local formulations 107
3.3.1 Integrating out the Stückelberg in the WZ case 109
3.3.2 Non-local counterterms: axial QED 111
3.4 BIM amplitudes, unitarity and the resonance pole 114
3.5 A realistic model with WZ counterterms 117

3.5.1 Prompt photons, the Landau-Yang theorem and the anomaly 118
3.6 Gauge parameter dependence in the physical basis 122
3.7 Unitarity bounds: the partonic contribution $gg \to \gamma\gamma$ 124
3.8 Couplings and Parameters in the Madrid Model 131
3.8.1 Anomalous and anomaly-free regions: numerical results 133
3.9 Conclusions 139
3.10 Appendix. The cross section 140

4 Axions and Anomaly-Mediated Interactions: The Green-Schwarz and Wess-Zumino Vertices at Higher Orders and $g-2$ of the muon 143
4.1 Introduction to the chapter 143
4.2 The GS and WZ vertices 145
4.2.1 The GS vertex in the AAA and AVV cases 146
4.2.2 Implications of the GS vertex: vanishing of (real) light-by-light scattering at two-loop 147
4.2.3 Embedding the GS vertex into higher-order diagrams 149
4.2.4 The vertex in the longitudinal/transverse (L/T) formulation 152
4.2.5 Examples of explicit GS counterterms: anomaly in muon decay 154
4.2.6 Self-energy and gauge invariance 155
4.3 Higher-order diagrams 157
4.3.1 Three-point functions 157
4.4 WZ and GS interactions, anomalous magnetic moment of the muon and muonium 160
4.4.1 The GS case 160
4.4.2 Anomalous corrections to a_μ 161
4.5 Two-loop Contributions to $g-2$: Anomalous Diagrams 162
4.5.0.1 The Wess-Zumino Counterterm 167
4.5.1 Corrections to muonium 168
4.6 The longitudinal subtraction and the broken Ward Identities of the GS vertex 170
4.7 Conclusions 172
4.8 Appendix. Some features of the GS and WZ vertices 173
4.8.1 Gauge choices 174
4.9 Appendix. Simplifications in some of the integrands on higher-point functions 174
4.9.1 Computation of the diagrams in Fig. 4.9 174
4.9.2 Simplifications of the integrands in Sec. 4.2.3 175

5 An Anomalous Extra Z' from Intersecting Branes with Drell-Yan and Direct Photons at the LHC 177
5.1 Introduction to the chapter 177
5.2 Anomaly-free versus an anomalous extra Z' in Drell-Yan 179
5.2.1 An anomalous extra Z' 181
5.3 The GS and WZ vertices and gluon fusion 182
5.3.1 Ward Identities 186
5.4 Invariant mass distributions in Drell-Yan 188
5.4.1 Precision studies on the Z resonance 191
5.4.2 Di-lepton production: numerical results 192
5.5 Direct Photons with GS and WZ interactions 196

5.5.1 Helicity amplitudes: massless box diagrams and anomalous interferences 200
5.5.2 Numerical analysis for direct photons 203
5.5.3 The *gg* sector 204
5.6 Conclusions 208
5.7 Appendix 210
5.8 Appendix. A comment on the unitarity breaking in WZ Lagrangians 210

Bibliography **211**

Acknowledgements

I wish to express an extreme gratitude to my advisor Claudio Corianò. His patience and firmness of purposes together with an exceptional passion for Physics have always been my guide during the last years and will be reason of real inspiration to me during all my life.

A special thank is due to my friend and collaborator Marco Guzzi for all the nice time we spent working together. I am grateful to him for his constant help and for pushing me to do better and better every time.

I wish to thank Nikos Irges for giving me the precious opportunity to work with him and for his support. Every discussion with him has always been illuminating and of great importance for my work.

A great thank is addressed to Cosmas K. Zachos for his kind hospitality and for the opportunity to work with him. I am particularly grateful to him for the three months we spent together in Chicago, for all the time he dedicated to me for discussions and last, but not least, for his "English lessons".

Many thanks are due to Marco Roncadelli, Francesco Fucito and Theodore Tomaras for their support and hospitality.

Finally, I cannot miss to thank all my friends and colleagues of the Department of Physics in Lecce for their sympathy and all the fun we had together. Their friendship has always been a safe shelter for me.

This work is dedicated to my family.

List of publications

The chapters presented in this thesis are based on the following research papers.

1. *Stueckelberg axions and the effective action of anomalous Abelian models. 1. A Unitarity analysis of the Higgs-axion mixing.*
   C. Corianò, N. Irges and S. Morelli, JHEP 07 (2007) 008, hep-ph/0701010.

2. *Stueckelberg axions and the effective action of anomalous Abelian models. 2. A* $SU(3)_C \times SU(2)_W \times U(1)_Y \times U(1)_B$ *model and its signature at the LHC.*
   C. Corianò, N. Irges and S. Morelli, Nucl. Phys. B789 (2008) 133, hep-ph/0703127.

3. *Unitarity Bounds for Gauged Axionic Interactions and the Green-Schwarz Mechanism.*
   C. Corianò, M. Guzzi and S. Morelli, Eur. Phys. J. C55 (2008) 629, arXiv:0801.2949 [hep-ph].

4. *Axions and Anomaly-Mediated Interactions: The Green-Schwarz and Wess-Zumino Vertices at Higher Orders and g-2 of the muon.*
   R. Armillis, C. Corianò, M. Guzzi and S. Morelli, JHEP 10 (2008) 034, arXiv:0808.1882 [hep-ph].

5. *An Anomalous Extra Z Prime from Intersecting Branes with Drell-Yan and Direct Photons at the LHC.*
   R. Armillis, C. Corianò, M. Guzzi and S. Morelli, Nucl. Phys. B814 (2009) 15679, arXiv:0809.3772 [hep-ph].

Introduction

One of the challenges of the next several years in the area of particle theory will be the search for confirmation of the Standard Model (SM) at the Large Hadron Collider, which has provided so far the fundamental scheme within which to explain a large part of the electroweak phenomenology and the physics of the strong interactions. Based on a Yang-Mills theory and incorporating the mechanism of spontaneous symmetry breaking in order to give mass to the electroweak gauge bosons, this theory remains, however, still to be proven to be correct in all of its sectors. For instance, the mechanism of spontaneous symmetry breaking itself, which is a structural part of the theory, while elegant and so far unchallenged as a theoretical model for the breaking of the gauge symmetry -while preserving the renormalizability and the unitarity of the theory- involves a scalar field, the Higgs field, which has not been found yet. Whether the mechanism is correct or not, at least experimentally, remains to be seen, although there are reasonable hopes to believe that the Higgs field will be found. Naturally, even the discovery of the Higgs and the confirmation of the correctness of the scalar sector of the model does not stop the hopes that in the next decade we will be able to enlarge quite substantially our knowledge of the physics of the fundamental interactions at the energy scale of several TeV's. One among the many possibilities is to look for minimal extensions of the SM which are characterized by modest departures from the $SU(3)\times SU(2)\times U(1)_Y$ gauge structure and which can be more easily tested at the Large Hadron Collider (LHC). Naturally, there are plenty of options and roads that one can take, from supersymmetry to extra dimensions to brane constructions.

Many scenarios have been put forward in the last few years in which many of these ideas have been blended and synthesized in new ways, providing a fertile ground for further elaborations and modeling of the fundamental interactions with a substantial enrichment of the spectrum of the physical possibilities.

It is clear, at this point, that, given all these new developements, the selection of the most promising directions to follow and on which contribute is not an issue with a straight "yes or not" answer, since there are personal tastes and motivations of different nature, some of them sociological, that motivate the pattern to follow, the theory to develope and to believe in, and the answer to give to these questions. If one assumes that unification is for sure an important issue in current and future elementary particle theory, then for sure, the simplest answer is provided within the context of Grand Unified theories (GUT), the most impressive result in favour of it being the unification of the gauge coupling in a supersymmetric extension of the SM. In all these scenarios, string theory has played a considerable role, especially after the discovery that special vacua of string/brane theory may show up in some way at future collider experiments. While string theory has always been connected with physics at the Planck scale, with the advent of brane theory and extra dimensional models, strings are expected to play a role also at rather modest energies, such as at the TeV scale. The study of this energy range will be at the center of the two major experiments planned at the LHC, that is ATLAS and CMS. In fact, a large effort has gone into the classification of these vacua of string theory, especially in the theoretical analysis of models of intersecting branes which are at the root of the class of theories that we are going to investigate in this thesis work.

In our study we will start with an analysis of these models in a rather simplified context, focusing on their basic structure and studying the class of effective actions wich are at the origins of these scenarios. Being the gauge structure of these gauge theories rather simple, we will be able to go quite far in the developement of the corresponding field theory and we will provide accurate predictions at the LHC for these models, having identified the key parameters which characterize them and which are the objects of experimental verification.

Our work is not a work in string theory, but is a study of what string theory may imply at field theory level in a special class of its vacua. One of the key discoveries of these class of vacua is the presence of a physical axion in the spectrum of this class of theories. The axion, termed the "axi-Higgs" in [1], is a natural by-product of the presence of anomalous symmetries in the gauge structure of these theories. The effective actions of these models, which contain several extra anomalous $U(1)$'s, have their anomaly cancelled by a Green-Schwarz mechanism, which involves an axion. At the same time, the axion appears in the form of a combination of Stückelberg fields and CP-odd contributions of an extended Higgs sector, characterized by two Higgs doublets, with the possibility of some "phases" (Peccei-Quinn breaking terms) added to its canonical structure.

In our analysis we will characterize these models from the ground up, working out at a very fine level of detail the effective action of these models, starting from the simplest ones and moving towards more general and complex analysis of them. The objective of these studies is to provide a firm characterization of the field theory and the phenomenology of these models, stressing on the various mechanisms of cancellation of the anomalies which are allowed in these types of constructions. A key role, in these scenarios, is played by the anomaly, and several of its properties are analyzed under a new light. One important point of our study concerns the discovery of a unitarity bound for this class of theories, which appears when a mechanism of anomaly cancellation involves a local counterterm of Wess-Zumino type. Other mechanisms are proposed and analyzed as well, one of them being the subtraction of the anomaly pole and its formulation in terms of an axion and a ghost.

As we have mentioned, our analysis stresses mostly the role of the physical (Stückelberg) axion, that survives after electroweak symmetry breaking as a physical field, and its potential significance as a new weakly interacting pseudoscalar which might play a role as a component of dark matter.

Chapter 1

Stückelberg Axions and the Effective Action of Anomalous Abelian Models 1. A unitarity analysis of the Higgs-axion mixing

1.1 Introduction to the chapter

The search for the identification of possible extensions of the Standard Model (SM) is a challenging area both from the theoretical and the experimental perspectives. It is even more so with the upcoming experiments at the LHC, where the hopes are that at least some among the many phenomenological scenarios that have been formulated in the last three decades can finally be tested. The presence of so many wide and diverse possibilities certainly render these studies very challenging. Surely, among these, the choice of simple Abelian extension of the basic gauge structure of the SM is one of the simplest to take into consideration. These extensions will probably be the easiest to test and be also the first to be confirmed or ruled out. Though $U(1)$ extensions are ubiquitous, they are far from being trivial. These theories predict new gauge bosons, the extra Z', with masses that are likely to be detected if they are up to $4 \div 5$ TeV (see for instance [2, 3, 4, 5, 6] for an overview and topical studies). These extensions are formulated, with a variety of motivations, within a well-defined theoretical framework and involve phenomenological studies which are far simpler than those required, for instance, in the case of supersymmetry, where a large set of parameters and soft-breaking terms clearly render the theoretical description much more involved.

On the other hand, simple Abelian extensions are also quite numerous, since new neutral currents are predicted both by Grand Unified Theories (GUT's) and/or by superstring inspired models based on E_6 and $SO(10)$ (see [7, 8, 9] for instance). One of the common features of these models is the absence of an anomalous fermion spectrum, as for the SM, with the anomaly cancellation mechanism playing a key role in fixing the couplings of the fermions to the gauge fields and in guaranteeing their inner consistency. In this respect, unitarity and renormalizability, tenets of the effective theory, are preserved.

When we move to enlarge the gauge symmetry of the SM, the unitarity has to be preserved, but not necessarily the renormalizability of the model. In fact, operators of dimension-5 and higher which may appear at higher energies have been studied and classified under quite general assumptions [10].

Anomalous Abelian models, differently from the non-anomalous ones, show some striking features, which have been exploited in various ways, for example in the generation of realistic hierarchies among the Yukawa couplings [11, 12] and to analyze neutrino mixing. There are obvious reasons that justify these studies: the mechanism of anomaly cancellation that Nature selects may not just be based on an anomaly-free spectrum, but may require a more complex pattern, similar to the Green-Schwarz (GS) anomaly cancellation mechanism of string theory, that invokes an axion. Interestingly enough, the same pattern appears if, for a completely different and purely dynamical reason, part of the fermion spectrum of an anomaly free theory is integrated out, together with part of the Higgs sector [13]. In both cases, the result is a theory that shows the features discussed in this work, though some differences between the two different realizations may remain in the effective theory. For instance, it has been suggested that the PVLAS result can be easily explained within this class of models incorporating a single anomalous $U(1)$. The anomaly can be real (due to anomaly inflow from extra dimensions, (see [14, 15] as an example), or effective, due to the partial decoupling of a heavy Higgs, and the Stückelberg field is the remnant phase of this partial decoupling. The result is a “gauging” of the PQ axion [13].

1.1.1 The quantization of anomalous Abelian models and the axion

The interest on the quantization of anomalous models and their proper field theoretical description has beeen a key topic for a long period, in an attempt to clarify under which conditions an anomalous gauge theory may be improved by the introduction of suitable interactions so to become unitary and renormalizable. The introduction of the Wess-Zumino term (WZ), a $\theta F \wedge F$ term, which involves a pseudoscalar θ times the divergence of a topological current, has been proposed as a common cure in order to restore the gauge invariance of the theory [16, 17]. Issues related to the unitarity of models incorporating Chern-Simons (CS) and anomalous interactions in lower dimensions have also been analyzed in the past [18, 19].

Along the same lines of thought, also non-local counterterms have been proposed as a way to achieve the same objective [20]. The gauge dependence of the WZ term and its introduction into the spectrum so to improve the power counting in the loop expansion of the theory has also been a matter of debate [21]. Either with or without a WZ term, renormalizability is clearly lost, while unitarity, in principle, can be maintained. As we are going to illustrate in specific and realistic examples, gauge invariance and anomaly cancellation play a subtle role in guaranteeing the gauge independence of matrix elements in the presence of symmetry breaking.

So far, the most interesting application of this line of reasoning in which the Wess-Zumino term acquires a physical meaning is in the Peccei-Quinn solution of the strong CP-problem of QCD [22], where the SM Lagrangian is augmented by a global anomalous U(1) and involves an axion.

The PQ symmetry, in its original form, is a global symmetry broken only by instanton effects. The corresponding axion, which in the absence of non perturbative effects would be the massless Nambu-Goldstone boson of the global (chiral) symmetry, acquires a tiny mass. In the PQ case the mass of the axion and its coupling to the gauge field are correlated, since both quantities are defined in terms of the same factor $1/f_a$, with f_a being the PQ-breaking scale, which is currently bounded, by terrestrial and astrophysical searches, to be very large ($\approx 10^9$ GeV) [23, 24].

This tight relation between the axion mass and the coupling is a specific feature of models of PQ type where a global symmetry is invoked and, as we are going to see, it can be relaxed if the anomalous interaction is gauged. The axion discussed in the thesis and its effective action has some special features that render it an interesting physical state, quite distinct from the PQ axion. The term “gauged axion” or “Stückelberg axion” or “axi-Higgs” all capture some of its main properties. Depending on the size of the PQ-breaking potential, the value of the axion mass gets corrected in the form of additional factors which are absent in the standard PQ axion.

Although some of the motivations to investigate this class of models come from the interest toward special vacua of string theory [1], the study of anomalous Abelian interactions, in the particular construction that we are going to discuss in this work, are applicable to a wide variety of models which share the typical features of those studied here.

1.1.2 The Case of String/Branes Inspired Models

As we have mentioned, we work under quite general assumptions that apply to Abelian anomalous models that combine both the Higgs and the Stückelberg mechanisms [25] in order to give mass to the extra (anomalous) gauge bosons. There are various low-energy effective theories which can be included into this framework, one example being low energy orientifold models, but we will try to stress on the generality of the construction rather than on its stringy motivations, which, from this perspective, are truly just optional.

These models have been proposed as a possible scenario for physics beyond the Standard Model, with motivations that have been presented in [1]. Certain features of these models have been studied in some generality [26], and their formulation relies on the Green-Schwarz mechanism of anomaly cancellation that incorporates axionic and Chern-Simons interactions. At low energy, the Green-Schwarz term is nothing but the long known Wess-Zumino term. In particular, the mechanism of spontaneous symmetry breaking, that now involves both the Stückelberg field (the axion) and the Standard Model Higgs, has been elucidated [1]. While the general features of the theory have been presented before, the selection of a specific gauge structure (the number of anomalous $U(1)$’s in [1] was generic), in our case of a single additional anomalous $U(1)$, allows us to specify the model in much more detail and discuss the structure of the effective action to a larger extent. This study is needed and provides a new step toward a phenomenological analysis for the LHC that we will present in the following chapters.

This requires the choice of a specific and simplified gauge structure which can be amenable to experimental testing. While in the minimal formulation of the models derived from intersecting branes the number of anomalous Abelian gauge groups is larger or equal to three, the simplest case (and the one for which a quantitative phenomenological analysis is possible) is the one in which a single anomalous $U(1)$ is present. This simplified structure appears once we make the assumption that the masses of the new Abelian gauge interactions are widely (but not too widely) separated so to guarantee an effective decoupling of the heavier Z's. Clearly, in this simplified setting, the analysis of [1] can be further specialized and, even more interestingly, one can try to formulate possible experimental predictions.

1.1.3 The content of this chapter

This chapter and the following address the construction of anomalous Abelian models in the presence of an extra anomalous $U(1)$, called $U(1)_B$. This extra gauge boson becomes massive via a combined Higgs-Stückelberg mechanism and is accompanied by one axion, b. We illustrate the physical role played by the axion when both the Higgs and the Stückelberg mechanisms are present. The physical axion, that emerges in the scalar sector when b is rotated into its physical component (the axi-Higgs, denoted by χ) interacts with the gauge bosons with dimension-5 operators (the WZ terms). The presence of these interactions renders the theory non-renormalizable and one needs a serious study of its unitarity in order to make sense of it, which is the objective of these two chapters. Here the analysis is exemplified in the case of two simple models (the A-B and Y-B Models) where the non-Abelian sector is removed. A complete model will be studied in Chap. 2. Beside the WZ term the theory clearly shows that additional Chern-Simons interactions become integral part of the effective action.

1.1.4 The role of the Chern-Simons interactions

There are some very interesting features of these models which deserve a careful study, and which differ from the case of the Standard Model (SM). In this last case the cancellation of the anomalies is enforced by charge assignments. As a result of this, before electroweak symmetry breaking, all the anomalous trilinear gauge interactions vanish. This cancellation continues to hold also after symmetry breaking if all the fermions of each generation are mass degenerate. Therefore, trilinear gauge interactions containing axial couplings are only sensitive to the mass differences among the fermions. In the case of extensions of the SM which include an anomalous $U(1)$ this pattern changes considerably, since the massless contributions in anomalous diagrams do not vanish. In fact, these theories become consistent only if a suitable set of axions and Chern-Simons (CS) interactions are included as counterterms in the defining Lagrangian. The role of the CS interactions is to re-distribute the partial anomalies among the vertices of a triangle in order to restaure the gauge invariance of the one-loop effective action before symmetry breaking. For instance, a hypercharge current involving a generator Y,would be anomalous at one-loop level in a trilinear interaction of the form YBB or YYB, if B is an anomalous gauge boson. In fact, while anomalous diagrams of the form YYY are automatically vanishing by charge assignment, the former ones are not. The theory requires that in these anomalous interactions the CS counterterm moves the partial anomaly from the Y vertex to the B vertex, rendering in these diagrams the hypercharge current effectively vector-like. The B vertex then carries all the anomaly of the trilinear interaction, but B is accompanied by a Green-Schwarz axion b and its anomalous gauge variation is canceled by the GS counterterm. It is then obvious that these theories show some new features which have never fully discussed in the past and require a very careful study. In particular, one is naturally forced to develope a regularization scheme that allows to keep track correctly of the distribution of the anomalies on the various vertices of the theory. This problem is absent in the case of the SM since the vanishing of the anomalous vertices in the massless phase renders any momentum parameterization of the diagrams acceptable. We describe in detail some of these more technical points in the appendices, where we illustrate how these theories can be treated consistently in dimensional regularization but with the addition of suitable shifts that take the form of CS counterterms.

1.2 Massive $U(1)$'s *à la* Stückelberg

One of the ways to render an Abelian $U(1)$ gauge theory massive is by the mechanism proposed by Stückelberg [25] and extensively studied in the past. Before that another mechanism, the Higgs mechanism, was proposed as a viable and renormalizable method to give mass both to Abelian and to non-Abelian gauge theories. There are various ways in which, nowadays, this mechanism is implemented, and Stückelberg fields appear quite naturally in the form of *compensator* fields in many supergravity and string models. On the phenomenological side, one of the first successful investigations of this mechanism for model building has been presented in [27], while, rather recently, supersymmetric extensions of this mechanism have been investigated [28, 29, 30]. In other recent work some of its perturbative aspects have also been addressed, in the case of non anomalous Abelian models.

In the seventies, the Stückelberg field (also called the "Stückelberg ghost") re-appared in the analysis of the properties of renormalization of Abelian massive Yang-Mills theory by Salam and Strathdee [31], Delbourgo [32] and others [33], while Gross and Jackiw [34] introduced it in their analysis of the role of the anomaly in the same theory. According to these analysis the perturbative properties of a massive Yang-Mills theory, which is not renormalizable in its direct formulation, can be ameliorated by the introduction of this field. Effective actions in massive Yang-Mills theory have been also investigated in the past, and shown to have some predictivity also without the use of the Stückelberg variables [35, 36], but clearly the advantages of the Higgs mechanism and its elegance remains a firm result of the current formulation of the Standard Model. We briefly review these points to make our treatment self-contained but also to show that the role of this field completely changes in the presence of an anomalous fermion spectrum, when the need to render the theory unitary requires the introduction of an interaction $bF\tilde{F}$, spoiling renormalizability, but leaving the resulting theory well defined as an *effective* theory. For this to happen one needs to check explicitly the unitarity of the theory, which is not obvious, especially if the Higgs and Stückelberg mechanisms are combined. This study is the main objective of the first part of this investigation, which is focused on the issues of unitarity of simple models which include both mechanisms. Various technical aspects of this analysis are important for the study of realistic models, as discussed in Chap. 2, where we move toward the study of an extension of the SM with two Abelian factors $U(1)_Y \times U(1)_B$, one of them being the standard hypercharge Y. The charge assignments for the anomalous diagrams involving a combinations of both gauge bosons are such that additional Ward Identities are needed to render the theory unitary, starting from gauge invariance. We study most of the features of this model in depth, and show how the neutral vertices of the model are affected by the new anomaly cancellation mechanism. We will work out an application of the theory in the process $Z \to \gamma\gamma$, which can be tested at forthcoming experiments at the LHC.

1.2.1 The Stückelberg action from a field-enlarging transformation

We start with a brief introduction on the derivation of an action of Stückelberg type to set the stage for further elaborations.

A massive Yang-Mills theory can be viewed as a gauge-fixed version of a more general action involving the Stückelberg scalar. A way to recognize this is to start from the standard Lagrangian

$$\mathcal{L} = -\frac{1}{4}F_{\mu\nu}F^{\mu\nu} + \frac{1}{2}M_1^2(B_\mu)^2 \tag{1.1}$$

with $F_{\mu\nu} = \partial_\mu B_\nu - \partial_\nu B_\mu$ and perform a field-enlarging transformation (see the general discussion presented in [37])

$$B_\mu = B'_\mu - \frac{1}{M_1}\partial_\mu b, \tag{1.2}$$

that brings the original (gauge-fixed) theory (1.1) into the new form

$$\mathcal{L} = -\frac{1}{4}F_{\mu\nu}F^{\mu\nu} + \frac{1}{2}M_1^2(B_\mu)^2 + \frac{1}{2}(\partial_\mu b)^2 - M_1 B_\mu \partial^\mu b \tag{1.3}$$

which now reveals a peculiar gauge symmetry. It is invariant under the transformation

$$\begin{aligned} b &\rightarrow b' = b - M_1\theta \\ B_\mu &\rightarrow B'_\mu = B_\mu + \partial_\mu\theta. \end{aligned} \tag{1.4}$$

We can trace back our steps and gauge-fix this Lagrangian in order to obtain a new version of the original Lagrangian that now contains a scalar. One can choose to remove the mixing between B_μ and b by the gauge-fixing condition

$$\mathcal{L}_{gf} = -\xi\left(\partial\cdot B + \frac{M_1}{2\xi}b\right)^2 \tag{1.5}$$

giving the gauge-fixed Lagrangian

$$\mathcal{L} = -\frac{1}{4}F_{\mu\nu}F^{\mu\nu} + \frac{1}{2}M_1^2(B_\mu)^2 + \frac{1}{2}(\partial_\mu b)^2 - \xi(\partial B)^2 - \frac{M_1^2}{4\xi}b^2. \tag{1.6}$$

It is easy to show that the BRST charge of this model generates exactly the Stückelberg condition on the physical subspace, decoupling the unphysical Faddeev-Popov ghosts from the physical spectrum.

Different gauge choices are possible. The choice of a unitary gauge ($b = 0$) in the Lagrangian (1.3) brings us back to the original massive Yang-Mills model (1.1). In the presence of a chiral fermion, the same field-enlarging transformation trick goes through, though this time we have to take into account the contribution of the anomaly

$$\mathcal{L} = -\frac{1}{4}F_B^2 + \frac{M_1^2}{2}(B_\mu + \frac{1}{M_1}\partial_\mu b)^2 + i\overline{\psi}_L\gamma^\mu(\partial_\mu + igB_\mu + ig\partial_\mu b)\psi_L, \tag{1.7}$$

where $\psi_L = \frac{1}{2}(1-\gamma^5)$ is the left-handed anomalous fermion. The Fujikawa method can be used to derive from the anomalous variation of the measure the relation

$$g\overline{\psi}_L\gamma^\mu\partial_\mu b\psi_L = \frac{g^3}{32\pi^2}\epsilon^{\mu\nu\rho\sigma}F_{\mu\nu}F_{\rho\sigma} \tag{1.8}$$

thereby obtaining the final anomalous action

$$\mathcal{L} = -\frac{1}{4}F_B^2 + \frac{M_1^2}{2}(B_\mu + \frac{1}{M_1}\partial_\mu b)^2 + i\overline{\psi}_L\gamma^\mu(\partial_\mu + igB_\mu)\psi_L - \frac{g^3}{32\pi^2}b\,\epsilon^{\mu\nu\rho\sigma}F_{\mu\nu}F_{\rho\sigma}. \tag{1.9}$$

Notice that the b field can be integrated out [34]. In this case one obtains an alternative effective action of the form

$$\begin{aligned}\mathcal{L} &= -\frac{1}{4}F_B^2 + \frac{M_1^2}{2}(B_\mu)^2 + i\overline{\psi}_L\gamma^\mu(\partial_\mu + igB_\mu)\psi_L \\ &\quad -\frac{g^3}{96\pi^2}\int d^4y F_B^{\alpha\beta}\tilde{F}_{B\alpha\beta}(x)D(x-y|M_1^2\xi)F^{\mu\nu}(y)\tilde{F}_{\mu\nu}(y)\end{aligned} \tag{1.10}$$

with $(\Box + M_1^2\xi^2)D(x|M_1^2) = -\delta^4(x)$. The locality of the description is clearly lost. It is also obvious that the role of the axion, in this case, is to be an unphysical field. However, in the case of a model incorporating both spontaneous symmetry breaking and the Stückelberg mechanism, the axion plays a physical role and can be massless or massive depending whether it is part of the scalar potential or not. Our interest, in this chapter, is to analyze in detail the contribution to the one-loop effective action of anomalous Abelian models, here defined as the classical Lagrangian plus its anomalous trilinear fermionic interactions. Anomalous Ward Identities in these effective actions are eliminated once the divergences from the triangles are removed either by 1) suitable charge assignments for some of generators, or by 2) shifting axions or by 3) a distribution of the partial anomalies on each vertex.

Since this approach of anomaly cancellations is more involved than in the SM case, we have decided to analyze it using some simple (purely Abelian) models as working examples, before considering a realistic extension of the Standard Model which will be developed in Chap. 2. There, all the methodology

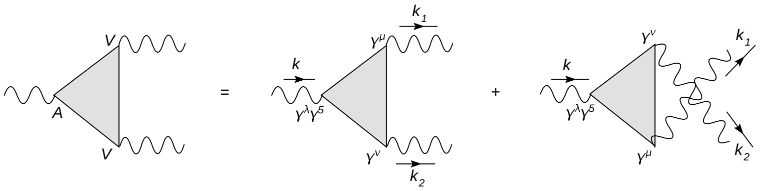

Figure 1.1: The **AVV** diagrams.

developed in this chapter will be widely applied to the analysis of a string-inspired model derived from the orientifold construction [1]. In fact, this analysis tries to clarify some unobvious issues that naturally appear once an effective anomaly-free gauge theory is generated at lower energies from an underlying renormalizable theory at a higher energy. For this purpose we will use a simple approach based on s-channel unitarity, inspired by the classic work of Bouchiat, Iliopoulos and Meyer [38].

1.2.2 Implications at the LHC

A second comment concerns the possible prospects for the discovery of a Z' of anomalous origin. Clearly Z' bosons being ubiquitous in GUT's and other SM extensions, discerning an anomalous Z' from a non-anomalous one is subtle, but possible. In Chap. 2 we propose the Drell-Yan mechanism as a possible way to make this distinction, since some new effects related to the treatment of the anomalies are already apparent near the Z resonance in this process. The numerical results for the anomalous corrections to Drell-Yan will be presented in Chap. 5. Anomalous vertices involving the Z gauge boson appear both in the production mechanism and in its decay into two gluons or two photons. In the usual Drell-Yan process of the SM, these contributions, because of anomaly cancellations, are sensitive only to the mass difference between the fermion of a given generation and are usually omitted in NNLO computations. If these resonances, predicted by theories with extra Abelian gauge structures, are very weakly coupled, then a precise determination of the QCD background is necessary to detect them (see [39] for details).

1.3 The Effective Action in the A-B Model

As we have already mentioned, we will focus our analysis on the anomalous effective actions of simple Abelian theories. We will analyze two models: a first one called "A-B", with a A vector-like (anomaly-free) and B axial-vector-like (anomalous) and a second model called the "Y-B" Model where B is anomalous and Y is anomaly-free with both vector and axial-vector interactions. We start defining the so called "A-B" Model by the Lagrangian

$$\begin{aligned}\mathcal{L}_0 &= |(\partial_\mu + i g_B q_B B_\mu)\phi|^2 - \frac{1}{4}F_A^2 - \frac{1}{4}F_B^2 + \frac{1}{2}(\partial_\mu b + M_1\, B_\mu)^2 - \lambda(|\phi|^2 - \frac{v^2}{2})^2 \\ &\quad + \overline{\psi} i \gamma^\mu (\partial_\mu + i e A_\mu + i g_B \gamma^5 B_\mu)\psi - \lambda_1 \overline{\psi}_L \phi \psi_R - \lambda_1 \overline{\psi}_R \phi^* \psi_L \qquad (1.11)\end{aligned}$$

which exhibits a non anomalous (A) and an anomalous (B) gauge interaction. Its couplings are summarized in Tabs. 1.1 and 1.2, where "S" refers to the presence of a Stückelberg mass term for the corresponding gauge boson, if present. We have indicated with a small lowercase b the corresponding axion. The $U(1)_A$ symmetry is unbroken while B gets its mass by the combined Higgs-Stückelberg mechanism. Another feature of the model, as we are going to see, is the presence of an Higgs-axion mixing generated not by a scalar potential (such as $V(\phi, b)$), as we will show in Sec. 1.4.1, but by the fact that both mechanisms

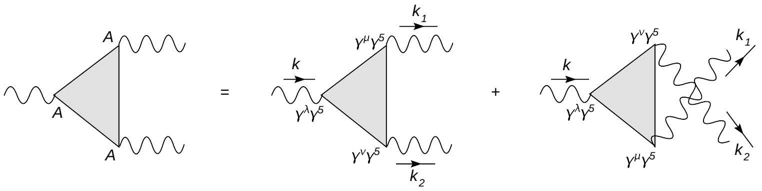

Figure 1.2: The **AAA** diagrams.

communicate their mass to the same gauge boson B. The axion remains a massless field in this case. Our discussion relies on the formalism of the one-loop effective action, which is the generating functional of the one-particle irreducible (1PI) correlation functions of a given model. The correlators are multiplied by external classical fields and the formalism allows to derive quite directly the anomalous Ward Identities of the theory. The reader can find a discussion of the formalism in the appendix, where we study the properties of the Chern-Simons and Wess-Zumino vertices of the model and their gauge variations.

	A	B
ψ	$q_L^A = q_R^A = 1$	$q_R^B = -q_L^B = 1$

Table 1.1: Fermion assignments, A-B Model.

	ϕ	S
A	$q^A = 0$	0
B	$q^B = -2$	b

Table 1.2: Gauge structure, A-B Model.

In the A-B Model, this will involve the classical defining action plus the anomaly diagrams with fermionic loops and we will require its invariance under gauge transformations. The structure of the (total) effective action is summarized, in the case of one vector (A) and one axial-vector (B) interaction by an expansion of the form

$$\begin{aligned} W[A,B] &= \sum_{n_1=1}^{\infty}\sum_{n_2=1}^{\infty} \frac{i^{n_1+n_2}}{n_1! n_2!} \int dx_1 ... dx_{n_1} dy_1 ... dy_{n_2} T^{\lambda_1 ... \lambda_{n_1} \mu_1 ... \mu_{n_2}}(x_1 ... x_{n_1}, y_1 ... y_{n_2}) \\ &\qquad B^{\lambda_1}(x_1) ... B^{\lambda_{n_1}}(x_{n_1}) A_{\mu_1}(y_1) ... A_{\mu_{n_2}}(y_{n_2}), \end{aligned} \tag{1.12}$$

corresponding to the diagrams in Fig. 1.3 where we sum, for each diagram, over the symmetric exchanges of all the indices (including the momentum) of the identical gauge bosons (see also Fig. 1.4). As we are going to discuss next, also higher-order diagrams of the form, for instance, AVVV will be affected by the presence of an undetermined shift in the triangle amplitudes, amounting to Chern-Simons interactions (CS). They turn to be well-defined once the distribution of the anomaly on three-point functions is

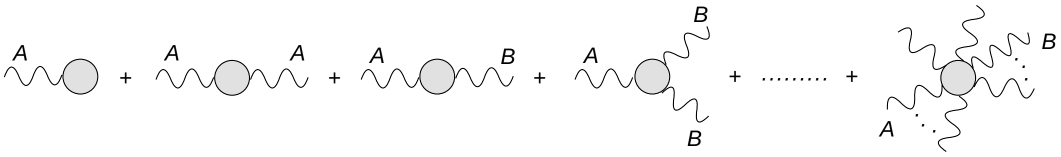

Figure 1.3: Expansion of the effective action.

performed according to the correct Bose symmetries of these correlators of lower order. Computing the

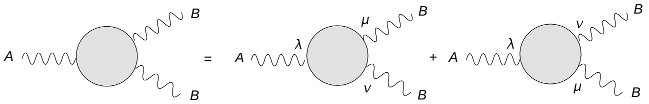

Figure 1.4: Triangle diagrams with permutations.

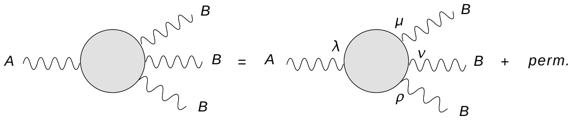

Figure 1.5: Symmetric expansion.

variation of the generating functional we obtain

$$\begin{aligned} \delta_B W^{an}[A,B] &= \frac{1}{2!}\int dx\, dy\, dz\, T^{\lambda\mu\nu}(z,x,y)\, \delta B_\lambda(z) A_\mu(x) A_\nu(y) \\ &+ \frac{1}{3!}\int dx\, dy\, dz\, dw\, T^{\lambda\mu\nu\rho}(z,x,y,w) B_\lambda(z) A_\mu(x) A_\nu(y) A_\rho(w), \end{aligned} \tag{1.13}$$

using $\delta B_\lambda(z) = \partial_\mu \theta_B(z)$ and integrating by parts we get

$$\begin{aligned} \delta_B W^{an}[A,B] &= -\frac{1}{2!}\int dx\, dy\, dz\, \frac{\partial}{\partial z^\lambda} T^{\lambda\mu\nu}(z,x,y)\, \theta_B(z) A_\mu(x) A_\nu(y) \\ &- \frac{1}{3!}\int dx\, dy\, dz\, dw\, \frac{\partial}{\partial z^\lambda} T^{\lambda\mu\nu\rho}(z,x,y,w)\, \theta_B(z) A_\mu(x) A_\nu(y) A_\rho(w). \end{aligned} \tag{1.14}$$

Notice that in configuration space the four- and the three- point function correlators are related by

$$\frac{\partial}{\partial z^\lambda}\overline{T}^{\lambda\mu\nu\rho}(z,x,y,w) = \delta(z-w)\overline{T}^{\rho\mu\nu}(w,x,y) - \delta(z-x)\overline{T}^{\mu\nu\rho}(x,y,w) + \text{ perm.} \tag{1.15}$$

For T we will be using the same conventions as for Δ, with $\overline{T}^{\lambda\mu\nu}$ indicating a single diagram with non-permuted external gauge lines, while $T^{\lambda\mu\nu}$ will denote the symmetrized one (in $\mu\nu$). Clearly, the one-loop effective theory of this model contains anomalous interactions that need to be cured by the introduction of suitable compensator fields. The role of the axion b is to remove the anomalies associated to the triangle diagrams which are correlators of one and three chiral currents respectively

$$T^{(\mathbf{AVV})}_{\lambda\mu\nu}(x,y,z) = \langle 0|T\left(J_\mu(x) J_\nu(y) J^5_\lambda(z)\right)|0\rangle \tag{1.16}$$

and

$$T^{(\mathbf{AAA})}_{\lambda\mu\nu}(x,y,z) = \langle 0|T\left(J^5_\mu(x) J^5_\nu(y) J^5_\lambda(z)\right)|0\rangle, \tag{1.17}$$

where

$$J_\mu = -\overline{\psi}\gamma_\mu\psi \qquad J^5_\mu = -\overline{\psi}\gamma_\mu\gamma_5\psi. \tag{1.18}$$

We denote by $\Delta(k_1,k_2)$ and $\Delta_3(k_1,k_2)$ their corresponding expressions in momentum space

$$(2\pi)^4\delta(k-k_1-k_2)\Delta^{\lambda\mu\nu}(k_1,k_2) = \int dx\, dy\, dz\, e^{ik_1\cdot x + ik_2\cdot y - ik\cdot z}\, T^{\lambda\mu\nu}_{(\mathbf{AVV})}(x,y,z) \tag{1.19}$$

$$(2\pi)^4\delta(k-k_1-k_2)\Delta_3^{\lambda\mu\nu}(k_1,k_2)=\int dx\,dy\,dz\,e^{ik_1\cdot x+ik_2\cdot y-ik\cdot z}\,T^{\lambda\mu\nu}_{(\mathbf{AAA})}(x,y,z). \tag{1.20}$$

Another point to remark is that the invariant amplitudes linear in momenta in the definition of the **AVV** triangle diagram correspond, in configuration space, to Chern-Simons interactions. In momentum space these are proportional to

$$V_{CS}^{\lambda\mu\nu}(k_1,k_2)=-i\epsilon^{\lambda\mu\nu\sigma}(k_1-k_2)_\sigma \tag{1.21}$$

and we denote with $T_{CS}^{\lambda\mu\nu}$ the corresponding contribution to the effective Lagrangian in Minkowski space (see App. 1.16 for an explicit computation)

$$\mathcal{L}_{CS,ABA}=\int dx\,A^\mu(x)B^\nu(x)F_A^{\rho\sigma}(x)\epsilon_{\mu\nu\rho\sigma}. \tag{1.22}$$

Moving to the anomalous part of the effective action, this takes the form, for generic gauge bosons A_i

$$\mathcal{S}_{eff}=\mathcal{S}_0+\mathcal{S}_1, \tag{1.23}$$

where

$$\mathcal{S}_1=\sum_{i\,j\,k}\frac{1}{n_i!n_j!n_k!}\,g_{ijk}\int dx\,dy\,dz\,A_i^\lambda(x)A_j^\mu(y)A_k^\nu(z)T^{\lambda\mu\nu}_{A_iA_jA_k}(x,y,z) \tag{1.24}$$

and where A_i indicates an A or a B gauge boson, while g_{ijk} is the product of the three coupling constants $g_{A_i}g_{A_j}g_{A_k}$, with an additional normalization due to a counting of identical external gauge bosons ($n_i!$). All the anomalous contributions are included in the definition. In order to derive its explicit structure in our simplified cases, we consider the case of the BAA vertex, the other examples being similar. We have, for instance, the partial contribution

$$\mathcal{S}^{BAA}=g_B\int dx\,dy\,dz\,B_\lambda(z)\langle J_5^\lambda(z)e^{ig_A\int d^4xJ^\mu(x)A_\mu(x)}\rangle, \tag{1.25}$$

where the gauge fields are treated as classical fields and $\langle,\rangle$ indicate the vacuum expectation value. Expanding to second order, we keep only the connected contributions obtaining for instance

$$\mathcal{S}^{BAA}=\frac{i^2}{2!}g_Bg_A^2\int dx\,dy\,dz\,B_\lambda(z)A_\mu(x)A_\nu(y)\langle J_5^\lambda(z)J^\mu(x)J^\nu(y)\rangle. \tag{1.26}$$

This expression is our starting point for all the further analysis. Most of the manipulations concerning the proof of gauge-invariance of the effective action are more easily worked out in this formalism. Moving from momentum space to configuration space and back, may also be quite useful in order to detail the Ward Identities of a given anomalous effective action.

In the presence of spontaneous symmetry breaking and of Stückelberg mass terms one has to decide whether the linear mixing between the Stückelberg field and the gauge boson is kept or not. One can keep the mixing and derive ordinary Ward Identities for a given model. This is a possibility which is clearly at hand and can be useful. The disadvantage of this approach is that there is no gauge-fixing parameter that can be used to analyze the gauge dependence of a given set of amplitudes and their cancellation. When the mixing is removed by going to a R_ξ gauge, one can identify the set of gauge-invariant contributions to a given amplitude and identify more easily the conditions under which a given model becomes unitary. We follow this second approach. We are then able to combine gauge-dependent contributions in such a way that the unphysical poles of a given amplitude cancel. The analysis that we perform is limited to the s-channel, but the results are easily generalizable to the t and u channels as well. From this simple analysis one can easily extract information on the perturbative expansion of the effective action.

1.3.1 The anomalous effective action of the A-B Model

In the A-B Model, defined in Eq. (1.11), the contribution to the anomalous effective action is given by

$$\begin{aligned}
\mathcal{S}_{an} &= \mathcal{S}_1 + \mathcal{S}_3 \\
\mathcal{S}_1 &= \int dx\, dy\, dz \left(\frac{g_B\, g_A^2}{2!}\, T^{\lambda\mu\nu}_{\mathbf{AVV}}(x,y,z) B_\lambda(z) A_\mu(x) A_\nu(y) \right), \\
\mathcal{S}_3 &= \int dx\, dy\, dz \left(\frac{g_B^3}{3!}\, T^{\lambda\mu\nu}_{\mathbf{AAA}}(x,y,z) B_\lambda(z) B_\mu(x) B_\nu(y) \right),
\end{aligned} \tag{1.27}$$

where we have collected all the anomalous diagrams of the form **AVV** and **AAA**. We can easily express the gauge transformations of A and B in the form

$$\begin{aligned}
\frac{1}{2!}\delta_B \langle T_{\mathbf{AVV}} BAA \rangle &= \frac{i}{2!} a_3(\beta) \frac{1}{4} \langle F_A \wedge F_A \theta_B \rangle, \\
\frac{1}{3!}\delta_B \langle T_{\mathbf{AAA}} BBB \rangle &= \frac{i}{3!} \frac{a_n}{3} \frac{3}{4} \langle F_B \wedge F_B \theta_B \rangle,
\end{aligned} \tag{1.28}$$

where we have left open the choice over the parameterization of the loop momentum, denoted by the presence of the arbitrary parameter β with

$$a_3(\beta) = -\frac{i}{4\pi^2} + \frac{i}{2\pi^2}\beta \qquad a_3 \equiv \frac{a_n}{3} = -\frac{i}{6\pi^2}, \tag{1.29}$$

while

$$\frac{1}{2!}\delta_A \langle T_{\mathbf{AVV}} BAA \rangle = \frac{i}{2!} a_1(\beta) \frac{2}{4} \langle F_B \wedge F_A \theta_A \rangle. \tag{1.30}$$

We have the following equations for the anomalous variations of the effective Lagrangian

$$\begin{aligned}
\delta_B \mathcal{L}_{an} &= \frac{i g_B g_A^2}{2!}\, a_3(\beta) \frac{1}{4} F_A \wedge F_A \theta_B + \frac{i g_B^3}{3!} \frac{a_n}{3} \frac{3}{4} F_B \wedge F_B \theta_B \\
\delta_A \mathcal{L}_{an} &= \frac{i g_B g_A^2}{2!}\, a_1(\beta) \frac{2}{4} F_B \wedge F_A \theta_A,
\end{aligned} \tag{1.31}$$

while the axionic contributions $\mathcal{L}_b$ (Wess-Zumino counterterms), needed to restore the gauge symmetry violated at one-loop level, are given by

$$\mathcal{L}_b = \frac{C_{AA}}{M} b\, F_A \wedge F_A + \frac{C_{BB}}{M} b\, F_B \wedge F_B. \tag{1.32}$$

Notice that since the axion shifts only under a gauge variation of the anomalous $U(1)$ gauge field B (and not under A), gauge invariance of the effective action under a gauge transformation of the gauge field A requires that

$$\delta_A \mathcal{L}_{an} = 0. \tag{1.33}$$

Clearly, this condition fixes $\beta = -1/2 \equiv \beta_0$ and is equivalent to the CVC condition on A that we had relaxed at the beginning. Imposing gauge invariance under B gauge transformations, on the other hand, we obtain

$$\delta_B \left(\mathcal{L}_b + \mathcal{L}_{an} \right) = 0 \tag{1.34}$$

which implies

$$C_{AA} = \frac{i\, g_B g_A^2}{2!}\frac{1}{4}\, a_3(\beta_0)\, \frac{M}{M_1}, \qquad C_{BB} = \frac{i g_B^3}{3!}\frac{1}{4}\, a_n\, \frac{M}{M_1}. \tag{1.35}$$

These conditions on the coefficients C are sufficient to render gauge-invariant the total Lagrangian. We observe that the presence of an Abelian symmetry which has to remain exact and is not accompanied by a shifting axion has important implications on the consistency of the theory. We have brought up this example because in more complex situations in which a given gauge symmetry is broken and the pattern of breakings is such to preserve a final symmetry (for instance $U(1)_{em}$), the structure of the anomalous correlators, in some case, is drastically constrained to assume the CVC form. However this is not a general result.

Under a more general assumption, we could have allowed some Chern-Simons contributions in the counterterm Lagrangian. This is an interesting variation that can be worked out at a diagrammatic level in order to identify the role played by the CS interactions. We will get back to this point once we start our diagrammatic analysis of these simple models.

1.4 Higgs-Axion Mixing in $U(1)$ Models: massless axi-Higgs

Having discussed the consistency to all orders of the effective action, we need to discuss the role played by the shifting axions in the spectrum of the theory. We have already pointed out that the axion will mix with the remaining scalars of the model. In the presence of a Higgs sector such a mixing can take place at the level of the scalar potential, with implications on the mass and the coupling of the axion to the remaining particles of the model. In order to understand how this mixing occurs, we consider the case of the A-B Model.

This model has two scalars: the Higgs and the Stückelberg fields. We assume that the Higgs field takes a non-zero v.e.v. and, as usual, the scalar field is expanded around the minimum $<\phi>= v$

$$\phi = \frac{1}{\sqrt{2}}\left(v + \phi_1 + i\phi_2\right), \tag{1.36}$$

while from the quadratic part of the Lagrangian we can easily read out the mass terms and the Goldstone mode present in the spectrum in the broken phase. This is given by

$$\begin{aligned}\mathcal{L}_q \;=\;& \frac{1}{2}\left(\partial_\mu\phi_1\right)^2 + \frac{1}{2}\left(\partial_\mu\phi_2\right)^2 + \frac{1}{2}\left(\partial_\mu b\right)^2 + \frac{1}{2}\left(M_1^2 + (q_B g_B v)^2\right) B_\mu B^\mu - \frac{1}{2} m_1^2 \phi_1^2 \\ & + B_\mu \partial^\mu \left(M_1 b + v g_B q_B \phi_2\right),\end{aligned} \tag{1.37}$$

from which, after diagonalization of the mass terms, we obtain

$$\begin{aligned}\mathcal{L}_q \;=\;& \frac{1}{2}\left(\partial_\mu\chi\right)^2 + \frac{1}{2}\left(\partial_\mu G_B\right)^2 + \frac{1}{2}\left(\partial_\mu h_1\right)^2 + \frac{1}{2} M_B^2 B_\mu B^\mu - \frac{1}{2} m_1^2 h_1^2 \\ & + M_B B^\mu \partial_\mu G_B\end{aligned} \tag{1.38}$$

where we have redefined $\phi_1(x) = h_1(x)$ and $m_1 = v\sqrt{2\lambda}$, for the Higgs field and its mass. We have identified the linear combinations

$$\begin{aligned}\chi &= \frac{1}{M_B}\left(-M_1\,\phi_2 + q_B g_B v\, b\right), \\ G_B &= \frac{1}{M_B}\left(q_B g_B v\,\phi_2 + M_1\, b\right),\end{aligned} \tag{1.39}$$

corresponding to a massless particle, the axi-Higgs χ, and a massless Goldstone mode G_B. The rotation matrix that allows the change of fields $(\phi_2, b) \rightarrow (\chi, G_B)$ is given by

$$U = \begin{pmatrix} -\cos\theta_B & \sin\theta_B \\ \sin\theta_B & \cos\theta_B \end{pmatrix} \tag{1.40}$$

with $\theta_B = \arccos(M_1/M_B) = \arcsin(q_B g_B v/M_B)$. The axion b can be expressed as linear combination of the rotated fields χ, G_B as

$$b = \alpha_1\chi + \alpha_2 G_B = \frac{q_B g_B v}{M_B}\chi + \frac{M_1}{M_B}G_B, \tag{1.41}$$

while the gauge field B_μ gets its mass M_B through the combined Higgs-Stückelberg mechanism

$$M_B = \sqrt{M_1^2 + (q_B g_B v)^2}. \tag{1.42}$$

To remove the mixing between the gauge field and the Goldstone mode we work in the R_ξ gauge. The gauge-fixing Lagrangian is given by

$$\mathcal{L}_{gf} = -\frac{1}{2}\mathcal{G}_B^2 \tag{1.43}$$

where

$$\mathcal{G}_B = \frac{1}{\sqrt{\xi_B}}\left(\partial \cdot B - \xi_B M_B G_B\right), \tag{1.44}$$

and the corresponding ghost Lagrangian

$$\mathcal{L}_{B\,gh} \quad = \quad \bar{c}_B\left(-\Box - \xi_B v(h_1 + v) - \xi_B M_1^2\right)c_B. \tag{1.45}$$

The full Lagrangian in the physical basis after diagonalization of the mass matrix becomes

$$\mathcal{L} \quad = \quad -\frac{1}{4}F_A^2 - \frac{1}{4}F_B^2 + \mathcal{L}_{Bgh} + \mathcal{L}_f + \mathcal{L}_B \tag{1.46}$$

where $\mathcal{L}_f$ denotes the fermion contribution. Its expression can be found in [40].

At this stage there are some observations to be made. In the Stückelberg phase the axion b is a Goldstone mode, since it can be set to vanish by a gauge transformation on the B gauge boson, while B is massive (with a mass M_1) and has 3 degrees of freedom (d.o.f.). Therefore in this phase the number of physical d.o.f.'s is 3 for B, 2 for A, 2 for the complex scalar Higgs ϕ, for a total of 7. After electroweak symmetry breaking we have 3 d.o.f.'s for B, 2 for A which remains massless, 1 real Higgs field h_1 and 1 physical axion χ, for a total of 7. The axion, in this case, on the contrary of what happens in the case of ordinary symmetry breaking is a *massless physical* scalar, being not part of the scalar potential. Not much surprise so far. Let's now move to the analysis of the case when the axion is part of the scalar potential. In this second case the physical axion (the axi-Higgs) gets its mass by the combined Higgs-Stückelberg mechanism.

1.4.1 Higgs-Axion Mixing in $U(1)$ Models: massive axi-Higgs

We now illustrate the mechanism of mass generation for the physical axion χ. We focus on the breaking of the $U(1)_B$ gauge symmetry of the A-B Model. We have a gauge-invariant Higgs potential given by

$$V_{PQ}(\phi) = \mu^2\phi^*\phi + \lambda\left(\phi^*\phi\right)^2 \tag{1.47}$$

plus the new PQ-breaking terms, allowed by the symmetry [1]

$$V_{\not{P}\not{Q}}(\phi, b) = b_1 \left(\phi\, e^{-i q_B g_B \frac{b}{M_1}}\right) + \lambda_1 \left(\phi\, e^{-i q_B g_B \frac{b}{M_1}}\right)^2 + 2\lambda_2 \left(\phi^* \phi\right) \left(\phi\, e^{-i q_B g_B \frac{b}{M_1}}\right) \tag{1.48}$$

so that the complete potential considered is given by

$$V(\phi, b) = V_{PQ} + V_{\not{P}\not{Q}} + V^*_{\not{P}\not{Q}} \, . \tag{1.49}$$

We require that the minima of the potential are located at

$$\langle b \rangle = 0 \qquad \langle \phi \rangle = v, \tag{1.50}$$

which imply that the mass parameter satisfies

$$\mu^2 = -\frac{b_1}{v} - 2v^2\lambda - 2\lambda_1 - 6v\lambda_2. \tag{1.51}$$

We are interested in the matrix describing the mixing of the CP-odd Higgs sector with the axion field b, given by

$$\left(\begin{array}{cc} \phi_2, & b \end{array} \right) \mathcal{M}_2 \left(\begin{array}{c} \phi_2 \\ b \end{array} \right) \tag{1.52}$$

where $\mathcal{M}_2$ is a symmetric matrix

$$\mathcal{M}_2 = -\frac{1}{2} c_\chi v^2 \left(\begin{array}{cc} 1 & -v \frac{q_B g_B}{M_1} \\ -v \frac{q_B g_B}{M_1} & v^2 \frac{q_B^2 g_B^2}{M_1^2} \end{array} \right) \tag{1.53}$$

and where the dimensionless coefficient multiplied in front is given by

$$c_\chi = 4 \left(\frac{b_1}{v^3} + \frac{4\lambda_1}{v^2} + \frac{2\lambda_2}{v} \right). \tag{1.54}$$

Notice that this parameter plays an important role in establishing the size of the mass of the physical axion, after diagonalization. It encloses all the dependence of the mass from the PQ corrections to the standard Higgs potential. They can be regarded as corrections of order p/v, with p being any parameter of the PQ potential. If p is very small, which is the case if the $V_{\not{P}\not{Q}}$ term of the potential is generated non-perturbatively (for instance by instanton effects in the case of QCD), the mass of the axi-Higgs can be pushed far below the typical mass of the electroweak breaking scenario (the Higgs mass), as discussed in [13].

The mass matrix has 1 zero eigenvalue corresponding to the Goldstone boson G_B and 1 non-zero eigenvalue corresponding to a physical axion field $-\chi-$ with mass

$$m_\chi^2 = -\frac{1}{2} c_\chi v^2 \left[1 + \frac{q_B^2 g_B^2 v^2}{M_1^2} \right] = -\frac{1}{2} c_\chi \, v^2 \, \frac{M_B^2}{M_1^2}. \tag{1.55}$$

The mass of this state is positive if $c_\chi < 0$. The rotation matrix that takes from the interaction eigenstates to the mass eigenstates is denoted by O^χ

$$\begin{pmatrix} \chi \\ G_B \end{pmatrix} = O^\chi \begin{pmatrix} \phi_2 \\ b \end{pmatrix} \tag{1.56}$$

so that we obtain the rotations

$$\begin{aligned} \phi_2 &= \frac{1}{M_B}(-M_1\,\chi + q_B g_B\,v\,G_B) && (1.57) \\ b &= \frac{1}{M_B}(q_B g_B\,v\,\chi + M_1\,G_B). && (1.58) \end{aligned}$$

The mass squared matrix can be diagonalized as

$$(\,\chi,\,G_B\,)O^\chi\mathcal{M}_2(O^\chi)^T\begin{pmatrix} \chi \\ G_B \end{pmatrix} = (\,\chi,\,G_B\,)\begin{pmatrix} m_\chi^2 & 0 \\ 0 & 0 \end{pmatrix}\begin{pmatrix} \chi \\ G_B \end{pmatrix} \tag{1.59}$$

so that G_B is a massless Goldstone mode and m_χ is the mass of the physical axion. In [13] one can find a discussion of some physical implications of this field when its mass is driven to be small in the instanton vacuum, similarly to the Peccei-Quinn axion of a global symmetry. However, given the presence of both mechanisms, the Stückelberg and the Higgs, it is not possible to decide whether this axion can be a valid dark-matter candidate. In the same work it is shown that the entire Stückelberg mechanism can be the result of a partial decoupling of a chiral fermion.

1.5 Unitarity issues in the A-B Model in the exact phase

In this section we start discussing the issue of unitarity of the model that we have introduced. This is a rather involved topic that can be addressed by a diagrammatic analysis of those amplitudes with s-channel exchanges of the gauge bosons, the axi-Higgs and the NG modes generated in the various phases of the theory (before and after symmetry breaking, with/without Yukawa couplings). The analysis could, of course, be repeated in the other channels (t, u) as well, but no further condition would be obtained. We will gather all the information coming from the study of the S-matrix amplitudes to set constraints on the parameters of the model. We have organized our analysis as a case-by-case study verifying the cancellation of the unphysical singularities in the amplitude in all the phases of the theory, establishing also their gauge independence. This is worked out in the R_ξ gauge so to make evident the disappearance of the gauge-fixing parameter in each amplitude. The scattering amplitudes are built out of two anomalous diagrams with s-channel exchanges of gauge dependent propagators, and in all the cases we are brought back to the analysis of a set of anomalous Ward Identities to establish our results.

1.5.1 Unitarity and CS interactions in the A-B Model

The first point that we address in this section concerns the role played by the CS interactions in the unitarity analysis of simple s-channel amplitudes. This analysis clarifies that CS interactions can be included or kept separately from the anomalous vertices with no consequence. To show this, we consider the following modification on the A-B Model, where the CS interactions are generically introduced as

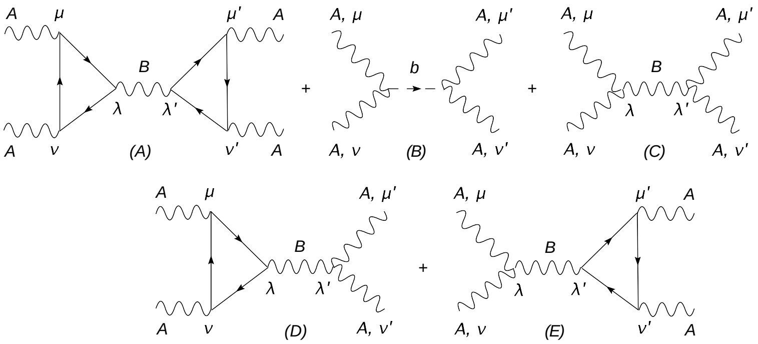

Figure 1.6: Diagrams involved in the unitarity analysis with external CS interactions.

possible counterterms in the one-loop effective action, which is given by

$$\mathcal{L} = \mathcal{L}_0 + \mathcal{L}_{GS} + \mathcal{L}_{CS}, \tag{1.60}$$

where $\mathcal{L}_0$ is already known from the previous sections, but in particular we focus on the components

$$\mathcal{L}_{GS} = \frac{C_{AA}}{M} b F_A \wedge F_A + \frac{C_{BB}}{M} b F_B \wedge F_B \tag{1.61}$$

and

$$\mathcal{L}_{CS} = d_1 B^{\mu} A^{\nu} F_A^{\rho\sigma} \epsilon_{\mu\nu\rho\sigma} \equiv d_1 B A \wedge F^A. \tag{1.62}$$

Under an A-gauge transformation we have [1]

$$\delta_A \mathcal{L} = \frac{d_1}{2}\, \theta_A F_B \wedge F_A + \frac{i}{2!} a_1(\beta) \frac{2}{4}\, \theta_A F_B \wedge F_A, \tag{1.63}$$

so that we obtain

$$\frac{d_1}{2} + \frac{i a_1(\beta)}{4} = 0 \quad \leftrightarrow \quad d_1 = -\frac{i}{2} a_1(\beta). \tag{1.64}$$

Analogously, under a B-gauge transformation we have

$$\begin{aligned}\delta_B \mathcal{L} = & -\frac{d_1}{2} \theta_B F_A \wedge F_A + \frac{i}{2!} a_3(\beta) \frac{1}{4} F_A \wedge F_A \theta_B - C_{AA} \frac{M_1 \theta_B}{M}\, F_A \wedge F_A \\ & - C_{BB} \frac{M_1 \theta_B}{M} F_B \wedge F_B + \frac{i}{3!} \frac{a_n}{3} \frac{3}{4} \theta_B F_B \wedge F_B,\end{aligned} \tag{1.65}$$

to obtain

$$-\frac{d_1}{2} - C_{AA} \frac{M_1}{M} + \frac{i}{2!} a_3(\beta) \frac{1}{4} = 0 \quad \leftrightarrow \quad C_{AA} = \left(-\frac{d_1}{2} + \frac{i}{2!} a_3(\beta) \frac{1}{4} \right) \frac{M}{M_1}. \tag{1.66}$$

We refer the reader to one of the appendices where the computation is performed in detail. We have shown that the presence of external Ward Identities forcing the invariant amplitudes of a given anomalous triangle diagram to assume a specific form, allow to re-absorb the CS coefficients inside the triangle, thereby simplifyig the computations. In this specific case the CVC condition for A is a property of the

---

[1] In the language of the effective action the multiplicity factors are proportional to the number ($n!$) of external gauge lines of a given type. We keep these factors explicitly to backtrack their origin.

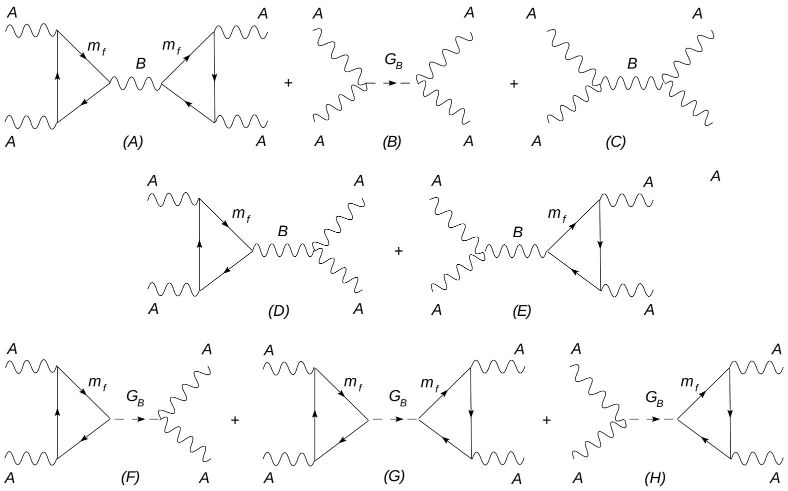

Figure 1.7: Unitarity issue for the A-B Model in the broken phase.

theory. In other cases this does not take place. For instance, instead of the condition $a_1(\beta) = 0$, a less familiar condition such as $a_3(\beta) = 0$ (conserved axial current, CAC) may be needed. In this sense, if we define the CVC condition to be the "standard case", the CAC condition points toward a *new* anomalous interaction. We remark once more that β remains "free" in the SM, since the anomaly traces cancel for all the generators, differently from this new situation. The theory allows new CS interactions, with the understanding that, at least in these cases, these interactions can be absorbed into a redefinition of the vertex. However, the presence of a WI, that allows us to re-express a_1 and a_2 in terms of $a_3 \ldots a_6$ in *different* ways (see Eq. (1.120) for the structure of the triangle diagram), at the same time allows us to come up with different gauge invariant expressions of the same vertex function (fixed by a CVC or a CAC condition, depending on the case). These different versions of these **AVV** three-point functions are characterized by different (gauge-variant) contact interactions since a_1 and a_2 in Minkowski space contain, indeed, CS interactions. We will elaborate on this point in a following section where we discuss the structure of the effective action in Minkowski space.

The extension of this pattern to the broken Higgs phase can be understood from Fig. 1.7 where the additional contributions have been explicitly included. We have depicted the CS terms as separate contributions and shown perfect cancellation also in this case. The complete set of diagrams is

$$S_\xi = A_\xi + B_\xi + C_\xi + D_\xi + E_\xi + F_\xi + G_\xi + H_\xi \tag{1.67}$$

and the total gauge dependence vanishes. Details on the calculation can be found in the App. 1.13.1.

1.6 Gauge independence of the A self-energy to higher orders and the loop counting

In this section we move to an analysis performed to higher orders that illustrates how the loop expansion and the counterterms get organized so to have a consistent gauge independent theory.

For this purpose, let's consider the diagrams in Fig. 1.8, which are relevant in order to verify this

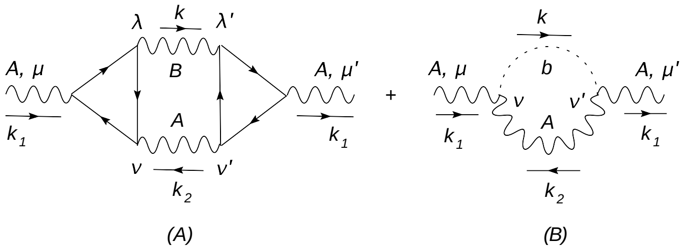

Figure 1.8: Three-loop cancellations of the gauge dependence.

cancellation in the massless fermion case. It shows the self-energy of the A gauge boson. From now on we are dropping all the coupling constants to simplify the notation, which can be re-inserted at the end. We have omitted diagrams which are symmetric with respect to the two intermediate lines of the B and A gauge bosons, for simplicity. This symmetrization is responsible for the cancellation of the gauge dependence of the propagator of A and the vector interaction of B, while the gauge dependence of the axial-vector contribution of B is canceled by the corresponding Goldstone (shown). Diagram (A) involves three loops and therefore we need to look for cancellations induced by a diagram involving the s-channel exchange both of an A and of a B gauge boson plus the one-loop interactions involving the relevant counterterms. In this case one easily identifies diagram (B) as the only possible additional contribution.

To proceed with the demonstration we first isolate the gauge dependence in the propagator for the gauge boson exchanged in the s-channel

$$\begin{aligned}\frac{-i}{k^2-M_1^2}\left[g^{\lambda\lambda'}-\frac{k^\lambda k^{\lambda'}}{k^2-\xi_B M_1^2}(1-\xi_B)\right] &= \frac{-i}{k^2-M_1^2}\left(g^{\lambda\lambda'}-\frac{k^\lambda k^{\lambda'}}{M_1^2}\right)+\frac{-i}{k^2-\xi_B M_1^2}\left(\frac{k^\lambda k^{\lambda'}}{M_1^2}\right)\\ &= P_0^{\lambda\lambda'}+P_\xi^{\lambda\lambda'}.\end{aligned} \tag{1.68}$$

and, using this separation, the sum involving the two diagrams gives

$$S=\int\frac{d^4k_2}{(2\pi)^4}(\mathcal{A}+\mathcal{B}), \tag{1.69}$$

with the gauge-dependent contributions being given by

$$\begin{aligned}\mathcal{A}_{\xi 0} &= \Delta^{\lambda\mu\nu}(-k_1,-k_2)P_\xi^{\lambda\lambda'}\Delta^{\lambda'\mu'\nu'}(k_1,k_2)P_o^{\nu\nu'}\\ &= \Delta^{\lambda\mu\nu}(-k_1,-k_2)\left[\frac{-i}{k^2-\xi_B M_1^2}\left(\frac{k^\lambda k^{\lambda'}}{M_1^2}\right)\right]\Delta^{\lambda'\mu'\nu'}(k_1,k_2)\left[\frac{-ig^{\nu\nu'}}{k_2^2}\right]\\ \mathcal{B}_{\xi 0} &= 4\times\left(\frac{4}{M}C_{AA}\right)^2\epsilon^{\mu\nu\rho\sigma}k_{1\rho}k_{2\sigma}\frac{i}{k^2-\xi_B M_1^2}\epsilon^{\mu'\nu'\rho'\sigma'}k_{1\rho'}k_{2\sigma'}P_o^{\nu\nu'}.\end{aligned} \tag{1.70}$$

Using the anomaly equations and substituting the appropriate value already obtained for the WZ-coefficient, we obtain a vanishing expression

$$\begin{aligned}\mathcal{A}_{\xi 0}+\mathcal{B}_{\xi 0} &= (-a_3(\beta)\epsilon^{\mu\nu\rho\sigma}k_{1\rho}k_{2\sigma})\left[\frac{-i}{k^2-\xi_B M_1^2}\frac{1}{M_1^2}\right](a_3(\beta)\epsilon^{\mu'\nu'\rho'\sigma'}k_{1\rho'}k_{2\sigma'})P_o^{\nu\nu'}\\ &+ 4\frac{16}{M^2}\left(\frac{i}{2!}\frac{1}{4}a_3(\beta)\frac{M}{M_1}\right)^2\epsilon^{\mu\nu\rho\sigma}k_{1\rho}k_{2\sigma}\frac{i}{k^2-\xi_B M_1^2}\epsilon^{\mu'\nu'\rho'\sigma'}k_{1\rho'}k_{2\sigma'}P_o^{\nu\nu'}=0.\end{aligned} \tag{1.71}$$

After symmetry breaking, with massive fermions, the pattern gets far more involved and is described in

Fig. 1.9. In this case we have the sum

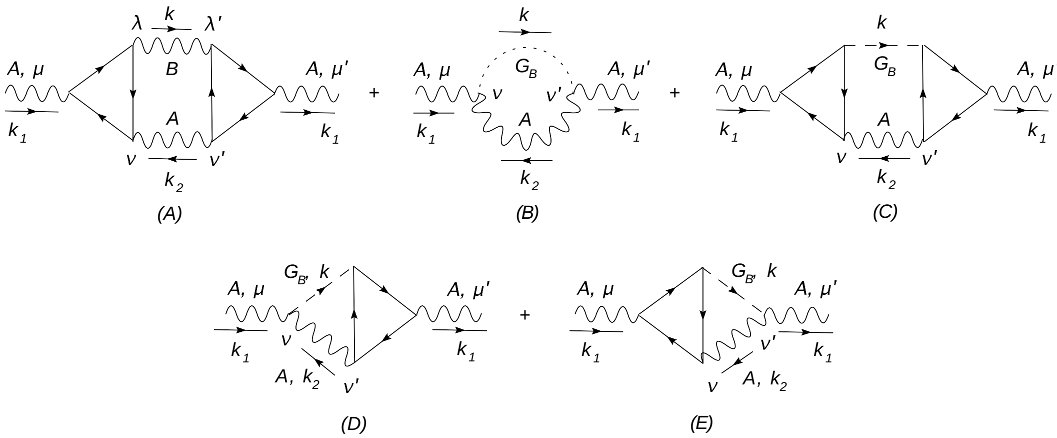

Figure 1.9: The complete set of diagrams in the broken phase.

$$S = \int \frac{d^4k_2}{(2\pi)^4}(\mathcal{A}+\mathcal{B}+\mathcal{C}+\mathcal{D}+\mathcal{E}) \tag{1.72}$$

and it can be shown by direct computation that the gauge dependences cancel in this combination. The details about this cancellation are given in App. 1.13.3. Notice that the pattern to follow in order to identify the relevant diagrams is quite clear, and it is not difficult to identify at each order of the loop expansion contributions with the appropriate s-channel exchanges that combine into gauge invariant amplitudes. These are built identifying direct contributions and counterterms in an appropriate fashion, counting the counterterms at their appropriate order in Planck's constant (h).

1.7 Unitarity Analysis of the A-B Model in the broken phase

In the broken phase and in the presence of Yukawa couplings there are some modifications that take place, since the s-channel exchange of the b axion is rotated on the two components (the Goldstone and physical axion χ) as shown later in Fig. 1.11. The introduction of the Yukawa interaction and the presence of a symmetry breaking phase determines an interaction of the axion with the fermions. Therefore, let's consider the Yukawa Lagrangian

$$\mathcal{L}_{Yuk} = -\lambda_1\,\overline{\psi}_L\phi\,\psi_R - \lambda_1\,\overline{\psi}_R\phi^*\psi_L, \tag{1.73}$$

which is needed to extract the coupling between the axi-Higgs and the fermions. We focus on the term

$$\mathcal{L}_{Yuk}(\phi_2) = -\frac{\lambda_1}{2}\left[\overline{\psi}(1+\gamma^5)\psi\,\frac{i\phi_2}{\sqrt{2}} - \overline{\psi}(1-\gamma^5)\psi\,\frac{i\phi_2}{\sqrt{2}}\right], \tag{1.74}$$

having expanded around the Higgs vacuum. Performing a rotation to express the pseudoscalar Higgs phase ϕ_2 in terms of the physical axion and the NG boson

$$\phi_2 = -\frac{M_1}{M_B}\chi + \frac{q_B g_B v}{M_B} G_B,$$

one extracts a $\chi\overline{\psi}\psi$ coupling of the kind

$$\mathcal{L}_{Yuk}(\chi) = \frac{\lambda_1}{\sqrt{2}}\frac{M_1}{M_B} i\,\overline{\psi}\chi\gamma^5\psi = \frac{m_f}{v}\frac{M_1}{M_B} i\,\overline{\psi}\chi\gamma^5\psi, \tag{1.75}$$

and a coupling $G\overline{\psi}\psi$ for the Goldstone mode

$$\mathcal{L}_{Yuk}(G_B) = -\frac{\lambda_1}{\sqrt{2}}\frac{q_B g_B v}{M_B} i\,\overline{\psi}\, G_B\gamma^5\psi = 2 g_B \frac{m_f}{M_B} i\overline{\psi}\gamma^5\psi G_B. \tag{1.76}$$

Having fixed the Yukawa couplings of the model, we move to the analysis of the same diagrams of the previous section in the broken phase. Preliminarily, we need to identify the structure of the anomaly equation for the fermionic three-point functions with their complete mass dependence. In the case of massive fermions the anomalous Ward Identities for an **AVV** triangle are of the form

$$\begin{aligned}
k_{1\mu}\Delta^{\lambda\mu\nu}(\beta, k_1, k_2) &= a_1(\beta)\epsilon^{\lambda\nu\alpha\beta}k_1^\alpha k_2^\beta, \\
k_{2\nu}\Delta^{\lambda\mu\nu}(\beta, k_1, k_2) &= a_1(\beta)\epsilon^{\lambda\mu\alpha\beta}k_2^\alpha k_1^\beta, \\
k_{\lambda}\Delta^{\lambda\mu\nu}(\beta, k_1, k_2) &= a_3(\beta)\epsilon^{\mu\nu\alpha\beta}k_1^\alpha k_2^\beta + 2m_f\Delta^{\mu\nu},
\end{aligned} \tag{1.77}$$

and in the case of **AAA** triangle $\Delta_3^{\lambda\mu\nu}(\beta, k_1, k_2) = \Delta_3^{\lambda\mu\nu}(k_1, k_2)$, with Bose symmetry providing a factor $1/3$ for the distribution of the anomalies among the 3 vertices

$$\begin{aligned}
k_{1\mu}\Delta_3^{\lambda\mu\nu}(k_1, k_2) &= \frac{a_n}{3}\epsilon^{\lambda\nu\alpha\beta}k_1^\alpha k_2^\beta + 2m_f\Delta^{\lambda\nu}, \\
k_{2\nu}\Delta_3^{\lambda\mu\nu}(k_1, k_2) &= \frac{a_n}{3}\epsilon^{\lambda\mu\alpha\beta}k_2^\alpha k_1^\beta + 2m_f\Delta^{\lambda\mu}, \\
k_{\lambda}\Delta_3^{\lambda\mu\nu}(k_1, k_2) &= \frac{a_n}{3}\epsilon^{\mu\nu\alpha\beta}k_1^\alpha k_2^\beta + 2m_f\Delta^{\mu\nu},
\end{aligned} \tag{1.78}$$

where we have dropped the appropriate coupling constants common to both sides. The amplitude $\Delta^{\mu\nu}$ is given by

$$\Delta^{\mu\nu} = \int \frac{d^4q}{(2\pi)^4}\frac{Tr\left[\gamma^5(\not{q} - \not{k} + m_f)\gamma^\nu\gamma^5(\not{q} - \not{k}_1 + m_f)\gamma^\mu\gamma^5(\not{q} + m_f)\right]}{[q^2 - m_f^2][(q-k)^2 - m_f^2][(q-k_1)^2 - m_f^2]} + \text{exch.} \tag{1.79}$$

and can be expressed as a two-dimensional integral using the Feynman parameterization. We find

$$\Delta^{\mu\nu} = \epsilon^{\alpha\beta\mu\nu}k_1^\alpha k_2^\beta m_f\left(\frac{1}{2\pi^2}\right) I, \tag{1.80}$$

with I denoting the formal expression of the integral

$$I \equiv \int_0^1 dx\int_0^{1-x} dy\frac{1}{\Delta(x, y, m_f, m_\chi, M_B)}. \tag{1.81}$$

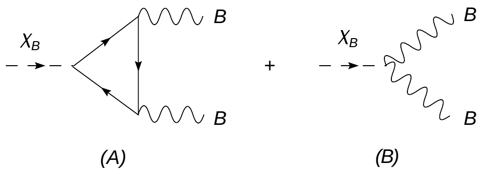

Figure 1.10: Decay amplitude for $\chi \to BB$.

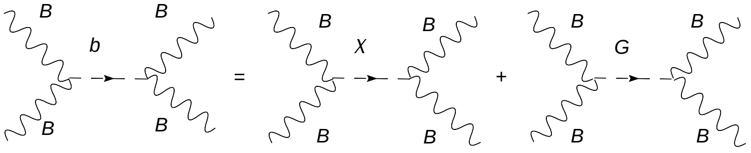

Figure 1.11: Diagrams from the Green-Schwarz coupling after symmetry breaking.

We have dropped the charge dependence since we have normalized the charges to unity and we have defined

$$\Delta(x, y, m_f, m_\chi, M_B) = \Sigma^2 - D = m_f^2 - x\, y\, m_\chi^2 + M_B^2 (x+y)^2 - x M_B^2 - y M_B^2 \equiv \Delta(x, y). \qquad (1.82)$$

We can use this amplitude to compute the one-loop decay of the axi-Higgs in this simple model, shown in Fig. 1.10, which is given by

$$\begin{aligned} \mathcal{M}^{\mu\nu}(\chi \to BB) &= \mathcal{A} + \mathcal{B} \\ &= i \frac{m_f}{v} \frac{M_1}{M_B} \Delta^{\mu\nu}(k_1, k_2) + \alpha_1 \frac{4}{M} C_{BB} \epsilon^{\alpha\beta\mu\nu} k_1^\alpha k_2^\beta \\ &= i \frac{m_f}{v} \frac{M_1}{M_B} \Delta^{\mu\nu}(k_1, k_2) - \frac{2 g_B v}{M_B} \left(\frac{4}{M} \frac{i}{3!} \frac{1}{4} a_n \frac{M}{M_1} \right) \epsilon^{\alpha\beta\mu\nu} k_1^\alpha k_2^\beta, \qquad (1.83) \end{aligned}$$

where α_1 is the coefficient that rotates the axion b on the axi-Higgs particle χ.

1.7.1 A-B Model: $BB \to BB$ mediated by a B gauge boson in the broken phase

A second class of contributions that require a different distribution of the partial anomalies are those involving BBB diagrams. They appear in the $BB \to BB$ amplitude, mediated by the exchange of a B gauge boson of mass $M_B = \sqrt{M_1^2 + (2 g_B v)^2}$. Notice that M_B gets its mass both from the Higgs and the Stückelberg sectors. The relevant diagrams for this check are shown in Fig. 1.12. We have not included the exchange of the physical axion, since this is not gauge-dependent. We have only left the gauge-dependent contributions. Notice that the expansion is valid at two-loop level and involves two-loop diagrams built as combinations of the original diagrams and of the one-loop counterterms. There are some comments that are due in order to appreciate the way the cancellations take place. If we neglect the Yukawa couplings the diagrams (B), (C) and (D) are absent, since the Goldstone does not couple to a massless fermion. In this case, the axion b is rotated, as in the previous sections, into a Goldstone mode G_B and a physical axion χ (see Fig. 1.11). On the other hand, if we include the Yukawa couplings then the entire set of diagrams is needed. From diagram (E) we obtain the partial contribution

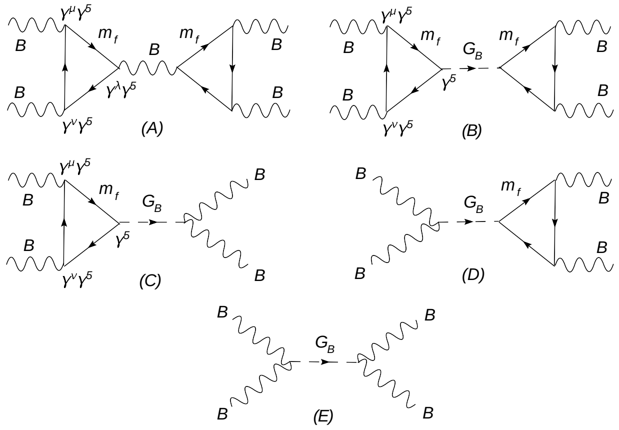

Figure 1.12: Cancellation of the gauge dependence after spontaneous symmetry breaking.

$$\mathcal{E}_\xi = 4 \times \left(\frac{4}{M}\alpha_2 C_{BB}\right)^2 \epsilon^{\mu\nu\rho\sigma} k_1^\rho k_2^\sigma \left(\frac{i}{k^2 - \xi_B M_B^2}\right) \epsilon^{\mu'\nu'\rho'\sigma'} k_1^{\rho'} k_2^{\sigma'}, \tag{1.84}$$

where the overall factor of 4 in front is a symmetry factor, the coefficient α_2 comes from the rotation of the b axion over the Goldstone boson ($\alpha_2 = \frac{M_1}{M_B}$), and the coefficient C_{BB} has already been determined from the condition of gauge invariance of the anomalous effective action before symmetry breaking. Similarly, from diagram (B) we get the term

$$\mathcal{B}_\xi = (g_B)^3 \Delta^{\mu\nu}(-k_1, -k_2) \left(2i\,\frac{m_f}{M_B}\right) \frac{i}{k^2 - \xi_B M_B^2} \left(2i\frac{m_f}{M_B}\right) (g_B)^3 \Delta^{\mu'\nu'}(k_1, k_2), \tag{1.85}$$

while diagram (C) gives

$$\mathcal{C}_\xi = 2 \times (g_B)^3 \Delta^{\mu\nu}(-k_1, -k_2) \left(2\,i\frac{m_f}{M_B}\right) \frac{i}{k^2 - \xi_B M_B^2} \left(\frac{4}{M}\alpha_2 C_{BB}\, \epsilon^{\mu'\nu'\rho'\sigma'} k_1^{\rho'} k_2^{\sigma'}\right), \tag{1.86}$$

having introduced also in this case a symmetry factor. Finally (D) gives

$$\mathcal{D}_\xi = 2 \times \left(\frac{4}{M}\alpha_2 C_{BB} \epsilon^{\mu\nu\rho\sigma} k_1^\rho k_2^\sigma\right) \frac{i}{k^2 - \xi_B M_B^2} \left(2\,i\frac{m_f}{M_B}\right) \Delta^{\mu'\nu'}(k_1, k_2)(g_B)^3. \tag{1.87}$$

We will be using the anomaly equation in the massive fermion case, having distributed the anomaly equally among the three B vertices

$$k^\lambda \Delta^{\lambda\mu\nu} = \frac{a_n}{3} \epsilon^{\mu\nu\alpha\beta} k_1^\alpha k_2^\beta + 2 m_f \Delta^{\mu\nu}. \tag{1.88}$$

Separating in diagram (A) the gauge dependent part of the propagator of the boson B from the rest we obtain

$$\begin{aligned}
\mathcal{A}_\xi &= \Delta^{\lambda\mu\nu} \frac{-i}{k^2 - \xi_B M_B^2} \left(\frac{k^\lambda k^{\lambda'}}{M_B^2}\right) \Delta^{\lambda'\mu'\nu'} \\
&= \left(\frac{a_n}{3} \epsilon^{\mu\nu\alpha\beta} k_1^\alpha k_2^\beta + 2 m_f \Delta^{\mu\nu}\right) (g_B)^3 \frac{i}{k^2 - \xi_B M_B^2} \frac{1}{M_B^2} \left(\frac{a_n}{3} \epsilon^{\mu'\nu'\alpha'\beta'} k_1^{\alpha'} k_2^{\beta'} + 2 m_f \Delta^{\mu'\nu'}\right) (g_B)^3 \\
&= \frac{i}{k^2 - \xi_B M_B^2} \frac{g_B^6}{M_B^2} \left[\left(\frac{a_n}{3}\right)^2 \epsilon^{\mu\nu\alpha\beta} \epsilon^{\mu'\nu'\alpha'\beta'} k_1^\alpha k_2^\beta k_1^{\alpha'} k_2^{\beta'}\right.
\end{aligned}$$

$$
\begin{aligned}
&+\frac{a_n}{3}\epsilon^{\mu\nu\alpha\beta}k_1^{\alpha}k_2^{\beta}\,2m_f\Delta^{\mu'\nu'}+2m_f\Delta^{\mu\nu}\frac{a_n}{3}\epsilon^{\mu'\nu'\alpha'\beta'}k_1^{\alpha'}k_2^{\beta'}\\
&+\left(2m_f\Delta^{\mu\nu}\right)\left(2m_f\Delta^{\mu'\nu'}\right)\Big]. \qquad (1.89)
\end{aligned}
$$

The first term in (1.89) is exactly canceled by the contribution from diagram (E). The last contribution cancels by the contribution from diagram (B). Finally diagrams (C) and (D) cancel against the second and third contributions from diagram (A).

1.8 The Effective Action in the Y-B Model

We anticipate in this section some of the methods that will be used in the next chapter for the analysis of a realistic model. In the A-B Model, in order to simplify the analysis, we have assumed that the coupling of the B gauge boson was purely axial-vector-like while A was purely vector-like. Here we discuss a gauge structure which allows both gauge bosons to have combined vector and axial-vector couplings. We will show that the external Ward Identities of the model involve a specific definition of the shift parameter in one of the triangle diagrams that forces the axial-vector current to be conserved ($a_3(\beta)=0$). This result, new compared to the case of the SM, shows the presence of an effective CS term in some amplitudes. The Lagrangian that we choose to exemplify this new situation is given by

$$
\begin{aligned}
\mathcal{L}_0 &= |(\partial_\mu + ig_Y q_u^Y Y_\mu + ig_B q_u^B B_\mu)\phi_u|^2 + |(\partial_\mu + ig_Y q_d^Y Y_\mu + ig_B q_d^B B_\mu)\phi_d|^2 - \frac{1}{4}F_Y^2 - \frac{1}{4}F_B^2\\
&+ \frac{1}{2}(\partial_\mu b + M_1 B_\mu)^2 - \lambda_u\left(|\phi_u|^2 - \frac{v_u}{2}\right)^2 - \lambda_d\left(|\phi_d|^2 - \frac{v_d}{2}\right)^2 + \mathcal{L}_f + \mathcal{L}_{Yuk}, \qquad (1.90)
\end{aligned}
$$

where the Yukawa couplings are given by

$$
\mathcal{L}_{Yuk} = -\lambda_1\overline{\psi}_{1L}\phi_u\psi_{1R} - \lambda_1\overline{\psi}_{1R}\phi_u^*\psi_{1L} - \lambda_2\overline{\psi}_{2L}\phi_d\psi_{2R} - \lambda_2\overline{\psi}_{2R}\phi_d^*\psi_{2L}, \qquad (1.91)
$$

with L and R denoting left- and right- handed fermions. The fermion currents are

$$
\begin{aligned}
\mathcal{L}_f &= \overline{\psi}_{1L}i\gamma^\mu\left[\partial_\mu + ig_Y q_{1L}^Y Y_\mu + ig_B q_{1L}^B B_\mu\right]\psi_{1L} + \overline{\psi}_{1R}i\gamma^\mu\left[\partial_\mu + ig_Y q_{1R}^Y Y_\mu + ig_B q_{1R}^B B_\mu\right]\psi_{1R}\\
&+ \overline{\psi}_{2L}i\gamma^\mu\left[\partial_\mu + ig_Y q_{2L}^Y Y_\mu + ig_B q_{2L}^B B_\mu\right]\psi_{2L} + \overline{\psi}_{2R}i\gamma^\mu\left[\partial_\mu + ig_Y q_{2R}^Y Y_\mu + ig_B q_{2R}^B B_\mu\right]\psi_{2R}
\end{aligned}
\qquad (1.92)
$$

so that, in general, without any particular charge assignment, both gauge bosons show vector and axial-vector couplings. In this case we realize an anomaly-free charge assignment for the hypercharge by requiring that $q_{2L}^Y = -q_{1L}^Y, q_{2R}^Y = -q_{1R}^Y$, which cancels the anomaly for a YYY triangle since

$$
\sum_{f=1,2}(q_f^Y)^3 = (q_{1R}^Y)^3 - (q_{1L}^Y)^3 + (q_{2R}^Y)^3 - (q_{2L}^Y)^3 = (q_{1R}^Y)^3 - (q_{1L}^Y)^3 - (q_{1R}^Y)^3 + (q_{1L}^Y)^3 = 0. \qquad (1.93)
$$

This condition is similar to the vanishing of the YYY anomaly for the hypercharge in the SM, and for this reason we will assume that it holds also in our simplified model. Before symmetry breaking the B gauge boson has a Goldstone coupling coming from the Stückelberg mass term due to the presence of a Higgs field. The effective action for this model is given by

$$
\mathcal{S}_{eff} = \mathcal{S}_{an} + \mathcal{S}_{WZ}, \qquad (1.94)
$$

which reads

$$\mathcal{S}_{an} = \frac{1}{3!}\langle T^{\lambda\mu\nu}_{BBB}(z,x,y)B^{\lambda}B^{\mu}B^{\nu}\rangle + \frac{1}{2!}\langle T^{\lambda\mu\nu}_{BYY}(z,x,y)B^{\lambda}Y^{\mu}Y^{\nu}\rangle + \frac{1}{2!}\langle T^{\lambda\mu\nu}_{YBB}(z,x,y)Y^{\lambda}B^{\mu}B^{\nu}\rangle \tag{1.95}$$

with

$$\mathcal{S}_{WZ} = \frac{C_{YY}}{M}\langle b\, F^{Y}\wedge F^{Y}\rangle + \frac{C_{BB}}{M}\langle b\, F^{B}\wedge F^{B}\rangle + \frac{C_{BY}}{M}\langle b\, F^{B}\wedge F^{Y}\rangle \tag{1.96}$$

denoting the WZ counterterms. Only for the triangle BBB we have assumed an anomaly symmetrically distributed, all the other anomalous diagrams having an **AVV** anomalous structure, given in momentum space by

$$\Delta^{\lambda\mu\nu}_{ijk} = \frac{i^3}{2}\sum_f \left[q^i_f q^j_f q^k_f\right]\int \frac{d^4p}{(2\pi)^4}\frac{Tr[\gamma^{\lambda}\gamma^5 \not{p}\ \gamma^{\mu}(\not{p}\ - \not{k}_1)\gamma^{\nu}(\not{p}\ - \not{k})]}{p^2(p-k_1)^2(p-k)^2} + \{\mu, k_1 \ \leftrightarrow\ \nu, k_2\}, \tag{1.97}$$

with indices running over i, j, k =Y, B. The sum over the fermionic spectrum involves the charge operators in the chiral basis

$$D_{ijk} = \frac{1}{2}\sum_{f=1,2}\left[q^i_f q^j_f q^k_f\right] \equiv \frac{1}{2}\sum_f \left(q^i_{fR}q^j_{fR}q^k_{fR} - q^i_{fL}q^j_{fL}q^k_{fL}\right). \tag{1.98}$$

Computing the Y-gauge variation for the effective one-loop anomalous action under the trasformations $Y_\mu \to Y_\mu + \partial_\mu \theta_Y$ we obtain

$$\delta_Y \mathcal{S}_{an} = \frac{i}{2!}a_1(\beta_1)\frac{2}{4}\theta_Y F_B\wedge F_Y D_{BYY} + \frac{i}{2!}a_3(\beta_2)\frac{1}{4}\theta_Y F_B\wedge F_B D_{YBB}, \tag{1.99}$$

and, similarly, for B-gauge transformations $B_\mu \to B_\mu + \partial_\mu\theta_B$ we obtain

$$\begin{aligned}\delta_B \mathcal{S}_{an} &= \frac{i}{3!}\frac{a_n}{3}\frac{3}{4}\theta_B F_B\wedge F_B D_{BBB} + \frac{i}{2!}a_3(\beta_1)\frac{1}{4}\theta_B F_Y\wedge F_Y D_{BYY}\\ &\quad + \frac{i}{2!}a_1(\beta_2)\frac{2}{4}\theta_B F_B\wedge F_Y D_{YBB},\end{aligned} \tag{1.100}$$

so that to get rid of the anomalous contributions due to gauge variance we have to fix the parameterization of the loop momenta with parameters

$$\beta_1 = \overline{\beta}_1 = -\frac{1}{2}, \qquad \beta_2 = \overline{\beta}_2 = +\frac{1}{2}. \tag{1.101}$$

Notice that while β_1 corresponds to a canonical choice (CVC condition), the second amounts to a condition for a conserved axial-vector current, which can be interpreted as a condition that forces a CS counterterm in the parameterization of the triangle amplitude. Having imposed these conditions to cancel the anomalous variations for the Y gauge boson, we can determine the WZ coefficients as

$$C_{BB} = \frac{M}{M_1}\frac{i}{3!}a_n\frac{1}{4}D_{BBB}, \quad C_{YY} = \frac{M}{M_1}\frac{i}{2!}a_3(\overline{\beta}_1)\frac{1}{4}D_{BYY}, \quad C_{BY} = \frac{M}{M_1}\frac{i}{2!}a_1(\overline{\beta}_2)\frac{2}{4}D_{YBB}. \tag{1.102}$$

Having determined all the parameters in front of the counterterms we can test the unitarity of the model. Consider the process $YY \to YY$ mediated by an B gauge boson depicted in Fig. 1.13, one can easily check that the gauge dependence vanishes. In fact we obtain

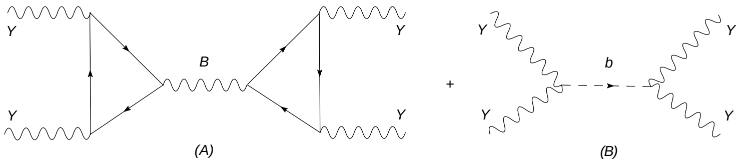

Figure 1.13: Unitarity diagrams in the Y-B Model.

$$
\begin{aligned}
\mathcal{S}_\xi &= \mathcal{A}_\xi + \mathcal{B}_\xi \\
&= \Delta^{\lambda\mu\nu}(-k_1,-k_2)\left[\frac{-i}{k^2-\xi_B M_1^2}\left(\frac{k^\lambda k^{\lambda'}}{M_1^2}\right)\right]\Delta^{\lambda'\mu'\nu'}(k_1,k_2)(D_{BYY})^2 \\
&\quad +4\left(\frac{4}{M}C_{YY}\right)^2 \epsilon^{\mu\nu\rho\sigma}k_1^\rho k_2^\sigma\left(\frac{i}{k^2-\xi_B M_1^2}\right)\epsilon^{\mu'\nu'\rho'\sigma'}k_1^{\rho'}k_2^{\sigma'} \\
&= \frac{-i}{k^2-\xi_B M_1^2}\frac{1}{M_1^2}\left(-a_3(\overline{\beta}_1)\epsilon^{\mu\nu\rho\sigma}k_1^\rho k_2^\sigma\right)\left(a_3(\overline{\beta}_1)\epsilon^{\mu'\nu'\rho'\sigma'}k_1^{\rho'}k_2^{\sigma'}\right)(D_{BYY})^2 \\
&+ 4\frac{16}{M^2}\left(\frac{M}{M_1}\frac{i}{2!}a_3(\overline{\beta}_1)\frac{1}{4}D_{BYY}\right)^2 \epsilon^{\mu\nu\rho\sigma}k_1^\rho k_2^\sigma\left(\frac{i}{k^2-\xi_B M_1^2}\right)\epsilon^{\mu'\nu'\rho'\sigma'}k_1^{\rho'}k_2^{\sigma'} = 0 \qquad (1.103)
\end{aligned}
$$

where we have included the corresponding symmetry factors. There are some comments that are in order. In the basis of the interaction eigenstates, characterized by Y and B before symmetry breaking, the CS counterterms can be absorbed into the diagrams, thereby obtaining a re-distribution of the partial anomalies on each anomalous gauge interaction. As we have already mentioned, the role of the CS terms is to render vector-like an axial-vector current at one-loop level in an anomalous trilinear coupling. The anomaly is moved from the Y vertex to the B vertex, and then canceled by a WZ counterterm. However, after symmetry breaking, in which Y and B undergo mixing, the best way to treat these anomalous interactions is to keep the CS term, rotated into the physical basis, separate from the triangular contribution. This separation is scheme dependent, being the CS term gauge variant. These theories are clearly characterized by direct interactions which are absent in the SM which can be eventually tested in suitable processes at the LHC (as suggested in Chap. 2 and developed in Chap. 5).

1.9 The fermion sector

Moving to analyze the gauge consistency of the fermion sector, we summarize some of the features of the organization of some typical fermionic amplitudes. These considerations, naturally, can also be generalized to more complex cases. For our discussion we work directly in the A-B Model for simplicity. Applications of this analysis can be found in the next chapter.

We start from Fig. 1.14 that describes the t-channel exchange of A-gauge bosons. We have explicitly shown the indices $(\lambda\mu\nu)$ over which we perform permutations. In the absence of axial-vector interactions the gauge independence of diagrams of these types is obtained just with the symmetrization of the A-lines, both in the massive and in the massless fermion (m_f=0) case. When, instead, we allow for a B exchange in diagrams of the same topology, the cases $m_f = 0$ and $m_f \neq 0$ involve a different (see Fig. 1.15) organization of the expansion. In the first case, the derivation of the gauge independence in this class of diagrams is obtained again just by a permutation of the attachments of the gauge boson lines. In the massive fermion case, instead, we need to add to this class of diagrams also the corresponding Goldstone exchanges together with their similar symmetrizations (Fig. 1.16). We illustrate in Figs. 1.17 and

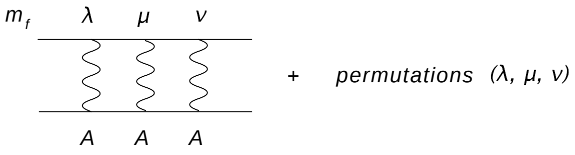

Figure 1.14: The massive fermion sector with massive vector exchanges in the t-channel.

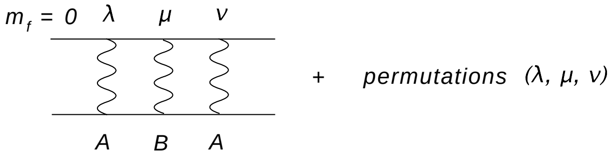

Figure 1.15: t-channel exchanges with vector and axial-vector interactions of massive gauge bosons. Being the fermion massless, permutation of the exchanges is sufficient to generate a gauge invariant result.

1.18 the organization of the expansion to lowest order for a process of the type $f\bar{f} \rightarrow AA$ which is the analogous of $q\bar{q} \rightarrow \gamma\gamma$ in this simple model. The presence of a Goldstone exchange takes place, obviously, only in the massive case. Finally, we have included the set of gauge-invariant diagrams describing the exchange of A and B gauge bosons in the t-channel and with an intermediate triangle anomaly diagram (BAA) (Figs. 1.19 and 1.20). In the massless fermion case gauge invariance is obtained simply by adding to the basic diagram all the similar ones obtained by permuting the attachments of the gauge lines (this involves both the lines at the top and at the bottom) and summing only over the topologically independent configurations. In the massive case one needs to add to this set of diagrams 2 additional sets: those containing a Goldstone exchange and those involving a WZ interaction. The contributions of these additional diagrams have to be symmetrized as well, by moving the attachments of the gauge boson/scalar lines.

1.10 The Effective Action in configuration space

Hidden inside the anomalous three-point functions are some Chern-Simons interactions. Their "extraction" can be done quite easily if we try to integrate out completely a given diagram and look at the structure of the effective action that is so generated directly in configuration space. The resulting action is non-local but contains a contact term that is present independently from the type of external Ward Identities that need to be imposed on the external vertices. This contact term is a dimension-4 contribution that is identified with a CS interaction, while the higher dimensional contributions have a non-trivial structure. The variation of both the local and the non-local effective vertex is still a local operator, proportional to $F \wedge F$. The coefficient in front of the local CS interaction changes, depending on the external conditions imposed on the diagram (the external Ward Identities). In this sense, different

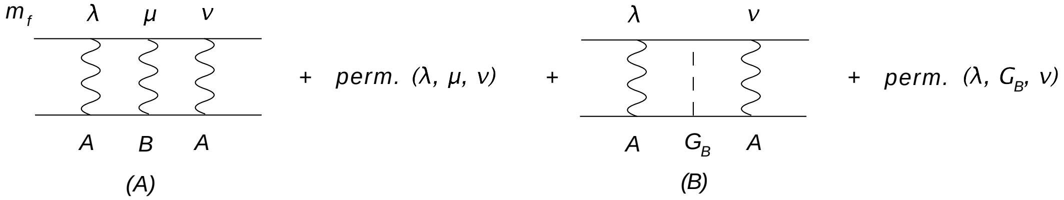

Figure 1.16: As in Fig. 1.15 but in the massive case and with a Goldstone.

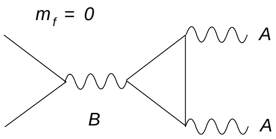

Figure 1.17: $f\overline{f}$ annihilation in the massless case.

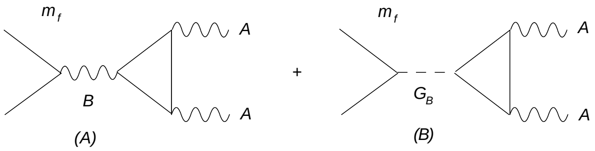

Figure 1.18: $f\overline{f}$ in the massive case.

vertices may carry different CS terms.

To illustrate this issue in a simple way, we proceed as follows. Consider the special case in which the two lines $\mu\nu$ are on-shell, so that $k_1^2 = k_2^2 = 0$. This simplifies our derivation, though a more general analysis can also be considered. We work in the specific parameterization in which the vertex satisfies the vector WI on the $\mu\nu$ lines, with the anomaly brought entirely on the λ line.

In this case we have

$$\begin{aligned} A_1(k_1,k_2) &= k_1\cdot k_2 A_3(k_1,k_2) \\ A_2(k_1,k_2) &= -A_1(k_2,k_1) \\ A_5(k_1,k_2) &= -A_4(k_2,k_1) \\ A_6(k_1,k_2) &= -A_3(k_2,k_1), \end{aligned} \tag{1.104}$$

and defining $s = 2k_1\cdot k_2 = k^2$, the explicit expressions of A_1 and A_2 are summarized in the form

$$A_1(k^2) = -i\frac{1}{4\pi^2} + iC_0(m_f^2, s) \tag{1.105}$$

with C_0 a given function of the ratio m_f^2/s that we redefine as $R(m_f^2/s)$. The typical expression of these functions can be found in the appendix. Here we assume that $s > 4m_f^2$, but other regions can be reached by suitable analytic continuations. The important point to be appreciated is the presence of a constant term in this invariant amplitude. Notice that the remaining amplitudes do not share this property. If we

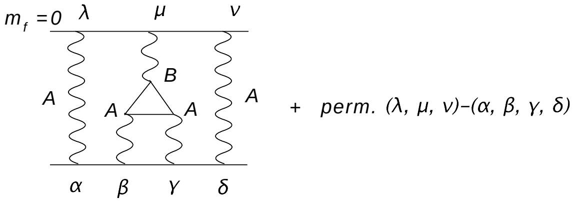

Figure 1.19: Anomaly in the t-channel.

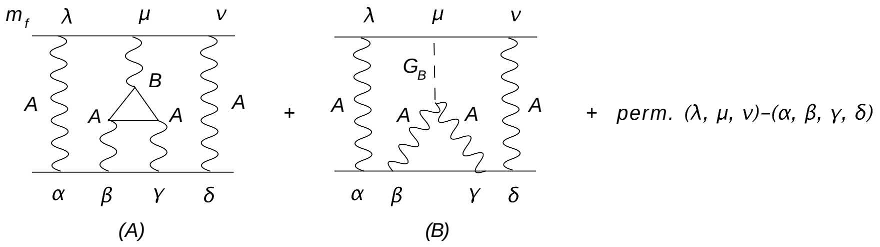

Figure 1.20: The WZ counterterm for the restauration of gauge invariance.

denote as T_c the vertex in configuration space, the contribution to the effective action becomes

$$\begin{aligned} &\langle T_c^{\lambda\mu\nu}(z,x,y)B_\lambda(z)A_\mu(x)A_\nu(y)\rangle \\ &= \frac{1}{4\pi^2}\langle\epsilon_{\mu\nu\rho\sigma}B^\lambda A^\mu F_A^{\rho\sigma}\rangle + \langle R\left(-m_f^2/\Box_z\right)\right)\left[\delta(x-z)\delta(y-z)\right]B^\lambda(z)A^\mu(x)A^\nu(y)\rangle \end{aligned} \tag{1.106}$$

where the $1/\Box_z$ operator acts only on the distributions inside the squared brackets ([ ]). It is not difficult to show that if we perform a gauge variation, say under B, of the vertex written in this form, then the first term trivially gives the $F_A \wedge F_A$ contribution, while the second (non-local) expression summarized in R, vanishes identically after an integration by parts. For this one needs to use the Bianchi identities of the A, B gauge bosons.

A similar computation on A_3, A_4 etc, can be carried out, but this time these contributions do not have a contact interaction as A_1 and A_2, but they are, exactly as the $R()$ term, purely non-local. Their gauge variations are also vanishing. When we impose a parameterization of the triangle diagram that redistributes the anomaly in such a way that some axial interactions are conserved or, for that reason, any other distribution of the partial anomalies on the single vertices, than we are actually introducing into the theory some specific CS interactions. We should think of these vertices as new effective vertices, fixed by the Ward Identities imposed on them. Their form is dictated by the conditions of gauge invariance. These conditions may appear with an axion term if the corresponding gauge boson, such as B in this case, is anomalous. Instead, if the gauge boson is not paired to a shifting axion, such as for Y, then gauge invariance under Y is restaured by suitable CS terms. The discussion of the phenomenological relevance of these vertices will be addressed in the next chapters.

1.11 Conclusions

We have analyzed in some detail unitarity issues that emerge in the context of anomalous Abelian models when the anomaly cancellation mechanism involves a WZ term, CS interactions and traceless conditions on some of the generators. We have investigated the features of these types of theories both in their exact and in their broken phases, and we have used s-channel unitarity as a simple strategy to achieve this. We have illustrated in a simple model (the "A-B Model") how the axion b is decomposed into a physical field χ and a Goldstone mode G_B (see Eq. (1.41)), and how the cancellation of the gauge dependences in the S-matrix involves either b or G_B, in the Stückelberg or the Higgs-Stückelberg phase respectively. In the Stückelberg phase the axion is a Goldstone mode. The physical component of the field, χ, appears after spontaneous symmetry breaking, and becomes massive via a combination of both the Stückelberg and the Higgs mechanism. Its mass can be driven to be light if the Peccei-Quinn breaking contributions in the scalar potential (see Eq. (1.49)) appear with small parameters $(b_1, \lambda_1, \lambda_2)$ compared to the Higgs v.e.v.

(see Eq. (1.54)). Then we have performed a unitarity analysis of this model first in the Stückelberg phase and then in the Higgs-Stückelberg phase, summarized in the set of diagrams collected in Figs. 1.6 and 1.7. A similar analysis has been presented for self-energy like diagrams, and is summarized in Figs. 1.8 and 1.9 respectively. In the broken phase, the most demanding pattern of cancellation is the one involving several anomalous interactions (BBB), and the analysis is summarized in Fig. 1.12. We have also shown that in the simple models discussed in this chapter, Chern-Simons interactions can be absorbed into the triangle diagrams by a re-definition of the momentum parameterization, if one rewrites a given amplitude in the basis of the interaction eigenstates. Isolation of the Chern-Simons terms may however help in the computation of trilinear gauge interactions in realistic extensions of the SM and can be kept separate from the fermionic triangles. Their presence is the indication that the theory requires external Ward Identities to be correctly defined at one-loop. Our results will be generalized in the following chapter and applied to the analysis of effective string models derived from the orientifold construction in the following chapters.

1.12 Appendix. The triangle diagrams and their ambiguities

We have collected in this and in the following appendices some of the more technical material which is summarized in the main sections. We present also a rather general analysis of the main features of anomalous diagrams, some of which are not available in the similar literature on the Standard Model, for instance due to the different pattern of cancellations of the anomalies required in our case study.

The consistency of these models, in fact, requires specific realizations of the vector WI for gauge trasformations involving the vector currents, which implies a specific parameterization of the fermionic triangle diagrams. While the analysis of these triangles is well known in the massless fermion case, for massive fermions it is slightly more involved. We have gathered here some results concerning these diagrams.

The typical **AVV** diagram with two vectors and one axial-vector current (see Fig. 1.1) is described here using a specific parameterization of the loop momenta given by

$$\Delta^{\lambda\mu\nu}_{\mathbf{AVV}} = \Delta^{\lambda\mu\nu} = i^3 \int \frac{d^4q}{(2\pi)^4} \frac{Tr\left[\gamma^\mu(\not{q}+m)\gamma^\lambda\gamma^5(\not{q}-\not{k}+m)\gamma^\nu(\not{q}-\not{k}_1+m)\right]}{(q^2-m^2)[(q-k_1)^2-m^2][(q-k)^2-m^2]} + \text{exch.} \tag{1.107}$$

Similarly, for the **AAA** diagram we will use the parameterization

$$\Delta^{\lambda\mu\nu}_{\mathbf{AAA}} = \Delta^{\lambda\mu\nu}_3 = i^3 \int \frac{d^4q}{(2\pi)^4} \frac{Tr\left[\gamma^\mu\gamma^5(\not{q}+m)\gamma^\lambda\gamma^5(\not{q}-\not{k}+m)\gamma^\nu\gamma^5(\not{q}-\not{k}_1+m)\right]}{(q^2-m^2)[(q-k_1)^2-m^2][(q-k)^2-m^2]} + \text{exch.} \tag{1.108}$$

In both cases we have included both the direct and the exchanged contributions [2].

In our notation $\overline{\Delta}^{\lambda\mu\nu}$ denotes a single diagram while we will use the symbol Δ to denote the Bose symmetric expression

$$\Delta^{\lambda\mu\nu} = \overline{\Delta}^{\lambda\mu\nu}(k_1,k_2) + \text{exchange of } \{(k_1,\mu),(k_2,\nu)\}. \tag{1.109}$$

To be noticed that the exchanged diagram is equally described by a diagram equal to the first diagram but with a reversed fermion flow. Reversing the fermion flow is sufficient to guarantee Bose symmetry of the two **V** lines. Similarly, for an **AAA** diagram, the exchange of any two **A** lines is sufficient to render the entire diagram completely symmetric under cyclic permutations of the three **AAA** lines.

Let's now consider the **AVV** contribution and work out some preliminaries. It is a simple exercise to show that the parameterization that we have used above indeed violates the vector WI on the $\mu\nu$ vector lines giving

$$\begin{aligned}
k_{1\mu}\Delta^{\lambda\mu\nu}(k_1,k_2) &= a_1\epsilon^{\lambda\nu\alpha\beta}k_1^\alpha k_2^\beta \\
k_{2\nu}\Delta^{\lambda\mu\nu}(k_1,k_2) &= a_2\epsilon^{\lambda\mu\alpha\beta}k_2^\alpha k_1^\beta \\
k_{\lambda}\Delta^{\lambda\mu\nu}(k_1,k_2) &= a_3\epsilon^{\mu\nu\alpha\beta}k_1^\alpha k_2^\beta,
\end{aligned} \tag{1.110}$$

where

$$a_1 = -\frac{i}{8\pi^2} \qquad a_2 = -\frac{i}{8\pi^2} \qquad a_3 = -\frac{i}{4\pi^2}. \tag{1.111}$$

Notice that $a_1 = a_2$, as expected from the Bose symmetry of the two **V** lines. It is also well known that the total anomaly $a_1 + a_2 + a_3 \equiv a_n$ is regularization scheme independent ($a_n = -\frac{i}{2\pi^2}$). We do not impose any WI on the **V** lines, conditions which would bring the anomaly only to the axial vertex, as done for the SM case, but we will determine consistently the value of the three anomalies at a later stage from the requirement of gauge invariance of the effective action, with the inclusion of the axion terms. To render our discussion self-contained, and define our notations, we briefly review the issue of the shift dependence of these diagrams.

---

[2] Our conventions differ from [41] by an overall (-1) since our currents are defined as $j^B_\mu = -q_B g_B \overline{\psi}\gamma_\mu\psi$

We recall that a shift of the momentum in the integrand ($p \rightarrow p + a$) where a is the most general momentum written in terms of the two independent external momenta of the triangle diagram ($a = \alpha(k_1 + k_2) + \beta(k_1 - k_2)$) induces on Δ changes that appear only through a dependence on one of the two parameters characterizing a, that is

$$\Delta^{\lambda\mu\nu}(\beta, k_1, k_2) = \Delta^{\lambda\mu\nu}(k_1, k_2) - \frac{i}{4\pi^2}\beta\epsilon^{\lambda\mu\nu\sigma}\left(k_{1\sigma} - k_{2\sigma}\right). \tag{1.112}$$

We have introduced the notation $\Delta^{\lambda\mu\nu}(\beta, k_1, k_2)$ to denote the shifted three-point function, while $\Delta^{\lambda\mu\nu}(k_1, k_2)$ denotes the original one, with a vanishing shift. In our parameterization, the choice $\beta = -\frac{1}{2}$ corresponds to conservation of the vector current and brings the anomaly to the axial vertex

$$\begin{aligned} k_{1\mu}\Delta^{\lambda\mu\nu}(a, k_1, k_2) &= 0, \\ k_{2\nu}\Delta^{\lambda\mu\nu}(a, k_1, k_2) &= 0, \\ k_{\lambda}\Delta^{\lambda\mu\nu}(a, k_1, k_2) &= -\frac{i}{2\pi^2}\epsilon^{\mu\nu\alpha\beta}k_1^{\alpha}k_2^{\beta} \end{aligned} \tag{1.113}$$

with $a_n = a_1 + a_2 + a_3 = -\frac{i}{2\pi^2}$ still equal to the total anomaly. Therefore, starting from generic values of $(a_1 = a_2, a_3)$, for instance from the values deduced from the basic parameterization (1.111), an additional shift with parameter β' gives

$$\Delta^{\lambda\mu\nu}(\beta', k_1, k_2) = \Delta^{\lambda\mu\nu}(\beta, k_1, k_2) - \frac{i\beta'}{4\pi^2}\epsilon^{\lambda\mu\nu\sigma}(k_1 - k_2)_{\sigma} \tag{1.114}$$

and will change the Ward Identities into the form

$$\begin{aligned} k_{1\mu}\Delta^{\lambda\mu\nu}(\beta', k_1, k_2) &= (a_1 - \frac{i\beta'}{4\pi^2})\epsilon^{\lambda\nu\alpha\beta}k_1^{\alpha}k_2^{\beta}, \\ k_{2\nu}\Delta^{\lambda\mu\nu}(\beta', k_1, k_2) &= (a_2 - \frac{i\beta'}{4\pi^2})\epsilon^{\lambda\mu\alpha\beta}k_2^{\alpha}k_1^{\beta}, \\ k_{\lambda}\Delta^{\lambda\mu\nu}(\beta', k_1, k_2) &= (a_3 + \frac{i\beta'}{2\pi^2})\epsilon^{\mu\nu\alpha\beta}k_1^{\alpha}k_2^{\beta}, \end{aligned} \tag{1.115}$$

where $a_2 = a_1$. There is an intrinsic ambiguity in the definition of the amplitude, which can be removed by imposing CVC on the vector vertices, as done, for instance, in Rosenberg's original paper [42] and discussed later. We remark once more that, in our case, this condition is not automatically required. The distribution of the anomaly may, in general, be different and we are defining, in this way, new effective parameterizations of the three-point anomalous vertices.

It is therefore convenient to introduce a notation that makes explicit this dependence and for this reason we define

$$a_1(\beta) = a_2(\beta) = -\frac{i}{8\pi^2} - \frac{i}{4\pi^2}\beta, \qquad a_3(\beta) = -\frac{i}{4\pi^2} + \frac{i}{2\pi^2}\beta, \tag{1.116}$$

with

$$a_1(\beta) + a_2(\beta) + a_3(\beta) = a_n = -\frac{i}{2\pi^2}. \tag{1.117}$$

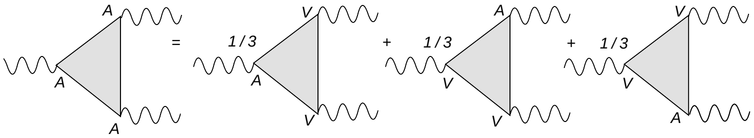

Figure 1.21: Distribution of the axial anomaly for the **AAA** diagram.

Notice that the additional β-dependent contribution amounts to a Chern-Simons interaction. Clearly, this contribution can be moved around at will and is related to the presence of two divergent terms in the general triangle diagram that need to be fixed appropriately using the underlying Bose symmetries of the three-point functions. The regularization of the **AAA** vertex, instead, has to respect the complete Bose symmetry of the diagram and this can be achieved with the symmetric expression

$$\Delta_3^{\lambda\mu\nu}(k_1,k_2)=\frac{1}{3}[\Delta^{\lambda\mu\nu}(k_1,k_2)+\Delta^{\mu\nu\lambda}(k_2,-k)+\Delta^{\nu\lambda\mu}(-k,k_1)]. \tag{1.118}$$

It is an easy exercise to show that this symmetric choice is independent from the momentum shift

$$\Delta_3^{\lambda\mu\nu}(\beta,k_1,k_2)=\Delta_3^{\lambda\mu\nu}(k_1,k_2) \tag{1.119}$$

and that the anomaly is equally distributed among the 3 vertices, $a_1=a_2=a_3=a_n/3$, as shown in Fig. 1.21. We conclude this section with some comments regarding the kind of invariant amplitudes appearing in the definition of Δ which help to clarify the role of the CS terms in the parameterization of these diagrams in momentum space. For $\overline{\Delta}^{(\mathbf{AVV})}_{\lambda\mu\nu}$, expressed using Rosenberg's parametrization, one obtains

$$\begin{aligned}\overline{\Delta}_{\lambda\mu\nu} \quad = \quad & \hat{a}_1\epsilon[k_1,\mu,\nu,\lambda]+\hat{a}_2\epsilon[k_2,\mu,\nu,\lambda]+\hat{a}_3\epsilon[k_1,k_2,\mu,\lambda]{k_1}^{\nu} \\ & +\hat{a}_4\epsilon[k_1,k_2,\mu,\lambda]k_2^{\nu}+\hat{a}_5\epsilon[k_1,k_2,\nu,\lambda]k_1^{\mu}+\hat{a}_6\epsilon[k_1,k_2,\nu,\lambda]k_2^{\mu},\end{aligned} \tag{1.120}$$

originally given in [42], with λ being the axial-vector vertex. By power-counting, two invariant amplitudes are divergent, a_1 and a_2, while the a_i with $i\geq 3$ are finite[3].

Instead, for the direct plus the exchanged diagrams we use the expression

$$\begin{aligned}\Delta_{\underline{\lambda}\mu\nu}+\Delta_{\underline{\lambda}\nu\mu} \quad = \quad & (\hat{a}_1-\hat{a}_2)\epsilon[k_1,\mu,\nu,\lambda]+(a_2-a_1)\epsilon[k_2,\mu,\nu,\lambda] \\ & +(\hat{a}_3-\hat{a}_6)\epsilon[k_1,k_2,\mu,\lambda]{k_1}^{\nu}+(\hat{a}_4-\hat{a}_5)\epsilon[k_1,k_2,\mu,\lambda]k_2^{\nu} \\ & +(\hat{a}_5-\hat{a}_4)\epsilon[k_1,k_2,\nu,\lambda]k_1^{\mu}+(\hat{a}_6-\hat{a}_3)\epsilon[k_1,k_2,\nu,\lambda]k_2^{\mu} \\ \quad = \quad & \underline{a}_1\epsilon[k_1,\mu,\nu,\lambda]+\underline{a}_2\epsilon[k_2,\mu,\nu,\lambda]+\underline{a}_3\epsilon[k_1,k_2,\mu,\lambda]{k_1}^{\nu} \\ & +\underline{a}_4\epsilon[k_1,k_2,\mu,\lambda]{k_2}^{\nu}+\underline{a}_5\epsilon[k_1,k_2,\nu,\lambda]k_1^{\mu}+\underline{a}_6\epsilon[k_1,k_2,\nu,\lambda]k_2^{\mu}\end{aligned} \tag{1.121}$$

where clearly $\underline{a}_2=-\underline{a}_1, \underline{a}_3=-\underline{a}_6$ and $\underline{a}_4=-\underline{a}_5$. The CS contributions are those proportional to the two terms linear in the external momenta. We recall that, in Rosenberg, these linear terms are re-expressed in terms of the remaining ones by imposing the vector Ward Identities on the **V**-lines. As already explained, we will instead assume, in our case, that the distribution of the anomaly among the 3 vertices of all the anomalous diagrams of the theory respects the requirement of Bose symmetry, with no additional constraint. A discussion of some technical points concerning the regularization of this and other diagrams both in 4 dimensions and in other schemes, such as Dimensional Regularization (DR) can be found below. For instance, one can find there the proof of the identical vanishing of $\Delta_{\mathbf{VVV}}$ worked out in both schemes. In this last case this result is obtained after removing the so called hat-momenta of the t'Hooft-Veltman scheme on the external lines. In this scheme this is possible since one can choose the external momenta to lay on a four-dimensional subspace (see [43, 44] for a discussion of these methods). We remark also that it is also quite useful to be able to switch from momentum space to configuration space with ease, and for this purpose we introduce the Fourier transforms of (1.19) and (1.20) in the anomaly equations, obtaining their expressions in configuration space

---

[3] We will be using the notation $\epsilon[a,b,\mu,\nu]\equiv\epsilon_{\alpha\beta\mu\nu}a^{\alpha}b^{\beta}$ to denote the structures in the expansion of the anomalous triangle diagrams.

$$\begin{aligned}
\frac{\partial}{\partial x^\mu} T^{\lambda\mu\nu}_{\mathbf{AVV}}(x,y,z) &= i a_1(\beta) \epsilon^{\lambda\nu\alpha\beta} \frac{\partial}{\partial x^\alpha} \frac{\partial}{\partial y^\beta} \left(\delta^4(x-z) \delta^4(y-z) \right), \\
\frac{\partial}{\partial y^\nu} T^{\lambda\mu\nu}_{\mathbf{AVV}}(x,y,z) &= i a_2(\beta) \epsilon^{\lambda\mu\alpha\beta} \frac{\partial}{\partial y^\alpha} \frac{\partial}{\partial x^\beta} \left(\delta^4(x-z) \delta^4(y-z) \right), \\
\frac{\partial}{\partial z^\lambda} T^{\lambda\mu\nu}_{\mathbf{AVV}}(x,y,z) &= i a_3(\beta) \epsilon^{\mu\nu\alpha\beta} \frac{\partial}{\partial x^\alpha} \frac{\partial}{\partial y^\beta} \left(\delta^4(x-z) \delta^4(y-z) \right),
\end{aligned} \tag{1.122}$$

with a_1, a_2 and a_3 as in (1.116), for the **AVV** case and

$$\begin{aligned}
\frac{\partial}{\partial x^\mu} T^{\lambda\mu\nu}_{\mathbf{AAA}}(x,y,z) &= i \frac{a_n}{3} \epsilon^{\lambda\nu\alpha\beta} \frac{\partial}{\partial x^\alpha} \frac{\partial}{\partial y^\beta} \left(\delta^4(x-z) \delta^4(y-z) \right), \\
\frac{\partial}{\partial y^\nu} T^{\lambda\mu\nu}_{\mathbf{AAA}}(x,y,z) &= i \frac{a_n}{3} \epsilon^{\lambda\mu\alpha\beta} \frac{\partial}{\partial y^\alpha} \frac{\partial}{\partial x^\beta} \left(\delta^4(x-z) \delta^4(y-z) \right), \\
\frac{\partial}{\partial z^\lambda} T^{\lambda\mu\nu}_{\mathbf{AAA}}(x,y,z) &= i \frac{a_n}{3} \epsilon^{\mu\nu\alpha\beta} \frac{\partial}{\partial x^\alpha} \frac{\partial}{\partial y^\beta} \left(\delta^4(x-z) \delta^4(y-z) \right),
\end{aligned} \tag{1.123}$$

for the **AAA** case. Notice that in this last case we have distributed the anomaly equally among the three vertices. These relations will be needed when we derive the anomalous variation of the effective action directly in configuration space.

1.13 Appendix. Chern-Simons cancellations

Having isolated the CS contributions, as shown in Fig. 1.6, the cancellation of the gauge dependence can be obtained combining all these terms so to obtain[4]

$$\begin{aligned}
S_\xi &= \Delta^{\lambda\mu\nu}(-k_1,-k_2) \left[\frac{-i}{k^2 - \xi_B M_1^2} \frac{k^\lambda k^{\lambda'}}{M_1^2} \right] \Delta^{\lambda'\mu'\nu'}(k_1,k_2) \\
&+ 4 \times \left(\frac{4}{M} C_{AA} \right)^2 \epsilon^{\mu\nu\rho\sigma} k_{1\rho} k_{2\sigma} \left[\frac{i}{k^2 - \xi_B M_1^2} \right] \epsilon^{\mu'\nu'\rho'\sigma'} k_{1\rho'} k_{2\sigma'} \\
&+ 4 \times \left(i d_1 \epsilon^{\mu\nu\lambda\sigma} (k_1 - k_2)_\sigma \right) \left[\frac{-i}{k^2 - \xi_B M_1^2} \frac{k^\lambda k^{\lambda'}}{M_1^2} \right] \left(-i d_1 \epsilon^{\mu'\nu'\lambda'\sigma'} (k_1 - k_2)_{\sigma'} \right) \\
&+ 2 \times \Delta^{\lambda\mu\nu}(-k_1,-k_2) \left[\frac{-i}{k^2 - \xi_B M_1^2} \frac{k^\lambda k^{\lambda'}}{M_1^2} \right] \left(-i d_1 \epsilon^{\mu'\nu'\lambda'\sigma'} (k_1 - k_2)_{\sigma'} \right) \\
&+ 2 \times \left(i d_1 \epsilon^{\mu\nu\lambda\sigma} (k_1 - k_2)_\sigma \right) \left[\frac{-i}{k^2 - \xi_B M_1^2} \frac{k^\lambda k^{\lambda'}}{M_1^2} \right] \Delta^{\lambda'\mu'\nu'}(k_1,k_2),
\end{aligned} \tag{1.124}$$

---

[4] The symmetry factor of each configuration is easily identified as the first factor in each separate contribution.

and using the relevant Ward Identities these simply to

$$\begin{aligned}
S_\xi &= (-a_3(\beta)\epsilon^{\mu\nu\rho\sigma}k_{1\rho}k_{2\sigma})\left[\frac{-i}{k^2-\xi_B M_1^2}\frac{1}{M_1^2}\right](a_3(\beta)\epsilon^{\mu'\nu'\rho'\sigma'}k_{1\rho'}k_{2\sigma'}) \\
&+ 4\times\frac{16}{M^2}\left[\left(-\frac{d_1}{2}+\frac{i}{2}a_3(\beta)\frac{1}{4}\right)^2\frac{M^2}{M_1^2}\right]\epsilon^{\mu\nu\rho\sigma}k_{1\rho}k_{2\sigma}\left[\frac{i}{k^2-\xi_B M_1^2}\right]\epsilon^{\mu'\nu'\rho'\sigma'}k_{1\rho'}k_{2\sigma'} \\
&+ 4\times d_1^2\left[\frac{-i}{k^2-\xi_B M_1^2}\frac{1}{M_1^2}\right]4\epsilon^{\mu\nu\rho\sigma}k_{1\rho}k_{2\sigma}\epsilon^{\mu'\nu'\rho'\sigma'}k_{1\rho'}k_{2\sigma'} \\
&+ 2\times(-a_3(\beta)\epsilon^{\mu\nu\rho\sigma}k_{1\rho}k_{2\sigma})\left[\frac{-i}{k^2-\xi_B M_1^2}\frac{1}{M_1^2}\right](+id_1 2\epsilon^{\mu'\nu'\lambda'\sigma'}k_1^{\lambda'}k_2^{\sigma'}) \\
&+ 2\times(-id_1 2\epsilon^{\mu\nu\lambda\sigma}k_1^{\lambda}k_2^{\sigma})\left[\frac{-i}{k^2-\xi_B M_1^2}\frac{1}{M_1^2}\right](a_3(\beta)\epsilon^{\mu'\nu'\rho'\sigma'}k_{1\rho'}k_{2\sigma'}) = 0. \qquad (1.125)
\end{aligned}$$

Having shown the cancellation of the gauge-dependent terms, the gauge independent contribution becomes

$$\begin{aligned}
S_0 &= \Delta^{\lambda\mu\nu}(-k_1,-k_2)\left[\frac{-i}{k^2-M_1^2}\left(g^{\lambda\lambda'}-\frac{k^\lambda k^{\lambda'}}{M_1^2}\right)\right]\Delta^{\lambda'\mu'\nu'}(k_1,k_2) \\
&+ 4\times(id_1\epsilon^{\mu\nu\lambda\sigma}(k_1-k_2)_\sigma)\left[\frac{-i}{k^2-M_1^2}\left(g^{\lambda\lambda'}-\frac{k^\lambda k^{\lambda'}}{M_1^2}\right)\right](-id_1\epsilon^{\mu'\nu'\lambda'\sigma'}(k_1-k_2)_{\sigma'}) \\
&+ 2\times\Delta^{\lambda\mu\nu}(-k_1,-k_2)\left[\frac{-i}{k^2-M_1^2}\left(g^{\lambda\lambda'}-\frac{k^\lambda k^{\lambda'}}{M_1^2}\right)\right](-id_1\epsilon^{\mu'\nu'\lambda'\sigma'}(k_1-k_2)_{\sigma'}) \\
&+ 2\times(id_1\epsilon^{\mu\nu\lambda\sigma}(k_1-k_2)_\sigma)\left[\frac{-i}{k^2-M_1^2}\left(g^{\lambda\lambda'}-\frac{k^\lambda k^{\lambda'}}{M_1^2}\right)\right]\Delta^{\lambda'\mu'\nu'}(k_1,k_2). \qquad (1.126)
\end{aligned}$$

At this point we need to express the triangle diagrams in terms of their shifting parameter β using the shift-relations

$$\Delta^{\lambda\mu\nu}(\beta,k_1,k_2) = \Delta^{\lambda\mu\nu}(k_1,k_2) - \frac{i}{4\pi^2}\beta\epsilon^{\lambda\mu\nu\sigma}(k_1-k_2)_\sigma, \qquad (1.127)$$

$$\Delta^{\lambda\mu\nu}(\beta,-k_1,-k_2) = \Delta^{\lambda\mu\nu}(-k_1,-k_2) + \frac{i}{4\pi^2}\beta\epsilon^{\lambda\mu\nu\sigma}(k_1-k_2)_\sigma, \qquad (1.128)$$

and with the substitution $d_1 = -ia_1(\beta)/2$ we obtain

$$\begin{aligned}
S_0 &= \left(\Delta^{\lambda\mu\nu}(-k_1,-k_2)+\frac{i}{4\pi^2}\beta\epsilon^{\lambda\mu\nu\sigma}(k_1-k_2)_\sigma\right)P_0^{\lambda\lambda'}\left(\Delta^{\lambda'\mu'\nu'}(k_1,k_2)-\frac{i}{4\pi^2}\beta\epsilon^{\lambda'\mu'\nu'\sigma'}(k_1-k_2)_{\sigma'}\right) \\
&+ 4\times\left(\frac{1}{2}a_1(\beta)\epsilon^{\mu\nu\lambda\sigma}(k_1-k_2)_\sigma\right)P_0^{\lambda\lambda'}\left(-\frac{1}{2}a_1(\beta)\epsilon^{\mu'\nu'\lambda'\sigma'}(k_1-k_2)_{\sigma'}\right) \\
&+ 2\times\left(\Delta^{\lambda\mu\nu}(-k_1,-k_2)+\frac{i}{4\pi^2}\beta\epsilon^{\lambda\mu\nu\sigma}(k_1-k_2)_\sigma\right)P_0^{\lambda\lambda'}\left(-\frac{1}{2}a_1(\beta)\epsilon^{\mu'\nu'\lambda'\sigma'}(k_1-k_2)_{\sigma'}\right) \\
&+ 2\times\left(\frac{1}{2}a_1(\beta)\epsilon^{\mu\nu\lambda\sigma}(k_1-k_2)_\sigma\right)P_0^{\lambda\lambda'}\left(\Delta^{\lambda'\mu'\nu'}(k_1,k_2)-\frac{i}{4\pi^2}\beta\epsilon^{\lambda'\mu'\nu'\sigma'}(k_1-k_2)_{\sigma'}\right). \qquad (1.129)
\end{aligned}$$

Introducing the explicit expression for $a_1(\beta)$, it is an easy exercise to show the equivalence between S_0 and diagram (A) of Fig. 1.6, with a choice of the shifting parameter that corresponds to the CVC condition ($\beta = -1/2$)

$$S_0 \equiv \left(\Delta^{\lambda\mu\nu}(-k_1,-k_2)-\frac{i}{8\pi^2}\epsilon^{\lambda\mu\nu\sigma}(k_1-k_2)_\sigma\right)P_0^{\lambda\lambda'}\left(\Delta^{\lambda'\mu'\nu'}(k_1,k_2)+\frac{i}{8\pi^2}\beta\epsilon^{\lambda'\mu'\nu'\sigma'}(k_1-k_2)_{\sigma'}\right).$$

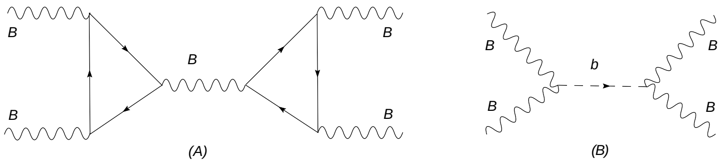

Figure 1.22: Relevant diagrams for the unitarity check before symmetry breaking.

(1.130)

1.13.1 Cancellation of gauge dependences in the broken Higgs phase

In this case we have (see Fig. 1.7)

$$\begin{aligned}
S_\xi &= A_\xi + B_\xi + C_\xi + D_\xi + E_\xi + F_\xi + G_\xi + H_\xi \\
&= \Delta^{\lambda\mu\nu}(-k_1,-k_2)\left[\frac{-i}{k^2-\xi_B M_B^2}\frac{k^\lambda k^{\lambda'}}{M_B^2}\right]\Delta^{\lambda'\mu'\nu'}(k_1,k_2) \\
&+ 4\times\left(\frac{4}{M}\alpha_2 C_{AA}\right)^2 \epsilon^{\mu\nu\rho\sigma}k_{1\rho}k_{2\sigma}\left[\frac{i}{k^2-\xi_B M_B^2}\right]\epsilon^{\mu'\nu'\rho'\sigma'}k_{1\rho'}k_{2\sigma'} \\
&+ 4\times\left(id_1\epsilon^{\mu\nu\lambda\sigma}(k_1-k_2)_\sigma\right)\left[\frac{-i}{k^2-\xi_B M_B^2}\frac{k^\lambda k^{\lambda'}}{M_B^2}\right]\left(-id_1\epsilon^{\mu'\nu'\lambda'\sigma'}(k_1-k_2)_{\sigma'}\right) \\
&+ 2\times\Delta^{\lambda\mu\nu}(-k_1,-k_2)\left[\frac{-i}{k^2-\xi_B M_B^2}\frac{k^\lambda k^{\lambda'}}{M_B^2}\right]\left(-id_1\epsilon^{\mu'\nu'\lambda'\sigma'}(k_1-k_2)_{\sigma'}\right) \\
&+ 2\times\left(id_1\epsilon^{\mu\nu\lambda\sigma}(k_1-k_2)_\sigma\right)\left[\frac{-i}{k^2-\xi_B M_B^2}\frac{k^\lambda k^{\lambda'}}{M_B^2}\right]\Delta^{\lambda'\mu'\nu'}(k_1,k_2) \\
&+ 2\times\Delta^{\mu\nu}(-k_1,-k_2)\left(2i\frac{m_f}{M_B}\right)\left[\frac{i}{k^2-\xi_B M_B^2}\right]\left(\frac{4}{M}\alpha_2 C_{AA}\epsilon^{\mu'\nu'\rho'\sigma'}k_{1\rho'}k_{2\sigma'}\right) \\
&+ \Delta^{\mu\nu}(-k_1,-k_2)\left(2i\frac{m_f}{M_B}\right)\left[\frac{i}{k^2-\xi_B M_B^2}\right]\left(2i\frac{m_f}{M_B}\right)\Delta^{\mu'\nu'}(k_1,k_2) \\
&+ 2\times\left(\frac{4}{M}\alpha_2 C_{AA}\epsilon^{\mu\nu\rho\sigma}k_{1\rho}k_{2\sigma}\right)\left[\frac{i}{k^2-\xi_B M_B^2}\right]\left(2i\frac{m_f}{M_B}\right)\Delta^{\mu\nu}(k_1,k_2).
\end{aligned} \tag{1.131}$$

The vanishing of this expression can be checked as in the previous case, using the massive version of the anomalous Ward Identities in the triangular graphs involving Δ.

1.13.2 Cancellations in the A-B Model: $BB \to BB$ mediated by a B gauge boson

Let's now discuss the exchange of a B gauge boson in the s-channel before spontaneous symmetry breaking. The relevant diagrams are shown in Fig. 1.22. We remark, obviously, that each diagram has to be inserted with the correct multiplicity factor in order to obtain the cancellation of the unphysical poles. In this case, from Bose-symmetry, the anomaly is equally distributed among the 3 vertices, $a_1 = a_2 = a_3 = a_n/3$, as we have discussed above. We recall that from the variations $\delta_B\mathcal{L}_{an}$ and $\delta_B\mathcal{L}_b$ the relevant terms are

$$\frac{1}{3!}\delta_B\langle T^{\lambda\mu\nu}_{BBB}B^\lambda(z)B^\mu(x)B^\nu(y)\rangle = \frac{ig_B^3}{3!}\,a_n\langle\theta_B\,\frac{F^B\wedge F^B}{4}\rangle$$

$$\delta_B \langle \frac{C_{BB}}{M} b F^B \wedge F^B \rangle \quad = \quad -C_{BB} \frac{M_1}{M} \langle \theta_B F^B \wedge F^B \rangle \quad \text{from} \quad \delta_B b = -M_1 \theta_B, \tag{1.132}$$

so that from the condition of anomaly cancellation we obtain

$$-C_{BB} \frac{M_1}{M} + \frac{i g_B^3}{3!} \frac{1}{4} a_n = 0 \iff C_{BB} = \frac{i g_B^3}{3!} \frac{1}{4} a_n \frac{M}{M_1}, \tag{1.133}$$

which fixes the appropriate value of the coefficient of the WZ term. One can easily show the correspondence between a Green-Schwarz term $\frac{C_{BB}}{M} b\, F^B \wedge F^B$ and a vertex $4 \frac{C_{BB}}{M} \epsilon^{\mu\nu\rho\sigma} k_1^\rho k_2^\sigma$ in momentum representation, as will be shown in App. 1.16. Taking into account only the gauge-dependent parts of the two diagrams, we have that the diagram with the exchange of the gauge boson B can be written as

$$\mathcal{A}_\xi = \Delta^{\lambda\,\mu\,\nu}(-k_1, -k_2) \left[\frac{-i}{k^2 - \xi_B M_1^2} \left(\frac{k^\lambda\, k^{\lambda'}}{M_1^2} \right) \right] \Delta^{\lambda'\,\mu'\,\nu'}(k_1, k_2) \tag{1.134}$$

and the diagram with the exchange of the axion b is

$$\mathcal{B}_\xi = 4 \times \left(\frac{4}{M} C_{BB} \right)^2 \epsilon^{\mu\nu\rho\sigma} k_1^\rho k_2^\sigma \left(\frac{i}{k^2 - \xi_B M_1^2} \right) \epsilon^{\mu'\nu'\rho'\sigma'} k_1^{\rho'} k_2^{\sigma'}. \tag{1.135}$$

Using the anomaly equations for the AAA vertex we can evaluate the first diagram

$$\begin{aligned} \mathcal{A}_\xi &= \frac{-i}{k^2 - \xi_B M_1^2} \frac{1}{M_1^2} \left(k^\lambda \Delta^{\lambda\mu\nu} \right) \left(k^{\lambda'} \Delta^{\lambda'\mu'\nu'} \right) \\ &= \frac{-i}{k^2 - \xi_B M_1^2} \frac{1}{M_1^2} \left(-(g_B)^3 \frac{a_n}{3} \epsilon^{\mu\nu\alpha\beta} k_1^\alpha k_2^\beta \right) \left((g_B)^3 \frac{a_n}{3} \epsilon^{\mu'\nu'\alpha'\beta'} k_1^{\alpha'} k_2^{\beta'} \right) \\ &= \frac{i}{k^2 - \xi_B M_1^2} \frac{1}{M_1^2} \left(\frac{a_n}{3} g_B^3 \right)^2 \epsilon^{\mu\nu\alpha\beta}\, \epsilon^{\mu'\nu'\alpha'\beta'}\, k_1^\alpha k_2^\beta\, k_1^{\alpha'} k_2^{\beta'}, \end{aligned} \tag{1.136}$$

while the axion exchange diagram gives

$$\begin{aligned} \mathcal{B}_\xi &= 4 \times \left(\frac{4 C_{BB}}{M} \right)^2 \left(\frac{i}{k^2 - \xi_B M_1^2} \right) \epsilon^{\mu\nu\alpha\beta}\, \epsilon^{\mu'\nu'\alpha'\beta'}\, k_1^\alpha k_2^\beta\, k_1^{\alpha'} k_2^{\beta'} \\ &= \frac{64\, C_{BB}^2}{M^2} \frac{i}{k^2 - \xi_B M_1^2} \epsilon^{\mu\nu\alpha\beta}\, \epsilon^{\mu'\nu'\alpha'\beta'}\, k_1^\alpha k_2^\beta\, k_1^{\alpha'} k_2^{\beta'}. \end{aligned} \tag{1.137}$$

Adding the contributions from the two diagrams we obtain

$$\mathcal{A}_\xi + \mathcal{B}_\xi = 0 \iff \frac{1}{M_1^2} \left(\frac{a_n}{3} g_B^3 \right)^2 + \frac{64\, C_{BB}^2}{M^2} = 0, \tag{1.138}$$

in fact substituting the proper value for the coefficient C_{BB} we obtain an identity

$$\frac{1}{M_1^2} \frac{a_n^2}{9} g_B^6 + \frac{64}{M^2} \left[\frac{i g_B^3}{3!} \frac{1}{4} a_n \frac{M}{M_1} \right]^2 = \frac{1}{M_1^2} \frac{a_n^2}{9} g_B^6 - \frac{64}{M_1^2} \frac{1}{64} \frac{a_n^2}{9} g_B^6 = 0. \tag{1.139}$$

This pattern of cancellations holds for a massless fermion ($m_f = 0$).

1.13.3 Gauge cancellations in the self-energy diagrams

In this case, following Fig. 1.9, we isolate the following gauge-dependent amplitudes

$$\begin{aligned}
\mathcal{A}_{\xi 0} &= \Delta^{\lambda\mu\nu}(-k_1,-k_2)\left[\frac{-i}{k^2-\xi_B M_B^2}\left(\frac{k^{\lambda}k^{\lambda'}}{M_B^2}\right)\right]\Delta^{\lambda'\mu'\nu'}(k_1,k_2)\,P_o^{\nu\nu'},\\
\mathcal{B}_{\xi 0} &= 4\times\left(\frac{4}{M}\alpha_2 C_{AA}\right)^2\epsilon^{\mu\nu\rho\sigma}k_{1\rho}k_{2\sigma}\frac{i}{k^2-\xi_B M_B^2}\epsilon^{\mu'\nu'\rho'\sigma'}k_{1\rho'}k_{2\sigma'}\,P_o^{\nu\nu'},\\
\mathcal{C}_{\xi 0} &= \Delta^{\mu\nu}(-k_1,-k_2)\left(2i\frac{m_f}{M_B}\right)\frac{i}{k^2-\xi_B M_B^2}\left(2i\frac{m_f}{M_B}\right)\Delta^{\mu'\nu'}(k_1,k_2)P_o^{\nu\nu'},\\
\mathcal{D}_{\xi 0} &= 2\times\left(\frac{4}{M}\alpha_2 C_{AA}\epsilon^{\mu\nu\rho\sigma}k_{1\rho}k_{2\sigma}\right)\frac{i}{k^2-\xi_B M_B^2}\left(2i\frac{m_f}{M_B}\right)\Delta^{\mu'\nu'}(k_1,k_2)P_o^{\nu\nu'},\\
\mathcal{E}_{\xi 0} &= 2\times\Delta^{\mu\nu}(-k_1,-k_2)\left(2i\frac{m_f}{M_B}\right)\frac{i}{k^2-\xi_B M_B^2}\left(\frac{4}{M}\alpha_2 C_{AA}\epsilon^{\mu'\nu'\rho'\sigma'}k_{1\rho'}k_{2\sigma'}\right)P_o^{\nu\nu'},
\end{aligned}\tag{1.140}$$

so that using the anomaly equations for the triangles

$$\begin{aligned}
k^{\lambda'}\Delta^{\lambda'\mu'\nu'}(k_1,k_2) &= a_3(\beta)\epsilon^{\mu'\nu'\rho'\sigma'}k_{1\rho'}k_{2\sigma'}+2m_f\Delta^{\mu'\nu'},\\
k^{\lambda}\Delta^{\lambda\mu\nu}(-k_1,-k_2) &= -a_3(\beta)\epsilon^{\mu\nu\rho\sigma}k_{1\rho}k_{2\sigma}-2m_f\Delta^{\mu\nu},
\end{aligned}$$

and substituting the appropriate value for the WZ coefficient, with the rotation coefficient of the axion b to the Goldstone boson given by $\alpha_2 = M_1/M_B$, one obtains quite straightforwardly that the condition of gauge independence is satisfied

$$\mathcal{A}_{\xi 0}+\mathcal{B}_{\xi 0}+\mathcal{C}_{\xi 0}+\mathcal{D}_{\xi 0}+\mathcal{E}_{\xi 0}=0. \tag{1.141}$$

1.14 Appendix. Ward Identities on the tetragon

As we have seen in the previous sections, the shift dependence from the anomaly on each vertex, parameterized by β, β_1, β_2, drops in the actual computation of the unitarity conditions on the s-channel amplitudes, which clearly signals the irrelevance of these shifts in the actual computation, as far as the Bose symmetry of the corresponding amplitudes that assign the anomaly on each vertex consistently, are respected. It is well known that all the contribution of the anomaly in correlators with more external legs is taken care of by the correct anomaly cancellation in three-point function. It is instructive to illustrate, for generic shifts, chosen so to respect the symmetries of the higher point functions, how a similar patterns holds. This takes place since anomalous Ward Identities for higher-order correlators are expressed in terms of standard triangle anomalies. This analysis and a similar analysis of other diagrams of this type, which we have included in an appendix, is useful for the investigation of some rare Z decays (such as $Z \to \gamma\gamma\gamma$) which takes place with an on-shell Z boson.

Then let's consider the tetragon diagram BAAA shown in Fig. 1.23, where B, being characterized by an axial-vector coupling, generates an anomaly in the related WI. We have the fermionic trace

$$\Delta^{\lambda\mu\nu\rho}(k_1,k_2,k_3)=\overline{\Delta}^{\lambda\mu\nu\rho}(k_1,k_2,k_3)+\text{perm.} \tag{1.142}$$

where perm. means permutations of $\{(k_1,\mu),(k_2,\nu),(k_3,\rho)\}$. One contribution to the axial WI comes

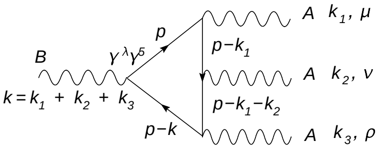

Figure 1.23: The tetragon contribution.

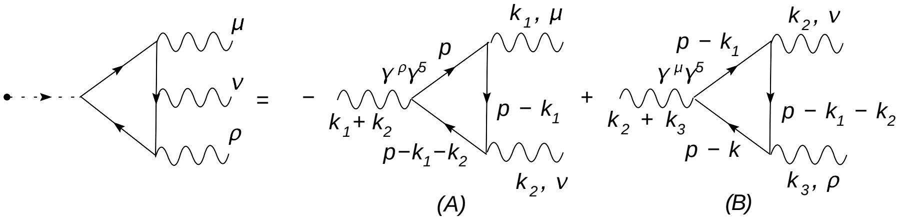

Figure 1.24: Momenta distribution for the external lines in a WI.

for instance from

$$\begin{aligned}
& k^\lambda Tr\left[\gamma^\lambda\gamma^5\frac{1}{\not p-\not k}\gamma^\rho\frac{1}{\not p-\not k_1-\not k_2}\gamma^\nu\frac{1}{\not p-\not k_1}\gamma^\mu\frac{1}{\not p}\right] \\
= & \ Tr\left[\not k\ \gamma^5\frac{1}{\not p-\not k}\gamma^\rho\frac{1}{\not p-\not k_1-\not k_2}\gamma^\nu\frac{1}{\not p-\not k_1}\gamma^\mu\frac{1}{\not p}\right] \\
= & -Tr\left[\gamma^5\frac{1}{\not p}\gamma^\rho\frac{1}{\not p-\not k_1-\not k_2}\gamma^\nu\frac{1}{\not p-\not k_1}\gamma^\mu\right] \\
& +Tr\left[\gamma^5\frac{1}{\not p-\not k}\gamma^\rho\frac{1}{\not p-\not k_1-\not k_2}\gamma^\nu\frac{1}{\not p-\not k_1}\gamma^\mu\right],
\end{aligned} \tag{1.143}$$

which has been rearranged in terms of triangle anomalies using

$$\frac{1}{\not p}\not k\ \gamma^5\frac{1}{\not p-\not k}=\gamma^5\frac{1}{\not p-\not k}-\gamma^5\frac{1}{\not p}. \tag{1.144}$$

Relation (1.143) is diagrammatically shown in Fig. 1.24. Explicitly these diagrammatic equations become

$$\begin{aligned}
k^\lambda\overline{\Delta}^{\lambda\mu\nu\rho} &= -\overline{\Delta}^{\rho\mu\nu}(k_1,k_2)+\overline{\Delta}^{\mu\nu\rho}(\beta_1,k_2,k_3), \\
k^\lambda\overline{\Delta}^{\lambda\mu\rho\nu} &= -\overline{\Delta}^{\nu\mu\rho}(k_1,k_3)+\overline{\Delta}^{\mu\rho\nu}(\beta_2,k_3,k_2), \\
k^\lambda\overline{\Delta}^{\lambda\nu\rho\mu} &= -\overline{\Delta}^{\mu\nu\rho}(k_2,k_3)+\overline{\Delta}^{\nu\rho\mu}(\beta_3,k_3,k_1), \\
k^\lambda\overline{\Delta}^{\lambda\nu\mu\rho} &= -\overline{\Delta}^{\rho\nu\mu}(k_2,k_1)+\overline{\Delta}^{\nu\mu\rho}(\beta_4,k_1,k_3), \\
k^\lambda\overline{\Delta}^{\lambda\rho\mu\nu} &= -\overline{\Delta}^{\nu\rho\mu}(k_3,k_1)+\overline{\Delta}^{\rho\mu\nu}(\beta_5,k_1,k_2), \\
k^\lambda\overline{\Delta}^{\lambda\rho\nu\mu} &= -\overline{\Delta}^{\mu\rho\nu}(k_3,k_2)+\overline{\Delta}^{\rho\nu\mu}(\beta_6,k_2,k_1),
\end{aligned} \tag{1.145}$$

where the usual (direct) triangle diagram is given for instance by

$$\overline{\Delta}^{\mu\nu\rho}=\int\frac{d^4p}{(2\pi)^4}Tr\left[\gamma^\mu\gamma^5\frac{1}{\not p-\not k}\gamma^\rho\frac{1}{\not p-\not k_1-\not k_2}\gamma^\nu\frac{1}{\not p-\not k_1}\right]. \tag{1.146}$$

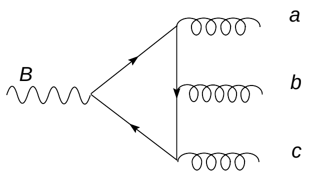

Figure 1.25: The tetragon diagram in the non-Abelian case.

Adding all the contributions we have

$$\begin{aligned} k^\lambda \Delta^{\lambda\mu\nu\rho}(k_1,k_2,k_3) &= [\Delta^{\rho\mu\nu}(\beta_5,\beta_6,k_1,k_2)+\Delta^{\nu\mu\rho}(\beta_3,\beta_4,k_1,k_3)+\Delta^{\mu\nu\rho}(\beta_1,\beta_2,k_2,k_3)] \\ &\quad -[\Delta^{\rho\mu\nu}(k_1,k_2)+\Delta^{\nu\mu\rho}(k_1,k_3)+\Delta^{\mu\nu\rho}(k_2,k_3)]\,. \end{aligned} \tag{1.147}$$

At this point, to show the validity of the WI independently of the chosen value of the CS shifts, we recall that under some shifts

$$\begin{aligned} \Delta^{\mu\nu\rho}(\beta_1,\beta_2,k_2,k_3) &= \Delta^{\mu\nu\rho}(k_2,k_3)-\frac{i(\beta_1+\beta_2)}{4\pi^2}\epsilon^{\mu\nu\rho\sigma}(k_2^\sigma-k_3^\sigma) \\ \Delta^{\nu\mu\rho}(\beta_3,\beta_4,k_2,k_3) &= \Delta^{\nu\mu\rho}(k_1,k_3)-\frac{i(\beta_3+\beta_4)}{4\pi^2}\epsilon^{\nu\mu\rho\sigma}(k_1^\sigma-k_3^\sigma) \\ \Delta^{\rho\mu\nu}(\beta_5,\beta_6,k_1,k_2) &= \Delta^{\rho\mu\nu}(k_1,k_2)-\frac{i(\beta_5+\beta_6)}{4\pi^2}\epsilon^{\rho\mu\nu\sigma}(k_1^\sigma-k_2^\sigma), \end{aligned} \tag{1.148}$$

and redefining the shifts by setting

$$\beta_5+\beta_6=\overline{\beta}_1 \qquad \beta_1+\beta_2=\overline{\beta}_3 \qquad \beta_3+\beta_4=\overline{\beta}_2 \tag{1.149}$$

we obtain

$$k^\lambda \Delta^{\lambda\mu\nu\rho}(k_1,k_2,k_3) = -\frac{i}{4\pi^2}\left[\overline{\beta}_1\epsilon^{\rho\mu\nu\sigma}(k_1^\sigma-k_2^\sigma)+\overline{\beta}_2\epsilon^{\nu\mu\rho\sigma}(k_1^\sigma-k_3^\sigma)+\overline{\beta}_3\epsilon^{\mu\nu\rho\sigma}(k_2^\sigma-k_3^\sigma)\right]. \tag{1.150}$$

Finally, using the Bose symmetry on the r.h.s. (indices μ,ν,ρ) of the original diagram we obtain

$$\overline{\beta}_1=\overline{\beta}_2=\overline{\beta}_3, \tag{1.151}$$

which is the correct WI: $k^\lambda\Delta^{\lambda\mu\nu\rho}=0$. We have shown that the correct choice of the CS shifts in tetragon diagrams, fixed by the requirements of Bose symmetries of the corresponding amplitude and of the underlying three-point functions, gives the correct Ward Identities for these correlators. This is not unexpected, since the anomaly appears only at the level of three-point functions, but shows how one can work in full generality with these amplitudes and determine their correct structure. It is also interesting to underline the modifications that take place once this study is extended to the non-Abelian case. In this case (shown in Fig. 1.25) one obtains the same result already shown for the axial Abelian WI, but modified by color factors. We obtain

$$\begin{aligned} & Tr(\{T^a,T^b\}T^c)\,[-\Delta^{\rho\mu\nu}+\Delta^{\rho\mu\nu}(\beta)]+Tr(\{T^c,T^b\}T^a)\,[-\Delta^{\mu\nu\rho}+\Delta^{\mu\nu\rho}(\beta)] \\ & +Tr(\{T^a,T^c\}T^b)\,[-\Delta^{\nu\mu\rho}+\Delta^{\nu\mu\rho}(\beta)] \\ = \; & d^{abc}\,[-\Delta^{\rho\mu\nu}+\Delta^{\rho\mu\nu}(\beta)]+d^{cba}\,[-\Delta^{\mu\nu\rho}+\Delta^{\mu\nu\rho}(\beta)]+d^{acb}\,[-\Delta^{\nu\mu\rho}+\Delta^{\nu\mu\rho}(\beta)], \end{aligned} \tag{1.152}$$

where we have used the usual definition of the symmetric d-tensor

$$d^{abc} = Tr(\left\{T^a, T^b\right\} T^c). \tag{1.153}$$

Simple manipulations give a result which is proportional to the result of the Abelian case

$$d^{abc}([-\Delta^{\rho\mu\nu} + \Delta^{\rho\mu\nu}(\beta)] + [-\Delta^{\mu\nu\rho} + \Delta^{\mu\nu\rho}(\beta)] + [-\Delta^{\nu\mu\rho} + \Delta^{\nu\mu\rho}(\beta)]). \tag{1.154}$$

The vanishing of the shift-dependence is related to the Bose symmetry under exchange of the indices

$$\{(a, \mu, k_1), (b, \nu, k_2), (c, \rho, k_3)\}.$$

This result is clearly expected, since the gauge current of B is Abelian and behaves as a gauge-singlet current under the gauge interaction of A, the latter having been promoted to a non-Abelian current.

1.15 Appendix. DR-HVBM

In this appendix we give some of the details for the computation of the direct plus exchanged diagrams in Dimensional Regularization using the HVBM scheme for a partially anticommuting γ_5 [45, 46]. There are various results presented in the previous literature on the computation of these diagrams, most of them using a momentum shift without actually enforcing a regularization, shift that brings the anomaly contribution to the axial-vector vertex of the triangle diagram, keeping the vector Ward Identities satisfied, which takes to Rosenberg's parameterization (1.120). We fill this gap by showing how the regularization works using an arbitrary tensor structure $T^{\lambda\mu\nu}$ rather than scalar amplitudes. We also keep the mass of the fermion arbitrary, so to obtain a general result concerning the mass dependence of the corrections to the anomaly contributions. We remind that momentum shift are allowed in DR-HVBM, once the integration measure is extended from 4 to $n = 4 - \epsilon$ dimensions and the Feynman parametrization can be used to reduce the integrals into symmetric forms. Symmetric integration can then be used exactly as in the standard DR case, but with some attention on how to treat the Lorentz indices in the two subspaces of dimensions 4 and $n - 4$, introduced by the regularization. These points are illustrated below.

In the following we will use the notation I_{xy} to denote the parametric integration after performing the loop integral

$$I_{xy}\left[...\right] \equiv 2 \int_0^1 \int_0^{1-x} dy \left[...\right]. \tag{1.155}$$

There are various ways to implement γ_5 in D-dimensions, but the prescription that works best and is not so difficult to implement is the t'Hooft-Veltman-Breitenlohner-Maison (simply denoted as HVBM) prescription. In the HVBM prescription γ_5 is only partially anticommuting. The gamma algebra in this case is split into $n = 4 + (n - 4)$, and the indices of the matrices are split accordingly: $\mu = (\tilde{\mu}, \hat{\mu})$. There are now two subspaces, and the indices carrying a ˜ are the 4-dimensional ones. The 4-dimensional part of the algebra is the same as usual, but now

$$\left[\gamma^{\hat{\mu}}, \gamma_5\right]_+ = 0, \tag{1.156}$$

where the commutators have been replaced by anticommutators. It is important to clarify some points regarding the use of symmetric integration. We recall that in DR the use of symmetric integration gives

$$\int d^n q \frac{q^{\hat{\alpha}}, q^{\tilde{\alpha}}}{(q^2-\Delta)^L} = 0, \tag{1.157}$$

and

$$\begin{aligned} \int d^n q \frac{q^{\hat{\mu}} q^{\hat{\nu}}}{(q^2-\Delta)^L} &= g^{\hat{\mu}\hat{\nu}} \int d^n q \frac{q^2/n}{(q^2-\Delta)^L}, \\ \int d^n q \frac{q^{\tilde{\mu}} q^{\tilde{\nu}}}{(q^2-\Delta)^L} &= g^{\tilde{\mu}\tilde{\nu}} \int d^n q \frac{q^2/n}{(q^2-\Delta)^L}. \end{aligned} \tag{1.158}$$

Integrals involving mixed indices are set to vanish. We now summarize other properties of this regularization. We denote by

$$g_{\mu\nu}, \qquad \tilde{g}_{\mu\nu}, \qquad \hat{g}_{\mu\nu} \tag{1.159}$$

respectively the n -, 4 - and (n-4) -dimensional parts of the metric tensor. An equivalent notation is to set $\hat{g}_{\mu\nu} = g_{\hat{\mu}\hat{\nu}}$ and $\tilde{g}_{\mu\nu} = g_{\tilde{\mu}\tilde{\nu}}$, $\gamma^{\hat{\mu}} = \hat{\gamma}^{\mu}$, etc. The contraction rules are

$$g^{\mu}_{\mu} = n, \qquad g_{\mu\lambda} g^{\lambda}_{\nu} = g_{\mu\nu}, \qquad \hat{g}^{\mu}_{\mu} = n-4, \qquad \tilde{g}^{\mu}_{\mu} = 4, \qquad \tilde{g}_{\mu\lambda}\hat{g}^{\lambda\nu} = 0. \tag{1.160}$$

Other properties of this regularization follow quite easily. For instance, from

$$\tilde{\gamma}_{\mu} = \gamma^{\sigma}\tilde{g}_{\sigma\mu}, \qquad \hat{\gamma}^{\mu} = \gamma_{\lambda}\hat{g}^{\lambda\mu}, \tag{1.161}$$

using (1.160) it follows straightforwardly that

$$\begin{aligned} \tilde{\gamma}_{\mu}\gamma_{a_1}\gamma_{a_2}...\gamma_{a_D}\hat{\gamma}^{\mu} &= 0, \\ \gamma_{\mu}\gamma_{a_1}\gamma_{a_2}...\gamma_{a_D}\hat{\gamma}^{\mu} &= \hat{\gamma}_{\mu}\gamma_{a_1}\gamma_{a_2}...\gamma_{a_D}\hat{\gamma}^{\mu}. \end{aligned} \tag{1.162}$$

The definition of γ_5 involves an antisymmetrization over the basic gamma matrices

$$\gamma_5 \equiv \frac{i}{4!}\epsilon_{\mu\nu\rho\sigma}\gamma^{\mu}\gamma^{\nu}\gamma^{\rho}\gamma^{\sigma}. \tag{1.163}$$

The definition is equivalent to the standard one $\gamma_5 = i\gamma_0\gamma_1\gamma_2\gamma_3$. The ϵ-tensor is a 4-dimensional projector that selects only the˜indices of a contraction,

$$\epsilon_{\mu\nu\rho\sigma}\gamma^{\mu}\gamma^{\nu}\gamma^{\rho}\gamma^{\sigma} = \epsilon_{\tilde{\mu}\tilde{\nu}\tilde{\rho}\tilde{\sigma}}\gamma^{\tilde{\mu}}\gamma^{\tilde{\nu}}\gamma^{\tilde{\rho}}\gamma^{\tilde{\sigma}}. \tag{1.164}$$

It is then easy to show that with this definition

$$\{\gamma_5, \tilde{\gamma}^{\mu}\} = 0, \qquad [\gamma_5, \hat{\gamma}^{\mu}] = 0. \tag{1.165}$$

These two relations can be summarized in the statement

$$\{\gamma_5, \gamma_{\mu}\} = 2\hat{\gamma}_{\mu}\gamma_5. \tag{1.166}$$

We compute the traces and remove the hat-momenta of the two external vector currents. We illustrate some steps of the computation. We denote by $I[...]$ a typical momentum integral that appears in the computation

$$I[...] \equiv \int \frac{d^n q}{(2\pi)^n} \frac{[...]}{\left(q^2-\Delta\right)^3}, \tag{1.167}$$

setting $n = 4 - \epsilon$, for instance we get

$$\begin{aligned} I\left[\epsilon[k_1,k_2,\mu,\nu]\right]\hat{q}_\lambda &= 0, \\ I\left[\epsilon[k_2,\lambda,\mu,\nu]\right]\hat{q}\cdot\hat{q} &= \epsilon[k_2,\lambda,\mu,\nu](n-4)I_2, \\ I\left[\epsilon[k_2,q,\mu,\nu]\right]\hat{q}_\lambda &= 0, \\ I\left[\epsilon[k_1,q,\mu,\nu]\right]\tilde{q}_\lambda &= \epsilon[k_1,\lambda,\mu,\nu]I_2, \\ I\left[\epsilon[k_2,q,\mu,\nu]\right]q_\lambda &= \epsilon[k_2,\lambda,\mu,\nu]I_2. \end{aligned} \tag{1.168}$$

Denoting by D and E the direct and the exchanged diagram (before the integration over the Feynman parameters x,y), we obtain

$$D + E = -iI_{xy}\left[a_1c_1 + a_2c_2 + a_3c_3 + a_4c_4 + a_5c_5\right], \tag{1.169}$$

where

$$\begin{aligned} c_1 &= -4iI_2[n(-2+x+y)+2(2+x+y)] \\ &\quad +4iI_1[m_f^2(-2+x+y)+sx(1-x+xy-y+y^2)], \\ c_2 &= -c_1, \\ c_3 &= 8iI_1x(x-y-1)(k_{1\lambda}+k_{2\lambda}), \\ c_4 &= 8iI_1(x+y-1)(yk_{1\mu}-xk_{2\mu}), \\ c_5 &= 8iI_1(x+y-1)(xk_{1\nu}-yk_{2\nu}), \\ a_1 &= \epsilon[k_1,\lambda,\mu,\nu], \\ a_2 &= \epsilon[k_2,\lambda,\mu,\nu], \\ a_3 &= \epsilon[k_1,k_2,\mu,\nu], \\ a_4 &= \epsilon[k_1,k_2,\lambda,\nu], \\ a_5 &= \epsilon[k_1,k_2,\lambda,\mu], \end{aligned} \tag{1.170}$$

and introducing the dimensionally regulated expressions of I_1 and I_2 and expanding in ϵ we obtain

$$\begin{aligned} c_1 &= \frac{1}{\epsilon}\frac{3x+3y-2}{4\pi^2} \\ &\quad + \frac{x(x+y-1)(2y-1)s + (3x+3y-2)\left(sxy-m_f^2\right)\log\left(\frac{m_f^2-sxy}{\mu^2}\right)}{8\pi^2\left(m_f^2-sxy\right)}, \\ c_3 &= -\frac{x(x-y-1)}{4\pi^2(sxy-m_f^2)}\left(k_{1\lambda}+k_{2\lambda}\right), \\ c_4 &= \frac{(x+y-1)(k_{2\mu}x-k_{1\mu}y)}{4\pi^2\left(sxy-m_f^2\right)}, \end{aligned}$$

$$c_5 \;=\; -\frac{(x+y-1)(k_{1\nu}x-k_{2\nu}y)}{4\pi^2\left(sxy-m_f^2\right)}, \tag{1.171}$$

where μ is the renormalization scale in the $\overline{MS}$ scheme with $\overline{\mu}^2=\mu^2 e^{\gamma}/(4\pi)$ and γ is the Euler-Mascheroni constant. The pole singularity is related to tensor structures which have a lower mass dependence on k_1 and k_2 (a_1 and a_2) which involve loop integrations with an additional powers of q and are, therefore, UV divergent. However, the pole contributions vanish after integration over the Feynman parameter, since

$$I_{xy}\left[3x+3y-2\right]=0. \tag{1.172}$$

Performing the integration over the Feynman parameters we obtain the result reported below in Eq. (1.181).

1.15.1 The vanishing of a massive AAV/VVV

The vanishing of **AAV** in DR in the general case (with non-vanishing fermion masses) can be established by a direct computation, beside using C-invariance (Furry's theorem). The vanishing of this diagram is due to the specific form of all the Feynman parameters which multiply every covariant structure in the corresponding tensor amplitude. Denoting by $X^{\lambda\mu\nu}$ any of these generic structures, the parametric integral is of the form

$$\Delta^{\lambda\mu\nu}_{AAV}=X^{\lambda\mu\nu}\int_0^1 dx\int_0^{1-x}dy\frac{f(x,y)}{\Delta(x,y)}+\dots \tag{1.173}$$

with $f(x,y)$ antisymmetric in x,y and $\Delta(x,y)$ symmetric, giving a vanishing result. For **VVV** the result is analogous.

1.15.2 AVV and shifts

If we decide to use a shift parameterization of the diagrams then the two values of the amplitudes $\underline{a_1}$ and $\underline{a_2}$, are arbitrary. This point has been discussed in the previous sections, although here we need to discuss with further detail and include in our analysis fermion mass effects as well. However, the use of Dimensional Regularization is such to determine an equal distribution of the anomaly among diagrams of the form **AAA**, no matter which parameterization of the momentum we choose in the graph. Therefore, in this case, if a current is conserved, there is no need to add CS interactions or, equivalently, perform a shift in order to remove the anomaly from vertices which are vector-like.

The first significant parameterization of the anomalus diagram can be found in Rosenberg's paper, later used by Adler in his work on the axial anomaly. The shift is fixed by requiring CVC, which is practical matter rather than a fundamental issue. We will show that this method can be mapped into the DR-HVBM result using the Schouten identity. We start from Rosenberg's parameterization

$$\begin{aligned}T^{\lambda\mu\nu} \;=\;& A_1\epsilon[k_1,\mu,\nu,\lambda]+A_2\epsilon[k_2,\mu,\nu,\lambda]+A_3\epsilon[k_1,k_2,\mu,\lambda]{k_1}^{\nu}+A_4\epsilon[k_1,k_2,\mu,\lambda]k_2^{\nu}\\ &+A_5\epsilon[k_1,k_2,\nu,\lambda]k_1^{\mu}+A_6\epsilon[k_1,k_2,\nu,\lambda]k_2^{\mu}\end{aligned} \tag{1.174}$$

given in [42]. By power-counting, two invariant amplitudes are divergent, A_1 and A_2, while the A_i with $i\geq 3$ are finite[5]. In general A_1 and A_2 are given by parametric integrals which are divergent and there are two free parameters in these integrals, amounting to momentum shifts, that can be chosen to render

---

[5] We will be using the notation $\epsilon[a,b,\mu,\nu]\equiv\epsilon_{\alpha\beta\mu\nu}a^{\alpha}b^{\beta}$ to denote the structures in the expansion of the anomalous triangle diagrams

A_1 and A_2 finite. It is possible to redefine the momentum shifts so that the divergences are removed, and this can be obtained by imposing the defining Ward Identities (conservation of the two vector currents) in the diagrams

$$k_{1\mu}T^{\lambda\mu\nu} = k_{2\nu}T^{\lambda\mu\nu} = 0. \tag{1.175}$$

This gives $A_1 = s/2\ A_3$ and $A_2 = s/2\ A_6$. The expressions of the invariant amplitudes A_i are given in Rosenberg as implicit parametric integrals. They can be arranged in the form

$$\begin{aligned} A_1 &= -\frac{i}{4\pi^2} + iC_0(m_f^2, s) \\ A_2 &= \frac{i}{4\pi^2} - iC_0(m_f^2, s) \\ A_3 &= -\frac{i}{2s\pi^2} + \frac{2i}{s}C_0(m_f^2, s) \\ A_4 &= \frac{i}{s\pi^2} - if(m_f^2, s) \\ A_5 &= -A_4 \\ A_6 &= -A_3 \end{aligned} \tag{1.176}$$

where we have isolated the mass-independent contributions, which will appear in the anomaly, from the mass corrections dependent on the fermion mass (m_f), and we have defined

$$C_0(m_f^2, s) = \frac{Li_2\left(\frac{2}{1-\sqrt{1-4m_f^2/s}}\right) m_f^2}{2s\pi^2} + \frac{Li_2\left(\frac{2}{1+\sqrt{1-4m_f^2/s}}\right) m_f^2}{2s\pi^2}, \tag{1.177}$$

$$f(m_f^2, s) = \frac{\sqrt{1-4m_f^2/s}\,\tanh^{-1}\left(\frac{1}{\sqrt{1-4m_f^2/s}}\right)}{s\pi^2}. \tag{1.178}$$

Eqs. (1.177) and (1.178) have been obtained integrating the parametric expressions of Rosenberg.

The axial vector WI is obtained from the contraction

$$\begin{aligned} &(k_{1\lambda} + k_{2\lambda})\, T^{\lambda\mu\nu} \\ =\ & \Bigg(-\frac{i}{2\pi^2} + \frac{iLi_2\left(\frac{2}{1-\sqrt{1-4m_f^2/s}}\right) m_f^2}{s\pi^2} + \frac{iLi_2\left(\frac{2}{1+\sqrt{1-4m_f^2/s}}\right) m_f^2}{s\pi^2} \Bigg) \epsilon[k_1, k_2, \mu, \nu] \\ =\ & \left(-\frac{i}{2\pi^2} + 2\, i\, C_0(m_f^2, s) \right) \times \epsilon[k_1, k_2, \mu, \nu] \end{aligned} \tag{1.179}$$

where the first contribution is the correct value of the anomaly. The remaining term, expressed in terms of dilogarithmic functions, is related to the scalar three-point function, as shown below.

1.15.3 DR-HVBM scheme

1.15.3.1 The AVV diagram

In this case if we use DR we obtain

$$\begin{aligned} T_{\lambda\mu\nu} \;=\; & -i\tau_1 \left(\epsilon[k_1, \lambda, \mu, \nu] - \ \epsilon[k_2, \lambda, \mu, \nu] \right) - i\tau_2\, (k_{1\lambda} + k_{2\lambda})\ \epsilon[k_1, k_2, \mu, \nu] \\ & -i\tau_3\, (k_{1\mu} - k_{2\mu})\ \epsilon[k_1, k_2, \lambda, \nu] - i\tau_3\, (k_{1\nu} - k_{2\nu})\ \epsilon[k_1, k_2, \lambda, \mu] \end{aligned} \tag{1.180}$$

$$
\begin{aligned}
\tau_1 &= -\frac{Li_2\left(\frac{2}{1-\sqrt{1-4m_f^2/s}}\right)m_f^2}{4s\pi^2}-\frac{Li_2\left(\frac{2}{1+\sqrt{1-4m_f^2/s}}\right)m_f^2}{4s\pi^2}\\
&\quad+\frac{3}{8\pi^2}-\frac{\sqrt{4m_f^2/s-1}\ \tan^{-1}\left(\frac{1}{\sqrt{4m_f^2/s-1}}\right)}{4\pi^2}\\
\tau_2 &= -\frac{Li_2\left(\frac{2}{1-\sqrt{1-4m_f^2/s}}\right)m_f^2}{2s^2\pi^2}-\frac{Li_2\left(\frac{2}{1+\sqrt{1-4m_f^2/s}}\right)m_f^2}{2s^2\pi^2}\\
&\quad+\frac{\sqrt{4m_f^2/s-1}\ \tan^{-1}\left(\frac{1}{\sqrt{4m_f^2/s-1}}\right)}{2s\pi^2}-\frac{1}{4s\pi^2}\\
\tau_3 &= \frac{Li_2\left(\frac{2}{1-\sqrt{1-4m_f^2/s}}\right)m_f^2}{2s^2\pi^2}+\frac{Li_2\left(\frac{2}{1+\sqrt{1-4m_f^2/s}}\right)m_f^2}{2s^2\pi^2}\\
&\quad+\frac{\sqrt{4m_f^2/s-1}\ \tan^{-1}\left(\frac{1}{\sqrt{4m_f^2/s-1}}\right)}{2s\pi^2}-\frac{3}{4s\pi^2}.
\end{aligned}
\tag{1.181}
$$

The expressions above require a suitable analytic continuation in order to cover all the kinematic range of the external invariant (virtuality) s. The position of the branch cut in the physical region is at $\sqrt{s}=2m$, corresponding to an s-channel cut, where the virtual axial-vector line can produce two on-shell collinear massive fermions.

It is interesting to see how the vector and the axial-vector Ward Identities are satisfied for a generic fermion mass m. For the vector WI we get

$$
\begin{aligned}
k_{1\mu}T^{\mu\nu\lambda} &= \frac{i}{2}\left(\tau_3 s+2\tau_1\right)\epsilon[k_1,k_2,\lambda,\nu]\\
k_{2\nu}T^{\mu\nu\lambda} &= -\frac{i}{2}\left(\tau_3 s+2\tau_1\right)\epsilon[k_1,k_2,\lambda,\nu].
\end{aligned}
\tag{1.182}
$$

One can check directly that the combination $(\tau_3 s+2\tau_1)$ vanishes so that $k_{1\mu}T^{\mu\nu\lambda}=k_{2\nu}T^{\mu\nu\lambda}=0$.

The second and third term in (1.179) are related to the scalar three-point function

$$
C_{00}(k^2,k_1^2,k_2^2,m_f^2,m_f^2,m_f^2)=\int d^4q\frac{1}{\left(q^2-m_f^2\right)\left((q+k_1)^2-m_f^2\right)\left((q+k_1+k_2)^2-m_f^2\right)}
\tag{1.183}
$$

$$
\begin{aligned}
C_{00}(k^2,0,0,m_f^2,m_f^2,m_f^2) &= -\frac{1}{k^2}\left(Li_2\left(\frac{1}{r_1}\right)+Li_2\left(\frac{1}{r_2}\right)\right)\\
r_{1,2} &= \frac{1}{2}\left[1\pm\sqrt{1-4\frac{m_f^2}{k^2}}\right]
\end{aligned}
\tag{1.184}
$$

giving the equivalent relation

$$
\left(k_{1\lambda}+k_{2\lambda}\right)T^{\lambda\mu\nu}=\left(-\frac{i}{2\pi^2}+\frac{iLi_2\left(\frac{2}{1-\sqrt{1-4m_f^2/s}}\right)m_f^2}{s\pi^2}+\frac{iLi_2\left(\frac{2}{1+\sqrt{1-4m_f^2/s}}\right)m_f^2}{s\pi^2}\right)\epsilon[k_1,k_2,\mu,\nu].
\tag{1.185}
$$

Our result for $T^{\lambda\mu\nu}$ can be easily matched to other parameterizations obtained by a shift of the momentum in the loop integral performed in 4 dimensions. We recall that in this case one needs to impose the defining Ward Identities on the amplitude, rather than obtaining them from a regularization, as in the case of the HVBM scheme. Before doing this, we present the analytically continued expressions of (1.181) which are valid for $\sqrt{s} > 2m_f$ and are given by

$$\begin{aligned}
\tau_1 &= -\frac{1}{2}C_0(s,m_f^2) + \frac{3}{8\pi^2} - \frac{1}{4\pi^2}\sqrt{1-4m_f^2/s}\ \tanh^{-1}\left(\frac{1}{\sqrt{1-4m_f^2/s}}\right) \\
&= -\frac{1}{2}C_0(s,m_f^2) + \frac{3}{8\pi^2} - \frac{s}{4}f(m_f^2,s), \\
\tau_2 &= -\frac{1}{s}C_0(s,m_f^2) - \frac{1}{4s\pi^2} + \frac{1}{2s\pi^2}\sqrt{1-4m_f^2/s}\ \tanh^{-1}\left(\frac{1}{\sqrt{1-4m_f^2/s}}\right) \\
&= -\frac{1}{s}C_0(s,m_f^2) - \frac{1}{4s\pi^2} + \frac{1}{2}f(m_f^2,s), \\
\tau_3 &= \frac{1}{s}C_0(s,m_f^2) - \frac{3}{4s\pi^2} + \frac{1}{2s\pi^2}\sqrt{1-4m_f^2/s}\ \tanh^{-1}\left(\frac{1}{\sqrt{1-4m_f^2/s}}\right) \\
&= \frac{1}{s}C_0(s,m_f^2) - \frac{3}{4s\pi^2} + \frac{1}{2}f(m_f^2,s). \qquad (1.186)
\end{aligned}$$

1.15.3.2 The AAA diagram

The second case that needs to be worked out in DR is that of a triangle diagram containing three axial-vector currents. We use the HVBM scheme for γ_5. The analysis is pretty similar to the case of a single γ_5. In this case we obtain

$$\begin{aligned}
T_3^{\lambda\mu\nu} &= -i\left(I_{xy}[c_1]\epsilon[k_1,\lambda,\mu,\nu] + I_{xy}[c_2]\epsilon[k_2,\lambda,\mu,\nu] + I_{xy}[c_3]\epsilon[k_1,k_2,\mu,\nu]\left(k_1^\lambda + k_2^\lambda\right)\right. \\
&\quad \left. + I_{xy}[c_4^\mu]\epsilon[k_1,k_2,\lambda,\nu] + I_{xy}[c_5^\nu]\epsilon[k_1,k_2,\lambda,\mu]\right) \qquad (1.187)
\end{aligned}$$

where I_{xy} is the integration over the Feynman parameters. Also in this case the coefficients c_1 and c_2 are divergent and are regulated in DR. We obtain

$$\begin{aligned}
c_1 &= 4i\left(I_2(n-6)(3x+3y-2) + I_1\left((-3x-3y+2)m_f^2 + sx\left(y^2-y+x(y-1)+1\right)\right)\right) \\
c_2 &= -c_1 \\
c_3 &= 8iI_1x(x-y-1) \\
c_4 &= -8iI_1(x+y-1)(xk_2{}^\mu - yk_1{}^\mu) \\
c_5 &= 8iI_1(x+y-1)(xk_1{}^\nu - yk_2{}^\nu), \qquad (1.188)
\end{aligned}$$

which in DR become

$$\begin{aligned}
c_1 &= \frac{3x+3y-2}{4\pi^2\epsilon} + \frac{(3x+3y-2)\left(sxy-m_f^2\right)\log\left(\frac{m_f^2-sxy}{\mu^2}\right) - sx(x+y-1)(2y+1)}{8\pi^2\left(m_f^2-sxy\right)} \\
c_3 &= \frac{x(x-y-1)}{4\pi^2\left(m_f^2-sxy\right)} \\
c_4 &= -\frac{(x+y-1)(k_2{}^\mu x - k_1{}^\mu y)}{4\pi^2\left(m_f^2-sxy\right)}
\end{aligned}$$

$$c_5 = \frac{(x+y-1)({k_1}^{\nu} x - {k_2}^{\nu} y)}{4\pi^2\left(m_f^2 - sxy\right)}. \tag{1.189}$$

After integration over x and y the pole contribution vanishes. We obtain

$$\begin{aligned} T^{(3)}_{\lambda\mu\nu} = & -i\Big(\tau_1^{(3)}\ (\epsilon[k_1,\lambda,\mu,\nu] - \ \epsilon[k_2,\lambda,\mu,\nu]) + \tau_2^{(3)}\,(k_{1\lambda}+k_{2\lambda})\ \epsilon[k_1,k_2,\mu,\nu] \\ & + \tau_3^{(3)}\,(k_{1\mu}-k_{2\mu})\ \epsilon[k_1,k_2,\lambda,\nu] + \tau_3^{(3)}\,(k_{1\nu}-k_{2\nu})\ \epsilon[k_1,k_2,\lambda,\mu]\Big)\,, \end{aligned} \tag{1.190}$$

$$\begin{aligned} \tau_1^{(3)} = & \frac{3Li_2\left(\frac{2}{1-\sqrt{1-4m_f^2/s}}\right)m_f^2}{4s\pi^2} + \frac{3Li_2\left(\frac{2}{1+\sqrt{1-4m_f^2/s}}\right)m_f^2}{4s\pi^2} \\ & + \frac{\left(64\,m_f^4/s^2 - 20\,m_f^2/s + 1\right)\ \tan^{-1}\left(\frac{1}{\sqrt{4m_f^2/s-1}}\right)}{4\pi^2\sqrt{4m_f^2/s-1}} - \frac{4m_f^2}{s\pi^2} + \frac{5}{24\pi^2}, \end{aligned} \tag{1.191}$$

$$\begin{aligned} \tau_2^{(3)} = & -\frac{Li_2\left(\frac{2}{1-\sqrt{1-4m_f^2/s}}\right)m_f^2}{2s^2\pi^2} - \frac{Li_2\left(\frac{2}{1+\sqrt{1-4m_f^2/s}}\right)m_f^2}{2s^2\pi^2} \\ & + \frac{\sqrt{4m_f^2/s-1}\tan^{-1}\left(\frac{1}{\sqrt{4m_f^2/s-1}}\right)}{2s\pi^2} - \frac{1}{4s\pi^2}, \end{aligned} \tag{1.192}$$

$$\begin{aligned} \tau_3^{(3)} = & \frac{Li_2\left(\frac{2}{1-\sqrt{1-4m_f^2/s}}\right)m_f^2}{2s^2\pi^2} + \frac{Li_2\left(\frac{2}{1+\sqrt{1-4m_f^2/s}}\right)m_f^2}{2s^2\pi^2} \\ & + \frac{\sqrt{4m_f^2/s-1}\tan^{-1}\left(\frac{1}{\sqrt{4m_f^2/s-1}}\right)}{2s\pi^2} - \frac{3}{4s\pi^2}. \end{aligned} \tag{1.193}$$

We present the analytically continued expressions of relations (1.191, 1.192, 1.193) valid for $\sqrt{s} > 2m_f$

$$\begin{aligned} \tau_1^{(3)} = & \frac{3Li_2\left(\frac{2}{1-\sqrt{1-4m_f^2/s}}\right)m_f^2}{4s\pi^2} + \frac{3Li_2\left(\frac{2}{1+\sqrt{1-4m_f^2/s}}\right)m_f^2}{4s\pi^2} \\ & - \frac{\left(64\,m_f^4/s^2 - 20\,m_f^2/s + 1\right)\ \tanh^{-1}\left(\frac{1}{\sqrt{1-4m_f^2/s}}\right)}{4\pi^2\sqrt{1-4m_f^2/s}} - \frac{4m_f^2}{s\pi^2} + \frac{5}{24\pi^2}, \end{aligned} \tag{1.194}$$

$$\begin{aligned} \tau_2^{(3)} = & -\frac{Li_2\left(\frac{2}{1-\sqrt{1-4m_f^2/s}}\right)m_f^2}{2s^2\pi^2} - \frac{Li_2\left(\frac{2}{1+\sqrt{1-4m_f^2/s}}\right)m_f^2}{2s^2\pi^2} \\ & + \frac{\sqrt{1-4m_f^2/s}\tanh^{-1}\left(\frac{1}{\sqrt{1-4m_f^2/s}}\right)}{2s\pi^2} - \frac{1}{4s\pi^2}, \end{aligned} \tag{1.195}$$

$$
\begin{aligned}
\tau_3^{(3)} &= \frac{Li_2\left(\frac{2}{1-\sqrt{1-4m_f^2/s}}\right) m_f^2}{2s^2\pi^2} + \frac{Li_2\left(\frac{2}{1+\sqrt{1-4m_f^2/s}}\right) m_f^2}{2s^2\pi^2} \\
&+ \frac{\sqrt{1-4m_f^2/s}\,\tanh^{-1}\left(\frac{1}{\sqrt{1-4m_f^2/s}}\right)}{2s\pi^2} - \frac{3}{4s\pi^2}. \qquad (1.196)
\end{aligned}
$$

In the massless case, the contribution to the WI is given by

$$
\begin{aligned}
k_3^\lambda T^{AAA}_{\lambda\mu\nu} &= -\frac{i}{6\pi^2}\epsilon[k_1,k_2,\mu,\nu] \\
k_1^\mu T^{AAA}_{\lambda\mu\nu} &= -\frac{i}{6\pi^2}\epsilon[k_2,k_3,\nu,\lambda] \\
k_2^\nu T^{AAA}_{\lambda\mu\nu} &= -\frac{i}{6\pi^2}\epsilon[k_3,k_1,\lambda,\mu] \qquad (1.197)
\end{aligned}
$$

where we have chosen a symmetric distribution of (outgoing) momenta (k_1, k_2, k_3) attached to vertices (μ, ν, λ), with $k_3 = -k = -k_1 - k_2$.

1.15.4 Equivalence of the shift-based (CVC) and of DR-HVBM schemes

The equivalence between the HVBM result and the one obtained using the defining Ward Identities (1.176) can be shown using the Schouten relation

$$
\begin{aligned}
& k_i^{\mu_1}\epsilon[\mu_2,\mu_3,\mu_4,\mu_5] + k_i^{\mu_2}\epsilon[\mu_3,\mu_4,\mu_5,\mu_1] + k_i^{\mu_3}\epsilon[\mu_4,\mu_5,\mu_1,\mu_2] \\
& + k_i^{\mu_4}\epsilon[\mu_5,\mu_1,\mu_2,\mu_3] + k_i^{\mu_5}\epsilon[\mu_1,\mu_2,\mu_3,\mu_4] = 0, \qquad (1.198)
\end{aligned}
$$

that allows to remove the $k_{1,2}^\lambda$ terms in terms of other contributions

$$
\begin{aligned}
k_1^\lambda\epsilon[k_1,k_2,\mu,\nu] &= \frac{s}{2}\epsilon[k_1,\mu,\nu,\lambda] - k_1^\mu\epsilon[k_1,k_2,\nu,\lambda] + k_1^\nu\epsilon[k_1,k_2,\mu,\lambda] \\
k_2^\lambda\epsilon[k_1,k_2,\mu,\nu] &= -\frac{s}{2}\epsilon[k_2,\mu,\nu,\lambda] - k_2^\mu\epsilon[k_1,k_2,\nu,\lambda] + k_2^\nu\epsilon[k_1,k_2,\mu,\lambda]. \qquad (1.199)
\end{aligned}
$$

The result in the HBVM scheme then becomes

$$
\begin{aligned}
T^{\lambda\mu\nu} &= -i\left(\tau_1 + \frac{s}{2}\tau_2\right)\epsilon[k_1,\mu,\nu,\lambda] - i\left(-\tau_1 - \frac{s}{2}\tau_2\right)\epsilon[k_2,\mu,\nu,\lambda] \\
&\quad -i\left(\tau_2 - \tau_3\right)\epsilon[k_1,k_2,\mu,\lambda]{k_1}^\nu - i\left(\tau_2 + \tau_3\right)\epsilon[k_1,k_2,\mu,\lambda]k_2^\nu \\
&\quad -i\left(-\tau_2 - \tau_3\right)\epsilon[k_1,k_2,\nu,\lambda]k_1^\mu - i\left(\tau_3 - \tau_2\right)\epsilon[k_1,k_2,\nu,\lambda]k_2^\mu \qquad (1.200)
\end{aligned}
$$

and it is easy to check using (1.176) and (1.186) that the invariant amplitudes given above coincide with those given by Rosenberg. Therefore we have the correspondence

$$
\begin{aligned}
A_1 &= -i(\tau_1 + \frac{s}{2}\tau_2) \\
A_2 &= -i(-\tau_1 - \frac{s}{2}\tau_2) \\
A_3 &= -i(\tau_2 - \tau_3) \\
A_4 &= -i(\tau_2 + \tau_3) \\
A_5 &= -i(-\tau_2 - \tau_3) \\
A_6 &= -i(\tau_3 - \tau_2). \qquad (1.201)
\end{aligned}
$$

A similar correspondence holds between the Rosenberg parameterization of **AAA** and the corresponding DR-HVBM result

$$\begin{aligned}
A_1^{(3)} &= -i(\tau_1^{(3)} + \frac{s}{2}\tau_2) \\
A_2^{(3)} &= -i(-\tau_1^{(3)} - \frac{s}{2}\tau_2^{(3)}) \\
A_3^{(3)} &= -i(\tau_2^{(3)} - \tau_3^{(3)}) \\
A_4^{(3)} &= -i(\tau_2^{(3)} + \tau_3^{(3)}) \\
A_5^{(3)} &= -i(-\tau_2^{(3)} - \tau_3^{(3)}) \\
A_6^{(3)} &= -i(\tau_3^{(3)} - \tau_2^{(3)}).
\end{aligned} \tag{1.202}$$

1.16 Appendix. The Chern-Simons and Wess-Zumino vertices

The derivation of the CS vertex is straightforward and is given by

$$\begin{aligned}
&\int dx\, dy\, dz\, T_{CS}^{\lambda\mu\nu}(z,x,y)\, B^\lambda(z) A^\mu(x) A^\nu(y) \\
=\;& \int dx\, dy\, dz \int \frac{dk_1}{(2\pi)^4}\frac{dk_2}{(2\pi)^4} e^{-ik_1(x-z)-ik_2(y-z)}\, \epsilon^{\lambda\mu\nu\alpha}\,(k_1^\alpha - k_2^\alpha)\, B^\lambda(z) A^\mu(x) A^\nu(y) \\
=\;& \int dx\, dy\, dz\, i\left(\frac{\partial}{\partial x^\alpha} - \frac{\partial}{\partial y^\alpha}\right)\left(\int \frac{dk_1}{(2\pi)^4}\frac{dk_2}{(2\pi)^4} e^{-ik_1(x-z)-ik_2(y-z)}\right) B^\lambda(z) A^\mu(x) A^\nu(y) \epsilon^{\lambda\mu\nu\alpha} \\
=\;& (-i)\int dx\, dy\, dz \int \frac{dk_1\, dk_2}{(2\pi)^8} e^{-ik_1(x-z)-ik_2(y-z)} B^\lambda(z)\left(\frac{\partial}{\partial x^\alpha}A^\mu(x)A^\nu(y) - \frac{\partial}{\partial y^\alpha}A^\nu(y)A^\mu(x)\right)\epsilon^{\lambda\mu\nu\alpha} \\
=\;& (-i)\int dx\, dy\, dz\, \delta(x-z)\delta(y-z) B^\lambda(z)\left(\frac{\partial}{\partial x^\alpha}A^\mu(x)A^\nu(y) - \frac{\partial}{\partial y^\alpha}A^\nu(y)A^\mu(x)\right)\epsilon^{\lambda\mu\nu\alpha} \\
=\;& i\int dx A^\lambda(x) B^\nu(x) F^A_{\rho\sigma}(x)\epsilon^{\lambda\nu\rho\sigma}.
\end{aligned} \tag{1.203}$$

Proceeding in a similar way we obtain the expression of the Wess-Zumino vertex

$$\begin{aligned}
&\int dx\, dy\, dz \int \frac{d^4k_1}{(2\pi)^4}\frac{d^4k_2}{(2\pi)^4}\epsilon^{\mu\nu\rho\sigma} k_1^\rho k_2^\sigma e^{-ik_1\cdot(x-z)-ik_2\cdot(y-z)}\, b(z) B^\mu(x) B^\nu(y) \\
=\;& \int dx\, dy\, dz \int \frac{d^4k_1}{(2\pi)^4}\frac{d^4k_2}{(2\pi)^4}\epsilon^{\mu\nu\rho\sigma}\left(\frac{1}{-i}\right)\frac{\partial}{\partial x^\rho} e^{-ik_1\cdot(x-z)}\left(\frac{1}{-i}\right)\frac{\partial}{\partial y^\sigma}e^{-ik_2\cdot(y-z)}\, b(z) B^\mu(x) B^\nu(y) \\
=\;& (-1)\int dx\, dy\, dz\, \delta^{(4)}(x-z)\delta^{(4)}(y-z)\, b(z)\, \frac{\partial B^\mu}{\partial x^\rho}(x)\, \frac{\partial B^\nu}{\partial y^{\,\sigma}}(y)\, \epsilon^{\mu\nu\rho\sigma} \\
=\;& -\frac{1}{4}\int dx\, b(x)\, F^B_{\rho\mu}(x)\, F^B_{\sigma\nu}(x)\, \epsilon^{\mu\nu\rho\sigma} = \frac{1}{4}\int dx\, b\, F^B_{\rho\mu}\, F^B_{\sigma\nu}\, \epsilon^{\rho\mu\sigma\nu}
\end{aligned} \tag{1.204}$$

so that we find the following correspondence between Minkowsky space and momentum space for the Green-Schwarz vertex

$$4\,\epsilon^{\mu\nu\rho\sigma}\, k_1^\rho k_2^\sigma \qquad \leftrightarrow \qquad bF^B \wedge F^B. \tag{1.205}$$

1.17 Appendix. Computation of the Effective Action

In this appendix we illustrate the derivation of the variation of the effective action for typical anomalous contributions involving **AVV** and **AAA** diagrams. We consider the case of the A-B Model described in the first few sections. We recall that we have the relations

$$\delta B^\mu = \partial_\mu \theta_B \qquad \delta A^\mu = \partial_\mu \theta_A. \tag{1.206}$$

We obtain the following gauge variations

$$\begin{aligned}
\delta_B \mathcal{S}_{BAA} &= \delta_B \int dx\, dy\, dz\, T^{\lambda\mu\nu}_{\mathbf{AVV}}(z,x,y)\, B^\lambda(z)\, A^\mu(x)\, A^\nu(y) \\
&= -\int dx\, dy\, dz\, \partial_{z^\lambda} T^{\lambda\mu\nu}_{\mathbf{AVV}}(z,x,y)\, A^\mu(x)\, A^\nu(y)\, \theta_B(z) \\
&= -i a_3(\beta) \epsilon^{\mu\nu\alpha\beta} \int dx\, dy\, dz\, \partial_{x^\alpha} \partial_{y^\beta} [\delta(x-z)\, \delta(y-z)]\, A^\mu(x)\, A^\nu(y) \theta_B(z) \\
&= -i a_3(\beta) \epsilon^{\mu\nu\alpha\beta} \int dx\, \partial_{x^\alpha} A^\mu(x)\, \partial_{x^\beta} A^\nu(x)\, \theta_B(x) \\
&= i \frac{a_3(\beta)}{4} \int dx\, \theta_B\, F^A_{\alpha\mu} F^A_{\beta\nu} \epsilon^{\alpha\mu\beta\nu},
\end{aligned} \tag{1.207}$$

$$\begin{aligned}
\delta_A \mathcal{S}_{BAA} &= \delta_A \int dx\, dy\, dz\, T^{\lambda\mu\nu}_{\mathbf{AVV}}(z,x,y)\, B^\lambda(z)\, A^\mu(x)\, A^\nu(y) \\
&= -\int dx\, dy\, dz\, \partial_{x^\mu} T^{\lambda\mu\nu}_{\mathbf{AVV}}(z,x,y)\, B^\lambda(z)\, \theta_A(x)\, A^\nu(y) \\
&\quad -\int dx\, dy\, dz\, \partial_{y^\nu} T^{\lambda\mu\nu}_{\mathbf{AVV}}(z,x,y)\, B^\lambda(z)\, A^\mu(x)\, \theta_A(y) \\
&= i a_1(\beta) \epsilon^{\lambda\nu\alpha\beta} \int dx\, dy\, dz\, \partial_{x^\alpha} \partial_{y^\beta} [\delta(x-z)\, \delta(y-z)]\, B^\lambda(z)\, \theta_A(x)\, A^\nu(y) \\
&= -i a_1(\beta) \epsilon^{\lambda\nu\alpha\beta} \int dx\ \partial_{x^\alpha} B^\lambda(x)\, \partial_{x^\beta} A^\nu(x)\, \theta_A(x) \\
&\quad + i a_1(\beta) \epsilon^{\lambda\mu\alpha\beta} \int dx\ \partial_{x^\beta}\, B^\lambda(x)\, \partial_{x^\alpha}\, A^\mu\, \theta_A(x) \\
&= i \frac{a_1(\beta)}{4} 2 \int dx\, \theta_A\, F^B_{\alpha\lambda} F^A_{\beta\nu}\, \epsilon^{\alpha\lambda\beta\nu}.
\end{aligned} \tag{1.208}$$

1.18 Appendix. Decay of the axi-Higgs: the pseudoscalar triangle χBB

The computation is standard and the result is finite. There are no problems with the handling of γ_5 and so we can stay in 4 dimensions.

We first compute the triangle diagram with the position of zero mass fermion $m_f = 0$

$$\int \frac{d^4 q}{(2\pi)^4} \frac{Tr\left[\gamma^5 (\not{q} - \not{k})\gamma^\nu (\not{q} - \not{k_1})\gamma^\mu \not{q}\right]}{q^2 (q-k)^2 (q-k_1)^2} + \text{exch.} \tag{1.209}$$

which trivially vanishes because of the γ-algebra. Then the relevant contribution to the diagram comes to be proportional to the mass $m_f \neq 0$, as we are now going to show.

We set $k = k_1 + k_2$ and set on-shell the B-bosons: $k_1^2 = k_2^2 = M_B^2$, so that $k^2 = 2M_B^2 + 2k_1 \cdot k_2 = m_\chi^2$

The diagram now becomes

$$\int \frac{d^4 q}{(2\pi)^4} \frac{Tr\left[\gamma^5 (\not{q} - \not{k} + m_f)\gamma^\nu (\not{q} - \not{k_1} + m_f)\gamma^\mu (\not{q} + m_f)\right]}{\left[q^2 - m_f^2\right] \left[(q-k)^2 - m_f^2\right] \left[(q-k_1)^2 - m_f^2\right]} + \text{exch.} \tag{1.210}$$

Using a Feynman parameterization we obtain

$$
\begin{aligned}
&= 2\int_0^1 dx \int_0^{1-x} \frac{1}{\Big[q^2 - 2q[k_2 y + k_1(1-x)] + [\,y m_\chi^2 - m_f^2 + m_B^2(1-x-y)\,]\Big]^3} \\
&= 2\int_0^1 dx \int_0^{1-x} dy \frac{1}{[q^2 - 2q\Sigma + D]^3} = 2\int_0^1 dx \int_0^{1-x} dy \frac{1}{[(q-\Sigma)^2 - (\Sigma^2 - D)\,]^3} \\
&= 2\int_0^1 dx \int_0^{1-x} dy\, \frac{1}{[(q-\Sigma)^2 - \Delta\,]^3}. \qquad (1.211)
\end{aligned}
$$

We define

$$\Sigma = y k_2 + k_1(1-x) \qquad (1.212)$$

and

$$D = y m_\chi^2 - m_f^2 + M_B^2(1-x-y), \qquad (1.213)$$

for the direct diagram and the function

$$\Delta = \Sigma^2 - D = m_f^2 - x\, y\, m_\chi^2 + m_B^2(x+y)^2 - x M_B^2 - y m_B^2 \equiv \Delta(x,y,m_f,m_\chi,M_B) \qquad (1.214)$$

and perform a shift of the loop momentum

$$q' = q - \Sigma \qquad (1.215)$$

obtaining

$$2\int_0^1 dx \int_0^{1-x} dy \int \frac{d^D q}{(2\pi)^D} \frac{Tr[\gamma^5(\not{q} \ + \not{\Sigma} \ - \not{k} \ + m_f)\gamma^\nu(\not{q} \ + \not{\Sigma} \ - \not{k_1} \ + m_f)\gamma^\mu(\not{q} \ + \not{\Sigma} \ + m_f)]}{[q^2 - \Delta]^3} \qquad (1.216)$$

Using symmetric integration we can drop linear terms in q, together with $q^\mu q^\nu = \frac{1}{D} q^2 g^{\mu\nu}$. Adding the exchanged diagram and after a routine calculation we obtain the amplitude for the decay

$$\Delta^{\mu\nu} = \epsilon^{\alpha\beta\mu\nu} k_1^\alpha k_2^\beta m_f \left(\frac{1}{2\pi^2}\right) I(m_f, m_\chi, m_B) \qquad (1.217)$$

with

$$I = \int_0^1 dx \int_0^{1-x} dy \frac{1}{\Delta(x,y,m_f,m_\chi,m_B)}. \qquad (1.218)$$

Chapter 2

Stückelberg Axions and the Effective Action of Anomalous Abelian Models 2. A $SU(3)_C \times SU(2)_W \times U(1)_Y \times U(1)_B$ Model and its signature at the LHC

2.1 Introduction to the chapter

Among the possible extensions of the Standard Model (SM), those where the $SU(3)_C \times SU(2)_W \times U(1)_Y$ gauge group is enlarged by a number of extra $U(1)$ symmetries are quite attractive for being modest enough departures from the SM so that they are computationally tractable, but at the same time predictive enough so that they are interesting and even perhaps testable at the LHC. Of particular popularity among these have been models where at least one of the extra $U(1)$'s is "anomalous", that is, some of the fermion triangle loops with gauge boson external legs are non-vanishing. The existence of this possibility was noticed in the context of the (compactified to four dimensions) heterotic superstring where the stability of the supersymmetric vacuum [47, 48] can trigger in the four-dimensional low energy effective action a non-vanishing Fayet-Iliopoulos term proportional to the gravitational anomaly, i.e. proportional to the anomalous trace of the corresponding $U(1)$. The mechanism was recognized to be the low energy manifestation of the Green-Schwarz anomaly (GS) cancellation mechanism of string theory.[1] Most of the consequent developments were concentrated around exploiting this idea in conjunction with supersymmetry and the Froggatt-Nielsen mechanism [49] in order to explain the mass hierarchies in the Yukawa sector of the SM [50], supersymmetry breaking [51, 52], inflation [53] and axion physics [54], in all of which the presence of the anomalous $U(1)$ is a crucial ingredient. In the context of theories with extra dimensions the analysis of anomaly localization and of anomaly inflow has also been at the center of interesting developments [55, 14, 15]. The recent explosion of string model building, in particular in the context of orientifold constructions and intersecting branes [56, 57, 58] but also in the context of the heterotic string [59], have enhanced even more the interest in anomalous $U(1)$ models. There are a few universal characteristics that these vacua seem to possess. One is the presence of $U(1)$ gauge symmetries that do not appear in the SM [60, 61]. In realistic 4-dim heterotic string vacua the SM gauge group comes as a subgroup of the 10-dim $SO(32)$ or $E_8 \times E_8$ symmetry [62, 63], and in practice there is at least one anomalous $U(1)$ factor that appears at low energies, tied to the SM sector in a particular way, which we will summarize next. For simplicity and reasons of tractability we concentrate on the simplest non-trivial case of a model with gauge group $SU(3)_C \times SU(2)_W \times U(1)_Y \times U(1)_B$ where Y is the hypercharge and B is the anomalous gauge boson and where the fermion spectrum is that of the SM. The mass term for the anomalous $U(1)_B$ appears through a Stückelberg coupling [61, 64, 65, 66, 67] and the cancellation of its anomalies is due to axionic and Chern-Simons terms (in the open string context see the recent works [61, 68, 1, 69, 70]).

---

[1] Conventionally in this paper we will use both the term “Green-Schwarz” (GS) to denote the mechanism of cancellation of the anomalies, to conform to the string context, though the term “Wess-Zumino” (WZ) would probably be more adequate and sufficient for our analysis. The corresponding counterterm will be denoted, GS or WZ, with no distinction.

Despite of all this theoretical insight both from the top-down and bottom-up approaches, the question that remains open is how to make concrete contact with experiment. However, as mentioned above, in models with anomalous $U(1)$'s one should quite generally expect the presence of a physical axion-like field χ and in fact in any decay that involves a non-vanishing fermion triangle like the decay $Z^*, Z^{'*} \longrightarrow \gamma\gamma$, $Z, Z' \longrightarrow Z\gamma$ etc., one should be able to see traces of the anomalous structure [1, 69, 70, 13, 40]. In this chapter we will mostly concentrate on the gauge boson decays which, even though hard to measure, contain clear differences with respect to the SM - as is the case of the $Z^* \longrightarrow \gamma\gamma$ decay - and in addition with respect to anomaly free $U(1)$ extensions - like the $Z^{'*} \longrightarrow \gamma\gamma$ decay - for example.

In [1] a theory which extends the SM with this minimal structure (for essentially an arbitrary number of extra $U(1)$ factors) was called "Minimal Low Scale Orientifold Model" or mLSOM for short, because in orientifold constructions one typically finds multiple anomalous $U(1)$'s. Here, even though we discuss the case of a single anomalous $U(1)$ which could also originate from heterotic vacua or some field theory extension of the SM, we will keep on using the same terminology keeping in mind that the results can apply to more general cases. We finally mention that other similar constructions with emphasis on other phenomenological signatures of such models have appeared before in [68, 71, 27, 28, 72, 73, 29, 74, 27]. A perturbative study of the renormalization of these types of models is in [75]. Other features of these models, in view of the recent activity connected to the claimed PVLAS result [76, 77, 78, 79, 80, 81, 82], have been discussed in [40].

The chapter is organized as follows. In the first sections we will specialize the analysis of [1] to the case of an extension of the SM that contains one additional anomalous Abelian $U(1)$, with an Abelian structure of the form $U(1)_Y \times U(1)_B$. We will determine the structure of the entire Lagrangian and fix the counterterms in the one-loop anomalous effective action which are necessary to restore the gauge invariance of the model at quantum level. The analysis that we provide is the generalization of what is discussed in Chap. 1 that was devoted primarily to the analysis of anomalous Abelian models and to the perturbative organization of the corresponding effective action. After determining the axion Lagrangian and after discussing Higgs-axion mixing in this extension of the SM, we will focus our attention on an analysis of the contributions to a simple process ($Z \rightarrow \gamma\gamma$). Our analysis, in this case, aims to provide an example of how the new contributions included in the effective action - in the form of one-loop counterterms that restore unitarity of the effective action - modify the perturbative structure of the process. A detailed phenomenological analysis will be performed in the Chap. 5, since it requires, to be practically useful for searches at the LHC, a very accurate determination of the QCD and electroweak background around the Z/Z' resonance.

2.2 Effective models at low energy: the $SU(3)_C \times SU(2)_W \times U(1)_Y \times U(1)_B$ case

We start by briefly recalling the main features of the mLSOM starting from the expression of the Lagrangian which is given by

$$\begin{aligned}
\mathcal{L} = & - \frac{1}{2}Tr\,[F^G_{\mu\nu}F^{G\mu\nu}] - \frac{1}{2}Tr[\,F^W_{\mu\nu}F^{W\mu\nu}] - \frac{1}{4}F^B_{\mu\nu}F^{B\mu\nu} - \frac{1}{4}F^Y_{\mu\nu}F^{Y\mu\nu} \\
& + |(\partial_\mu + ig_2\frac{\tau^j}{2}W^j_\mu + ig_Y q^Y_u A^Y_\mu + ig_B\frac{q^B_u}{2}B_\mu)H_u|^2 \\
& + |(\partial_\mu + ig_2\frac{\tau^j}{2}W^j_\mu + ig_Y q^Y_d A^Y_\mu + ig_B\frac{q^B_d}{2}B_\mu)H_d|^2 \\
& + \overline{Q}_{Li}\, i\gamma^\mu \left(\partial_\mu + ig_3\frac{\lambda^a}{2}G^a_\mu + ig_2\frac{\tau^j}{2}W^j_\mu + ig_Y q^{(Q_L)}_Y A^Y_\mu + ig_B q^{(Q_L)}_B B_\mu\right) Q_{Li} \\
& + \overline{u}_{Ri}\, i\gamma^\mu \left(\partial_\mu + ig_Y q^{(u_R)}_Y A^Y_\mu + ig_B q^{(u_R)}_B B_\mu\right) u_{Ri} + \overline{d}_{Ri}\, i\gamma^\mu \left(\partial_\mu + ig_Y q^{(d_R)}_Y A^Y_\mu + ig_B q^{(d_R)}_B B_\mu\right) d_{Ri} \\
& + \overline{L}_i\, i\gamma^\mu \left(\partial_\mu + ig_2\frac{\tau^j}{2}W^j_\mu + ig_Y q^{(L)}_Y A^Y_\mu + ig_B q^{(L)}_B B_\mu\right) L_i \\
& + \overline{e}_{Ri}\, i\gamma^\mu \left(\partial_\mu + ig_Y q^{(e_R)}_Y A^Y_\mu + ig_B q^{(e_R)}_B B_\mu\right) e_{Ri} + \overline{\nu}_{Ri}\, i\gamma^\mu \left(\partial_\mu + ig_Y q^{(\nu_R)}_Y A^Y_\mu + ig_B q^{(\nu_R)}_B B_\mu\right) \nu_{Ri} \\
& - \Gamma^d\, \overline{Q}_L H_d d_R - \Gamma^u\, \overline{Q}_L (i\sigma_2 H^*_u) u_R + c.c. \\
& - \Gamma^e\, \overline{L} H_d e_R - \Gamma^\nu\, \overline{L} (i\sigma_2 H^*_u) \nu_R + c.c. \\
& + \frac{1}{2}(\partial_\mu b + M_1 B_\mu)^2 \\
& + \frac{C_{BB}}{M} b F_B \wedge F_B + \frac{C_{YY}}{M} b F_Y \wedge F_Y + \frac{C_{YB}}{M} b F_Y \wedge F_B \\
& + \frac{F}{M} b Tr[F^W \wedge F^W] + \frac{D}{M} b Tr[F^G \wedge F^G] \\
& + d_1 BY \wedge F_Y + d_2 YB \wedge F_B + c_1 \epsilon^{\mu\nu\rho\sigma} B_\mu C^{SU(2)}_{\nu\rho\sigma} + c_2 \epsilon^{\mu\nu\rho\sigma} B_\mu C^{SU(3)}_{\nu\rho\sigma} \\
& + V(H_u, H_d, b),
\end{aligned} \tag{2.1}$$

where we have summed over the $SU(3)$ index $a = 1, 2, ..., 8$, over the $SU(2)$ index $j = 1, 2, 3$ and over the fermion index $i = 1, 2, 3$ denoting a given generation. We have denoted with $F^G_{\mu\nu}$ the field-strength for the gluons and with $F^W_{\mu\nu}$ the field-strength of the weak gauge bosons W_μ. $F^Y_{\mu\nu}$ and $F^B_{\mu\nu}$ are the field-strengths related to the Abelian hypercharge and the extra Abelian gauge boson B, which has anomalous interactions with a typical generation of the Standard Model. The fermions in Eq. (2.1) are either left- or right-handed Dirac spinors f_L, f_R and they fall in the usual $SU(3)_C$ and $SU(2)_W$ representations of the Standard Model. The additional anomalous $U(1)_B$ is accompanied by a shifting Stückelberg axion b. The c_i, $i = 1, 2$, are the coefficients of the Chern-Simons trilinear interactions [1, 69, 70] and we have also introduced a mass term M_1 at tree level for the B gauge boson, by means of the Stückelberg term. As usual, the hypercharge is anomaly-free and its embedding in the so called "D-brane basis" has been discussed extensively in the previous literature [60, 71, 64, 65]. Most of the features of the orientifold construction are preserved, but we don't work with the more general multiple $U(1)$ structure since our goal is to analyze as close as possible this model making contact with direct phenomenological applications, although our results and methods can be promptly generalized to more complex situations.

Before moving to the specific analysis presented in this chapter, some comments are in order concerning the possible range of validity of effective actions of this type and the relation between the value of the cutoff parameter Λ and the Stückelberg mass M_1. This point has been addressed before in great detail in [21]

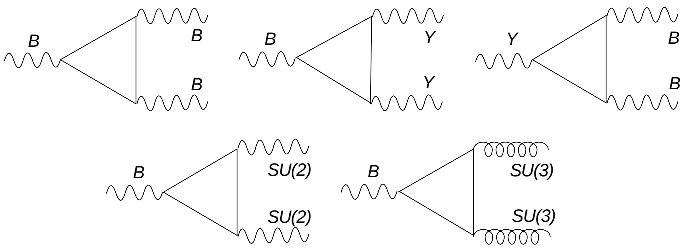

Figure 2.1: Anomalous triangle diagrams for the mLSOM.

and we omit any further elaboration, quoting the result. Lagrangians containing dimension-5 operators in the form of a Wess-Zumino term may have a range of validity constrained by $M_1 \geq g_1 g^2/(64\pi^3) a_n \Lambda$, where g_1 is the coupling at the chiral vertex where the anomaly a_n is assigned and g is the coupling constant of the other two vector-like currents in a typical AVV diagram. More quantitatively, this bound can be reasonably assumed to be of the order of 10^5 GeV, by a power-counting analysis. Notice that the arguments of [21], though based on the picture of "partial decoupling" of the fermion spectrum, in which the pseudoscalar field is the phase of a heavier Higgs, remain fully valid in this context (see [21] for more details). The actual value of M_1 is left undetermined, although in the context of string model building there are suggestions to relate them to specific properties of the compactified extra dimensions (see for instance [60, 64, 65]).

2.3 The Effective Action of the mLSOM with a single anomalous $U(1)$

Having derived the essential components of the classical Lagrangian of the model, now we try to extend our study to the quantum level, determining the anomalous effective action both for the Abelian and the non-Abelian sectors, fixing the D, F and C coefficients in front of the Green-Schwarz terms in Eq. (2.1). Notice that the only anomalous contributions to $\mathcal{S}_{an}$ in the Y-basis before symmetry breaking come from the triangle diagrams depicted in Fig. 2.1. Since hypercharge is anomaly-free, the only relevant non-Abelian anomalies to be canceled are those involving one boson B with two $SU(2)_W$ bosons, or two $SU(3)_C$ bosons, while the Abelian anomalies are those containing three $U(1)$ bosons, with the Y^3 triangle excluded by the hypercharge assignment. These $(BSU(2)SU(2))$ and $(BSU(3)SU(3))$ anomalies must be canceled respectively by Green-Schwarz terms of the kind

$$F\, b\, Tr[F^W \wedge F^W], \qquad D\, b\, Tr[F^G \wedge F^G],$$

with F and D to be fixed by the conditions of gauge invariance. In the Abelian sector we have to focus on the BBB, BYY and YBB triangles which generate anomalous contributions that need to be canceled, respectively, by the Green-Schwarz terms $C_{BB}\, b\, F^B \wedge F^B$, $C_{YY}\, b\, F^Y \wedge F^Y$ and $C_{YB}\, b\, F^Y \wedge F^B$. Denoting by $\mathcal{S}_{YM}$ the anomalous effective action involving the classical non-Abelian terms plus the non-Abelian anomalous diagrams, and with $\mathcal{S}_{ab}$ the analogous Abelian one, the complete anomalous effective action is given by

$$\mathcal{S}_{eff} = \mathcal{S}_0 + \mathcal{S}_{YM} + \mathcal{S}_{ab} \tag{2.2}$$

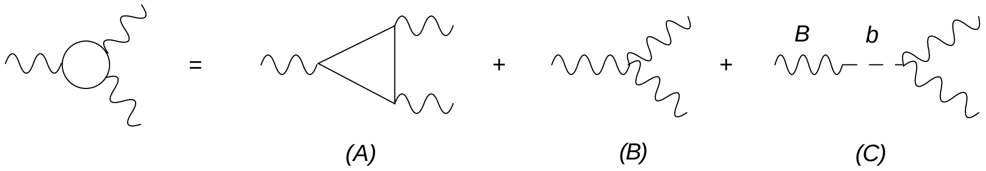

Figure 2.2: Contributions to a three Abelian gauge boson amplitude before the removal of the $B - \partial b$ gauge boson- Stückelberg mixing.

with $\mathcal{S}_0$ being the classical Lagrangian and

$$\mathcal{S}_{YM} = \int dx\, dy\, dz \left(\frac{1}{2!} T^{\lambda\mu\nu,ij}_{BWW}(z,x,y) B^\lambda(z) W^\mu_i(x) W^\nu_j(y) + \frac{1}{2!} T^{\lambda\mu\nu,ab}_{BGG}(z,x,y) B^\lambda(z) G^\mu_a(x) G^\nu_b(y) \right), \tag{2.3}$$

$$\begin{aligned} \mathcal{S}_{ab} = \int dx\, dy\, dz & \left(\frac{1}{3!} T^{\lambda\mu\nu}_{BBB}(z,x,y) B^\lambda(z) B^\mu(x) B^\nu(y) + \frac{1}{2!} T^{\lambda\mu\nu}_{BYY}(z,x,y) B^\lambda(z) Y^\mu(x) Y^\nu(y) \right. \\ & \left. + \frac{1}{2!} T^{\lambda\mu\nu}_{YBB}(z,x,y) Y^\lambda(z) B^\mu(x) B^\nu(y) \right). \end{aligned} \tag{2.4}$$

The corresponding three-point functions, for instance, are given by

$$\begin{aligned} T^{\lambda\mu\nu,\,ij}_{BWW} B^\lambda W^\mu_i W^\nu_j &= \langle 0|T(J^{\lambda,\,f}_B J^{\mu,\,f}_{Wi} J^{\nu,\,f}_{Wj})|0\rangle B^\lambda W^\mu_i W^\nu_j \\ &\equiv \langle 0|T(J^{\lambda,\,f_L}_B J^{\mu,\,f_L}_{Wi} J^{\nu,\,f_L}_{Wj})|0\rangle B^\lambda W^\mu_i W^\nu_j, \end{aligned} \tag{2.5}$$

and similarly for the others. Here we have defined the chiral currents

$$J^{\lambda,f}_B = J^{\lambda,fR}_B + J^{\lambda,fL}_B = -g_B q^{fR}_B \overline{\psi}_f \gamma^\lambda P_R \psi_f - g_B q^{fL}_B \overline{\psi}_f \gamma^\lambda P_L \psi_f. \tag{2.6}$$

The non-Abelian W-current being chiral

$$J^{\mu,f}_{Wi} \equiv J^{\mu,fL}_{Wi} = -g_2 \overline{\psi}_f \gamma^\mu \tau^i P_L \psi_f, \tag{2.7}$$

it forces the other currents in the triangle diagram to be of the same chirality, as shown in Fig. 2.7.

2.4 Three gauge boson amplitudes and gauge-fixing

2.4.1 The non-Abelian sector before symmetry breaking

Before we get into the discussion of the gauge invariance of the model, it is convenient to elaborate on the cancellations of the spurious s-channel poles coming from the gauge-fixing conditions. These are imposed to remove the $\partial b - B$ mixing in the effective action. We will perform our analysis in the basis of the interaction eigenstates since in this basis recovering gauge independence is more straightforward, at least before we enforce symmetry breaking via the Higgs mechanism. The procedure that we follow is to gauge fix the B gauge boson in the symmetric phase by removing the $B - \partial b$ mixing (see Fig. 2.2 (C)), so to derive simple Ward Identities involving only fermionic triangle diagrams and contact trilinear

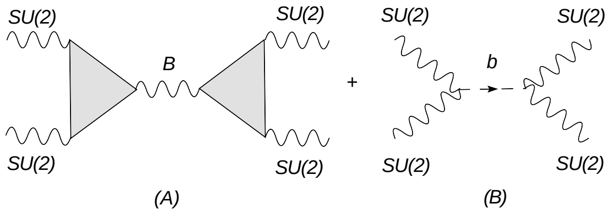

Figure 2.3: Unitarity check in the SU(2) sector for the mLSOM.

interactions with gauge bosons. For this purpose to the Stückelberg term

$$\frac{1}{2}(\partial_\mu b + M_1 B_\mu)^2 \tag{2.8}$$

we add the gauge-fixing term

$$\mathcal{L}_{gf} = -\frac{1}{2}\mathcal{G}_B^2 \tag{2.9}$$

to remove the bilinear mixing, where

$$\mathcal{G}_B = \frac{1}{\sqrt{\xi_B}}\left(\partial\cdot B - \xi_B M_1 b\right), \tag{2.10}$$

with a propagator for the massive B gauge boson separated in a gauge independent part P_0 and a gauge dependent one P_ξ:

$$\frac{-i}{k^2 - M_1^2}\left(g^{\lambda\lambda'} - \frac{k^\lambda k^{\lambda'}}{M_1^2}\right) + \frac{-i}{k^2 - \xi_B M_1^2}\left(\frac{k^\lambda k^{\lambda'}}{M_1^2}\right) \quad = \quad P_0^{\lambda\lambda'} + P_\xi^{\lambda\lambda'}. \tag{2.11}$$

We will briefly illustrate here how the cancellation of the gauge dependence due to b and B exchanges in the s-channel goes in this (minimally) gauge-fixed theory. In the exact phase we have no mixing between all the Y, B, W gauge bosons and the gauge dependence of the B propagator is canceled by the Stückelberg axion. In the broken phase things get more involved, but essentially the pattern continues to hold. In that case the Stückelberg scalar has to be rotated into its physical component χ and the two Goldstones G_Z and $G_{Z'}$ which are linear combinations of G_1^0 and G_2^0. The cancellation of the spurious s-channel poles takes place, in this case, via the combined exchange of the Z propagator and of the corresponding Goldstone mode G_Z. Naturally the GS interaction will be essential for this to happen.

For the moment we simply work in the exact symmetry phase and in the basis of the interaction eigenstates. We gauge fix the action to remove the $B - \partial b$ mixing, but for the rest we set the v.e.v. of the scalars to zero. For definiteness let's consider the process $WW \to WW$ mediated by a B boson as shown in Fig. 2.3. We denote by a bold-faced $\mathbf{V}$ the BWW vertex, constructed so to have gauge invariance on the W-lines. This vertex, as we are going to discuss next, requires a generalized CS counterterm to have such a property on the W-lines. Gauge invariance on the B-line, instead, which is clearly necessary to remove the gauge dependence in the gauge fixed action, is obtained at a diagrammatical level by the the axion exchange (Fig. 2.3). The expressions of the two diagrams are

$$\begin{aligned} A_\xi + B_\xi \quad &= \quad \frac{-i}{k^2 - \xi_B M_1^2}\frac{1}{M_1^2}\left(k^\lambda \mathbf{V}_{BWW}^{\lambda\mu\nu}(-k_1,-k_2)\right)\left(k^{\lambda'}\mathbf{V}_{BWW}^{\lambda'\mu'\nu'}(k_1,k_2)\right)\left(g_B g_2^2 D_B^{(L)}\right)^2 \\ &+ 4\times\left(\frac{4F}{M}\right)^2\left(\frac{i}{k^2 - \xi_B M_1^2}\right)\epsilon^{\mu\nu\alpha\beta}k_1^\alpha k_2^\beta\,\epsilon^{\mu'\nu'\alpha'\beta'}k_1^{\alpha'}k_2^{\beta'}. \end{aligned} \tag{2.12}$$

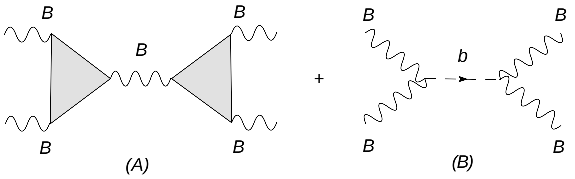

Figure 2.4: Unitarity check in the Abelian sector for the mLSOM.

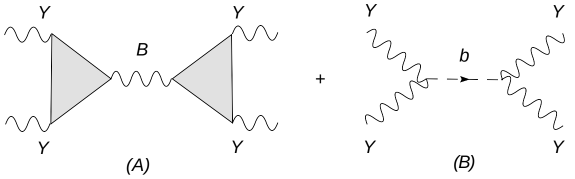

Figure 2.5: Unitarity check in Abelian sector for the mLSOM.

Using the equations for the anomalies and the correct value for the Green-Schwarz coefficient F given in Eq. (2.60) (determined in the next section), we obtain

$$\begin{aligned} A_\xi + B_\xi &= \frac{-i}{k^2-\xi_B M_1^2}\frac{1}{M_1^2}\Big(-4a_n \epsilon k_1 k_2\Big)\Big(4a_n \epsilon' k_1' k_2'\Big)\Big(g_B g_2^2 D_B^{(L)}\Big)^2 \\ &+ \frac{64}{M^2}\frac{M^2}{M_1^2}\Big(i g_B g_2^2 \frac{a_n}{2} D_B^{(L)}\Big)^2\Big(\frac{i}{k^2-\xi_B M_1^2}\Big)\epsilon k_1 k_2 \epsilon' k_1' k_2' \end{aligned} \tag{2.13}$$

so that the cancellation is easily satisfied. [2] The treatment of the $SU(3)$ sector is similar and we omit it.

2.4.2 The Abelian sector before symmetry breaking

In the Abelian sector the procedure is similar. For instance, to test the cancellation of the gauge parameter ξ_B in a process $BB \to BB$ mediated by a B gauge boson we sum the two gauge dependent contributions coming from the diagrams in Fig. 2.4 (we consider only the gauge dependent part of the s-channel exchange diagrams)

$$\begin{aligned} A_\xi + B_\xi &= \frac{-i}{k^2-\xi_B M_1^2}\frac{1}{M_1^2}\Big(4\,k^\lambda \Delta^{\lambda\mu\nu}_{\mathbf{AAA}}(-k_1,-k_2)\Big)\Big(4\,k^{\lambda'} \Delta^{\lambda'\mu'\nu'}_{\mathbf{AAA}}(k_1,k_2)\Big)\left(g_B^3 D_{BBB}\right)^2 \\ &+ 4\times\left(\frac{4}{M}C_{BB}\right)^2 \frac{i}{k^2-\xi_B M_1^2}\,\epsilon k_1 k_2\,\epsilon' k_1' k_2', \end{aligned} \tag{2.14}$$

and cancellation of the gauge dependences implies that the following identity must hold

$$\frac{16}{M_1^2}\left(\frac{a_n}{3}\right)^2\left(g_B^3 D_{BBB}\right)^2 + 4\times\left(\frac{4}{M}C_{BB}\right)^2 = 0, \tag{2.15}$$

which can be easily shown to be true after substituting the value of the GS coefficient given in relation (2.75). In Fig. 2.5 we have depicted the anomalous triangle diagram BYY (A) which has to be canceled by the Green-Schwarz term $\frac{C_{YY}}{M} b F^Y \wedge F^Y$, that generates diagram (B). In this case the two diagrams give

$$A_\xi + B_\xi = \frac{-i}{k^2-\xi_B M_1^2}\frac{1}{M_1^2}\Big(k^\lambda \mathbf{V}^{\lambda\mu\nu}_{BYY}(-k_1,-k_2)\Big)\Big(k^{\lambda'} \mathbf{V}^{\lambda'\mu'\nu'}_{BYY}(k_1,k_2)\Big)\left(g_B g_Y^2 D_{BYY}\right)^2$$

---

[2] For brevity we have adopted the notation $\epsilon k_1 k_2 = \epsilon^{\mu\mu\rho\sigma} k_{1\rho} k_{2\sigma}$.

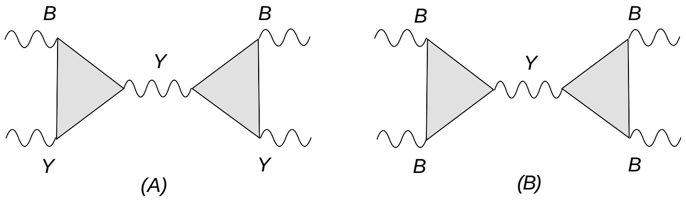

Figure 2.6: Unitarity check in the Abelian sector for the mLSOM.

$$+4\times\left(\frac{4}{M}C_{YY}\right)^2\frac{i}{k^2-\xi_B M_1^2}\,\epsilon k_1 k_2\,\epsilon' k_1' k_2'. \tag{2.16}$$

The condition of unitarity of the amplitude requires the validity of the identity

$$\frac{16}{M_1^2}\,{a_n}^2\left(g_B g_Y^2 D_{BYY}\right)^2+4\times\left(\frac{4}{M}C_{YY}\right)^2=0, \tag{2.17}$$

which can be easily checked substituting the value of the GS coefficient C_{YY} given in relation (2.76). We will derive the expressions of these coefficients and the factors of all the other counterterms in the next section. The gauge dependences appearing in the diagrams shown in Fig. 2.6 are analyzed in a similar way and we omit repeating the previous steps, but it should be obvious by now how the perturbative expansion is organized in terms of tree-level vertices and one-loop counterterms, and how gauge invariance is checked at higher orders when the propagators of the B gauge boson and of the axion b are both present. Notice that in the exact phase the axion b is not coupled to the fermions and the pattern of cancellations to ensure gauge independence, in this specific case, is simplified. At this point we pause to make some comments. The mixed anomalies analyzed above involve a non-anomalous Abelian gauge boson and the remaining gauge interactions (Abelian/non-Abelian). To be specific, in our model with a single non-anomalous $U(1)$, which is the hypercharge $U(1)_Y$ gauge group, these mixed anomalies are those involving triangle diagrams with the Y and B generators or the B accompanied by the non-Abelian sector. Consider, for instance, the BYY triangle, which appears in the $YB\to YB$ amplitude. There are two options that we can follow. Either we require that the corresponding traces of the generators over each generation vanish identically

$$Tr[q_Y^2 q_B]=-2\left(-\frac{1}{2}\right)^2 q_B^{(L)}+(-1)^2 q_B^{(e_R)}+3\left[-2\left(\frac{1}{6}\right)^2 q_B^{(Q_L)}+\left(\frac{2}{3}\right)^2 q_B^{(u_R)}+\left(-\frac{1}{3}\right)^2 q_B^{(d_R)}\right]=0,$$

which can be viewed as a specific condition on the charges of the model or, if this is not the case, we require that suitable one-loop counterterms balance the anomalous gauge variation. We are allowed, in other words, to fix the two divergent invariant amplitudes of the triangle diagram so that the corresponding Ward Identities for the BYY vertex and similar anomalous vertices are satisfied. This is a condition on the parameterization of the Feynman vertex rather than on the charges and is, in principle, allowed. It is not necessary to have a specific determination of the charges for this to occur, as far as the counterterms are fixed accordingly. For instance, in the Abelian sector the diagrams in question are

$$\begin{aligned}
YB\to YB \text{ mediated by Y} &\quad\propto\quad Tr[q_Y^2 q_B]\\
YY\to YY\text{mediated by B} &\quad\propto\quad Tr[q_Y^2 q_B]\\
BB\to BB \text{ mediated by Y} &\quad\propto\quad Tr[q_Y q_B^2]
\end{aligned}$$

$$YB \rightarrow YB \text{ mediated by B} \quad \propto \quad Tr[q_Y q_B^2].$$

In the mLSOM these traces are, in general, non vanishing and therefore we need to introduce defining Ward Identities to render the effective action anomaly free.

2.5 Ward Identities, Green-Schwarz and Chern-Simons counterterms in the Stückelberg phase

Having discussed the structure of the theory in the basis of the interaction eigenstates, we come now to identify the coefficients needed to enforce cancellation of the anomalies in the one-loop effective action. In the basis of the physical gauge bosons we will be dropping, with this choice, a gauge dependent ($B\partial b$ mixing) term that is vanishing for physical polarizations. At the same time, for exchanges of virtual gauge bosons, the gauge dependence of the corresponding propagators is canceled by the associated Goldstone exchanges.

Starting from the non-Abelian contributions, the BWW amplitude, we separate the charge/coupling constant dependence of a given diagram from the rest of its parametric structure $\mathbf{T}$ using, in the $SU(2)$ case, the relations

$$\begin{aligned}
T^{\lambda\mu\nu,ij}_{BWW} B^{\lambda} W^{\mu}_{i} W^{\nu}_{j} &= g_B g_2^2 \sum_{i,j} Tr[\tau_i \tau_j] \frac{1}{8} Tr[q_B^L]\, \mathbf{T}^{\lambda\mu\nu} B^{\lambda} W^{\mu}_{i} W^{\nu}_{j} \\
&= \frac{1}{2} g_B g_2^2 \sum_{i} D_B^{(L)}\, \mathbf{T}^{\lambda\mu\nu} B^{\lambda} W^{\mu}_{i} W^{\nu}_{i},
\end{aligned} \tag{2.18}$$

where $D_B^{(L)} = \frac{1}{8} Tr[q_B^L] = -\frac{1}{8} \sum_f q_B^{fL}$ and $\mathbf{T}^{\lambda\mu\nu}$ is the three-point function in configuration space, with all the couplings and the charges factored out, symmetrized in $\mu\nu$. Similarly, for the coupling of B to the gluons we obtain

$$\begin{aligned}
T^{\lambda\mu\nu,ab}_{BGG} B^{\lambda} G^{\mu}_{a} G^{\nu}_{b} &= g_B g_3^2 \sum_{a,b} Tr[T_a T_b] \frac{1}{8} Tr[q_B^Q]\, \mathbf{T}^{\lambda\mu\nu} B^{\lambda} G^{\mu}_{a} G^{\nu}_{b} \\
&= \frac{1}{2} g_B g_3^2 \sum_{a} D_B^{(Q)}\, \mathbf{T}^{\lambda\mu\nu} B^{\lambda} G^{\mu}_{a} G^{\nu}_{a},
\end{aligned} \tag{2.19}$$

having defined $D_B^{(Q)} = \frac{1}{8} Tr[q_B^Q] = \frac{1}{8} \sum_Q [q_B^{Q_R} - q_B^{Q_L}]$, while the Abelian triangle diagrams are given by

$$T^{\lambda\mu\nu}_{BBB} B^{\lambda} B^{\mu} B^{\nu} = g_B^3 \frac{1}{8} Tr[q_B^3]\, \mathbf{T}^{\lambda\mu\nu} B^{\lambda} B^{\mu} B^{\nu} = g_B^3\, D_{BBB}\, \mathbf{T}^{\lambda\mu\nu} B^{\lambda} B^{\mu} B^{\nu}, \tag{2.20}$$

$$\begin{aligned}
T^{\lambda\mu\nu}_{BYY} B^{\lambda} Y^{\mu} Y^{\nu} &= g_B g_Y^2 \frac{1}{8} Tr[q_B q_Y^2]\, \mathbf{T}^{\lambda\mu\nu} B^{\lambda} Y^{\mu} Y^{\nu} \\
&= g_B g_Y^2\, D_{BYY}\, \mathbf{T}^{\lambda\mu\nu} B^{\lambda} Y^{\mu} Y^{\nu},
\end{aligned} \tag{2.21}$$

$$\begin{aligned}
T^{\lambda\mu\nu}_{YBB} Y^{\lambda} B^{\mu} B^{\nu} &= g_Y g_B^2 \frac{1}{8} Tr[q_Y q_B^2]\, \mathbf{T}^{\lambda\mu\nu} Y^{\lambda} B^{\mu} B^{\nu} \\
&= g_Y g_B^2\, D_{YBB}\, \mathbf{T}^{\lambda\mu\nu} Y^{\lambda} B^{\mu} B^{\nu},
\end{aligned} \tag{2.22}$$

with the following definitions for the traces

$$D_{BBB} = \frac{1}{8} Tr[q_B^3] = \frac{1}{8} \sum_f \left[(q_B^{fR})^3 - (q_B^{fL})^3 \right], \tag{2.23}$$

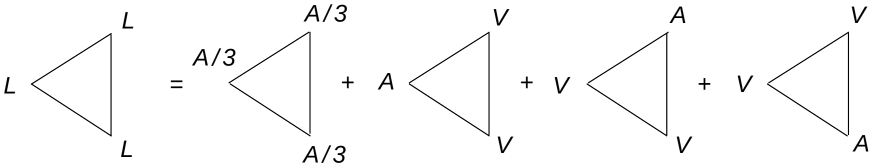

Figure 2.7: All the anomalous contributions to a triangle diagram in the non-Abelian sector in the massless fermion case.

$$
\begin{aligned}
D_{BYY} &= \frac{1}{8}Tr[q_B q_Y^2] = \frac{1}{8}\sum_f \left[q_B^{fR}(q_Y^{fR})^2 - q_B^{fL}(q_Y^{fL})^2\right], && (2.24)\\
D_{YBB} &= \frac{1}{8}Tr[q_Y q_B^2] = \frac{1}{8}\sum_f \left[q_Y^{fR}(q_B^{fR})^2 - q_Y^{fL}(q_B^{fL})^2\right]. && (2.25)
\end{aligned}
$$

The $\mathbf{T}$ vertex is given by the usual combination of vector and axial-vector components

$$
\mathbf{T}^{\lambda\mu\nu} = T^{\lambda\mu\nu}_{\mathbf{AAA}} + T^{\lambda\mu\nu}_{\mathbf{AVV}} + T^{\lambda\mu\nu}_{\mathbf{VAV}} + T^{\lambda\mu\nu}_{\mathbf{VVA}}, \qquad (2.26)
$$

and we denote by $\mathbf{\Delta}(k_1, k_2)$ its expression in momentum space

$$
(2\pi)^4\delta(k - k_1 - k_2)\mathbf{\Delta}^{\lambda\mu\nu}(k_1, k_2) = \int dx\, dy\, dz\, e^{ik_1\cdot x + ik_2\cdot y - ik\cdot z}\, \mathbf{T}^{\lambda\mu\nu}(z, x, y). \qquad (2.27)
$$

We denote similarly with $\mathbf{\Delta}^{\lambda\mu\nu}_{\mathbf{AVV}}, \mathbf{\Delta}^{\lambda\mu\nu}_{\mathbf{VAV}}, \mathbf{\Delta}^{\lambda\mu\nu}_{\mathbf{VVA}}$ the momentum space expressions of the corresponding x-space vertices $\mathbf{T}^{\lambda\mu\nu}_{\mathbf{AVV}}, \mathbf{T}^{\lambda\mu\nu}_{\mathbf{VVA}}, \mathbf{T}^{\lambda\mu\nu}_{\mathbf{VAV}}$ respectively. As illustrated in Fig. 2.7 and Fig. 2.8, the complete structure of $\mathbf{T}$ is given by

$$
\begin{aligned}
\mathbf{\Delta}^{\lambda\mu\nu}(k_1, k_2) &= \frac{1}{3}\left[\Delta^{\lambda\mu\nu}(-1/2, k_1, k_2) + \Delta^{\mu\nu\lambda}(-1/2, k_2, -k) + \Delta^{\nu\lambda\mu}(-1/2, -k, k_1)\right]\\
&\quad + \Delta^{\lambda\mu\nu}(-1/2, k_1, k_2) + \Delta^{\mu\nu\lambda}(-1/2, k_2, -k) + \Delta^{\nu\lambda\mu}(-1/2, -k, k_1)\\
&= \frac{4}{3}\left[\Delta^{\lambda\mu\nu}(-1/2, k_1, k_2) + \Delta^{\mu\nu\lambda}(-1/2, k_2, -k) + \Delta^{\nu\lambda\mu}(-1/2, -k, k_1)\right]\\
&= 4\Delta^{\lambda\mu\nu}_{\mathbf{AAA}}, && (2.28)
\end{aligned}
$$

where we have used the relation between the $\mathbf{\Delta_{AAA}}$ (bold-faced) vertex and the usual Δ vertex, which is of the form $\mathbf{AVV}$. Notice that

$$
\begin{aligned}
\mathbf{\Delta}^{\lambda\mu\nu}_{\mathbf{AVV}} &= \Delta^{\lambda\mu\nu}(-1/2, k_1, k_2),\\
\mathbf{\Delta}^{\mu\nu\lambda}_{\mathbf{AVV}} &= \Delta^{\mu\nu\lambda}(-1/2, k_2, -k),\\
\mathbf{\Delta}^{\nu\lambda\mu}_{\mathbf{AVV}} &= \Delta^{\nu\lambda\mu}(-1/2, -k, k_1), && (2.29)
\end{aligned}
$$

are the usual vertices with conserved vector current (CVC) on two lines and the anomaly on a single axial vertex.

The $\mathbf{AAA}$ vertex is constructed by symmetrizing the distribution of the anomaly on each of the three chiral currents, which is the content of (2.28). The same vertex can be obtained from the basic $\mathbf{AVV}$ vertex by a suitable shift, with $\beta = 1/6$, and then repeating the same procedure on the other indices and external momenta, with a cyclic permutation. We obtain

$$
\Delta^{\lambda\mu\nu}_{\mathbf{AAA}}(1/6, k_1, k_2) = \Delta^{\lambda\mu\nu}(-1/2, k_1, k_2) - \frac{i}{4\pi^2}\frac{2}{3}\epsilon^{\lambda\mu\nu\sigma}(k_1 - k_2)_\sigma \qquad (2.30)
$$

and its corresponding anomaly equations are given by

$$\begin{aligned}
k_\lambda \Delta^{\lambda\mu\nu}_{\mathbf{AAA}}(1/6, k_1, k_2) &= \frac{a_n}{3}\epsilon^{\mu\nu\alpha\beta}k_{1\alpha}k_{2\beta} \\
k_{1\mu} \Delta^{\lambda\mu\nu}_{\mathbf{AAA}}(1/6, k_1, k_2) &= \frac{a_n}{3}\epsilon^{\lambda\nu\alpha\beta}k_{1\alpha}k_{2\beta} \\
k_{2\nu} \Delta^{\lambda\mu\nu}_{\mathbf{AAA}}(1/6, k_1, k_2) &= \frac{a_n}{3}\epsilon^{\lambda\mu\alpha\beta}k_{2\alpha}k_{1\beta},
\end{aligned} \tag{2.31}$$

typical of a symmetric distribution of the anomaly.

These identities are obtained from the general shift-relation

$$\Delta^{\lambda\mu\nu}(\beta', k_1, k_2) = \Delta^{\lambda\mu\nu}(\beta, k_1, k_2) + \frac{i}{4\pi^2}(\beta - \beta')\epsilon^{\lambda\mu\nu\sigma}(k_1 - k_2)_\sigma. \tag{2.32}$$

Vertices with conserved axial currents (CAC) can be related to the symmetric **AAA** vertex in a similar way

$$\Delta^{\lambda\mu\nu}_{\mathbf{AAA}}(+1/6, k_1, k_2) = \{\Delta^{\lambda\mu\nu}(+1/2, k_1, k_2)\}_{CAC} + \frac{i}{4\pi^2}\,\frac{1}{3}\,\epsilon^{\lambda\mu\nu\sigma}(k_1 - k_2)_\sigma. \tag{2.33}$$

At this point we are ready to introduce the complete vertices for this model, which are given by the amplitude (2.27) with the addition of the corresponding Chern-Simons counterterms, were required. These will be determined later in this section by imposing the conservation of the $SU(2)$, $SU(3)$ and Y gauge currents. Following this definition for all the anomalous vertices, the amplitudes can then be written as

$$\begin{aligned}
\mathcal{V}^{\lambda\mu\nu,\,aa}_{BGG}B^\lambda G^\mu_a G^\nu_a &= \frac{1}{2}g_B g_3^2 D_B^{(Q)}\mathbf{T}^{\lambda\mu\nu}B^\lambda G^\mu_a G^\nu_a + c_2\epsilon^{\mu\nu\rho\sigma}B_\mu C^{SU(3)}_{\nu\rho\sigma} \\
\mathcal{V}^{\lambda\mu\nu,\,ii}_{BWW}B^\lambda W^\mu_i W^\nu_i &= \frac{1}{2}g_B g_2^2 D_B^{(L)}\mathbf{T}^{\lambda\mu\nu}B^\lambda W^\mu_i W^\nu_i + c_1\epsilon^{\mu\nu\rho\sigma}B_\mu C^{SU(2)}_{\nu\rho\sigma} \\
\mathcal{V}^{\lambda\mu\nu}_{BYY}B^\lambda Y^\mu Y^\nu &= g_B g_Y^2 D_{BYY}\mathbf{T}^{\lambda\mu\nu}B^\lambda Y^\mu Y^\nu + d_1 BY\wedge F_Y \\
\mathcal{V}^{\lambda\mu\nu}_{YBB}Y^\lambda B^\mu B^\nu &= g_Y g_B^2 D_{YBB}\mathbf{T}^{\lambda\mu\nu}Y^\lambda B^\mu B^\nu + d_2 YB\wedge F_B, \\
\mathcal{V}^{\lambda\mu\nu}_{BBB}B^\lambda B^\mu B^\nu &= g_B^3 D_{BBB}\mathbf{T}^{\lambda\mu\nu}B^\lambda B^\mu B^\nu
\end{aligned} \tag{2.34}$$

which are the anomalous vertices of the effective action, corrected when necessary by suitable CS interactions in order to conserve all the gauge currents at one-loop.

Before we proceed with our analysis, which has the goal to determine explicitly the counterterms in each of these vertices, we pause for some considerations. It is clear that the scheme that we have followed in order to determine the structure of the vertices of the effective action has been to assign the anomaly only to the chiral vertices and to impose conservation of the vector current. There are regularization schemes in the literature that enforce this principle, the most famous one being dimensional regularization with the t'Hooft Veltman prescription for γ_5 (see also the discussion in Chap. 1). In this scheme the anomaly is equally distributed for vertices of the form **AAA** and is assigned only to the axial-vector vertex in triangles of the form **AVV** and similar. Diagrams of the form **AAV** are zero by Furry's theorem, being equivalent to **VVV**.

We could also have proceeded in a different way, for instance by defining each $\mathcal{V}$, for instance $\mathcal{V}_{BYY}$, to have an anomaly only on the B vertex and not on the Y vertices, even if Y has both a vector and an axial-vector components at tree level and is, indeed, a chiral current. This implies that at one-loop the chiral projector has to be moved from the Y to to the B vertex "by hand", no matter if it appears on the Y current or on the B current, rendering the Y current effectively vector-like at one-loop. This is also what a CS term does. In both cases we are anyhow bond to define separately the one-loop vertices as new entities, unrelated to the tree level currents. However, having explicit Chern-Simons counterterms renders the treatment compatible with dimensional regularization in the t'Hooft-Veltman prescription. It is clear, however, that one way or the other, the quantum action is not fixed at classical level since the counterterms are related to quantum effects and the corresponding Ward Identities, which force the cancellation of the anomaly to take place in a completely new way respect to the SM case, are indeed *defining conditions* on the theory.

Having clarified this point, we return to the determination of the gauge invariance conditions for our anomalous vertices.

Under B-gauge transformations we have the following variations (singlet anomalies) of the effective action

$$\frac{1}{2!}\delta_B < T_{BWW}BWW >= i\frac{g_B g_2^2}{2!}\,\frac{4}{3}a_n\,\frac{1}{4}\langle\theta_B F_i^W \wedge F_j^W\rangle\, Tr[\tau^i\tau^j]\, D_B^{(L)}, \tag{2.35}$$

$$\frac{1}{2!}\delta_B < T_{BGG}BGG >= i\frac{g_B g_3^2}{2!}\,\frac{4}{3}a_n\,\frac{1}{4}\langle\theta_B F_a^G \wedge F_b^G\rangle\, Tr[T^a T^b]\, D_B^{(Q)}, \tag{2.36}$$

and with the normalization given by

$$Tr[\tau^i\tau^j] = \frac{1}{2}\delta^{ij} \qquad Tr[T^a T^b] = \frac{1}{2}\delta^{ab} \tag{2.37}$$

we obtain

$$\begin{aligned}
\frac{1}{2!}\delta_B < T_{BSU(2)SU(2)}BWW > &= i\frac{g_B g_2^2}{2!}\,\frac{a_n}{6}\,\langle\theta_B F_i^W \wedge F_i^W\rangle D_B^{(L)}, &(2.38)\\
\frac{1}{2!}\delta_B < T_{BSU(3)SU(3)}BGG > &= i\frac{g_B g_3^2}{2!}\,\frac{a_n}{6}\,\langle\theta_B F_a^G \wedge F_a^G\rangle D_B^{(Q)}. &(2.39)
\end{aligned}$$

Note, in particular, that the covariantization of the anomalous contributions requires the entire non-Abelian field-strengths $F^W_{i,\,\mu\nu}$ and $F^G_{a,\,\mu\nu}$

$$\begin{aligned}
F^W_{i,\,\mu\nu} &= \partial_\mu W^i_\nu - \partial_\nu W^i_\mu - g_2\varepsilon_{ijk}W^j_\mu W^k_\nu = \hat{F}^W_{i,\,\mu\nu} - g_2\varepsilon_{ijk}W^j_\mu W^k_\nu &(2.40)\\
F^G_{a,\,\mu\nu} &= \partial_\mu G^a_\nu - \partial_\nu G^a_\mu - g_3 f_{abc}G^b_\mu G^c_\nu = \hat{F}^G_{a,\,\mu\nu} - g_3 f_{abc}G^b_\mu G^c_\nu. &(2.41)
\end{aligned}$$

The covariantization of the right-hand-side (r.h.s.) of the anomaly equations takes place via higher-order corrections, involving correlators with more external gauge lines. It is well known, though, that the cancellation of the anomalies in these higher-order non-Abelian diagrams (in d=4) is only related to the triangle diagram (see [40]). Under the non-Abelian gauge transformations we have the following variations

$$\begin{aligned}
\frac{1}{2!}\delta_{SU(2)}\langle T_{BWW}BWW\rangle &= i\frac{g_B g_2^2}{2!}\frac{8}{3}a_n\frac{1}{4}\langle F^B \wedge Tr[\theta\hat{F}^W]\rangle D_B^{(L)} &(2.42)\\
\frac{1}{2!}\delta_{SU(3)}\langle T_{BGG}BGG\rangle &= i\frac{g_B g_3^2}{2!}\frac{8}{3}a_n\frac{1}{4}\langle F^B \wedge Tr[\vartheta\hat{F}^G]\rangle D_B^{(Q)}, &(2.43)
\end{aligned}$$

where the "hat" field-strengths $\hat{F}^W$ and $\hat{F}^G$ refer to the Abelian part of the non-Abelian field-strengths

W and G. Introducing the notation

$$\begin{aligned} Tr[\theta \hat{F}^W] &= Tr[\tau^i \tau^j]\theta_i \hat{F}^W_j = \frac{1}{2}\theta_i \hat{F}^W_i \qquad i,j=1,2,3 && (2.44)\\ Tr[\vartheta \hat{F}^G] &= Tr[T^a T^b]\vartheta_a \hat{F}^G_b = \frac{1}{2}\vartheta_a \hat{F}^G_a \qquad a,b=1,2,..,8 && (2.45)\end{aligned}$$

the expressions of the variations become

$$\begin{aligned} \frac{1}{2!}\delta_{SU(2)}\langle T_{BWW} BWW\rangle &= i\frac{g_B g_2^2}{2!}\frac{a_n}{3}\langle \theta_i F^B \wedge \hat{F}^W_i\rangle D_B^{(L)} && (2.46)\\ \frac{1}{2!}\delta_{SU(3)}\langle T_{BGG} BGG\rangle &= i\frac{g_B g_3^2}{2!}\frac{a_n}{3}\langle \vartheta_a F^B \wedge \hat{F}^G_a\rangle D_B^{(Q)}. && (2.47)\end{aligned}$$

We have now to introduce the Chern-Simons counterterms for the non-Abelian gauge variations

$$\mathcal{S}^{CS}_{non-ab} = \mathcal{S}^{CS}_{BWW} + \mathcal{S}^{CS}_{BGG} = c_1\langle \epsilon^{\mu\nu\rho\sigma} B_\mu C^{SU(2)}_{\nu\rho\sigma}\rangle + c_2\langle \epsilon^{\mu\nu\rho\sigma} B_\mu C^{SU(3)}_{\nu\rho\sigma}\rangle, \tag{2.48}$$

with the non-Abelian CS forms given by

$$\begin{aligned} C^{SU(2)}_{\mu\nu\rho} &= \frac{1}{6}\left[W^i_\mu \left(F^W_{i,\,\nu\rho} + \frac{1}{3}\,g_2\,\varepsilon^{ijk} W^j_\nu W^k_\rho\right) + cyclic\right], && (2.49)\\ C^{SU(3)}_{\mu\nu\rho} &= \frac{1}{6}\left[G^a_\mu \left(F^G_{a,\,\nu\rho} + \frac{1}{3}\,g_3\,f^{abc} G^b_\nu G^c_\rho\right) + cyclic\right], && (2.50)\end{aligned}$$

whose variations under non-Abelian gauge transformations are

$$\begin{aligned} \delta_{SU(2)} C^{SU(2)}_{\mu\nu\rho} &= \frac{1}{6}\left[\partial_\mu \theta^i\,(\hat{F}^W_{i,\,\nu\rho}) + cyclic\right], && (2.51)\\ \delta_{SU(3)} C^{SU(3)}_{\mu\nu\rho} &= \frac{1}{6}\left[\partial_\mu \vartheta^a\,(\hat{F}^G_{a,\,\nu\rho}) + cyclic\right]. && (2.52)\end{aligned}$$

The variations of the Chern-Simons counterterms then become

$$\begin{aligned} \delta_{SU(2)}\mathcal{S}^{CS}_{BWW} &= \frac{c_1}{2}\frac{1}{2}\langle \theta^i F^B \wedge \hat{F}^W_i\rangle && (2.53)\\ \delta_{SU(3)}\mathcal{S}^{CS}_{BGG} &= \frac{c_2}{2}\frac{1}{2}\langle \vartheta^a F^B \wedge \hat{F}^G_a\rangle, && (2.54)\end{aligned}$$

and we can choose the coefficients in front of the CS counterterms to obtain anomaly cancellations for the non-Abelian contributions

$$c_1 = -i g_B g_2^2 \frac{2}{3} a_n D_B^{(L)} \qquad c_2 = -i g_B g_3^2 \frac{2}{3} a_n D_B^{(Q)}. \tag{2.55}$$

The variations under B-gauge transformations for the related CS counterterms are then given by

$$\begin{aligned} \delta_B\mathcal{S}^{CS}_{BWW} &= -\frac{c_1}{2}\frac{1}{2}\langle \theta_B F^W_i \wedge F^W_i\rangle && (2.56)\\ \delta_B\mathcal{S}^{CS}_{BGG} &= -\frac{c_2}{2}\frac{1}{2}\langle \theta_B F^G_a \wedge F^G_a\rangle, && (2.57)\end{aligned}$$

where the coefficients c_i are given in (2.55). The variations under the B-gauge transformations for the $SU(2)$ and $SU(3)$ Green-Schwarz counterterms are respectively given by

$$\frac{F}{M}\,\delta_B\langle\, b\, Tr[F^W \wedge F^W]\,\rangle = -F\frac{M_1}{M}\frac{1}{2}\langle \theta_B F^W_i \wedge F^W_i\rangle, \tag{2.58}$$

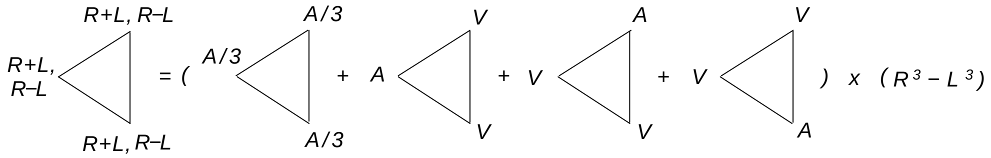

Figure 2.8: All the anomalous contributions to a triangle diagram in the Abelian sector for generic vector/axial-vector trilinear interactions in the massless fermion case.

$$\frac{D}{M}\,\delta_B\langle\, b\,Tr[F^G\wedge F^G]\,\rangle \;=\; -D\frac{M_1}{M}\frac{1}{2}\langle\theta_B F^G_a\wedge F^G_a\rangle, \tag{2.59}$$

and the cancellation of the anomalous contributions coming from the B-gauge transformations determines F and D as

$$F=\frac{M}{M_1}ig_B g_2^2\,\frac{a_n}{2}\,D_B^{(L)},\qquad D=\frac{M}{M_1}ig_B g_3^2\,\frac{a_n}{2}\,D_B^{(Q)}. \tag{2.60}$$

There are some comments to be made concerning the generalized CS terms responsible for the cancellation of the mixed anomalies. These terms, in momentum space, generate standard trilinear CS interactions, whose momentum structure is exactly the same as that due to the Abelian ones (see the appendix of Chap. 1 for more details), plus additional quadrilinear (contact) gauge interactions. These will be neglected in our analysis since we will be focusing in the next sections on the characterization of neutral tri-linear interactions. In processes such as $Z\rightarrow\gamma\gamma\gamma$ they re-distribute the anomaly appropriately in higher-point functions.

For the Abelian part $\mathcal{S}_{ab}$ of the effective action we first focus on gauge variations on B, obtaining

$$\frac{1}{3!}\delta_B\langle T^{\lambda\mu\nu}_{BBB}B^\lambda(z)B^\mu(x)B^\nu(y)\rangle = i\frac{g_B^3}{3!}\frac{4}{3}a_n\frac{3}{4}\langle F^B\wedge F^B\theta_B\rangle\, D_{BBB}, \tag{2.61}$$

$$\frac{1}{2!}\delta_B\langle T^{\lambda\mu\nu}_{BYY}B^\lambda(z)Y^\mu(x)Y^\nu(y)\rangle = i\frac{g_B g_Y^2}{2!}\frac{4}{3}a_n\frac{1}{4}\langle F^Y\wedge F^Y\theta_B\rangle\, D_{BYY}, \tag{2.62}$$

$$\frac{1}{2!}\delta_B\langle T^{\lambda\mu\nu}_{YBB}Y^\lambda(z)B^\mu(x)B^\nu(y)\rangle = i\frac{g_Y g_B^2}{2!}\frac{4}{3}a_n\frac{2}{4}\langle F^Y\wedge F^B\theta_B\rangle\, D_{YBB}, \tag{2.63}$$

and variations for Y that give

$$\frac{1}{2!}\delta_Y\langle T^{\lambda\mu\nu}_{BYY}B^\lambda(z)Y^\mu(x)Y^\nu(y)\rangle = i\frac{g_B g_Y^2}{2!}\frac{4}{3}a_n\frac{2}{4}\langle F^Y\wedge F^B\theta_Y\rangle\, D_{BYY}, \tag{2.64}$$

$$\frac{1}{2!}\delta_Y\langle T^{\lambda\mu\nu}_{YBB}Y^\lambda(z)B^\mu(x)B^\nu(y)\rangle = i\frac{g_Y g_B^2}{2!}\frac{4}{3}a_n\frac{1}{4}\langle F^B\wedge F^B\theta_Y\rangle\, D_{YBB}. \tag{2.65}$$

Also in this case we introduce the corresponding Abelian Chern-Simons counterterms

$$\mathcal{S}_{ab}^{CS}=\mathcal{S}_{BYY}^{CS}+\mathcal{S}_{YBB}^{CS}=d_1\langle BY\wedge F_Y\rangle+d_2\langle YB\wedge F_B\rangle \tag{2.66}$$

whose variations are given by

$$\begin{align}
\delta_Y \mathcal{S}^{CS}_{BYY} &= \frac{d_1}{2} \langle \theta_Y F^B \wedge F^Y \rangle, \tag{2.67}\\
\delta_Y \mathcal{S}^{CS}_{YBB} &= -\frac{d_2}{2} \langle \theta_Y F^B \wedge F^B \rangle, \tag{2.68}
\end{align}$$

and we can fix their coefficients so to obtain the cancellation of the Y-anomaly

$$d_1 = -i g_B g_Y^2 \frac{2}{3} a_n D_{BYY} \qquad d_2 = i g_Y g_B^2 \frac{a_n}{3} D_{YBB}. \tag{2.69}$$

Similarly, the gauge variation of B in the corresponding Green-Schwarz terms gives

$$\begin{align}
\frac{C_{BB}}{M} \delta_B \langle b\, F^B \wedge F^B \rangle &= -C_{BB} \frac{M_1}{M} \langle \theta_B F^B \wedge F^B \rangle \tag{2.70}\\
\frac{C_{YY}}{M} \delta_B \langle b\, F^Y \wedge F^Y \rangle &= -C_{YY} \frac{M_1}{M} \langle \theta_B F^Y \wedge F^Y \rangle \tag{2.71}\\
\frac{C_{YB}}{M} \delta_B \langle b\, F^Y \wedge F^B \rangle &= -C_{YB} \frac{M_1}{M} \langle \theta_B F^Y \wedge F^B \rangle \tag{2.72}
\end{align}$$

and on the other hand the B-variations of the fixed CS counterterms are

$$\begin{align}
\delta_B \mathcal{S}^{CS}_{BYY} &= -\frac{d_1}{2} \langle \theta_B F^Y \wedge F^Y \rangle, \tag{2.73}\\
\delta_B \mathcal{S}^{CS}_{YBB} &= \frac{d_2}{2} \langle \theta_B F^Y \wedge F^B \rangle. \tag{2.74}
\end{align}$$

Finally the cancellation of the anomalous contributions from the Abelian part of the effective action requires following conditions

$$\begin{align}
C_{BB} &= \frac{M}{M_1} \frac{i g_B^3}{3!} a_n D_{BBB}, \tag{2.75}\\
C_{YY} &= \frac{M}{M_1} i g_B g_Y^2 \frac{a_n}{2} D_{BYY}, \tag{2.76}\\
C_{YB} &= \frac{M}{M_1} i g_Y g_B^2 \frac{a_n}{2} D_{YBB}. \tag{2.77}
\end{align}$$

Regarding the Y-variations $\propto Tr[q_B q_Y^2]$ and $\propto Tr[q_B^2 q_Y]$, in general these traces are not identically vanishing and we introduce the CS and GS counterterms to cancel them. Having determined the factors in front of all the counterterms, we can summarize the structure of the one-loop anomalous effective action plus the counterterms as follows

$$\begin{aligned}
\mathcal{S} &= \mathcal{S}_0 + \mathcal{S}_{an} + \mathcal{S}_{GS} + \mathcal{S}_{CS}\\
&= \mathcal{S}_0 + \frac{1}{2!} \langle T_{BWW} BWW \rangle + \frac{1}{2!} \langle T_{BGG} BGG \rangle + \frac{1}{3!} \langle T_{BBB} BBB \rangle\\
&\quad + \frac{1}{2!} \langle T_{BYY} BYY \rangle + \frac{1}{2!} \langle T_{YBB} YBB \rangle\\
&\quad + \frac{C_{BB}}{M} \langle b F_B \wedge F_B \rangle + \frac{C_{YY}}{M} \langle b F_Y \wedge F_Y \rangle + \frac{C_{YB}}{M} \langle b F_Y \wedge F_B \rangle\\
&\quad + \frac{F}{M} \langle b Tr[F^W \wedge F^W] \rangle + \frac{D}{M} \langle b Tr[F^G \wedge F^G] \rangle\\
&\quad + d_1 \langle BY \wedge F_Y \rangle + d_2 \langle YB \wedge F_B \rangle\\
&\quad + c_1 \langle \epsilon^{\mu\nu\rho\sigma} B_\mu C^{SU(2)}_{\nu\rho\sigma} \rangle + c_2 \langle \epsilon^{\mu\nu\rho\sigma} B_\mu C^{SU(3)}_{\nu\rho\sigma} \rangle,
\end{aligned} \tag{2.78}$$

where $\mathcal{S}_0$ is the classical action. At this point we are ready to define the expressions in momentum space of the vertices introduced in Eq. (2.34), denoted by $\mathbf{V}$, obtaining

$$\begin{aligned}
\mathbf{V}^{\lambda\mu\nu}_{BGG} &= 4\,\frac{1}{2}D_B^{(Q)}\, g_B g_3^2\, \Delta^{\lambda\mu\nu}_{\mathbf{AAA}}(+1/6,k_1,k_2) + D_B^{(Q)}\, g_B g_3^2 \frac{1}{2}\frac{i}{\pi^2}\,\frac{2}{3}\,\epsilon^{\lambda\mu\nu\sigma}(k_1-k_2)_\sigma && (2.79)\\
\mathbf{V}^{\lambda\mu\nu}_{BWW} &= 4\,\frac{1}{2}D_B^{(L)}\, g_B g_2^2\, \Delta^{\lambda\mu\nu}_{\mathbf{AAA}}(+1/6,k_1,k_2) + D_B^{(L)}\, g_B g_2^2 \frac{1}{2}\frac{i}{\pi^2}\,\frac{2}{3}\,\epsilon^{\lambda\mu\nu\sigma}(k_1-k_2)_\sigma && (2.80)\\
\mathbf{V}^{\lambda\mu\nu}_{BYY} &= 4D_{BYY}\, g_B g_Y^2\, \Delta^{\lambda\mu\nu}_{\mathbf{AAA}}(+1/6,k_1,k_2) + D_{BYY}\, g_B g_Y^2 \frac{i}{\pi^2}\,\frac{2}{3}\,\epsilon^{\lambda\mu\nu\sigma}(k_1-k_2)_\sigma && (2.81)\\
\mathbf{V}^{\lambda\mu\nu}_{YBB} &= 4D_{YBB}\, g_Y g_B^2\, \Delta^{\lambda\mu\nu}_{\mathbf{AAA}}(+1/6,k_1,k_2) - D_{YBB}\, g_Y g_B^2 \frac{i}{\pi^2}\,\frac{1}{3}\,\epsilon^{\lambda\mu\nu\sigma}(k_1-k_2)_\sigma . && (2.82)\\
\mathbf{V}^{\lambda\mu\nu}_{BBB} &= 4D_{BBB}\, g_B^3\, \Delta^{\lambda\mu\nu}_{\mathbf{AAA}}(+1/6,k_1,k_2). && (2.83)
\end{aligned}$$

where for the generalized CS terms we consider only the trilinear CS interactions whose momentum structure is the same as the Abelian ones as already discussed in Sec. 2.5. The factor $1/2$ overall in the non-Abelian vertices comes from the trace over the generators. These vertices satisfy standard Ward Identities on the external Standard Model lines, with an anomalous WI only on the B-line

$$\begin{aligned}
k_{1\mu}\mathbf{V}^{\lambda\mu\nu}_{BYY}(k_1,k_2) &= 0 && (2.84)\\
k_{2\nu}\mathbf{V}^{\lambda\mu\nu}_{BYY}(k_1,k_2) &= 0 && (2.85)\\
k_{\lambda}\mathbf{V}^{\lambda\mu\nu}_{BYY}(k_1,k_2) &= 4D_{BYY} g_B g_Y^2\, a_n\, \epsilon^{\mu\nu\alpha\beta}k_{1\alpha}k_{2\beta}, && (2.86)
\end{aligned}$$

and obviously the B-currents contain the total anomaly $a_n = -\frac{i}{2\pi^2}$. The same anomaly equations given above for $\mathbf{V}^{\lambda\mu\nu}_{BYY}$ hold for the $\mathbf{V}^{\lambda\mu\nu}_{BGG}$ and $\mathbf{V}^{\lambda\mu\nu}_{BWW}$ vertices but with a $1/2$ factor overall. The anomaly equations for the YBB vertex are

$$\begin{aligned}
k_{1\mu}\mathbf{V}^{\lambda\mu\nu}_{YBB}(k_1,k_2) &= 4D_{YBB}\, g_Y g_B^2\, \frac{a_n}{2}\, \epsilon^{\lambda\nu\alpha\beta}k_{1\alpha}k_{2\beta} && (2.87)\\
k_{2\nu}\mathbf{V}^{\lambda\mu\nu}_{YBB}\,(k_1,k_2) &= 4D_{YBB}\, g_Y g_B^2\, \frac{a_n}{2}\, \epsilon^{\lambda\mu\alpha\beta}k_{2\alpha}k_{1\beta} && (2.88)\\
k_{\lambda}\mathbf{V}^{\lambda\mu\nu}_{YBB}(k_1,k_2) &= 0, && (2.89)
\end{aligned}$$

where the chiral current Y has to be conserved so to render the one-loop effective action gauge invariant. Introducing a symmetric distribution of the anomaly, in the BBB case the analogous equations are

$$\begin{aligned}
k_{1\mu}\mathbf{V}^{\lambda\mu\nu}_{BBB}(k_1,k_2) &= 4\,D_{BBB}\, g_B^3\, \frac{a_n}{3}\, \epsilon^{\lambda\nu\alpha\beta}k_{1\alpha}k_{2\beta} && (2.90)\\
k_{2\nu}\mathbf{V}^{\lambda\mu\nu}_{BBB}\,(k_1,k_2) &= 4\,D_{BBB}\, g_B^3\, \frac{a_n}{3}\, \epsilon^{\lambda\mu\alpha\beta}k_{2\alpha}k_{1\beta} && (2.91)\\
k_{\lambda}\mathbf{V}^{\lambda\mu\nu}_{BBB}(k_1,k_2) &= 4\,D_{BBB}\, g_B^3\, \frac{a_n}{3}\, \epsilon^{\mu\nu\alpha\beta}k_{1\alpha}k_{2\beta}, && (2.92)
\end{aligned}$$

A study of the issue of the gauge dependence in these types of models can be found in Chap. 1. The cancellation of the gauge dependendent terms in specific classes of diagrams can be performed both in the exact phase and in the broken phase, similarly to the discussion presented in the previous chapter, having re-expressed the fields in the basis of the mass eigenstates. The approach that we follow is then clear: we worry about the cancellation of the anomalies in the exact phase, having performed a minimal gauge-fixing to remove the B mixing with the axion b, then we rotate the fields and re-parameterize the Lagrangian around the non trivial vacuum of the potential. We will see in the next sections that with this simple procedure we can easily discuss simple basic processes involving neutral and charged currents exploiting the invariance of the effective action under re-parameterizations of the fields.

2.6 The neutral currents sector in the mLSOM

In this section we move toward the phenomenological analysis of a typical process which exhibits the new trilinear gauge interactions at one-loop level. As we have mentioned in the introduction, our goal here is to characterize this analysis at a more formal level, leaving to the following chapters the numerical results with accurate studies of its predictions for applications at the LHC in the future.

We proceed with our illustration starting from the definition of the neutral current in the model, which is given by

$$-\mathcal{L}_{NC} = \overline{\psi}_f \gamma^\mu \left[g_2 W^3_\mu T^3 + g_Y Y A^Y_\mu + g_B Y_B B_\mu \right] \psi_f, \tag{2.93}$$

that we express in the two basis, the basis of the interaction eigenstates and of the mass eigenstates. Clearly in the interaction basis the bosonic operator in the covariant derivative becomes

$$\begin{aligned} \mathcal{F} &\equiv g_2 W^3_\mu T^3 + g_Y Y A^Y_\mu + g_B Y_B B_\mu \\ &= g_Z Q_Z Z_\mu + g_{Z'} Q_{Z'} Z'_\mu + e\, Q A^\gamma_\mu, \end{aligned} \tag{2.94}$$

where $Q = T^3 + Y$. The rotation in the photon basis gives

$$W^3_\mu = O^A_{W_3\gamma} A^\gamma_\mu + O^A_{W_3 Z} Z_\mu + O^A_{W_3 Z'} Z'_\mu \tag{2.95}$$

$$A^Y_\mu = O^A_{Y\gamma} A^\gamma_\mu + O^A_{YZ} Z_\mu + O^A_{YZ'} Z'_\mu \tag{2.96}$$

$$B_\mu = O^A_{BZ} Z_\mu + O^A_{BZ'} Z'_\mu \tag{2.97}$$

and performing the rotation on $\mathcal{F}$ we obtain

$$\begin{aligned} \mathcal{F} = \; & A^\gamma_\mu \left[g_2 O^A_{W_3\gamma} T^3 + g_Y O^A_{Y\gamma} Y \right] + Z_\mu \left[g_2 O^A_{W_3 Z} T^3 + g_Y O^A_{YZ} Y + g_B O^A_{BZ} Y_B \right] \\ & + Z'_\mu \left[g_2 O^A_{W_3 Z'} T^3 + g_Y O^A_{YZ'} Y + g_B O^A_{BZ'} Y_B \right], \end{aligned} \tag{2.98}$$

where the electromagnetic current can be written in the usual way

$$A^\gamma_\mu \left[g_2 O^A_{W_3\gamma} T^3 + g_Y O^A_{Y\gamma} Y \right] = e A^\gamma_\mu Q, \tag{2.99}$$

with the definition of the electric charge as

$$e = g_2 O^A_{W_3\gamma} = g_Y O^A_{Y\gamma} = \frac{g_Y g_2}{\sqrt{g_Y^2 + g_2^2}}. \tag{2.100}$$

Similarly for the neutral Z current we obtain

$$\begin{aligned} & Z_\mu \left[g_2 O^A_{W_3 Z} T^3 + g_Y O^A_{YZ} Y + g_B O^A_{BZ} Y_B \right] \\ = \; & Z_\mu \left[T^3 (g_2 O^A_{W_3 Z} - g_Y O^A_{YZ}) + g_Y O^A_{YZ} Q + g_B O^A_{BZ} Y_B \right] \\ = \; & Z_\mu g_Z \left[T^3 + \frac{g_Y O^A_{YZ}}{g_2 O^A_{W_3 Z} - g_Y O^A_{YZ}} Q + \frac{g_B O^A_{BZ}}{g_2 O^A_{W_3 Z} - g_Y O^A_{YZ}} Y_B \right], \end{aligned} \tag{2.101}$$

where we have defined

$$g_Z = g_2 O^A_{W_3 Z} - g_Y O^A_{YZ} \simeq g = \frac{g_2}{\cos\theta_W}. \tag{2.102}$$

We can easily work out the structure of the covariant derivative interaction applied on a left-handed or on a right-handed fermion. For this reason it is convenient to introduce some notation. We define

$$\mu_Q^Z = \frac{g_Y O^A_{YZ}}{g_Z} \simeq -\sin^2\theta_W, \tag{2.103}$$

$$\mu_B^Z = \frac{g_B O^A_{BZ}}{g_Z} \simeq \frac{g_B}{2}\epsilon_1 \quad \text{so that} \quad \lim_{M_1\to\infty}\mu_B^Z = 0, \tag{2.104}$$

and similarly for the Z' neutral current

$$g_{Z'} = g_2 O^A_{W_3 Z'} - g_Y O^A_{YZ'}, \qquad \mu_Q^{Z'} = \frac{g_Y O^A_{YZ'}}{g_{Z'}}, \qquad \mu_B^{Z'} = \frac{g_B O^A_{BZ'}}{g_{Z'}}. \tag{2.105}$$

We can easily identify the generators in the (Z, Z', A_γ) basis. These are given by

$$\begin{aligned}
\hat{Q}_Z &= \hat{Q}^R_Z + \hat{Q}^L_Z = T^{3L} + \mu_Q^Z Q^L + \mu_B^Z Y_B^L + \mu_Q^Z Q^R + \mu_B^Z Y_B^R \\
\hat{Q}_{Z'} &= \hat{Q}^R_{Z'} + \hat{Q}^L_{Z'} = T^{3L} + \mu_Q^{Z'} Q^L + \mu_B^{Z'} Y_B^L + \mu_Q^{Z'} Q^R + \mu_B^{Z'} Y_B^R \\
\hat{Q} &= \hat{Q}_L + \hat{Q}_R
\end{aligned} \tag{2.106}$$

which will be denoted as $Q_{\overline{p}} = (\hat{Q}, \hat{Q}_Z, \hat{Q}_{Z'})$. To express a given correlator, say $\langle Z A_\gamma A_\gamma \rangle$ in the (W_3, A_Y, B) basis we proceed as follows. We denote with $Q_{\overline{p}} = (\hat{Q}, \hat{Q}_Z, \hat{Q}_{Z'})$ the generators in the photon basis (A_γ, Z, Z') and with $g_{\overline{p}} = (e, g_Z, g_{Z'})$ the corresponding couplings. Similarly, $Q_p = (T^3, Y, Y_B)$ are the generators in the interaction basis (W_3, A_Y, B) and $g_p = (g_2, g_Y, g_B)$ the corresponding couplings, so that

$$\begin{aligned}
-\mathcal{L}_{NC} &= \overline{\psi}\gamma^\mu \left[g_Z \hat{Q}_Z Z_\mu + g_{Z'} \hat{Q}_{Z'} Z'_\mu + e\,\hat{Q} A^\gamma_\mu \right]\psi \\
&= \overline{\psi}\gamma^\mu \left[g_2 T^3 W^3_\mu + g_Y Y A^Y_\mu + g_B Y_B B_\mu \right]\psi.
\end{aligned} \tag{2.107}$$

2.7 The $Z\gamma\gamma$ vertex in the Standard Model

Before coming to the computation of this vertex in the mLSOM we first start reviewing its structure in the SM.

We show in Fig. 2.9 the $Z\gamma\gamma$ vertex in the SM, where we have separated the QED contributions from the remaining corrections R_W. This vertex vanishes at all orders when all the three lines are on-shell, due to the Landau-Yang theorem. A direct proof of this property for the fermionic one-loop corrections will be shown in App. 2.9.3.

The QED contribution contains the fermionic triangle diagrams (direct plus exchanged) while R_W includes all the remaining contributions at one-loop level. Specifically, as shown in Fig. 2.10, R_W contains ghosts, Goldstones and all other exchanges. An exhaustive computation of all these contributions is not needed for our discussion. We have omitted diagrams of the type shown in Figs. 2.11, 2.12. These are removed by working in the R_ξ gauge for the Z boson. Notice, however, that even without a gauge-fixing these decouple from the anomaly diagrams in the massless fermion limit since the Goldstone does not couple to massless fermions. In Fig. 2.13 we show how the anomaly is re-distributed in an AAA diagram by a CS interaction, generating an AVV vertex.

To appreciate the role played by the anomaly in this vertex we perform a direct computation of the two anomaly diagrams and include the fermionic mass terms. A direct computation gives

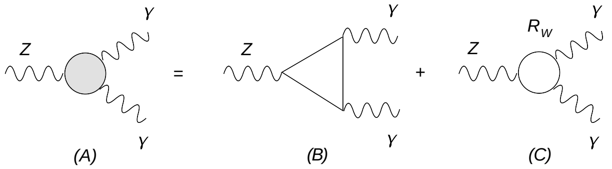

Figure 2.9: The $Z\gamma\gamma$ vertex to lowest order in the SM, with the anomalous contributions and the remaining weak corrections shown separately.

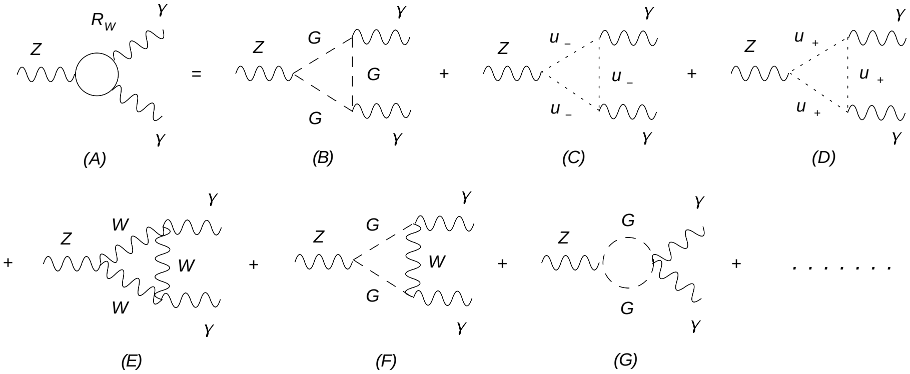

Figure 2.10: Some typical electroweak corrections, involving the charged Goldstones (here denoted by G, ghosts contributions $(u_\pm)$ and W exchanges.

$$
\begin{aligned}
G^{\rho\nu\mu}(k,k_1,k_2) &= -\frac{e^2 g}{\cos\theta_W}\sum_f g_A^f Q_f^2 \int \frac{d^4 p}{(2\pi)^4}\, Tr\left(\frac{1}{\not{p}-m_f}\gamma^\rho\gamma^5\frac{1}{\not{p}-\not{k}-m_f}\gamma^\nu\frac{1}{\not{p}-\not{k}_1-m_f}\gamma^\mu\right)\\
&\quad +(k_1\rightarrow k_2,\mu\rightarrow\nu).
\end{aligned}
\tag{2.108}
$$

which can be cast in the form

$$
\begin{aligned}
G^{\rho\nu\mu}(k,k_1,k_2) &= -\frac{e^2 g}{2\pi^2\cos\theta_W}\sum_f g_A^f Q_f^2\int_0^1 dx_1\int_0^{1-x_1}dx_2\\
&\quad \cdot\frac{1}{\Delta}\Big[\epsilon^{\rho\nu\mu\alpha}(1-x_1-x_2)(x_2k_1-x_1k_2)_\beta(k_2^\beta k_{1\alpha}+k_1^\beta k_{2\alpha})\\
&\quad +(1-x_1-x_2)(\epsilon^{\alpha\rho\beta\nu}k_{1\alpha}k_{2\beta}(x_2k_1^\mu-x_1k_2^\mu)+(\mu\rightarrow\nu))\\
&\quad +\epsilon^{\alpha\nu\beta\mu}k_{1\alpha}k_{2\beta}(x_2(x_2-x_1-1)k_1^\rho-x_1(x_2-x_1+1)k_2^\rho)\Big],
\end{aligned}
\tag{2.109}
$$

where

$$
\Delta = m_f^2 + x_2(x_2-1)k_1^2 + x_1(x_1-1)k_2^2 - 2x_1x_2\,k_1\cdot k_2, \tag{2.110}
$$

and we have introducing the $g_{Z,A}^f$ and $g_{Z,V}^f$ couplings of the Z with

$$
g_{Z,A}^f = \frac{1}{2}T_3^f, \qquad g_{Z,V}^f = \frac{1}{2}T_3^f - Q_f\sin^2\theta_W. \tag{2.111}
$$

This form of the amplitude is obtained if we use the standard Rosenberg definition of the anomalous diagrams and it agrees with [83]. In this case the Ward Identities on the photon lines are defining conditions for the vertex. Naturally, with the standard fermion multiplet assignment the anomaly vanishes

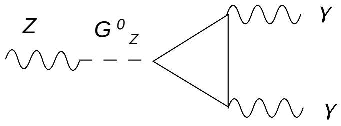

Figure 2.11: $Z - G^0_Z$ mixing in the broken phase in the SM.

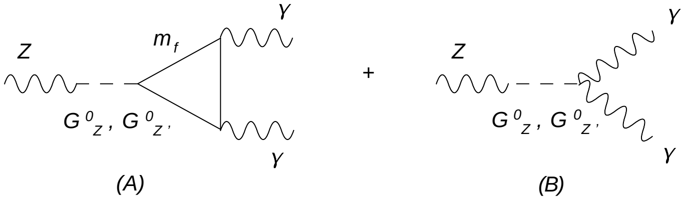

Figure 2.12: Same as in Fig. 2.11 but for the mLSOM.

since

$$\sum_f g^f_A Q^2_f = 0. \tag{2.112}$$

Because of the anomaly cancellation, the fermionic vertex is zero also off-shell, if the masses of all the fermions in each generation are degenerate, in particular if they are massless. Notice that this is not a consequence of the Landau-Yang theorem.

Let us now move to the WI on the Z-line. A direct computation gives

$$\begin{aligned} k_\rho \, G^{\rho\nu\mu} &= (k_1 + k_2)_\rho \, G^{\rho\nu\mu} \\ &= \frac{e^2 g}{\pi^2 \cos\theta_W} \sum_f g^f_A Q^2_f \, \epsilon^{\nu\mu\alpha\beta} k_{1\alpha} k_{2\beta} \left[\frac{1}{2} - m^2_f \int_0^1 dx_1 \int_0^{1-x_1} dx_2 \, \frac{1}{\Delta} \right]. \end{aligned} \tag{2.113}$$

The presence of a mass-dependent term on the r.h.s. of (2.113) constitutes a break-down of axial current conservation for massive fermions, as expected.

2.7.1 The $Z\gamma\gamma$ vertex in anomalous Abelian models: the Higgs-Stückelberg phase

The presence of anomalous generators in a given vertex renders some trilinear interactions non-vanishing also for massless fermions. In fact, as we have shown in the previous section, in the SM the anomalous triangle diagrams vanish if we neglect the masses of all the fermions, and this occurs both on-shell and off-shell. The only left over corrections are related to the fermion mass and these will also vanish (off-shell) if all the fermions of a given generation are mass degenerate. The on-shell vanishing of the same vertices is a consequence of the structure of the amplitude, as we show in the appendix. The extraction of the contribution of the anomalous generators in the trilinear vertices can be obtained starting from the 1-particle-irreducible (1PI) effective action, written in the basis of the interaction eigenstates, and performing the rotation of the trilinear interaction that project onto the $Z\gamma\gamma$ vertex.

In order to appreciate the differences between the SM result and the analogous one in the anomalous extensions that we are considering, we start by observing that only in the Stückelberg phase ($M_1 \neq 0$

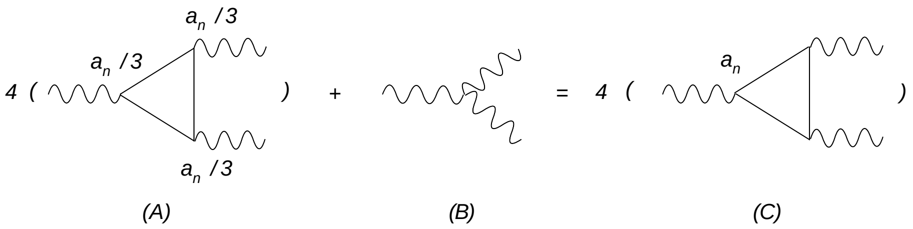

Figure 2.13: Re-distribution of the anomaly via the CS counterterm.

and $v_u = v_d = 0$) the anomaly-free traces vanish,

$$\begin{aligned} \langle YYY\rangle \, g_Y^3 \, Tr[Q_Y^3] &= 0 \\ \langle YW_3W_3\rangle \, g_Y g_2^2 \, Tr[Q_Y T^3 T^3] &= 0 \,, \end{aligned} \tag{2.114}$$

because of charge assignment. A similar result is valid also in the HS phase if the Yukawa couplings are neglected. Coming to extract the $Z\gamma\gamma$ vertex we rotate the anomalous diagrams of the effective action into the mass eigenstates, being careful to separate the massless from the massive fermion contributions.

Hence, we split the $\langle YYY\rangle$ vertex into its chiral contributions and performing the rotation of the fields we get the following contributions

$$\begin{aligned} &\frac{1}{3!}\,\langle YYY\rangle \, g_Y^3 \, Tr[Q_Y^3] = \\ &\qquad \sum_f \Big[g_Y^3 \frac{1}{8} (Q^L_{Y,f})^3 \langle LLL\rangle^{\lambda\mu\nu} + g_Y^3 \frac{1}{8} (Q^R_{Y,f})^3 \langle RRR\rangle^{\lambda\mu\nu} \\ &\qquad + g_Y^3 \frac{1}{8} Q^L_{Y,f} (Q^R_{Y,f})^2 \langle LRR\rangle^{\lambda\mu\nu} + g_Y^3 \frac{1}{8} Q^L_{Y,f} Q^R_{Y,f} Q^L_{Y,f} \langle LRL\rangle^{\lambda\mu\nu} \\ &\qquad + g_Y^3 \frac{1}{8} (Q^L_{Y,f})^2 Q^R_{Y,f} \langle LLR\rangle^{\lambda\mu\nu} + g_Y^3 \frac{1}{8} Q^R_{Y,f} (Q^L_{Y,f})^2 \langle RLL\rangle^{\lambda\mu\nu} \\ &\qquad + g_Y^3 \frac{1}{8} Q^R_{Y,f} Q^L_{Y,f} Q^R_{Y,f} \langle RLR\rangle^{\lambda\mu\nu} + g_Y^3 \frac{1}{8} (Q^R_{Y,f})^2 Q^L_{Y,f} \langle RRL\rangle^{\lambda\mu\nu} \Big] Z^\lambda A^\mu_\gamma A^\nu_\gamma \frac{1}{3!} R^{YYY} + \ldots \end{aligned} \tag{2.115}$$

where the dots indicate all the other projections of the type $ZZ\gamma, Z'\gamma\gamma$ etc. Here $\langle LLL\rangle$, $\langle RLR\rangle$ etc., indicate the (clockwise) insertion of L/R chiral projectors on the $\lambda\mu\nu$ vertices of the anomaly diagrams.

For the $\langle YWW\rangle$ vertex the structure is more simple because the generator associated to W_3 is left-chiral

$$\begin{aligned} \frac{1}{2!}\,\langle YWW\rangle \, g_Y g_2^2 \, Tr[Q_Y (T^3)^2] = \sum_f \Big[& g_Y g_2^2 \frac{1}{8} Q^L_{Y,f} (T^3_{L,f})^2 \langle LLL\rangle^{\lambda\mu\nu} \\ & + g_Y g_2^2 \frac{1}{8} Q^R_{Y,f} (T^3_{L,f})^2 \langle RLL\rangle^{\lambda\mu\nu} \Big] Z^\lambda A^\mu_\gamma A^\nu_\gamma \frac{1}{2!} R^{YWW} + \ldots \end{aligned} \tag{2.116}$$

The $\langle BYY\rangle$ vertex works in same way of $\langle YYY\rangle$

$$\begin{aligned} &\frac{1}{2!}\,\langle BYY\rangle \, g_B g_Y^2 \, Tr[Q_B Q_Y^2] = \\ &\qquad \sum_f \Big[g_B g_Y^2 \frac{1}{8} Q^L_{B,f} (Q^L_{Y,f})^2 \langle LLL\rangle^{\lambda\mu\nu} + g_B g_Y^2 \frac{1}{8} Q^R_{B,f} (Q^R_{Y,f})^2 \langle RRR\rangle^{\lambda\mu\nu} \end{aligned}$$

$$
\begin{aligned}
&+g_B g_Y^2 \frac{1}{8} Q^L_{B,f} (Q^R_{Y,f})^2 \langle LRR \rangle^{\lambda\mu\nu} + g_B g_Y^2 \frac{1}{8} Q^L_{B,f} Q^R_{Y,f} Q^L_{Y,f} \langle LRL \rangle^{\lambda\mu\nu} \\
&+g_B g_Y^2 \frac{1}{8} Q^L_{B,f} Q^L_{Y,f} Q^R_{Y,f} \langle LLR \rangle^{\lambda\mu\nu} + g_B g_Y^2 \frac{1}{8} Q^R_{Y,f} (Q^L_{Y,f})^2 \langle RLL \rangle^{\lambda\mu\nu} \\
&+g_B g_Y^2 \frac{1}{8} Q^R_{B,f} Q^L_{Y,f} Q^R_{Y,f} \langle RLR \rangle^{\lambda\mu\nu} + g_B g_Y^2 \frac{1}{8} Q^R_{B,f} Q^R_{Y,f} Q^L_{Y,f} \langle RRL \rangle^{\lambda\mu\nu} \Big] Z^\lambda A^\mu_\gamma A^\nu_\gamma \frac{1}{2!} R^{BYY} + \dots
\end{aligned}
\tag{2.117}
$$

Finally, the $\langle BWW \rangle$ vertex is similar to $\langle YWW \rangle$

$$
\begin{aligned}
\frac{1}{2!} \langle BWW \rangle \, g_Y g_2^2 \, Tr[Q_B (T^3)^2] = \sum_f \Big[& g_B g_2^2 \frac{1}{8} Q^L_{B,f} (T^3_{L,f})^2 \langle LLL \rangle^{\lambda\mu\nu} \\
&+ g_B g_2^2 \frac{1}{8} Q^R_{B,f} (T^3_{L,f})^2 \langle RLL \rangle^{\lambda\mu\nu} \Big] Z^\lambda A^\mu_\gamma A^\nu_\gamma \frac{1}{2!} R^{BWW} + \dots
\end{aligned}
\tag{2.118}
$$

where we have defined

$$
\begin{aligned}
R^{YYY} &= 3 \left[(O^{A\,T})_{22} (O^{A\,T})^2_{21} \right] \\
R^{YWW} &= \left[2 (O^{A\,T})_{11} (O^{A\,T})_{12} (O^{A\,T})_{21} + (O^{A\,T})^2_{11} (O^{A\,T})_{22} \right] \\
R^{BYY} &= (O^{A\,T})^2_{21} (O^{A\,T})_{32} \\
R^{BWW} &= \left[(O^{A\,T})^2_{11} (O^{A\,T})_{32} \right] .
\end{aligned}
\tag{2.119}
$$

which are the product of rotation matrices that project the anomalous effective action from the interaction eigenstate basis over the Z, γ gauge bosons.

We have expressed the generators in their chiral basis, and their mixing is due to mass insertions over each fermion line in the loop. The ellypsis refers to additional contributions which do not project on the vertex that we are interested in but which are present in the analysis of the remaining neutral vertices, $ZZ\gamma, Z'\gamma\gamma$ etc. The notation O^{AT} indicates the transposed of the rotation matrix from the interaction to the mass eigenstates. To obtain the final expression of the amplitude in the interaction eigenstate basis one can easily observe that in the chiral amplitudes $\langle LLL \rangle$ and $\langle RRR \rangle$ the mass dependence in the fermion loops is all contained in the denominators of the propagators, not in the Dirac traces. The only diagrams that contain a mass dependence at the numerators are those involving chirality flips ($\langle LLR \rangle, \langle RRL \rangle$) which contribute with terms proportional to m_f^2. These terms contribute only to the invariant amplitudes A_1 and A_2 of the Rosenberg representation (see Chap. 1, Eq. 1.120) and, although finite, they disappear once we impose a WI on the two photon lines, as requested by CVC for the two photons. A similar result is valid for the SM, as one can easily figure out from Eq. (2.109). Therefore, the amplitudes can be expressed just in terms of LLL and RRR correlators, and since the mass dependence is at the denominators of the propagators, one can easily show the relation

$$
\langle LLL \rangle = - \langle RRR \rangle
\tag{2.120}
$$

valid for any fermion mass m_f. Defining $\langle LLL \rangle \equiv \Delta^{\lambda\mu\nu}_{LLL}(m_f \neq 0)$, we can express the only independent chiral graph as sum of two contributions

$$
\Delta^{\lambda\mu\nu}_{LLL}(m_f \neq 0) = \Delta^{\lambda\mu\nu}_{LLL}(0) + \Delta^{\lambda\mu\nu}_{LLL}(m_f)
\tag{2.121}
$$

where we define

$$\begin{aligned}
&\Delta^{\lambda\mu\nu}_{LLL}(0) \equiv \Delta^{\lambda\mu\nu}_{LLL}(m_f = 0) \\
&\Delta^{\lambda\mu\nu}_{LLL}(m_f) \equiv \Delta^{\lambda\mu\nu}_{LLL}(m_f \neq 0) - \Delta^{\lambda\mu\nu}_{LLL}(m_f = 0).
\end{aligned} \tag{2.122}$$

Also, one can verify quite easily that

$$\begin{aligned}
\Delta^{\lambda\mu\nu}_{LLL}(0) &= \Delta^{\lambda\mu\nu}_{AVV}(0) + \Delta^{\lambda\mu\nu}_{VAV}(0) + \Delta^{\lambda\mu\nu}_{VVA}(0) + \Delta^{\lambda\mu\nu}_{AAA}(0) \\
&= 4\Delta^{\lambda\mu\nu}_{AAA}(0).
\end{aligned} \tag{2.123}$$

A second contribution to the effective action comes from the one-loop counterterms containing generalized CS terms. There are two ways to express these counterterms: either as separate trilinear interactions or as modifications of the two invariant amplitudes of the Rosenberg parameterization A_1, A_2. These amplitudes depend linearly on the momenta of the vertex (see App. 1.16). For instance we use

$$\Delta_{AAA}(0) - \frac{a_n}{3}\epsilon^{\lambda\mu\nu\alpha}(k_{1\alpha} - k_{2\alpha}) = \Delta_{AVV}(0), \tag{2.124}$$

which allows to absorb completely the CS term, giving conserved Y/W_3 currents in the interaction eigenstate basis. In this case we move from a symmetric distribution of the anomaly in the AAA diagram, to an AVV diagram. These currents interpolate with the vector-like vertices (V) of the AVV graph.

Notice that once the anomaly is moved from any vertex involving a Y/W_3 current to a vertex with a B current, it is then canceled by the GS interaction. The extension of this analysis to the complete m_f-dependent case for $\Delta_{LLL}(m_f \neq 0)$ is quite straightforward. In fact, after some re-arrangements of the $Z\gamma\gamma$ amplitude, we are left with the following contributions in the physical basis in the broken phase

$$\begin{aligned}
\langle Z\gamma\gamma\rangle|_{m_f\neq 0} = \frac{1}{4}\sum_f \Delta^{\lambda\mu\nu}_{AVV}(m_f \neq 0)\,\big[&g_Y^3\theta_f^{YYY}R^{YYY} + g_Y g_2^2\theta_f^{YWW}R^{YWW} \\
&+ g_B g_Y^2\theta_f^{BYY}R^{BYY} + g_B g_2^2\theta_f^{BWW}R^{BWW}\big]\,Z^\lambda A^\mu_\gamma A^\nu_\gamma
\end{aligned} \tag{2.125}$$

where we have defined the anomalous chiral asymmetries as

$$\begin{aligned}
&\theta_f^{BYY} = \left[Q^L_{B,f}(Q^L_{Y,f})^2 - Q^R_{B,f}(Q^R_{Y,f})^2\right] \\
&\theta_f^{BWW} = Q^L_{B,f}(T^3_{L,f})^2.
\end{aligned} \tag{2.126}$$

The conditions of gauge invariance force the coefficients in front of the CS terms to be

$$\begin{aligned}
D_{BYY} &= \frac{1}{8}\sum_f \theta_f^{BYY} \\
D_{BWW} &= \frac{1}{8}\sum_f \theta_f^{BWW},
\end{aligned} \tag{2.127}$$

which have been absorbed and do not appear explicitly, while the SM chiral asymmetries are defined as

$$\begin{aligned}
&\theta_f^{YYY} = \left[(Q^L_{Y,f})^3 - (Q^R_{Y,f})^3\right] \\
&\theta_f^{YWW} = Q^L_{Y,f}(T^3_{L,f})^2,
\end{aligned} \tag{2.128}$$

and the triangle $\Delta_{AVV}(m_f \neq 0)$ is given as in (2.109). Notice that Eq. (2.125) is in complete agreement with the SM result shown in (2.109), obtained by removing the contributions proportional to the B gauge bosons and setting the chiral asymmetries of Y and W_3 to zero. In particular, if the gauge bosons are not anomalous and in the chiral limit ($m_f = 0$ or $m_f = m$) this trilinear amplitude vanishes. As we have already pointed out, the amplitude for the $\langle Z\gamma\gamma\rangle$ process is espressed in terms of six invariant amplitudes that can be easily computed and take the form

$$\begin{aligned}\Delta^{\lambda\mu\nu}_{AVV} &= A_1(k_1,k_2)\epsilon[k_1,\mu,\nu,\lambda] + A_2(k_1,k_2)\epsilon[k_2,\mu,\nu,\lambda] + A_3(k_1,k_2)\epsilon[k_1,k_2,\mu,\lambda]{k_1}^{\nu} \\ &+A_4(k_1,k_2)\epsilon[k_1,k_2,\mu,\lambda]{k_2}^{\nu} + A_5(k_1,k_2)\epsilon[k_1,k_2,\nu,\lambda]k_1^{\mu} + A_6(k_1,k_2)\epsilon[k_1,k_2,\nu,\lambda]k_2^{\mu},\end{aligned} \tag{2.129}$$

with

$$\begin{aligned}A_1(k_1,k_2) &= k_1\cdot k_2 A_3(k_1,k_2) + k_2^2 A_4(k_1,k_2) \\ A_2(k_1,k_2) &= -A_1(k_2,k_1) \\ A_5(k_1,k_2) &= -A_4(k_2,k_1) \\ A_6(k_1,k_2) &= -A_3(k_2,k_1).\end{aligned} \tag{2.130}$$

Also $A_1(k_1,k_2) = A_1(k_2,k_1)$ as one can easily check by a direct computation. We obtain

$$\begin{aligned}A_3(k_1,k_2) &= -\frac{1}{2}\int_0^1 dx \int_0^{1-x} dy \frac{xy}{y(1-y)k_1^2 + x(1-x)k_2^2 + 2xy\, k_1\cdot k_2 - m_f^2} \\ A_4(k_1,k_2) &= \frac{1}{2}\int_0^1 dx \int_0^{1-x} dy \frac{x(1-x)}{y(1-y)k_1^2 + x(1-x)k_2^2 + 2xy\, k_1\cdot k_2 - m_f^2}\end{aligned} \tag{2.131}$$

The computation of these integrals can be done analytically and the various regions $0 < s < 4m_f^2$, $m_f >> \sqrt{s}/2$, and $m_f \to 0$ can be studied in detail. In the case of both photons on-shell, for instance, and $s > 4m_f^2$ we obtain

$$\begin{aligned}A_3(k_1,k_2) &= \frac{1}{2s} - \frac{m_f^2}{s}\mathrm{Li}_2\left(\frac{2}{1-\sqrt{1-4m_f^2/s}}\right) - \frac{m_f^2}{s}\mathrm{Li}_2\left(\frac{2}{1+\sqrt{1-4m_f^2/s}}\right) \\ A_4(k_1,k_2) &= -\frac{1}{s} + \frac{\sqrt{1-4m_f^2/s}}{s}\mathrm{ArcTanh}\left(\frac{1}{\sqrt{1-4m_f^2/s}}\right)\end{aligned} \tag{2.132}$$

Notice that the case in which the two photons are on-shell and light fermions are running in the loop, then the evaluation of the integral requires particular care because of infrared effects which render the parameteric integrals ill-defined. The situation is similar to the case of the coupling of the axial anomaly to on-shell gluons in spin physics [84], when the correct isolation of the massless quarks contributions is carried out by moving off-shell on the external lines and then performing the $m_f \to 0$ limit.

2.7.2 $q\bar{q} \to \gamma\gamma$ with an intermediate Z

In this section we are going to describe the role played by the new anomaly cancellation mechanism in simple processes which can eventually be studied with accuracy at the LHC. A numerical analysis of processes involving neutral currents can be performed along the lines of [85] and we will return to this point in Chap. 5 . Here we intend to discuss some of the phenomenological implications which might be of interest. Since the anomaly is canceled by a combination of Chern-Simons and Green-Schwarz contributions, the study of a specific process, such as $Z \to \gamma\gamma$, which differs from the SM prediction, requires, in general, a combined analysis both of the gauge sector and of the scalar sector.

We start from the case of a quark-antiquark annihilation mediated by a Z that later undergoes a decay into two photons. At leading order this process is at parton level described by the annihilations of a valence quark q and a sea antiquark $\bar{q}$ from the two incoming hadrons, both of them collinear and massless. In Fig. 2.14 we have depicted all the diagrams by which the process can take place to lowest order. Radiative corrections from the initial state are accurately known up to next-to-next-to-leading order, and are universal, being the same of the Drell-Yan cross section. In this respect, precise QCD predictions for the rates are available, for instance around the Z resonance [85].

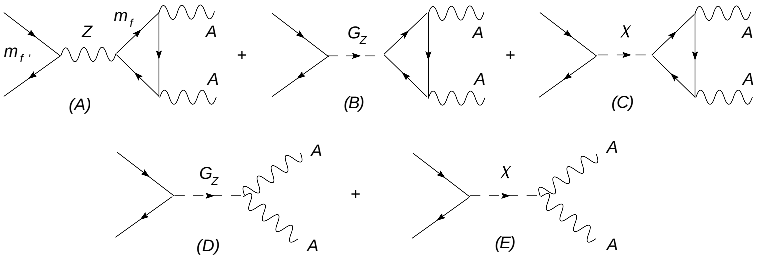

Figure 2.14: Two photon processes initiated by a $q\bar{q}$ annihilation with a Z exchange.

In the SM, gauge invariance of the process requires both a Z gauge boson exchange and the exchange of the corresponding Goldstone G_Z, which involves diagrams (A) and (B). In the mLSOM a direct Green-Schwarz coupling to the photon (which is gauge dependent) is accompanied by a gauge independent axion exchange. If the incoming quark-antiquark pair is massless, then the Goldstone has no coupling to the incoming fermion pair, and therefore (B) is absent, while gauge invariance is trivially satisfied because of the massless condition on the fermion pair of the initial state. In this case only diagram (A) is relevant. Diagram (B) may also be set to vanish, for instance in suitable gauges, such as the unitary gauge. Notice also that the triangle diagrams have a dependence on m_f, the mass of the fermion in the loop, and show two contributions: a first contribution which is proportional to the anomaly (mass independent) and a correction term which depends on m_f.

As we have shown above, the first contribution, which involves an off-shell vertex, is absent in the SM, while it is non vanishing in the mLSOM. In both cases, on the other hand, we have m_f dependent contributions. It is then clear that in the SM the largest contribution to the process comes from the top quark circulating in the triangle diagram, the amplitude being essentially proportional only to the heavy top mass. On the Z resonance and for on-shell photons, the cross section vanishes in both cases, as we have explained, in agreement with the Landau-Yang theorem. We have checked these properties explicitly, but they hold independently of the perturbative order at which they are analyzed, being based on the Bose symmetry of the two photons. The cross section, therefore, has a dip at $Q = M_Z$, where it vanishes, and where Q^2 is the virtuality of the intermediate s-channel exchange.

An alternative scenario is to search for neutral exchanges initiated by gluon-gluon fusion. In this case we replace the annihilation pair with a triangle loop (the process is similar to Higgs production via gluon fusion), as shown in Fig. 2.15. As in the decay mechanism discussed above, the production mechanism in

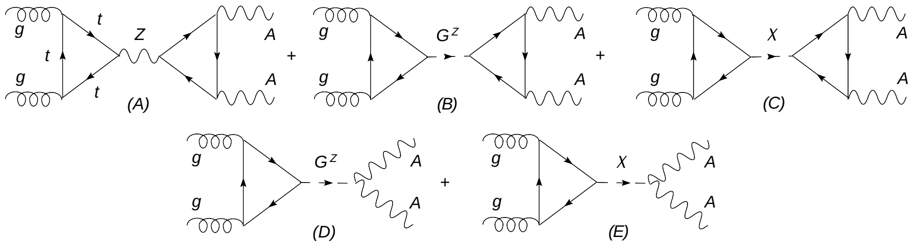

Figure 2.15: Gluon fusion contribution to double-photon production. Shown are also the scalar exchanges (B) and (D) that restore gauge invariance and the axi-Higgs exchange (E).

the SM and in the mLSOM are again different. In fact, in the mLSOM there is a massless contribution appearing already at the massless fermion level, which is absent in the SM. The production mechanism by gluon fusion has some special features as well. In ggZ production and $Z\gamma\gamma$ decay, the relevant diagrams are (A) and (B) since we need the exchange of a G_Z to obtain gauge invariance. As we probe smaller values of the Bjorken variable x, the gluon density raises, and the process becomes sizable. On the other hand, in a pp collider, although the quark annihilation channel is suppressed since the antiquark density is smaller than in a $p\bar{p}$ collision, this channel still remains rather significant. We have also shown in this figure one of the scalar channels, due to the exchange of an axi-Higgs.

Other channels such as those shown in Fig. 2.16 can also be studied. These involve a lepton pair

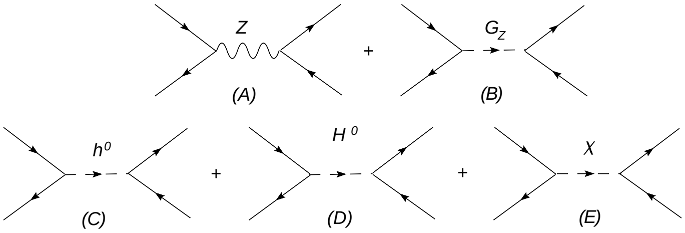

Figure 2.16: The $q\bar{q}$ annihilation channel (A,B). Scalar exchanges in the neutral sector involving the two Higsses and the axi-Higgs (C,D,E).

in the final state, and their radiative corrections also show the appearance of a triangle vertex. This is the classical Drell-Yan process, that we will briefly describe below. In this case, both the total cross section and the rapidity distributions of the lepton pair and/or an analysis of the charge asymmetry in s-channel exchanges of W's would be of major interest in order to disentangle the anomaly inflow. At the moment, errors on the parton distributions and scale dependences induce indeterminations which, just for the QCD background, are around 4% [85], as shown in a high precision study. It is expected, however, that the statistical accuracy on the Z resonance at the LHC is going to be a factor 10^2 better. In fact this is a case in which the experiment can do better than the theory.

2.7.3 Isolation of the massless limit: the $Z^* \to \gamma^*\gamma^*$ amplitude

The isolation of the massless from the massive contributions can be analyzed in the case of resolved photons in the final state. As we have already mentioned in the prompt photon case the amplitude, on the Z resonance, vanishes because of Bose symmetry and angular momentum conservation. We can, however, be on the Z resonance and produce one or two off-shell photons that undergo fragmentation. Needless to say, these contributions are small. However, the separation of the massless from the massive case is well defined. One can increase the rates by asking just for one single resolved photon and one prompt photon. Rates for this process in pp-collisions have been determined in [43]. We start from the case of off-shell external photons of virtuality s_1 and s_2 and an off-shell Z (Z^*). Following [86], we introduce the total vertex $V^{\lambda\mu\nu}(k_1, k_2, m_f)$, which contains both the massive m_f dependence (corresponding to the triangle amplitude $\Delta^{\lambda\mu\nu}$) and its massless counterpart $\mathbf{V}^{\lambda\mu\nu}(0) \equiv V(k_1, k_2, m_f = 0)$, obtained by sending the fermion mass to zero. The Rosenberg vertex and the V vertex are trivially related by a Schoutens transformation, moving the λ index from the Levi-Civita tensor to the momenta of the photons

$$
\begin{aligned}
& V_{\lambda\mu\nu}(k_1, k_2, m_f) \\
& = A(k_1, k_2, m_f)\epsilon[\lambda, \mu, \nu, k_2]s_1 - A(k_2, k_1, m_f)\epsilon[\lambda, \mu, \nu, k_1]s_2 + A(k_1, k_2, m_f)\epsilon[\lambda, \nu, k_1, k_2]k_1^\mu \\
& + A(k_2, k_1, m_f)\epsilon[\lambda, \mu, k_2, k_1]k_2^\nu - B(k_1, k_2, m_f)\epsilon[\mu, \nu, k_1, k_2]k^\lambda
\end{aligned}
\tag{2.133}
$$

with $k - k_1 - k_2 = 0$ and $s_i = k_i^2$ $(i = 1, 2)$, and

$$
\begin{aligned}
A(k_1, k_2, m_f) \quad = \quad & \frac{1}{\lambda}\Bigg[-\frac{1}{2}(s - s_1 + s_2) - \left(\frac{1}{2}(s + s_2) + (6/\lambda)ss_1s_2\right)\Delta_{\#1} \\
& + s_2\left[\frac{1}{2} - (3/\lambda)s(s - s_1 - s_2)\right]\Delta_{\#2} \\
& + \left[ss_2 + (m_f^2 + (3/\lambda)ss_1s_2)(s - s_1 + s_2)\right]C_{\#0}\Bigg]
\end{aligned}
\tag{2.134}
$$

$$
\begin{aligned}
B(k_1, k_2, m_f) \quad = \quad & \frac{1}{\lambda}\Bigg[\frac{1}{2}(s - s_1 - s_2) + s_1\left[\frac{1}{2} + (3/\lambda)s_2(s + s_1 - s_2)\right]\Delta_{\#1} \\
& + s_2\left[\frac{1}{2} + (3/\lambda)s_1(s - s_1 + s_2)\right]\Delta_{\#2} \\
& + \left[s_1s_2 - (m_f^2 + (3/\lambda)ss_1s_2)(s - s_1 - s_2)\right]C_{\#0}\Bigg]
\end{aligned}
\tag{2.135}
$$

with

$$
\lambda = \lambda(s, s_1, s_2),
\tag{2.136}
$$

being the usual Mandelstam function and where the analytic expressions for $\Delta_{\#i}$ and $C_{\#0}$ are given by

$$
\begin{aligned}
\Delta_{\#i} \quad & = \quad a_i \ln\frac{a_i + 1}{a_i - 1} - a_3 \ln\frac{a_3 + 1}{a_3 - 1}, \quad \text{(i=1,2)} \\
C_{\#0} \quad & = \quad \frac{1}{\sqrt{\lambda}} \sum_{i=1}^{3}\left[\mathrm{Li}_2\left(\frac{b_i - 1}{a_i + b_i}\right) - \mathrm{Li}_2\left(\frac{-b_i - 1}{a_i - b_i}\right) + \mathrm{Li}_2\left(\frac{-b_i + 1}{a_i - b_i}\right) - \mathrm{Li}_2\left(\frac{b_i + 1}{a_i + b_i}\right)\right],
\end{aligned}
\tag{2.137}
$$

and

$$
t_i = -s_i - i\epsilon, \qquad a_i = \sqrt{1 + (2m_f)^2/t_i}, \ \text{(i=1,2,3)},
$$

$$\lambda = \lambda(t_1, t_2, t_3), \qquad b_1 = (t_1 - t_2 - t_3)/\sqrt{\lambda} \text{ or cyclic} \tag{2.138}$$

For $m_f = 0$ the two expressions above become

$$\begin{aligned} \Delta_{\#i} &= \ln(t_i/t_3), \; (i = 1, 2), \\ C_{\#0} &= (1/\sqrt{\lambda})\left[2\left(\zeta(2) - \mathrm{Li}_2(x_1) - \mathrm{Li}_2(x_2) + \mathrm{Li}_2\left(\frac{1}{x_3}\right)\right) + \ln x_1 \ln x_2\right] \end{aligned} \tag{2.139}$$

with

$$x_i = \frac{(b_i + 1)}{(b_i - 1)}, \; (i = 1, 2, 3). \tag{2.140}$$

These can be inserted into (2.134) and (2.135) together with $m_f = 0$ to generate the corresponding $\mathbf{V}^{\lambda\mu\nu}(0)$ vertex needed for the computation of the massless contributions to the amplitude.

With these notations we clearly have

$$\begin{aligned} \Delta^{\lambda\mu\nu} &= V^{\lambda\mu\nu}(k_1, k_2, m_f) \\ \Delta^{\lambda\mu\nu}(0) &= \mathbf{V}^{\lambda\mu\nu}(k_1, k_2) \\ \Delta^{\lambda\mu\nu}(m_f) &= V^{\lambda\mu\nu}(k_1, k_2, m_f) - \mathbf{V}^{\lambda\mu\nu}(k_1, k_2). \end{aligned}$$

2.7.4 Extension to $Z \rightarrow \gamma^*\gamma$

To isolate the contribution to the decay on the resonance, we keep one of the two photons off-shell (resolved). We choose $s_1 = 0$, and s_2 virtual. We denote by $\Gamma^{\lambda\mu\nu}$ the corresponding vertex in this special kinematical configuration. The Z boson is on-shell. In this case at one-loop the result simplifies considerably [87]

$$\Gamma_{\lambda\mu\nu} = F_2(s_2\epsilon[\lambda, \mu, \nu, k_1] + k_2^\nu \epsilon[\lambda, \mu, k_1, k_2]), \tag{2.141}$$

with F_2 expressed as a Feynman parametric integral

$$F_2 = \frac{1}{2\pi^2}\int_0^1 dz_1 dz_2 dz_3 \delta(1 - z_1 - z_2 - z_3)\frac{-z_2 z_3}{m_f^2 - z_2 z_3 s_2 - z_1 z_3 M_Z^2}. \tag{2.142}$$

Setting $F_2 \equiv -F(z, r_f)$ where $f(z, r)$ is a dimensionless function of

$$z = s_2/M_Z^2, \qquad r_f = m_Z^2/4m_f^2, \tag{2.143}$$

and for vanishing m_f ($r_f = M_Z^2/4m_f^2 \rightarrow \infty$), the corresponding massless contribution is expressed as $F(z, \infty)$ with, in general

$$F(z, r_f) = \frac{1}{4(1-z)^2}(I(r_f z, r_f) - I(r_f, r_f) + 1 - z), \tag{2.144}$$

where

$$I(x, r_f) = 2\sqrt{\frac{x-1}{x^-}}\ln(\sqrt{-x} + \sqrt{1-x}) - \frac{1}{r_f}(\ln(\sqrt{-x} + \sqrt{1-x}))^2 \quad \text{for x} < 0$$

$$
\begin{aligned}
&= 2\sqrt{\frac{1-x}{x}}\sin^{-1}\sqrt{x}+\frac{1}{r_f}(\sin^{-1}\sqrt{x})^2 \quad \text{for } 0<\text{x}<1 \\
&= 2\sqrt{\frac{x-1}{x}}\left(\ln(\sqrt{x}+\sqrt{x-1})-\frac{i\pi}{2}\right)-\frac{1}{r_f}\left(\ln(\sqrt{x}+\sqrt{x-1})-\frac{i\pi}{2}\right)^2, \\
&\quad \text{for } \text{x}>1. \qquad (2.145)
\end{aligned}
$$

The $m_f = 0$ contribution is obtained in the $r_f \to +\infty$ limit,

$$
\begin{aligned}
F(z,\infty) &= \frac{1}{4(1-z)^2}(\ln z + 1 - z) \qquad \text{for} \quad \text{z} > 0, \\
&= \frac{1}{4(1-z)^2}(\ln|z| + i\pi + 1 - z) \quad \text{for} \quad \text{z} < 0. \qquad (2.146)
\end{aligned}
$$

In these notations, the infinite fermion mass limit ($m_f \to \infty$ or $r \to 0$), gives $F(z,0) = 0$ and we find

$$
\begin{aligned}
\Delta^{\lambda\mu\nu} &= \Gamma^{\lambda\mu\nu} = F(z,r_f) \\
\Delta^{\lambda\mu\nu}(0) &= \Gamma^{\lambda\mu\nu}(0) = F(z,\infty) \\
\Delta^{\lambda\mu\nu}(m_f) &= \Gamma^{\lambda\mu\nu} - \Gamma^{\lambda\mu\nu}(m_f) = F(z,r_f) - F(z,\infty), \qquad (2.147)
\end{aligned}
$$

which can be used for a numerical evaluation. The decay rate for the process is given by

$$
\Gamma(Z\to\gamma^*\gamma) = \frac{1}{4M_Z}\int d^4k_1 d^4k_2 \delta(k_1^2)\,\delta(k_2^2-Q_*^2)|\mathcal{M}_{Z\to\gamma\gamma^*}|^2\,(2\pi)^4\delta(k-k_1-k_2), \qquad (2.148)
$$

where

$$
\begin{aligned}
|\mathcal{M}_{Z\to\gamma\gamma^*}|^2 &= -A^{\lambda\mu\nu}_{Z\to\gamma\gamma^*}\Pi_Z^{\lambda\lambda'}A^{\lambda'\mu\nu'}_{Z\to\gamma\gamma^*}\Pi_{Q^*}^{\nu\nu'} \\
\Pi_Z^{\lambda\lambda'} &= -g^{\lambda\lambda'}+\frac{k^\lambda k^{\lambda'}}{M_Z^2} \\
\Pi_{Q^*}^{\nu\nu'} &= -g^{\lambda\lambda'}+\frac{k^\lambda k^{\lambda'}}{Q_*^2}. \qquad (2.149)
\end{aligned}
$$

We have indicated with Q_* the virtuality of the photon. A complete evaluation of this expression, to be of practical interest, would need the fragmentation functions of the photon (see [43] for an example). We briefly summarize the main points involved in the analysis of this and similar processes at the LHC, where the decay rate is folded with the (NLO/NNLO) contribution from the initial state using QCD factorization.

Probably one of the best way to search for neutral current interactions in hadronic collisions at the LHC is in lepton pair production via the Drell-Yan mechanism (all the details of the numerical analysis will be presented in Chap. 5). QCD corrections are known for this process up to $\mathrm{O}(\alpha_s^2)$ (next-to-next-to-leading order, NNLO), which can be folded with the NNLO evolution of the parton distributions to provide accurate determinations of the hadronic pp cross sections at the 4 % level of accuracy [85]. The same computation for Drell-Yan can be used to analyze the $pp \to Z \to \gamma\gamma^*$ process since the W_V (hadronic) part of the process is universal, with W_V defined below. An appropriate (and very useful) way to analyze this process would be to perform this study defining the invariant mass distribution

$$
\frac{d\sigma}{dQ^2} = \tau\sigma_{Z\to\gamma^*\gamma}(Q^2, M_V^2)\,W_V(\tau, Q^2) \qquad (2.150)
$$

where $\tau = Q^2/S$, which is separated into a point-like contribution $\sigma_{Z\to\gamma\gamma^*}$

$$\sigma_V(Q^2, M_V^2) = \frac{\pi\alpha}{4M_Z \sin\theta_W^2 \cos\theta_W^2 N_c} \frac{\Gamma(Z \to \gamma\gamma^*)}{(Q^2 - M_Z^2)^2 + M_Z^2\Gamma_Z^2}. \tag{2.151}$$

and a hadronic structure functions W_Z. This is defined via the integral over parton distributions and coefficient functions Δ_{ij}

$$W_Z(Q^2, M_Z^2) = \int_0^1 dx_1 \int_0^1 dx_2 \int_0^1 dx\, \delta(\tau - x x_1 x_2) PD_{ij}^V(x_1, x_2, \mu_f^2)\Delta_{ij}(x, Q^2, \mu_f^2) \tag{2.152}$$

where μ_f is the factorization scale. The choice $\mu_f = Q$, with Q the invariant mass of the $\gamma\gamma^*$ pair , removes the $\log(Q/M)$ for the computation of the coefficient functions, which is, anyhow, arbitrary. The non-singlet coefficient functions are given by

$$\begin{aligned}
\Delta_{q\bar{q}}^{(0)} &= \delta(1-x) \\
\Delta_{q\bar{q}}^{(1)} &= \frac{\alpha_S(M_V^2)}{4\pi} C_F \left[\delta(1-x)(8\zeta(2) - 16) + 16\left(\frac{\log(1-x)}{1-x}\right)_+ \right. \\
&\qquad \left. -8(1+x)\log(1-x) - 4\frac{1+x^2}{1-x}\log x\right]
\end{aligned} \tag{2.153}$$

with $C_F = (N_c^2 - 1)/(2N_c)$ and the "+" distribution is defined by

$$\left(\frac{\log(1-x)}{1-x}\right)_+ = \theta(1-x)\frac{\log(1-x)}{1-x} - \delta(1-x)\int_0^{1-\delta} dx\, \frac{\log(1-x)}{1-x}, \tag{2.154}$$

while at NLO appears also a qg sector

$$\Delta_{qg}^{(1)} = \frac{\alpha_S(M_V^2)}{4\pi} T_F \left[2(1 + 2x^2 - 2x)\log\left(\frac{(1-x)^2}{x}\right) + 1 - 7x^2 + 6x\right]. \tag{2.155}$$

Other sectors do not appear at this order. Explicitly one gets

$$\begin{aligned}
W_Z(Q^2, M_Z^2) &= \sum_i \int_0^1 dx_1 \int_0^1 dx_2 \int_0^1 dx \delta(\tau - x x_1 x_2) \\
&\quad \times\Big\{\Big(q_i(x_1, \mu_f^2)\bar{q}_i(x_2, \mu_f^2) + \bar{q}_i(x_1, \mu_f^2) q_i(x_2, \mu_f^2)\Big)\Delta_{q\bar{q}}(x, Q^2, \mu_f^2) \\
&\quad + \Big(q_i(x_1, \mu_f^2) g(x_2, \mu_f^2) + q_i(x_2, \mu_f^2) g(x_1, \mu_f^2)\Big)\Delta_{qg}(x, Q^2, \mu_f^2)\Big\}
\end{aligned} \tag{2.156}$$

where the sum is over the quark flavours. The identification of the generalized mechanism of anomaly cancellation requires that this description be extended to NNLO. It involves a slight modification of the NNLO hard scatterings. An explicit computation will be performed in Chap. 5 together with the numerical results.

2.8 Conclusions

We have presented a study of a model inspired by the structure encountered in a typical string theory derivation of the Standard Model. In particular we have focused our investigation on the characterization of the effective action and worked out its expression in the context of an extension containing one additional anomalous $U(1)$. This analysis specializes and, at the same time, extends a previous study of models belonging to this class. The results that we have presented are generic for models where the Stückelberg and the Higgs mechanism are combined and where an effective Abelian anomalous interaction is present. Our analysis has then turned toward the study of simple processes mediated by neutral current exchanges, and we have focused, specifically, on one of them, the one involving the $Z\gamma\gamma$ vertex. In particular our findings clearly show that new massless contributions are presented at one-loop level when anomalous generators are involved in the fermionic triangle diagrams and the interplay between massless and massive fermion effects is modified respect to the SM case. The typical processes considered in our analysis deserve a special attention, given the forthcoming experiments at the LHC, since they may provide a way to determine whether anomaly effects are present in some specific reactions. Other similar processes, involving the entire neutral sector should be considered, though the two-photon signal is probably the most interesting one phenomenologically. Given the high statistical precision (.05% and below on the Z peak, for 10 fb^{-1} of integrated luminosity) which can be easily obtained at the LHC, there are realistic chances to prove or disprove theories of these types.

2.9 Appendix. A Summary on the single anomalous $U(1)$ Model.

We summarize here some results concerning the model with a single anomalous $U(1)$ discussed in the main sections. These results specialize and simplify the general discussion of [1] to which we refer for further details. The hypercharge values used for our analysis are

f	Q_L	u_R	d_R	L	e_R	ν_R
q_Y	$1/6$	$2/3$	$-1/3$	$-1/2$	-1	0

and general $U(1)_B$ charge assignments

f	Q_L	u_R	d_R	L	e_R	ν_R
q_B	$q_B^{(Q_L)}$	$q_B^{(u_R)}$	$q_B^{(d_R)}$	$q_B^{(L)}$	$q_B^{(e_R)}$	$q_B^{(\nu_R)}$

The covariant derivatives act on the fermions f_L, f_R as

$$\mathcal{D}_\mu f_L = \left(\partial_\mu + i\mathbf{A}_\mu + iq_l^{(f_L)} g_l A_{l,\mu}\right) f_L$$
$$\mathcal{D}_\mu f_R = \left(\partial_\mu + i\mathbf{A}_\mu + iq_l^{(f_R)} g_l A_{l,\mu}\right) f_R \tag{2.157}$$

with $l = Y, B$ Abelian index, where $\mathbf{A}_\mu$ is a non-Abelian Lie algebra element and write the lepton doublet as

$$L_i = \begin{pmatrix} \nu_{Li} \\ e_{Li} \end{pmatrix}. \tag{2.158}$$

We will also use standard notations for the $SU(2)_W$ and $SU(3)_C$ gauge bosons

$$W_\mu = \frac{\sigma_i}{2} W_\mu^i = \tau_i W_\mu^i, \quad \text{with} \quad i = 1, 2, 3 \tag{2.159}$$
$$G_\mu = \frac{\lambda_a}{2} G_\mu^a = T_a G_\mu^a \quad \text{with} \quad a = 1, 2, ..., 8 \tag{2.160}$$

with the normalizations

$$Tr[\tau^i\tau^j]=\frac{1}{2}\delta_{ij},\qquad Tr[T^aT^b]=\frac{1}{2}\delta_{ab}. \tag{2.161}$$

The interaction Lagrangian for the leptons becomes

$$\begin{aligned}\mathcal{L}^{lep}_{int} &= (\,\overline{\nu}_{Li}\quad \overline{e}_{Li}\,)\,\gamma^\mu\left[-g_2\frac{\tau^a}{2}W^a_\mu - g_Y\,q^{(L)}_Y A^Y_\mu - g_B q^{(L)}_B B_\mu\right]\begin{pmatrix}\nu_{Li}\\ e_{Li}\end{pmatrix}+\\ &+\overline{e}_{Ri}\,\gamma^\mu\left[-g_Y q^{(e_R)}_Y A^Y_\mu - g_B q^{(e_R)}_B B_\mu\right]e_{Ri}\\ &+\overline{\nu}_{Ri}\,\gamma^\mu\left[-g_Y q^{(\nu_R)}_Y A^Y_\mu - g_B q^{(\nu_R)}_B B_\mu\right]\nu_{Ri}.\end{aligned} \tag{2.162}$$

As usual we define the left-handed and right-handed currents

$$J^L_\mu=\frac{1}{2}(J_\mu-J^5_\mu),\qquad J^R_\mu=\frac{1}{2}(J_\mu+J^5_\mu),\qquad J_\mu=J^R_\mu+J^L_\mu,\qquad J^5_\mu=J^R_\mu-J^L_\mu. \tag{2.163}$$

Writing the quark doublet as

$$Q_{Li}=\begin{pmatrix}u_{Li}\\ d_{Li}\end{pmatrix}, \tag{2.164}$$

we obtain the interaction Lagrangian

$$\begin{aligned}\mathcal{L}^{quarks}_{int} &= (\,\overline{u}_{Li}\quad \overline{d}_{Li}\,)\,\gamma^\mu\left[-g_3\frac{\lambda^a}{2}G^a_\mu - g_2\frac{\tau^i}{2}W^i_\mu - g_Y\,q^{(Q_L)}_Y A^Y_\mu - g_B q^{(Q_L)}_B B_\mu\right]\begin{pmatrix}u_{Li}\\ d_{Li}\end{pmatrix}+\\ &+\overline{u}_{Ri}\,\gamma^\mu\left[-g_Y q^{(u_R)}_Y A^Y_\mu - g_B q^{(u_R)}_B B_\mu\right]u_{Ri}\\ &+\overline{d}_{Ri}\,\gamma^\mu\left[-g_Y q^{(d_R)}_Y A^Y_\mu - g_B q^{(d_R)}_B B_\mu\right]d_{Ri}.\end{aligned} \tag{2.165}$$

As we have already mentioned in the introduction, we work with a two-Higgs doublet model, and therefore we parameterize the Higgs fields in terms of eight real degrees of freedom as

$$H_u=\begin{pmatrix}H^+_u\\ H^0_u\end{pmatrix}\qquad H_d=\begin{pmatrix}H^+_d\\ H^0_d\end{pmatrix} \tag{2.166}$$

where H^+_u, H^+_d and H^0_u, H^0_d are complex fields. Specifically

$$H^+_u=\frac{H^+_{uR}+iH^+_{uI}}{\sqrt{2}},\qquad H^-_d=\frac{H^-_{dR}+iH^-_{dI}}{\sqrt{2}},\qquad H^-_u=H^{+*}_u,\qquad H^+_d=H^{-*}_d. \tag{2.167}$$

Expanding around the vacuum we get for the neutral components

$$H^0_u=v_u+\frac{H^0_{uR}+iH^0_{uI}}{\sqrt{2}},\qquad H^0_d=v_d+\frac{H^0_{dR}+iH^0_{dI}}{\sqrt{2}}. \tag{2.168}$$

The Weinberg angle is defined via $\cos\theta_W=g_2/g,\sin\theta_W=g_Y/g$, with the following relation between the couplings

$$g^2=g_Y^2+g_2^2. \tag{2.169}$$

We also define $\cos\beta = v_d/v$, $\sin\beta = v_u/v$, related by

$$v^2 = v_d^2 + v_u^2. \tag{2.170}$$

2.9.1 The neutral gauge sector

The mass-matrix of the neutral gauge bosons is given by

$$\mathcal{L}_{mass} = \begin{pmatrix} W_3 & A^Y & B \end{pmatrix} \mathbf{M}^2 \begin{pmatrix} W_3 \\ A^Y \\ B \end{pmatrix}, \tag{2.171}$$

where explicitly

$$\mathbf{M}^2 = \frac{1}{4} \begin{pmatrix} {g_2}^2 v^2 & -g_2\, g_Y v^2 & -g_2\, x_B \\ -g_2\, g_Y v^2 & {g_Y}^2 v^2 & g_Y x_B \\ -g_2\, x_B & g_Y x_B & 2M_1^2 + N_{BB} \end{pmatrix} \tag{2.172}$$

with

$$N_{BB} = \left(q_u^{B\,2}\, v_u^2 + q_d^{B\,2}\, v_d^2\right)\, g_B^2, \tag{2.173}$$

$$x_B = \left(q_u^B v_u^2 + q_d^B v_d^2\right)\, g_B. \tag{2.174}$$

The orthonormalized mass squared eigenstates corresponding to this matrix are given by

$$\begin{pmatrix} O_{11}^A \\ O_{12}^A \\ O_{13}^A \end{pmatrix} = \begin{pmatrix} \frac{g_Y}{\sqrt{g_2^2+g_Y^2}} \\ \frac{g_2}{\sqrt{g_2^2+g_Y^2}} \\ 0 \end{pmatrix}, \tag{2.175}$$

$$\begin{pmatrix} O_{21}^A \\ O_{22}^A \\ O_{23}^A \end{pmatrix} = \begin{pmatrix} \frac{g_2\left(2M_1^2-g^2v^2+N_{BB}+\sqrt{\left(2M_1^2-g^2v^2+N_{BB}\right)^2+4g^2x_B^2}\right)}{g^2x_B\sqrt{4+\frac{g^2}{g^4x_B^2}\left(2M_1^2-g^2v^2+N_{BB}+\sqrt{\left(2M_1^2-g^2v^2+N_{BB}\right)^2+4g^2x_B^2}\right)^2}} \\ -\frac{g_Y\left(2M_1^2-g^2v^2+N_{BB}+\sqrt{\left(2M_1^2-g^2v^2+N_{BB}\right)^2+4g^2x_B^2}\right)}{g^2x_B\sqrt{4+\frac{g^2}{g^4x_B^2}\left(2M_1^2-g^2v^2+N_{BB}+\sqrt{\left(2M_1^2-g^2v^2+N_{BB}\right)^2+4g^2x_B^2}\right)^2}} \\ \frac{2}{\sqrt{4+\frac{g^2}{g^4x_B^2}\left(2M_1^2-g^2v^2+N_{BB}+\sqrt{\left(2M_1^2-g^2v^2+N_{BB}\right)^2+4g^2x_B^2}\right)^2}} \end{pmatrix}. \tag{2.176}$$

One can see that these results reproduce the analogous relations of the SM in the limit of very large M_1

$$\lim_{M_1\to\infty} O_{21}^A = \frac{g_2}{g}, \qquad \lim_{M_1\to\infty} O_{22}^A = -\frac{g_Y}{g},$$
$$O_{23}^A \simeq \frac{g}{2}\frac{x_B}{M_1^2} \equiv \frac{g}{2}\epsilon_1 \quad \text{so that} \quad \lim_{M_1\to\infty} O_{23}^A = 0.$$

Similarly, for the other matrix elements of the rotation matrix O^A we obtain

$$\begin{pmatrix} O^A_{31} \\ O^A_{32} \\ O^A_{33} \end{pmatrix} = \begin{pmatrix} -\frac{g_2\left(-2M_1^2+g^2v^2-N_{BB}+\sqrt{\left(2M_1^2-g^2v^2+N_{BB}\right)^2+4g^2x_B^2}\right)}{g^2x_B\sqrt{4+\frac{g^2}{g^4x_B^2}\left(-2M_1^2+g^2v^2-N_{BB}+\sqrt{\left(2M_1^2-g^2v^2+N_{BB}\right)^2+4g^2x_B^2}\right)^2}} \\ \frac{g_Y\left(-2M_1^2+g^2v^2-N_{BB}+\sqrt{\left(2M_1^2-g^2v^2+N_{BB}\right)^2+4g^2x_B^2}\right)}{g^2x_B\sqrt{4+\frac{g^2}{g^4x_B^2}\left(-2M_1^2+g^2v^2-N_{BB}+\sqrt{\left(2M_1^2-g^2v^2+N_{BB}\right)^2+4g^2x_B^2}\right)^2}} \\ \frac{2}{\sqrt{4+\frac{g^2}{g^4x_B^2}\left(-2M_1^2+g^2v^2-N_{BB}+\sqrt{\left(2M_1^2-g^2v^2+N_{BB}\right)^2+4g^2x_B^2}\right)^2}} \end{pmatrix}, \tag{2.177}$$

whose asymptotic behavior is described by the limits

$$O^A_{31} \simeq -\frac{g_2}{2}\frac{x_B}{M_1^2} \equiv -\frac{g_2}{2}\epsilon_1, \qquad O^A_{32} \simeq \frac{g_Y}{2}\frac{x_B}{M_1^2} \equiv \frac{g_Y}{2}\epsilon_1, \qquad O^A_{33} \simeq 1, \tag{2.178}$$

$$\lim_{M_1\to\infty} O^A_{31} = 0, \qquad \lim_{M_1\to\infty} O^A_{32} = 0, \qquad \lim_{M_1\to\infty} O^A_{33} = 1. \tag{2.179}$$

These mass-squared eigenstates correspond to one zero mass eigenvalue for the photon A_γ, and two non-zero mass eigenvalues for the Z and for the Z' vector bosons, corresponding to the mass values

$$\begin{aligned} m_Z^2 &= \frac{1}{4}\left(2M_1^2+g^2v^2+N_{BB}-\sqrt{\left(2M_1^2-g^2v^2+N_{BB}\right)^2+4g^2x_B^2}\right) \\ &\simeq \frac{g^2v^2}{2}-\frac{1}{M_1^2}\frac{g^2x_B^2}{4}+\frac{1}{M_1^4}\frac{g^2x_B^2}{8}(N_{BB}-g^2v^2), \end{aligned} \tag{2.180}$$

$$\begin{aligned} m_{Z'}^2 &= \frac{1}{4}\left(2M_1^2+g^2v^2+N_{BB}+\sqrt{\left(2M_1^2-g^2v^2+N_{BB}\right)^2+4g^2x_B^2}\right) \\ &\simeq M_1^2+\frac{N_{BB}}{2}. \end{aligned} \tag{2.181}$$

The mass of the Z gauge boson gets corrected by terms of the order v^2/M_1, converging to the SM value as $M_1 \to \infty$, with M_1 the Stückelberg mass of the B gauge boson, the mass of the Z' gauge boson can grow large with M_1. The physical gauge fields can be obtained from the rotation matrix O^A

$$\begin{pmatrix} A_\gamma \\ Z \\ Z' \end{pmatrix} = O^A \begin{pmatrix} W_3 \\ A^Y \\ B \end{pmatrix} \tag{2.182}$$

which can be approximated at the first order as

$$O^A \simeq \begin{pmatrix} \frac{g_Y}{g} & \frac{g_2}{g} & 0 \\ \frac{g_2}{g}+O(\epsilon_1^2) & -\frac{g_Y}{g}+O(\epsilon_1^2) & \frac{g}{2}\epsilon_1 \\ -\frac{g_2}{2}\epsilon_1 & \frac{g_Y}{2}\epsilon_1 & 1+O(\epsilon_1^2) \end{pmatrix}. \tag{2.183}$$

The mass squared matrix (2.172) can be diagonalized as

$$\begin{pmatrix} A_\gamma & Z & Z' \end{pmatrix} O^A \mathbf{M}^2 (O^A)^T \begin{pmatrix} A_\gamma \\ Z \\ Z' \end{pmatrix} = \begin{pmatrix} A_\gamma & Z & Z' \end{pmatrix} \begin{pmatrix} 0 & 0 & 0 \\ 0 & m_Z^2 & 0 \\ 0 & 0 & m_{Z'}^2 \end{pmatrix} \begin{pmatrix} A_\gamma \\ Z \\ Z' \end{pmatrix}. \tag{2.184}$$

It is straightforward to verify that the rotation matrix O^A satisfies the proper orthogonality relation

$$O^A (O^A)^T = 1. \tag{2.185}$$

2.9.2 Rotation matrix O^χ on the axi-Higgs

This matrix is needed in order to rotate into the mass eigenstates of the CP-odd sector, relating the axion χ and the two neutral Goldstones of this sector to the Stückelberg field b and the CP-odd phases of the two Higgs doublets

$$\begin{pmatrix} \mathrm{Im} H_u^0 \\ \mathrm{Im} H_d^0 \\ b \end{pmatrix} = O^\chi \begin{pmatrix} \chi \\ G_1^0 \\ G_2^0 \end{pmatrix}. \tag{2.186}$$

We refer to [1] for a more detailed discussion of the scalar sector of the model, where, in the presence of explicit phases (PQ-breaking terms), the mass of the axion becomes massive from the massless case. The PQ symmetric contribution is given by

$$V_{PQ}(H_u, H_d) = \sum_{a=u,d} \left(\mu_a^2 H_a^\dagger H_a + \lambda_{aa} (H_a^\dagger H_a)^2 \right) - 2\lambda_{ud} (H_u^\dagger H_u)(H_d^\dagger H_d) + 2\lambda'_{ud} |H_u^T \tau_2 H_d|^2, \tag{2.187}$$

while the PQ-breaking terms are

$$\begin{aligned} V_{\not{P}\not{Q}}(H_u, H_d, b) \quad = \quad & b_1 \left(H_u^\dagger H_d \, e^{-i(q_u^B - q_d^B)\frac{b}{M_1}} \right) + \lambda_1 \left(H_u^\dagger H_d \, e^{-i(q_u^B - q_d^B)\frac{b}{M_1}} \right)^2 \\ & + \lambda_2 \left(H_u^\dagger H_u \right) \left(H_u^\dagger H_d \, e^{-i(q_u^B - q_d^B)\frac{b}{M_1}} \right) + \lambda_3 \left(H_d^\dagger H_d \right) \left(H_u^\dagger H_d \, e^{-i(q_u^B - q_d^B)\frac{b}{M_1}} \right) + c.c. \end{aligned} \tag{2.188}$$

where b_1 has mass squared dimension, while λ_1, λ_2, λ_3 are dimensionless. From the scalar potential one can extract the mass eigenvalues of the model for the scalar sector. The mass matrix has two zero eigenvalues and one non-zero eigenvalue that corresponds to a physical axion field, χ, with mass

$$m_\chi^2 = -\frac{1}{2} c_\chi v^2 \left[1 + \left(\frac{q_u^B - q_d^B}{M_1} \frac{v \sin 2\beta}{2} \right)^2 \right] = -\frac{1}{2} c_\chi v^2 \left[1 + \frac{(q_u^B - q_d^B)^2}{M_1^2} \frac{v_u^2 v_d^2}{v^2} \right], \tag{2.189}$$

where

$$c_\chi = 4 \left(4\lambda_1 + \lambda_3 \cot\beta + \frac{b_1}{v^2} \frac{2}{\sin 2\beta} + \lambda_2 \tan\beta \right), \tag{2.190}$$

and $v_d = v\cos\beta, v_u = v\sin\beta$ together with

$$\cot\beta = \frac{\cos\beta}{\sin\beta} = \frac{v_d}{v_u}, \qquad \tan\beta = \frac{\sin\beta}{\cos\beta} = \frac{v_u}{v_d}. \tag{2.191}$$

The mass of this state is positive if $c_\chi < 0$. Notice that the mass of the axi-Higgs is the result of two effects: the presence of the Higgs v.e.v.'s and the presence of a PQ-breaking potential whose parameters can be small enough to drive the mass of this particle to be very light. We refer to Sec. 1.4.1 for a simple illustration of this effect in an Abelian model. The rotation matrix O^χ is shown below.

Introducing N given by

$$N = \frac{1}{\sqrt{1 + \frac{(q_u^B - q_d^B)^2}{M_1^2} \frac{v_d^2 v_u^2}{v^2}}} = \frac{1}{\sqrt{1 + \frac{(q_u^B - q_d^B)^2}{M_1^2} \frac{v^2 \sin^2 2\beta}{4}}} \tag{2.192}$$

and defining

$$Q_1 = -\frac{(q_u^B - q_d^B)}{M_1} v_u = -\frac{(q_u^B - q_d^B)}{M_1} v \sin\beta, \tag{2.193}$$

$$N_1 = \frac{1}{\sqrt{1 + Q_1^2}}, \tag{2.194}$$

O^χ is the following matrix

$$O^\chi = \begin{pmatrix} -N\cos\beta & \sin\beta & \overline{N}_1 \overline{Q}_1 \cos\beta \\ N\sin\beta & \cos\beta & -\overline{N}_1 \overline{Q}_1 \sin\beta \\ N Q_1 \cos\beta & 0 & \overline{N}_1 \end{pmatrix}, \tag{2.195}$$

where we defined

$$\overline{Q}_1 = Q_1 \cos\beta \tag{2.196}$$

and

$$\begin{aligned} \overline{N}_1 &= \frac{1}{\sqrt{1 + \overline{Q}_1^2}} = \frac{1}{\sqrt{1 + Q_1^2 \cos^2\beta}} \\ &= \frac{1}{\sqrt{1 + \frac{(q_u^B - q_d^B)^2}{M_1^2} v^2 \sin^2\beta \cos^2\beta}} = \frac{1}{\sqrt{1 + \frac{(q_u^B - q_d^B)^2}{M_1^2} \frac{v_u^2 v_d^2}{v^2}}}. \end{aligned} \tag{2.197}$$

One can see from (2.192) that $\overline{N}_1 = N$, and the explicit elements of the 3-by-3 rotation matrix O^χ can be written as

$$\begin{aligned} (O^\chi)_{11} &= -\frac{1}{\frac{-(q_u^B - q_d^B)}{M_1} v_u \sqrt{\frac{M_1^2}{(q_u^B - q_d^B)^2} \frac{v^2}{v_u^2 v_d^2} + 1}} \\ &= -\frac{1}{v_u \, \frac{v}{v_u v_d}} N = -N\cos\beta \end{aligned} \tag{2.198}$$

$$\begin{aligned} (O^\chi)_{21} &= \frac{1}{\frac{-(q_u^B - q_d^B)}{M_1} v_d \sqrt{\frac{M_1^2}{(q_u^B - q_d^B)^2} \frac{v^2}{v_u^2 v_d^2} + 1}} \\ &= \frac{1}{v_d \, \frac{v}{v_u v_d}} N = N\sin\beta \end{aligned} \tag{2.199}$$

$$
\begin{aligned}
(O^{\chi})_{31} &= \frac{1}{\sqrt{\frac{M_1^{\,2}}{(q_u^B-q_d^B)^2}\frac{v^2}{v_u^2 v_d^2}+1}} \\
&= \frac{1}{\frac{M_1}{-(q_u^B-q_d^B)\,v_u}\;v_u\sqrt{\frac{(q_u^B-q_d^B)^2}{M_1^{\,2}}+\frac{v^2}{v_u^2 v_d^2}}} = N Q_1 \cos\beta
\end{aligned}
\tag{2.200}
$$

$$
(O^{\chi})_{12} = \frac{v_u}{\sqrt{v_u^2+v_d^2}} = \sin\beta \tag{2.201}
$$

$$
(O^{\chi})_{22} = \frac{v_d}{\sqrt{v_u^2+v_d^2}} = \cos\beta \tag{2.202}
$$

$$
(O^{\chi})_{32} = 0 \tag{2.203}
$$

$$
\begin{aligned}
(O^{\chi})_{13} &= \frac{1}{\sqrt{1+\frac{(q_u^B-q_d^B)^2}{M_1^{\,2}}\frac{v_u^{\,2}v_d^{\,2}}{v^2}}}\left(-\frac{(q_u^B-q_d^B)}{M_1}\right)\frac{v_u v_d^2}{v^2} \\
&= N\left[-\frac{(q_u^B-q_d^B)}{M_1}v_u\cos\beta\right]\cos\beta = N\overline{Q}_1\cos\beta
\end{aligned}
\tag{2.204}
$$

$$
\begin{aligned}
(O^{\chi})_{23} &= -\frac{1}{\sqrt{1+\frac{(q_u^B-q_d^B)^2}{M_1^{\,2}}\frac{v_u^{\,2}v_d^{\,2}}{v^2}}}\left(-\frac{(q_u^B-q_d^B)}{M_1}\right)\frac{v_u^2 v_d}{v^2} \\
&= -N\left[\frac{-(q_u^B-q_d^B)}{M_1}v_u\cos\beta\right]\sin\beta = -N\overline{Q}_1\sin\beta
\end{aligned}
\tag{2.205}
$$

$$
(O^{\chi})_{33} = \frac{1}{\sqrt{1+\frac{(q_u^B-q_d^B)^2}{M_1^{\,2}}\frac{v_u^{\,2}v_d^{\,2}}{v^2}}} = N. \tag{2.206}
$$

It can be easily checked that this is an orthogonal matrix

$$
(O^{\chi})^T O^{\chi} = 1_{3\times 3}. \tag{2.207}
$$

2.9.3 Appendix. Vanishing of $\Delta^{\lambda\mu\nu}$ for on-shell external physical states

An important property of the triangle amplitude is its vanishing for on-shell external physical states.

The vanishing of the amplitude Δ for on-shell physical states can be verified once we have assumed conservation of the vector currents. This is a simple example of a result that, in general, goes under the name of the Landau-Yang theorem. In our case we use only the expression of the triangle in Rosenberg parametrization [42] and its gauge invariance to obtain this result. We stress this point here since if we modify the WI on the correlator, as we are going to discuss next, additional interactions are needed in the analysis of processes mediated by this diagram in order to obtain consistency with the theorem.

We introduce the three polarization four-vectors for the λ, μ, and ν lines, denoted by $\mathbf{e}$, $\epsilon_{\mathbf{1}}$ and $\epsilon_{\mathbf{2}}$ respectively, and we use the Sudakov parameterization of each of them, using the massless vectors k_1 and k_2 as a longitudinal basis on the light-cone, plus transversal ($\perp$) components which are orthogonal to the longitudinal ones. We have

$$
\mathbf{e} \;=\; \alpha(k_1-k_2)+\mathbf{e}_{\perp} \qquad \varepsilon_{\mathbf{1}} = a k_1 + \varepsilon_{\mathbf{1}\perp} \qquad \varepsilon_{\mathbf{2}} = b k_2 + \varepsilon_{\mathbf{2}\perp}, \tag{2.208}
$$

where we have used the condition of transversality $\mathbf{e}\cdot k = 0, \varepsilon_{\mathbf{1}}\cdot k_1 = 0, \varepsilon_{\mathbf{2}}\cdot k_2 = 0$, the external lines being now physical. Clearly $\mathbf{e}_{\perp}\cdot k_1 = \mathbf{e}_{\perp}\cdot k_2 = 0$, and similar relations hold also for $\varepsilon_{\mathbf{1}\perp}$ and $\varepsilon_{\mathbf{2}\perp}$, all the transverse polarization vectors being orthogonal to the light-cone spanned by k_1 and k_2. From gauge invariance on the $\mu\nu$ lines in the invariant amplitude, we are allowed to drop the light-cone components of the polarizators for these two lines

$$\Delta^{\lambda\mu\nu}\mathbf{e}_\lambda\varepsilon_{\mathbf{1}\mu}\varepsilon_{\mathbf{2}\nu} = \Delta^{\lambda\mu\nu}\mathbf{e}_\lambda\varepsilon_{\mathbf{1}\mu\perp}\varepsilon_{\mathbf{2}\nu\perp}, \tag{2.209}$$

and a simple computation then gives (introducing $\mathbf{e}_\perp \equiv (0,\vec{\mathbf{e}})$ and similar)

$$\begin{aligned}\Delta^{\lambda\mu\nu}\mathbf{e}_\lambda\varepsilon_{\mathbf{1}\mu\perp}\varepsilon_{\mathbf{2}\nu\perp} &= \underline{a}_1\epsilon[k_1-k_2,\varepsilon_{\mathbf{1}\perp},\varepsilon_{\mathbf{2}\perp},\mathbf{e}] = \underline{a}_1\epsilon[k_1-k_2,\varepsilon_{\mathbf{1}\perp},\varepsilon_{\mathbf{2}\perp},\alpha(k_1-k_2)+\mathbf{e}_\perp]\\ &\propto (\vec{\varepsilon}_{1\perp}\times\vec{\varepsilon}_{2\perp})\cdot\vec{\mathbf{e}}_\perp = 0,\end{aligned} \tag{2.210}$$

since the three transverse polarizations are linearly dependent. Notice that this proof shows that $Z \rightarrow \gamma\gamma$ with all three particles on-shell does not occur.

2.10 Appendix. Anomalous traces

Here we briefly discuss the computation of the anomalous traces in front of the triangle amplitudes. We work with massless fermion amplitudes. The anomaly coefficient in Eq. (2.18) can be obtained starting from the triangle diagram in momentum space. For instance we get

$$\begin{aligned}&\Delta^{\lambda\mu\nu,ij}_{BSU(2)SU(2)} = g_B g_2^2\, Tr[\tau^i\tau^j]\sum_f q_B^{fL}\mathbf{\Delta}^{L\lambda\mu\nu}\\ =\;& g_B g_2^2\, Tr[\tau^i\tau^j]\sum_f q_B^{fL}(i)^3\int\frac{d^4q}{(2\pi)^4}\frac{Tr[\gamma^\lambda P_L(\not q-\not k)\gamma^\nu P_L(\not q-\not k_1)\gamma^\mu P_L\not q]}{q^2(q-k_1)^2(q-k)^2}\\ &+(k_1\rightarrow k_2,\mu\rightarrow\nu)\\ =\;& g_B g_2^2\, Tr[\tau^i\tau^j]\frac{1}{8}\sum_f q_B^{fL}(i)^3\int\frac{d^4q}{(2\pi)^4}\frac{Tr[\gamma^\lambda(1-\gamma^5)(\not q-\not k)\gamma^\nu(1-\gamma^5)(\not q-\not k_1)\gamma^\mu(1-\gamma^5)\not q]}{q^2(q-k_1)^2(q-k)^2}\\ &+(k_1\rightarrow k_2,\mu\rightarrow\nu)\end{aligned} \tag{2.211}$$

and isolating the four anomalous contributions of the form **AAA**, **AVV**, **VAV** and **VVA** we obtain

$$D_B^{(L)} = \frac{1}{8}Tr[q_B^{fL}] \equiv -\frac{1}{8}\sum_f q_B^{fL}. \tag{2.212}$$

Similarly in the Abelian case we obtain

$$\begin{aligned}&\Delta^{\lambda\mu\nu}_{BBB} = g_B^3\sum_f (q_B^{fR})^3\mathbf{\Delta}^{R\lambda\mu\nu} + g_B^3\sum_f (q_B^{fL})^3\mathbf{\Delta}^{L\lambda\mu\nu}\\ =\;& g_B^3\sum_f (q_B^{fR})^3(i)^3\int\frac{d^4q}{(2\pi)^4}\frac{Tr[\gamma^\lambda P_R(\not q-\not k)\gamma^\nu P_R(\not q-\not k_1)\gamma^\mu P_R\not q]}{q^2(q-k_1)^2(q-k)^2}\\ &+g_B^3\sum_f (q_B^{fL})^3(i)^3\int\frac{d^4q}{(2\pi)^4}\frac{Tr[\gamma^\lambda P_L(\not q-\not k)\gamma^\nu P_L(\not q-\not k_1)\gamma^\mu P_L\not q]}{q^2(q-k_1)^2(q-k)^2}\\ &+\,(k_1\rightarrow k_2,\mu\rightarrow\nu)\\ =\;& g_B^3\frac{1}{8}\sum_f (q_B^{fR})^3(i)^3\int\frac{d^4q}{(2\pi)^4}\frac{Tr[\gamma^\lambda(1+\gamma^5)(\not q-\not k)\gamma^\nu(1+\gamma^5)(\not q-\not k_1)\gamma^\mu(1+\gamma^5)\not q]}{q^2(q-k_1)^2(q-k)^2}\end{aligned}$$

$$
\begin{aligned}
&+ g_B^3 \, \frac{1}{8} \sum_f (q_B^{fL})^3 (i)^3 \int \frac{d^4 q}{(2\pi)^4} \frac{Tr[\gamma^\lambda (1-\gamma^5)(\not{q} - \not{k})\gamma^\nu (1-\gamma^5)(\not{q} - \not{k}_1)\gamma^\mu (1-\gamma^5)\not{q}]}{q^2 (q-k_1)^2 (q-k)^2} \\
&+(k_1 \rightarrow k_2, \mu \rightarrow \nu)
\end{aligned}
\tag{2.213}
$$

with the related coefficient

$$
D_{BBB} = \frac{1}{8} Tr[q_B^3] = \frac{1}{8} \sum_f \left[(q_B^{fR})^3 - (q_B^{fL})^3 \right].
$$

The other coefficients reported in Eq. (2.25) are obtained similarly.

2.11 Appendix. CS and GS terms rotated

The rotation of the CS and the GS terms into the physical fields and the Goldstone gives

$$
\begin{aligned}
V_{CS}^{BYY} &= d_1 \langle BY \wedge F_Y \rangle = (-i) d_1 \epsilon^{\lambda\mu\nu\alpha} (k_{1\alpha} - k_{2\alpha}) \left[(O^{A\,T})_{21}^2 (O^{A\,T})_{32} \right] Z^\lambda A_\gamma^\mu A_\gamma^\nu + \ldots \\
V_{CS}^{BWW} &= c_1 \langle \epsilon^{\mu\nu\rho\sigma} B_\mu C_{\nu\rho\sigma}^{Abelian} \rangle = (-i) c_1 \epsilon^{\lambda\mu\nu\alpha} (k_{1\alpha} - k_{2\alpha}) \left[(O^{A\,T})_{11}^2 (O^{A\,T})_{32} \right] Z^\lambda A_\gamma^\mu A_\gamma^\nu + \ldots \\
V_{GS}^{bYY} &= \frac{C_{YY}}{M} b F_Y \wedge F_Y = 4 \frac{C_{YY}}{M} b \epsilon^{\mu\nu\rho\sigma} k_\mu k_\nu Y_\rho Y_\sigma = 4 \frac{C_{YY}}{M} \epsilon^{\mu\nu\rho\sigma} k_\mu k_\nu \left[O_{31}^\chi (O^{A\,T})_{21}^2 \, \chi A_\gamma^\mu A_\gamma^\nu \right. \\
&\qquad \left. + (O_{32}^\chi C_1 + O_{33}^\chi C_1')(O^{A\,T})_{21}^2 G_Z A_\gamma^\mu A_\gamma^\nu \right] + \ldots \\
V_{GS}^{bWW} &= \frac{F}{M} b Tr \left[F_W \wedge F_W \right] = 4 \frac{C_{YY}}{M} \frac{b}{2} \epsilon^{\mu\nu\rho\sigma} k_\mu k_\nu W_\rho^i W_\sigma^i = 4 \frac{F}{M} \epsilon^{\mu\nu\rho\sigma} k_\mu k_\nu \left[O_{31}^\chi (O^{A\,T})_{11}^2 \, \chi A_\gamma^\mu A_\gamma^\nu \right. \\
&\qquad \left. + (O_{32}^\chi C_1 + O_{33}^\chi C_1')(O^{A\,T})_{11}^2 \right] G_Z A_\gamma^\mu A_\gamma^\nu + \ldots
\end{aligned}
\tag{2.214}
$$

These vertices appear in the cancellation of the gauge dependence in s-channel exchanges of Z gauge bosons in the R_ξ gauge. The dots refer to the additional contributions, proportional to interactions of χ, the axi-Higgs, with the neutral gauge bosons of the model.

Chapter 3

Unitarity Bounds for Gauged Axionic Interactions and the Green-Schwarz Mechanism

3.1 Introduction to the chapter

The cancellation of gauge anomalies in the Standard Model is a landmark of modern particle theory that has contributed to shape our knowledge on the fermion spectrum, its chiral charges and couplings. Other mechanisms of cancellation, based on the introduction of both local and non-local counterterms, have also received a lot of attention in the last two decades, from the introduction of the Wess-Zumino term in gauge theories [88] (which is local) to the Green-Schwarz mechanism of string theory [89] (which is non-local). The field theory realization of this second mechanism is rather puzzling also on phenomenological grounds since it requires, in 4 dimensions, the non-local exchange of a pseudoscalar to restore gauge invariance in the anomalous vertices. In higher dimensions, for instance in 10 dimensions, the violation of the Ward Identities due to the hexagon diagram is canceled by the exchange of a 2-form [89, 62, 63]. In this chapter we are going to analyze the similarities between the two approaches and emphasize the differences as well. We will try, along the way, to point out those unclear aspects of the field theory realization of this mechanism - in the absence of supersymmetry and gravitational interactions - which, apparently, suffers from the presence of an analytic structure in the energy plane that is in apparent disagreement with unitarity. Moving to the WZ case, here we show that the restoration of gauge invariance in the corresponding one-loop effective Lagrangian via a local axion counterterm is not able to guarantee unitarity beyond a certain scale, although this deficiency is expected [21, 13], given the local nature of the counterterm. In the GS case, the restoration of the Ward Identities suffers from the presence of unphysical massless poles in the trilinear gauge vertices that, as we are going to show, are similar to those present in a non-local version of axial electrodynamics, which has been studied extensively in the past [20] with negative conclusions concerning its unitarity properties. In particular, in the case of scalar potentials that include Higgs-axion mixing, the phenomenological interpretation of the GS mechanism remains problematic in the field theoretical construction.

We comment on the relation between the two mechanisms, when the axion is integrated out of the partition function of the anomalous theory, and on other issues of the gauge dependence of the perturbative expansions, which emerge in the different formulations. In the second part of the chapter we apply our analysis to a realistic model characterizing numerically the bounds in effective actions of WZ type and discuss the possibility to constrain brane and axion-like models at the LHC.

3.1.1 WZ and GS counterterms

Anomalous Abelian models are variations of the SM in which the gauge structure of this is enlarged by one or more Abelian factors. The corresponding anomalies are canceled by the introduction of a pseudoscalar, an axion (b), that couples to 4-forms $F_I \wedge F_J$ (via $b/M F_I \wedge F_J$, the Wess-Zumino term) of the gauge fields (I, J). M is a scale that is apparently unrelated to the rest of the theory and simply describes the range in which the anomalous model can be used as a good approximation to the underlying complete theory. The latter can be resolved at an energy $E > M$, by using either a renormalizable Lagrangian with an anomaly-free chiral fermion spectrum or a string theory. The motivations for introducing such models are several, ranging from the study of the flavor sector, where several attempts have been performed in the last decade to reproduce the neutrino mixing matrix using theories of this type, to effective string models, in which the extra $U(1)$ abound. We also recall that in effective string models and in models characterized by extra dimensions the axion (b) appears together with a mixing to the anomalous gauge boson ($\partial b B$), which is, by coincidence, natural in a (Higgs) theory in a broken phase. In a way, theories of this type have several completions at higher energy [13].

Coming to the specific models that we analyze, these are complete mLSOM-like [1, 12, 26, 71, 90] models with three anomalous $U(1)$ [91, 92], while most of the unitarity issues are easier to address in simple models with two U(1) [40]. In our phenomenological analysis, which concerns only effective actions of WZ type, we will choose the charge assignments and the construction of [93, 60], but we will work in the region of parameter space where only the lowest Stückelberg mass eigenvalue is taken into account, while the remaining two extra Z' decouple. This configuration is not the most general but is enough to clarify the key physical properties of these models.

3.2 Anomaly cancellation and gauge dependences: the GS and the WZ mechanisms in field theory

In this section we start our discussion of the unitarity properties of the GS and WZ mechanisms, illustrating the critical issues. We illustrate a pure diagrammatic construction of the WZ effective action using a set of basic local counterterms and show how a certain class of amplitudes have an anomalous behavior that grows beyond their unitarity limit at high energy. The arguments being rather subtle, we have decided to illustrate the construction of the effective action for both mechanisms in parallel. A re-arrangement of the same basic counterterms of the WZ case generates the GS effective action, which, however, is non-local. The two mechanisms are different even if they share a common origin. In a following section we will integrate out the axion of the WZ formulation to generate a non-local form of the same mechanism that resembles more closely the GS counterterm. The two differ by a set of extra non-local interactions in their respective effective actions. One could go the other way and formulate the GS mechanism in a local form using (two or more) extra auxiliary fields. These points are relevant in order to understand the connection between the two ways to cancel the anomaly.

3.2.1 The Lagrangian

Specifically, the toy model that we consider has a single fermion with a vector-like interaction with the gauge field A and a purely axial-vector interaction with B. The Lagrangian is given by

$$\mathcal{L}_0 \quad = \quad -\frac{1}{4}F_A^2 - \frac{1}{4}F_B^2 + \frac{1}{2}(\partial_\mu b + M_1 \; B_\mu)^2 + \overline{\psi} i\gamma^\mu(\partial_\mu + ieA_\mu + ig_B\gamma^5 B_\mu)\psi, \tag{3.1}$$

where, for simplicity, we have taken all the charges to be unitary, and we have allowed for a Stückelberg term for B, with M_1 being the Stückelberg mass [1]. A is massless and takes the role of a photon. The Lagrangian has a Stückelberg-like symmetry with $b \to b - M_1\theta_B$ under a gauge transformation of B_μ, $\delta B_\mu = \partial_\mu \theta_B$. The axion is a singlet under gauge transformations of A. We call this simplified theory the "A-B" Model. We are allowed not to perform any gauge-fixing on B and keep the coupling of the longitudinal component of B to the axion, ∂Bb, as an interaction vertex. If we remove A, we call the simplified model the "B Model". We will be interchanging between these two models for illustrative purposes and to underline the essential features of theories of this type.

In the A-B Model, the $U(1)_A$ gauge freedom can be gauge-fixed in a generic Lorentz gauge, with polarization vectors that carry a dependence on the gauge parameter ξ_A, but A being non-anomalous we will assume trivially the validity of the Ward Identities on vector-like currents. This will erase any dependence on ξ_A both of the polarization vectors of A and of the propagators of the same gauge boson. At the same time Chern-Simons (CS) interactions such as $AB \wedge F_B$ or $AB \wedge F_A$, which are present if we define triangle diagrams with a symmetric distribution of the partial anomalies of each vertex both in the **AVV** (axial-vector/vector/vector) and **AAA** cases [40, 92], can be absorbed by a re-distribution of the anomaly. For instance, if we assume vector Ward Identities on the A-current and move the whole anomaly to the axial-vector currents, then the CS terms can be omitted. The anomalous corrections in the one-loop effective action are due to triangle diagrams of the form BAA (**AVV**, with conserved vector currents) and BBB (**AAA** with a symmetric distribution of the anomalies) which require two WZ counterterms, given in S_{WZ} below, for anomaly cancellation. Since the analysis of anomalous gauge theories containing WZ terms has been the subject of various analyses with radically different conclusions regarding the issue of unitarity of these theories, we refer to the literature for more details [20, 94, 95, 96, 97, 98]. Our goal here is to simply stress the relevance of these analyses in order to understand the difference between the WZ and GS cancellation mechanism and clarify that Higgs-axion mixing does not find a suitable description within the standard formulation of the GS mechanism. A detailed analysis of the unitarity issue will be presented in Chap. 4.

3.3 Local and non-local formulations

The GS mechanism is closely related to the WZ mechanism [88]. The latter, in this case, consists in restoring gauge invariance of an anomalous theory by introducing a shifting pseudoscalar, an axion, that couples to the divergence of an anomalous current. It can be formulated starting from a massive Abelian theory and performing a *field-enlarging transformation* [40] so as to generate a complete gauge invariant model in which the usual Abelian symmetry is accompanied by a shifting axion. The original Lagrangian of the massive gauge theory is interpreted as the gauge-fixed case of the field-enlarged Lagrangian. The

---

[1] Even if (3.1) is not the most general invariant Lagrangian under the gauge group $U(1)_A \times U(1)_B$, our considerations are the same. In fact, since b shifts only under a gauge variation of the anomalous $U(1)$ gauge field B (and not under A), the gauge invariance of the effective action under a gauge transformation of the gauge field A requires that there are no terms of the type $bF_A \wedge F_B$.

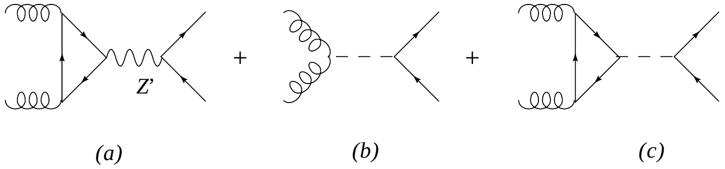

Figure 3.1: One-loop vertices and counterterms in the R_ξ gauge for the A-B Model for the WZ case.

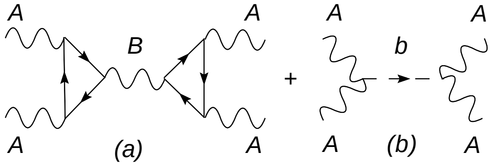

Figure 3.2: A typical Bouchiat-Iliopoulos-Meyer amplitude and the axion counterterm to restore gauge invariance in the R_ξ gauge in the WZ effective action.

gauge variation of the anomalous effective action is compensated by the WZ term, so as to have a gauge invariant formulation of the model. We will show next that a theory built in this way has a unitarity bound that we will be able to quantify. The appearance of the axion in these theories seems to be an artifact, since the presence of a symmetry allows one to set the axion to vanish, choosing a unitary gauge. In brane models, in the presence of a suitable scalar potential, the axion ceases to be a gauge artifact and cannot be gauged away, as shown in [1, 12]. This point is rather important, since it shows that the GS counterterm is unable to describe Higgs-axion mixing, which takes place when the Peccei-Quinn [22, 99] symmetry of the scalar potential is broken. The reason is quite obvious: the GS virtual axion is a massless exchange whose presence is just to guarantee the decoupling of the longitudinal component of the gauge boson from the anomaly and that does not describe a physical state. But before coming to a careful analysis of this point, let us discuss the counterterms of the Lagrangian.

In the A-B Model the WZ counterterms are

$$\mathcal{L}_{WZ} = \frac{C_{AA}}{2!M_1} b F_A \wedge F_A + \frac{C_{BB}}{2!M_1} b F_B \wedge F_B, \tag{3.2}$$

which are fixed by the condition of gauge invariance of the Lagrangian. The best way to proceed in the analysis of this theory is to work in the R_ξ gauge in order to remove the $B-b$ mixing [40]. Alternatively, we are entitled to keep the mixing and perform a perturbative expansion of the model using the Proca propagator for the massive gauge boson, and treat the $b\partial B$ term as a bilinear vertex. This second approach can be the source of some confusion, since one could be misled and identify the perturbative expansion obtained by using the WZ theory with that of the GS mechanism, which involves, at a field theory level, only a re-definition of the trilinear fermionic vertex with a pole-like counterterm. In the WZ effective action, treated with the $b-B$ mixing (and not in the R_ξ gauge), similar counterterms appear.

We show in Fig. 3.1 the vertices of the effective action in the R_ξ gauge approach, and we combine them to describe the process $AA \to AA$, as shown in Fig. 3.2. Graph a) of Fig. 3.2 is a typical BIM amplitude [38], first studied in '72 by Bouchiat, Iliopoulos and Meyer to analyze the gauge independence of anomaly-mediated processes in the Standard Model. The gauge independence of this process is a necessary condition in a gauge theory in order to have a consistent S-matrix free of spurious singularities [40], but is not sufficient to guarantee the absence of a unitarity bound. Typically, gauge cancellations help to identify the correct power counting (in $1/M_1$ and in the coupling constants) of the theory and

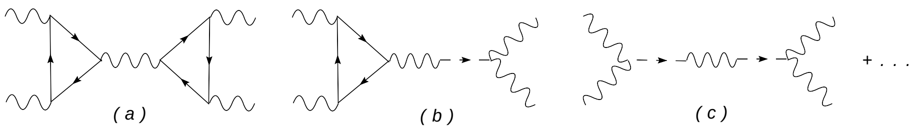

Figure 3.3: Perturbative expansion of the $AA \to AA$ amplitude in the presence of $B-b$ mixing.

are essential to establish the overall correctness of the perturbative computations using the vertices of the effective action. In our example, this can be established as follows: diagram b) of Fig. 3.2 cancels the gauge dependence of diagram a) but leaves an overall remnant, which is the contribution of diagram a) computed in the unitary gauge ($\xi \to \infty$) in which the propagator takes the Proca form

$$D_P^{\lambda\lambda'}(k) = -\frac{i}{k^2 - M_1^2}\left(g^{\lambda\lambda'} - \frac{k^\lambda k^{\lambda'}}{M_1^2}\right). \tag{3.3}$$

Due to this cancellation, the total contribution of the two diagrams is

$$\Delta_A^{\lambda\mu\nu}(k,p_1,p_2) D_P^{\lambda\lambda'} \Delta_A^{\lambda'\mu'\nu'}(k,k_1,k_2), \tag{3.4}$$

where Δ_A is given by the Dolgov-Zakharov parameterization

$$\Delta_A^{\lambda\mu\nu}(k,p_1,p_2) = A_6(s)(k_1+k_2)^\lambda \epsilon\left[k_1,k_2,\nu,\mu\right], \tag{3.5}$$

where the coefficient $A_6(s)$ in the massless case is $A_6(s) = 1/2(\pi^2 s)$.

We call Δ_B the triangle with a symmetric distribution of the anomaly ($a_n/3$ for each vertex), which is obtained from Δ_A by the addition of suitable CS terms [91, 92]. The bad behavior of this amplitude at high energy is then trivially given by [2]

$$\frac{1}{M_1^2}\Delta_A^{\lambda\mu\nu}\frac{k_\lambda k_{\lambda'}}{k^2 - M_1^2}\Delta_A^{\lambda'\mu'\nu'}(k,k_1,k_2) = \frac{1}{M_1^2}\frac{a_n^2}{k^2 - M_1^2}\epsilon[\mu,\nu,p_1,p_2]\epsilon[\mu',\nu',k_1,k_2], \tag{3.6}$$

with $a_n = i/(2\pi^2)$. Squaring the amplitude, the corresponding cross section grows linearly with $s = k^2$, which signals the breaking of unitarity, as expected in Proca theory, if the corresponding Ward Identities are violated. A similar result holds for the BBB case. In the alternative formulation, in which the $b-B$ term is treated as a vertex, the perturbative expansion is formulated diagrammatically as in Fig. 3.3. Though the expansion is less transparent in this case, it is still expected to reproduce the results of the R_ξ gauge and of the unitary gauge. Notice that the expansion seems to generate the specific GS counterterms (Graph 3b)) that limits the interaction of the gauge field with the anomaly to its transverse component, together with some extra graphs, which are clearly not absorbed by a re-definition of the gauge vertex.

3.3.1 Integrating out the Stückelberg in the WZ case

We can make a forward step and try to integrate out the axion from the partition function and obtain the non-local version of the WZ effective action. Notice that this is straightforward only in the case in which Higgs- axion mixing is absent. The partition function in this case is given by

$$Z = \int D\psi\, D\bar{\psi}\, DA\, DB\, Db\, \exp\left(i\langle\mathcal{L}(\psi,\bar{\psi},A,B,b)\rangle\right), \tag{3.7}$$

---

[2] We will use the coincise notation $\epsilon[\lambda,p,k,\nu] \equiv \epsilon^{\lambda\alpha\beta\nu}p_\alpha k_\beta$

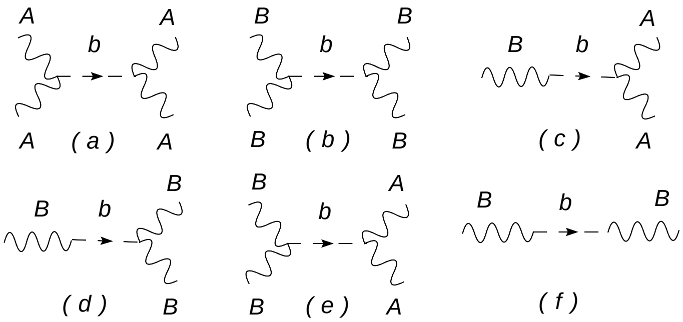

Figure 3.4: The structure of the WZ effective action having integrated out the axion.

where $\langle\,\rangle$ denote integration over x and

$$\mathcal{L} = \mathcal{L}_0 + \mathcal{L}_{WZ}, \tag{3.8}$$

with $\mathcal{L}_0$ and $\mathcal{L}_{WZ}$ given in (3.1) and (3.2), respectively. Indicating with $\mathcal{L}_b$ the b sector of $\mathcal{L}$, a partial integration on the axion gives [3]

$$\mathcal{L}_b = -\frac{1}{2} b \Box b + b\, J, \tag{3.9}$$

where

$$J = M\partial B - \frac{\kappa_A}{M} F_A \wedge F_A - \frac{\kappa_B}{M} F_B \wedge F_B, \tag{3.10}$$

and performing the path integration over b we obtain

$$\int Db \exp\left(i\langle\mathcal{L}\rangle\right) = \det\left(\Box - M_1^2\right)^{-1/2} \exp\left(\frac{i}{2} J \Box^{-1} J\right), \tag{3.11}$$

where

$$\langle J\Box^{-1}J\rangle_{WZ} = \langle\left(M_1\partial B - \frac{\kappa_A}{M_1} F_A \wedge F_A - \frac{\kappa_B}{M_1} F_B \wedge F_B\right)\Box^{-1}\left(M_1\partial B - \frac{\kappa_A}{M_1} F_A \wedge F_A - \frac{\kappa_B}{M_1} F_B \wedge F_B\right)\rangle. \tag{3.12}$$

The additional contributions to the effective action are now non-local and are represented by the set of diagrams in Fig. 3.4. Among these diagrams there are two GS counterterms, diagrams c) and d), but there are also other contributions. To generate only the GS counterterms one needs an additional pseudoscalar called a in order to enforce the cancellation of the extra terms. There are various ways of doing this [94, 95, 96, 100]. In [100] the non-local counterterm $\partial B \Box^{-1} F \wedge F$ of axial QED, which corresponds to the diagrams b) and c) of Fig. 3.5, is obtained by performing the functional integral over a and b of the following action [100]

$$\begin{aligned}\mathcal{L} &= \overline{\psi}\left(i\partial\!\!\!/ + eB\!\!\!/\gamma_5\right)\psi - \frac{1}{4}F_B^2 + \frac{e^3}{48\pi^2 M_1} F_B \wedge F_B (a+b) \\ &\quad + \frac{1}{2}\left(\partial_\mu b - M_1 B_\mu\right)^2 - \frac{1}{2}\left(\partial_\mu a - M_1 B_\mu\right)^2 . \end{aligned}\tag{3.13}$$

The integral on a and b are gaussians and their contributions to the effective action, after integrating them out, are shown in Fig. 3.5. Notice that b has a positive kinetic term and a is ghost-like. The role of the two pseudoscalars is to cancel the contributions in Fig. 3.5 a) and d), leaving only the contribution given by graphs b) and c), which has the pole structure typical of the GS non-local counterterm. Due to

---

[3] We have re-defined the coefficients in front of the counterterms absorbing the multiplicity factors.

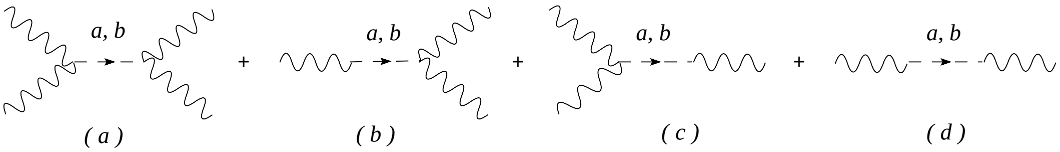

Figure 3.5: Effective action with two pseudoscalars, one of them ghost-like, a.

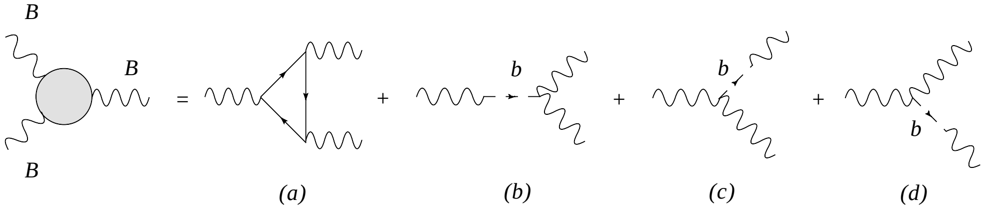

Figure 3.6: The GS vertex with the non-local contributions for the BBB diagram symmetrized on each leg.

these cancellations, the effective action now reduces to

$$\langle \partial B(x) \Box^{-1}(x-y) F(y) \wedge F(y) \rangle \tag{3.14}$$

besides the anomaly vertex and is represented by interactions of the form b) and c) of Fig. 3.5. This shows that the WZ and the GS effective actions organize the perturbative expansions in a rather different way. It is also quite immediate that the cleanest way to analyze the expansion is to use the R_ξ gauge, as we have already stressed. It is then also quite clear that in the WZ case we require the gauge invariance of the Lagrangian *but not* of the trilinear gauge interactions, while in the GS case, which is realized via Eq. (3.13) or, analogously, by the Lagrangians proposed in [94, 95, 96], it is the trilinear vertex that is rendered gauge invariant (together with the Lagrangian). The presence of a ghost-like particle in the GS case renders the local description quite unappealing and for sure the best way to define the mechanism is just by adding the non-local counterterms. In the WZ case the local description is quite satisfactory and allows one to treat the bFF interaction as a real trilinear vertex, which takes an important role in the presence of a broken phase. The GS counterterms are, in practice, the same ones as appearing in the analysis of axial QED with a non-local counterterm, as we are going to discuss next.

3.3.2 Non-local counterterms: axial QED

The use of non-local counterterms to cancel the anomaly is for sure a debated issue in quantum field theory since most of the results concerning the BRS analysis of these theories may not apply [95, 96]. In the GS case we may ignore all the previous constructions and just require ab initio that the anomalous vertices are modified by the addition of a non-local counterterm that cancels the anomaly on the axial lines.

Consider, for instance, the case of the BBB vertex of Fig. 3.6, where the regularization of the anomalies has been obtained by adding the three GS counterterms in a symmetric way [69]. In the BAA case only a single countertem is needed, but for the rest the discussion is quite similar to the BBB case, with just a few differences. These concern the distribution of the partial anomalies on the A- and B-lines in the case in which also BAA is treated symmetrically (equal partial anomalies). In this particular case we need to compensate the vertex with CS interactions, which are not, anyhow, observable if the A-lines correspond to conserved gauge currents such as in QED. In this situation the Ward Identities would force the CS counterterms to vanish. We will stick to the *consistent* definition of the anomaly in which only B carries the total anomaly a_n and A is anomaly-free. The counterterm used in the GS mechanism both for BAA and BBB is nothing else but the opposite of the Dolgov-Zakharov (DZ) expression [101], which in the BAA case takes the form

$$C^{\lambda\mu\nu}_{AVV}(k,k_1,k_2) = -\frac{a_n}{k^2}k^\lambda \epsilon[\mu,\nu,k_1,k_2]. \tag{3.15}$$

In the BBB case a similar expression is obtained by creating a Bose symmetric combination of DZ poles,

$$C^{\lambda\mu\nu}_{AAA}(k,k_1,k_2) = -\left(\frac{1}{3}\frac{a_n}{k^2}k^\lambda \epsilon[\mu,\nu,k_1,k_2] + \frac{1}{3}\frac{a_n}{k_1^2}k_1^\mu \epsilon[\nu,\lambda,k_2,k] + \frac{1}{3}\frac{a_n}{k_2^2}k_2^\nu \epsilon[\lambda,\mu,k,k_1]\right). \tag{3.16}$$

We have denoted by k the incoming momenta of the axial-vector vertex and by k_1 and k_2 the outgoing momenta of the vector vertices. We keep this notation also in the AAA case, since k will denote the momentum exchange in the s-channel when we glue together these amplitudes to obtain an amplitude of BIM type; this, we will analyze in the next sections. These expressions are consistent with the following equations of the anomaly for the BAA triangle

$$\begin{aligned} k_{1\mu}C^{\lambda\mu\nu}_{AVV}(k,k_1,k_2) &= 0, \\ k_{2\nu}C^{\lambda\mu\nu}_{AVV}(k,k_1,k_2) &= 0, \\ k_\lambda C^{\lambda\mu\nu}_{AVV}(k,k_1,k_2) &= -a_n\epsilon[\mu,\nu,k_1,k_2], \end{aligned} \tag{3.17}$$

and for the BBB anomalous triangle

$$\begin{aligned} k_{1\mu}C^{\lambda\mu\nu}_{AAA}(k,k_1,k_2) &= -\frac{a_n}{3}\epsilon[\lambda,\nu,k,k_2], \\ k_{2\nu}C^{\lambda\mu\nu}_{AAA}(k,k_1,k_2) &= -\frac{a_n}{3}\epsilon[\lambda,\mu,k,k_1], \\ k_\lambda C^{\lambda\mu\nu}_{AAA}(k,k_1,k_2) &= -\frac{a_n}{3}\epsilon[\mu,\nu,k_1,k_2]. \end{aligned} \tag{3.18}$$

So we can define a gauge invariant triangle amplitude, in both the BBB and BAA cases, by

$$\begin{aligned} \Delta^{\lambda\mu\nu\,GS}_{AAA}(k,k_1,k_2) &= \Delta^{\lambda\mu\nu}_{AAA}(k,k_1,k_2) + C^{\lambda\mu\nu}_{AAA}(k,k_1,k_2) \\ \Delta^{\lambda\mu\nu\,GS}_{AVV}(k,k_1,k_2) &= \Delta^{\lambda\mu\nu}_{AVV}(k,k_1,k_2) + C^{\lambda\mu\nu}_{AVV}(k,k_1,k_2). \end{aligned} \tag{3.19}$$

Notice that the (fermionic) triangle diagrams, in the symmetric limit $k_1^2 = k_2^2 = k_3^2$, is exactly the opposite of the DZ counterterms, as we will discuss in the next section,

$$\Delta_{AVV}(k_1^2 = k_2^2 = k^2) = -C_{AVV} \qquad \Delta_{AAA}(k_1^2 = k_2^2 = k^2) = -C_{AAA}, \tag{3.20}$$

so the cancellation is identical at that point (only at that point), and the two vertices Δ^{GS} vanish. It is rather obvious that the cancellations of these poles in BIM amplitudes, corrected by the GS counterterms, is identical only for on-shell external gauge lines. It is also quite straightforward to realize that the massless B-model with the GS vertex correction is equivalent to axial QED corrected by a non-local term [20] that

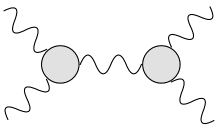

Figure 3.7: BIM amplitude with full GS vertices. For on-shell external lines the contributions from the extra poles disappear.

is described by the Lagrangian

$$\mathcal{L}_{5\,QED} = \overline{\psi}\left(i\partial\!\!\!/ + eB\!\!\!/\gamma_5\right)\psi - \frac{1}{4}F_B^2 \tag{3.21}$$

plus the counterterm

$$\mathcal{S}_{ct} = \frac{1}{24\pi^2}\langle \partial B(x)\Box^{-1}(x-y)F(y)\wedge F(y)\rangle. \tag{3.22}$$

This theory is equivalent to the (local) formulation given in Eq. (3.5) and in [95, 96], where the transversality constraint ($\partial B = 0$) is directly imposed on the Lagrangian via a multiplier. Unitarity requires these DZ poles in the C counterterms to disappear from a physical amplitude. In general, consider the diagrams depicted in Figs. 3.7 and 3.8. The structure of the GS vertex is, for BBB, given by (3.19) with the three massless poles generated by the exchange of the pseudoscalar on the three legs, as shown in Fig. 3.6. For on-shell external lines, in this diagram the contributions from the extra poles cancel due to the transversality condition satisfied by the polarizators of the gauge bosons. However, once these amplitudes are embedded into more general amplitudes, such as those shown in Figs. 3.8, 3.9, the cancellation of the DZ extra poles introduced by the counterterm requires a more detailed analysis that we postpone to Chap. 4, where this cancellation will be proven up to three-loop order.

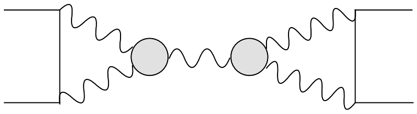

Figure 3.8: Embedding of the BIM amplitude with GS vertices in a fermion/antifermion scattering.

We can summarize the issues that we have raised in the following points.

1) The GS and the WZ mechanism have different formulations in terms of auxiliary fields.

2) Previous analyses of axial gauge theories, though distinct in their Lagrangian formulation, are all equivalent to axial QED plus a non-local counterterm. The regularization of the gauge interactions, in these theories, coincides with that obtained by using the GS counterterm on the gauge vertex. In particular, the massless poles introduced by the regularization are not completely understood in the context of perturbative unitarity.

A special comment is needed when we move to the analysis of Higgs-axion mixing. This has been shown to take place after electroweak symmetry breaking for a special class of potentials, which are not supersymmetric. The axion, which in the Stückelberg phase is essentially a Goldstone mode, develops a physical component and this component appears as a physical pole. It is then clear, from the analysis presented above, that the regularization procedure introduced by the GS counterterm involves a virtual massless state and not a physical pole. This is at variance with the WZ mechanism, in which the bFF vertex is introduced from the beginning as a vertex and not just as a virtual state. In this second case, b can be decomposed in terms of a Goldstone mode and a physical pseudoscalar, the *axi-Higgs*, which

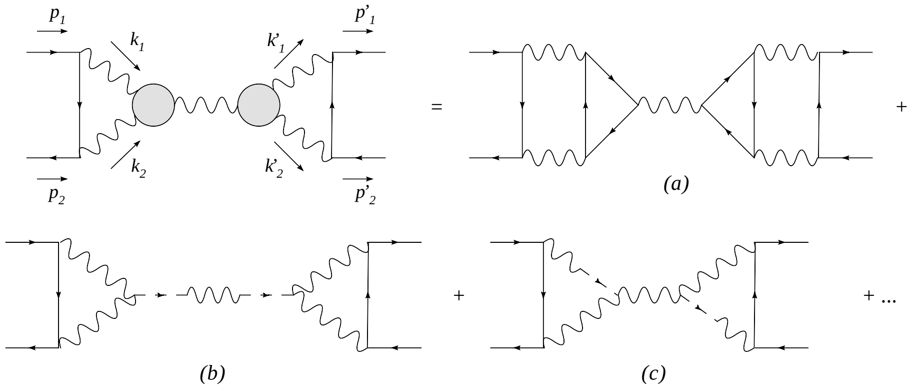

Figure 3.9: The structure of the fermionic scattering amplitudes with spurious massless poles (graphs b) and c)).

takes the role of a gauged Peccei-Quinn axion [1, 12]. This is entitled to appear as a physical state (and a physical pole, massless or massive) in the spectrum. The re-formulation of the GS counterterm in terms of a pseudoscalar comes also at a cost, due to the presence of a ghost-like (phantom) particle in the spectrum, which is absent in the WZ case. There are some advantages though, since the theory has, apparently, a nice UV behavior, given the gauge invariance condition on the vertex. The presence of these spurious poles requires further investigations to see how they are really embedded into higher-order diagrams and we will return to this point in Chap. 4.

In the next section we will move to the analysis of the unitarity bound in the WZ case. As we have shown, in this case it is possible to characterize it explicitly. We will work in a specific model, but the implications of our analysis are general and may be used to constrain significantly entire classes of models containing WZ interactions at the LHC. Before coming to the specific phenomenological applications we elaborate on the set of amplitudes that are instrumental in order to spot the bad high energy behavior of the chiral anomaly in s-channel processes: the so called BIM amplitudes.

3.4 BIM amplitudes, unitarity and the resonance pole

The uncontrolled growth of the cross section in the WZ case can be studied in a class of amplitudes that have two anomalous (**AVV** or **AAA**) vertices connected by an s-channel exchange as in Fig. 3.3 a). We are interested in the expressions of these amplitudes in the chiral limit, when all the fermions are massless. Processes such as $AA \to AA$, mediated by an anomalous gauge boson B, with on-shell external A-lines and massless fermions, can be expressed in a simplified form, which is, also in this case, the DZ form. We therefore set $k_1^2 = k_2^2 = 0$ and $m_f = 0$, which are the correct kinematical conditions to obtain DZ poles. We briefly elaborate on this point.

We start from the Rosenberg form of the AVV amplitude, which is given by

$$\begin{aligned} T^{\lambda\mu\nu} &= A_1 \epsilon[k_1, \lambda, \mu, \nu] + A_2 \epsilon[k_2, \lambda, \mu, \nu] + A_3 k_1^{\mu} \epsilon[k_1, k_2, \nu, \lambda] \\ &+ A_4 k_2^{\mu} \epsilon[k_1, k_2, \nu, \lambda] + A_5 k_1^{\nu} \epsilon[k_1, k_2, \mu, \lambda] + A_6 k_2^{\nu} \epsilon[k_1, k_2, \mu, \lambda] \, , \end{aligned} \tag{3.23}$$

and imposing the Ward Identities we obtain

$$\begin{aligned} A_1 &= k_2^2 A_4 + k_1 \cdot k_2 A_3 \\ A_2 &= k_1^2 A_5 + k_1 \cdot k_2 A_6 \end{aligned}$$

$$\begin{aligned} A_3(k_1,k_2) &= -A_6(k_1,k_2) \\ A_4(k_1,k_2) &= -A_5(k_1,k_2), \end{aligned} \tag{3.24}$$

where the invariant amplitudes $A_3,\dots,A_6$ are free from singularities. In this specific kinematical limit we can use the following relations to simplify our amplitude

$$\begin{aligned} \epsilon[k_2,\lambda,\mu,\nu] &= \frac{2}{s}\left(k_2^\lambda\epsilon[k_1,k_2,\nu,\mu] + k_2^\nu\epsilon[k_1,k_2,\mu,\lambda] + k_2^\mu\epsilon[k_1,k_2,\nu,\lambda]\right) \\ \epsilon[k_1,\lambda,\mu,\nu] &= -\frac{2}{s}\left(k_1^\lambda\epsilon[k_1,k_2,\nu,\mu] + k_1^\nu\epsilon[k_1,k_2,\mu,\lambda] + k_1^\mu\epsilon[k_1,k_2,\nu,\lambda]\right) \end{aligned} \tag{3.25}$$

where $k^2 = (k_1+k_2)^2 = s$ is the center of mass energy. These combinations allow us to re-write the expression of the trilinear amplitude as

$$T^{\mu\nu\lambda} = A_6 k^\lambda \epsilon[k_1,k_2,\nu,\mu] + (A_4+A_6)\left(k_2^\nu\epsilon[k_1,k_2,\mu,\lambda] - k_1^\mu\epsilon[k_1,k_2,\nu,\lambda]\right)\,. \tag{3.26}$$

It is not difficult to see that the second piece drops off for physical external on-shell A-lines, and we see that only one invariant amplitude contributes to the result

$$T^{\mu\nu\lambda} = A_6^f(s)(k_1+k_2)^\lambda \epsilon\left[k_1,k_2,\nu,\mu\right]. \tag{3.27}$$

There are some observations to be made concerning this result. Notice that A_6 multiplies a longitudinal momentum exchange and, as discussed in the literature on the chiral anomaly in QCD [101, 102, 103], brings about a *massless* pole in s. We just recall that A_6 satisfies an unsubtracted dispersion relation in s at a fixed invariant mass of the two photons, $(k_1^2 = k_2^2 = p^2)$

$$A_6(s,p^2) = \frac{1}{\pi^2}\int_{4m_f^2}^{\infty} dt\,\frac{Im A_6(t,p^2)}{t-s} \tag{3.28}$$

and a sum rule

$$\int_{4m_f^2}^{\infty} Im A_6(t,p^2)\,dt = \frac{1}{2\pi}, \tag{3.29}$$

while for on-shell external photons one can use the DZ relation [101]

$$Im A_6(k^2,0) = \frac{1}{\pi}\delta(k^2), \tag{3.30}$$

to show that the only pole of the amplitude is actually at $s = k^2 = 0$. It can be simplified using the identity

$$Li_2(1-a) + Li_2(1-a^{-1}) \quad = \quad -\frac{1}{2}\log^2(a), \tag{3.31}$$

with

$$a = \frac{\rho_f+1}{\rho_f-1} \qquad \rho_f = \sqrt{1-4\frac{m_f^2}{s}}\,, \tag{3.32}$$

to give [103]

$$A_6^f(s) = \frac{1}{2\pi^2 s}\left(1 - \frac{m_f^2}{s}\log^2\frac{\rho_f + 1}{\rho_f - 1}\right). \tag{3.33}$$

We can use this amplitude to discuss both the breaking of unitarity and the cancellation of the resonance pole in this simple model. The first point has already been addressed in the previous section, where the computation of the diagrams in Fig. 3.2 has shown that only a BIM amplitude survives in the WZ case in the scattering process $AA \to AA$. If the sum of those two diagrams gives a gauge invariant result, with the exchange of the Z' described by a Proca propagator, there is a third contribution that should be added to this amplitude. This comes from the exchange of the physical axion χ. We recall, in fact, that in the presence of Higgs-axion mixing, when b is the sum of a Goldstone mode and a physical axion χ, each anomalous Z' is accompanied by the exchange of the χ [1, 12]. This is generated in the presence of electroweak symmetry breaking, after expansion of the Higgs scalar ϕ around a vacuum v

$$\phi = \frac{1}{\sqrt{2}}\left(v + \phi_1 + i\phi_2\right), \tag{3.34}$$

with the axion b expressed as linear combination of the rotated fields χ and G_B

$$b = \alpha_1\chi + \alpha_2 G_B = \frac{q_B g_B v}{M_B}\chi + \frac{M_1}{M_B}G_B. \tag{3.35}$$

We also recall that the gauge fields B_μ get their masses M_B through the combined Higgs-Stückelberg mechanism,

$$M_B = \sqrt{M_1^2 + (q_B g_B v)^2}. \tag{3.36}$$

In the phenomenological analysis presented in the next sections the contribution due to χ has been included. Therefore, in the WZ case, the total contributions coming from the several BIM amplitudes related to the additional anomalous neutral currents should be accompanied not only by the set of Goldstone bosons, to restore gauge invariance, but also by the exchange of the axi-Higgs.

The cancellation of the resonance pole for $s = M_B$ is an important characteristic of BIM amplitudes, which does not occur in any other (anomaly-free) amplitude. This cancellation is the result of some trivial algebra already seen at work in the first two chapters. For instance, given a BIM amplitude and a Proca propagator, we have

$$\begin{aligned}
A_{BIM}^{\mu\nu\mu'\nu'} &= \frac{a_n}{k^2}k^\lambda\epsilon[\mu,\nu,k_1,k_2]\,\frac{-i}{k^2 - M_1^2}\left(g^{\lambda\lambda'} - \frac{k^\lambda k^{\lambda'}}{M_1^2}\right)\frac{a_n}{k^2}(-k^{\lambda'})\epsilon[\mu',\nu',k_1',k_2'] \\
&= \frac{a_n}{k^2}\epsilon[\mu,\nu,k_1,k_2]\,\frac{-i}{k^2 - M_1^2}\,\frac{k^{\lambda'}(M_1^2 - k^2)}{M_1^2}\,\frac{a_n}{k^2}(-k^{\lambda'})\epsilon[\mu',\nu',k_1',k_2'] \\
&= \frac{a_n}{k^2}\epsilon[\mu,\nu,k_1,k_2]\left(\frac{-ik^2}{M_1^2}\right)\frac{a_n}{k^2}\epsilon[\mu',\nu',k_1',k_2'] \\
&= -\frac{a_n}{M_1}\epsilon[\mu,\nu,k_1,k_2]\,\frac{i}{k^2}\,\frac{a_n}{M_1}\epsilon[\mu',\nu',k_1',k_2'].
\end{aligned} \tag{3.37}$$

This result implies that the amplitude is described - in the chiral limit and for massless external states - by a diagram with the exchange of a pseudoscalar (see Fig. 3.2 b)) and that the resonance pole has disappeared. It is clear, from (3.37), that these amplitudes break unitarity and give a contribution to the cross section that grows quadratically in energy ($\sim s$). Therefore, searching for BIM amplitudes at the

LHC can be a way to uncover the anomalous behavior of extra neutral (or charged) gauge interactions. There is one thing that might tame this growth, and this is the exchange of the physical axion. We will show, working in a complete brane model, that the exchange of the χ does lower the cross section, but insignificantly, independently from the mass of the axion.

3.5 A realistic model with WZ counterterms

Clarified the relation between the WZ and GS mechanisms using a toy-model, we now move towards the analysis of the issue of unitarity violation in the WZ Lagrangian at high energy. Details on the structure of the effective action of the complete model that we are going to analyze can be found in Chap. 2. We just mention that this is characterized by a gauge structure of the form $SU(3) \times SU(2) \times U(1) \times U(1)_B$, where the $U(1)_B$ is anomalous. We work in the context of a two-Higgs doublet model with H_u and H_d. In our analysis the charge assignments are those of a realistic brane model with three extra anomalous $U(1)$, but we will assume that only the lowest mass eigenvalue taking part is significant, since the remaining two additional gauge bosons are heavy and, essentially, decoupled.

We recall that the single anomalous gauge boson B, that we consider for this analysis, is characterized by a generator Y_B which is anomalous ($Tr\left[Y_B^3\right] \neq 0$) but at the same time has mixed anomalies with the remaining generators of SM and in particular with the hypercharge Y. In the presence of this anomalous $U(1)_B$ both the Z and the (extra) Z' gauge boson have an anomalous component, proportional to B. We also recall that the effective action of the anomalous theory is rendered gauge invariant using both CS and WZ counterterms, while a given gauge invariant sector involves the exchange both of the anomalous gauge boson and of the axion in the s-, t- and u-channels.

In [92] it has been shown how the trilinear vertices of the effective WZ Lagrangian can be determined consistently for a generic number of extra anomalous $U(1)$. Here, the goal is to identify and quantify the contributions that cause a violation of unitarity in this Lagrangian. For phenomenological reasons it is then convenient to select those BIM amplitudes that have a better chance, at the experimental level, to be measured at the LHC and for this reason we will focus on the process $g\,g \rightarrow \gamma\gamma$. The gluon density grows at high energy especially at smaller (Bjorken variable) x-values. We choose to work with *prompt* final state photons for obvious reasons, the signal being particularly clean. To begin with, we will be needing the expressions of the $Z\gamma\gamma$ and the Zgg vertices. In the presence of three anomalous $U(1)$'s, here denoted as $U(1)_B$, both the Z and the (extra) Z' gauge boson have an anomalous component, which is proportional to the $B_{i\mu}$, the anomalous gauge bosons of the interaction eigenstate basis (i=1,2,3). The photon vertex is given by [92]

$$\begin{aligned}
\langle Z_l\gamma\gamma\rangle|_{m_f\neq 0} = -\frac{1}{2} Z_l^{\lambda} A_\gamma^{\mu} A_\gamma^{\nu} \sum_f \Big[& g_Y^3 \theta_f^{YYY} \bar{R}_{Z_l\gamma\gamma}^{YYY} + g_2^3 \theta_f^{WWW} \bar{R}_{Z_l\gamma\gamma}^{WWW} + g_Y g_2^2 \theta_f^{YWW} R_{Z_l\gamma\gamma}^{YWW} \\
& + g_Y^2 g_2 \theta_f^{YYW} R_{Z_l\gamma\gamma}^{YYW} + \sum_i g_{B_i} g_Y g_2 \theta_f^{B_i YW} R_{Z_l\gamma\gamma}^{B_i YW} \\
& + \sum_i g_{B_i} g_Y^2 \theta_f^{B_i YY} R_{Z_l\gamma\gamma}^{B_i YY} + g_{B_i} g_2^2 \theta_f^{B_i WW} R_{Z_l\gamma\gamma}^{B_i WW} \Big] \Delta_{AVV}^{\lambda\mu\nu}(m_f \neq 0) \qquad (3.38)
\end{aligned}$$

with $l = 1,2,3$ enumerating the extra anomalous neutral currents. The explicit expressions of the rotation matrix O^A can be found in App. 2.9.1. We have defined

$$\bar{R}_{Z_l\gamma\gamma}^{YYY} = (O^A)_{YZ_l} (O^A)_{Y\gamma}^2, \qquad \bar{R}_{Z_l\gamma\gamma}^{WWW} = (O^A)_{W_3 Z_l} (O^A)_{W_3\gamma}^2, \qquad (3.39)$$

and the triangle $\Delta_{AVV}(m_f \neq 0)$ is given by [92]

$$\begin{aligned}
\Delta^{\lambda\mu\nu}_{AVV}(m_f \neq 0, k_1, k_2) = \frac{1}{\pi^2}\int_0^1 dx \int_0^{1-x} dy \frac{1}{\Delta(m_f)} \\
\big\{\epsilon[k_1, \lambda, \mu, \nu]\left[y(y-1)k_2^2 - xy k_1 \cdot k_2\right] \\
+\epsilon[k_2, \lambda, \mu, \nu]\left[x(1-x)k_1^2 + xy k_1 \cdot k_2\right] \\
+\epsilon[k_1, k_2, \lambda, \nu]\left[x(x-1)k_1^\mu - xy k_2^\mu\right] \\
+\epsilon[k_1, k_2, \lambda, \mu]\left[xy k_1^\nu + (1-y)y k_2^\nu\right]\big\} ,
\end{aligned}$$

$$\Delta(m_f) = m_f^2 + x(x-1)k_1^2 + y(y-1)k_2^2 - 2xy k_1 \cdot k_2 \,. \tag{3.40}$$

We have defined the following chiral asymmetries

$$\begin{aligned}
\theta_f^{B_l YY} &= Q^L_{B_j,f}(Q^L_{Y,f})^2 - Q^R_{B_l,f}(Q^R_{Y,f})^2, \\
\theta_f^{B_l WW} &= Q^L_{B_l,f}(T^3_{L,f})^2, \\
\theta_f^{WWW} &= (T^3_{L,f})^3, \\
\theta_f^{YYW} &= \left[(Q^L_{Y,f})^2 T^3_{L,f}\right], \\
\theta_f^{B_l YW} &= \left[Q^{B_l,f} Q^L_{Y,f} T^3_{L,f}\right],
\end{aligned} \tag{3.41}$$

with $Q_B^{L/R}$ and $Q_Y^{L/R}$ denoting the charges of the chiral fermions and T^3_L is the generator of the third component of the weak isospin, while the R factors are products of O^A matrix elements. The matrix O^A relates the interaction eigenstate basis of the generators (Y_B, Y, T_3) to those of the mass eigenstate basis $(T_Z, T_{Z'}, Q)$, of the physical gauge bosons of the neutral sector, Z, Z' and A_γ. They are given by

$$\begin{aligned}
R^{YYY}_{Z_l\gamma\gamma} &= 3\left[(O^A)_{YZ_l}(O^A)^2_{Y\gamma}\right] \\
R^{YWW}_{Z_l\gamma\gamma} &= \left[2(O^A)_{W_3\gamma}(O^A)_{YZ_l}(O^A)_{Y\gamma} + (O^A)^2_{W_3\gamma}(O^A)_{YZ_l}\right] \\
R^{WWW}_{Z_l\gamma\gamma} &= \left[3(O^A)_{B_iZ_l}(O^A)^2_{W_3\gamma}\right] \\
R^{YYW}_{Z_l\gamma\gamma} &= \left[2(O^A)_{YZ_l}(O^A)_{Y\gamma}(O^A)_{W_3\gamma} + (O^A)_{W_3Z_l}(O^A)^2_{Y\gamma}\right] \\
R^{B_iYY}_{Z_l\gamma\gamma} &= (O^A)^2_{Y\gamma}(O^A)_{B_iZ_l} \\
R^{B_iWW}_{Z_l\gamma\gamma} &= \left[(O^A)^2_{W_3\gamma}(O^A)_{B_iZ_l}\right] \\
R^{B_iYW}_{Z_l\gamma\gamma} &= \left[2(O^A)_{B_iZ_l}(O^A)_{W_3\gamma}(O^A)_{Y\gamma}\right] \,.
\end{aligned} \tag{3.42}$$

These expressions will be used extensively in the next section and computed numerically in a complete brane model.

3.5.1 Prompt photons, the Landau-Yang theorem and the anomaly

Since the analysis of the unitarity bound will involve the study of amplitudes with direct photons in the final state mediated by a Z or a Z' in the s-channel, we briefly recall some facts concerning the structure of these amplitude and in particular the Landau-Yang theorem. The condition of transversality of the Z' boson $(e_{Z'} \cdot k = 0)$ is essential for the vanishing of this amplitude.

The theorem states that a spin 1 particle cannot decay into two on-shell spin 1 photons because of

Bose symmetry and angular momentum conservation. Angular momentum conservation tells us that the two photons must be in a spin 1 state (which forces their angular momentum wave function to be antisymmetric), while their spatial part is symmetric. The total wave function is therefore antisymmetric and violates the requirement of Bose statistics. For these reasons the amplitude has to vanish. For a virtual exchange mediated by a Z' the contribution is vanishing -after summing over the fermions in each generation of the SM-, the theory being anomaly-free, in the chiral limit. The amplitude is non-vanishing only in the presence of chiral symmetry breaking terms (fermion masses), which can be induced both by the QCD vacuum and by the Yukawa couplings of SM in the presence of electroweak symmetry breaking. For this reason it is strongly suppressed also in the SM.

However, the situation in the case of an anomalous vertex is more subtle. The BIM amplitude is non-vanishing, but at the same time, as we have explained, is *non-resonant*, which means that the particle pole due to the Z' has disappeared. For the rest it will break unitarity at a certain stage.

In fact, a cursory look at the AVV vertex shows that if the external photons are on-shell and transverse, the amplitude mediated by this diagram is proportional to the momentum of the virtual Z, k^μ. This longitudinal momentum exchange does not set the amplitude to zero unless the production mechanism is also anomalous. We will show first that in the SM these processes are naturally suppressed, though not identically zero, since they are proportional to the fermion masses, due to anomaly cancellation. We start our analysis by going back to the AVV diagram, which summarizes the kinematical behavior of the $Z\gamma\gamma$ amplitude.

Let k_1 and k_2 denote the momenta of the two final state photons. We contract the AVV diagram with the polarization vectors of the photons, $\varepsilon_{1\mu}$ and $\varepsilon_{2\nu}$ of the Z boson, e_λ, obtaining

$$
\begin{aligned}
e_\lambda \varepsilon_{1\mu}\varepsilon_{2\nu}\Delta^{\lambda\mu\nu}_{AVV}(k_1,k_2,m_f\neq 0) = &-\frac{1}{\pi^2}\int_0^1 dx\int_0^{1-x} dy\,\frac{xy}{m_f^2-2xyk_1\cdot k_2} \\
&e_\lambda\varepsilon_{1\mu}\varepsilon_{2\nu}\left\{\epsilon_{\lambda\nu\mu\alpha}\left(k_2^\alpha-k_1^\alpha\right)+k_1^\alpha k_2^\beta\left(\epsilon_{\alpha\lambda\beta\nu}k_2^\mu-\epsilon_{\alpha\lambda\beta\mu}k_1^\nu\right)\right\}\,, \qquad (3.43)
\end{aligned}
$$

where we have used the conditions

$$
\begin{aligned}
&k_1^2 = k_2^2 = 0 \\
&\varepsilon_{1\mu}k_1^\mu = \varepsilon_{2\nu}k_2^\nu = 0. \qquad (3.44)
\end{aligned}
$$

It is important to observe that if we apply Schouten's identity we can reduce this expression to the form

$$
e_\lambda \varepsilon_{1\mu}\varepsilon_{2\nu}\Delta^{\lambda\mu\nu}_{AVV}(k_1,k_2,m_f\neq 0) = e_\lambda\left(k_1^\lambda+k_2^\lambda\right)\mathcal{F}_f(k^2,m_f) \qquad (3.45)
$$

with

$$
\begin{aligned}
\mathcal{F}_f(k^2,m_f) &= \mathcal{J}_f(k^2)\epsilon[k_1,k_2,\varepsilon_1,\varepsilon_2] \\
\mathcal{J}_f(k^2) &\equiv -\frac{1}{\pi^2}\int_0^1 dx\int_0^{1-x} dy\,\frac{xy}{m_f^2-2xyk_1\cdot k_2}, \qquad (3.46)
\end{aligned}
$$

which vanishes only if we impose the transversality condition on the polarization vector of the Z boson, $e_\lambda k^\lambda = 0$. Alternatively, this amplitude vanishes if the anomalous $Z\gamma\gamma$ vertex is contracted with another gauge invariant vertex, as discussed above. The amplitude has an anomalous behavior. In fact,

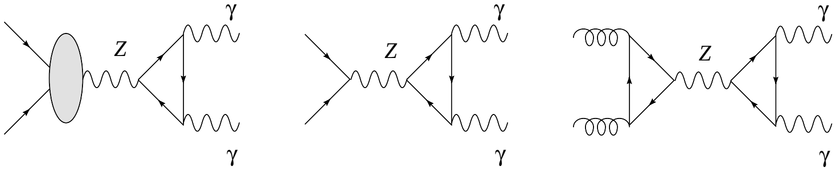

Figure 3.10: Vanishing and non-vanishing amplitudes mediated by an axial-vector spin 1.

contracting with the k_λ four-vector we obtain

$$\begin{aligned}
k_\lambda \varepsilon_{1\mu}\varepsilon_{2\nu}\Delta^{\lambda\mu\nu}_{AVV}(k_1,k_2,m_f\neq 0) &= \left(-\frac{1}{\pi^2}\int_0^1 dx\int_0^{1-x} dy\frac{k_\lambda k^\lambda xy}{m_f^2-2xyk_1\cdot k_2}\right)\epsilon[k_1,k_2,\varepsilon_1,\varepsilon_2]\\
&= \left(\frac{1}{\pi^2}\int_0^1 dx\int_0^{1-x} dy\frac{-2k_1\cdot k_2 xy}{m_f^2-2xyk_1\cdot k_2}\right)\epsilon[k_1,k_2,\varepsilon_1,\varepsilon_2]\\
&= \left(\frac{1}{\pi^2}+\frac{m_f^2}{\pi^2}\int_0^1 dx\int_0^{1-x} dy\frac{1}{m_f^2-2xyk_1\cdot k_2}\right)\epsilon[k_1,k_2,\varepsilon_1,\varepsilon_2]
\end{aligned}\tag{3.47}$$

where the mass-independent and mass-dependent contributions have been separated. Summing over an anomaly-free generation, the first of these two contributions cancel. For this reason, it is also convenient to isolate the following quantity

$$\mathcal{G}_f(k^2,m_f)=\frac{m_f^2}{\pi^2}\int_0^1 dx\int_0^{1-x} dy\frac{1}{m_f^2-2xyk_1\cdot k_2}\epsilon[k_1,k_2,\varepsilon_1,\varepsilon_2]\tag{3.48}$$

which is the only contribution to the triangle amplitude in the SM for a given fermion flavor f.

We illustrate in Fig. 3.10 the contributions to the $q\bar{q}$ annihiliation channel at all orders (first graph), at leading order (second graph), and the BIM amplitude (third graph), all attached to an AVV final state. In an anomaly-free theory all these processes are only sensitive to the difference in masses among the flavors, since degeneracy in the fermion mass sets these contributions to zero. Only the second graph vanishes identically due to the WI on the $q\bar{q}$ channel also away from the chiral limit. For instance in the third diagram chiral symmetry breaking is sufficient to induce violations of the WI on the initial state vertex, due to the different quark masses within a given fermion generation.

To illustrate, in more detail, how chiral symmetry breaking can induce the exchange of a scalar component in the process with two prompt photons, we start from the SM case, where the $Z^*\gamma\gamma$ vertex, multiplied by external physical polarizations for the two photons becomes

$$V^\lambda_{Z^*\gamma\gamma}=k^\lambda\frac{g_2}{2\cos\theta_W}e^2\sum_f (Q_f)^2 g^Z_{A,f}\mathcal{F}_f(k^2,m_f)\tag{3.49}$$

and consider the quark antiquark annihilation channel $q\bar{q}\to Z^*\to\gamma\gamma$. We work in the parton model with massless light quarks. We can rewrite the amplitude as

$$\mathcal{M} \quad = \quad V^\lambda_{ffZ^*}\Pi_{\lambda,\lambda',\xi}V^{\lambda'}_{Z^*\gamma\gamma},\tag{3.50}$$

where we have introduced the $Zq\bar{q}$ vertex

$$V_{ffZ}=\bar{v}(p_1)\Gamma^{\lambda'}u(p_2) \qquad \Gamma^\lambda=ig_Z\gamma^\lambda(g_V-g_A\gamma^5),\tag{3.51}$$

and the expression of the propagator of the Z in the R_ξ gauge

$$\Pi_{\lambda,\lambda',\xi} = \frac{-i}{k^2 - M_Z^2}\left[g^{\lambda\lambda'} - \frac{k^\lambda k^{\lambda'}}{k^2 - \xi M_Z^2}(1-\xi)\right]. \tag{3.52}$$

To move to the unitary gauge, we split the propagator of the Z boson as

$$\Pi_{\lambda,\lambda',\xi} = \frac{-i}{k^2 - M_Z^2}\left[g^{\lambda\lambda'} - \frac{k^\lambda k^{\lambda'}}{M_Z^2}\right] + \frac{-i}{k^2 - \xi M_Z^2}\left(\frac{k^\lambda k^{\lambda'}}{M_Z^2}\right) \tag{3.53}$$

and go to the unitary gauge by choosing $\xi \to \infty$. The amplitude will then be written as

$$\begin{aligned}\mathcal{M} &= \bar{v}(p_1)\Gamma^\lambda u(p_2)\frac{-i}{k^2 - M_Z^2}\left[g^{\lambda\lambda'} - \frac{k^\lambda k^{\lambda'}}{M_Z^2}\right] k^{\lambda'}\left(\frac{g_2}{2\cos\theta_W}e^2\sum_f (Q_f)^2 g^Z_{A,f}\mathcal{F}_f(k^2, m_f)\right) \\ &= \frac{i}{M_Z^2}\bar{v}(p_1)\Gamma^\lambda u(p_2)k^\lambda\left(\frac{g_2}{2\cos\theta_W}e^2\sum_f (Q_f)^2 g^Z_{A,f}\mathcal{F}_f(k^2, m_f)\right). \end{aligned}\tag{3.54}$$

Clearly, at the Born level, using the WI on the left V_{ffZ^*} vertex, we find that the amplitude is zero. This result remains unchanged if we include higher-order corrections (strong/electroweak), since the structure of this vertex is just modified by a Pauli (weak-electric) form factor and the additional contribution vanishes after contraction with the momentum k^λ. This amplitude is however non-vanishing if we replace the V_{ffZ^*} vertex with a V_{ggZ^*} vertex, where now we assume that the new vertex is computed for non-zero fermion masses (i.e. away from the chiral limit). In this case we use the WI

$$\begin{aligned} k_\rho\, V^{\rho\nu\mu}_{ggZ^*} &= (p_1 + p_2)_\rho\, G^{\rho\nu\mu} \\ &= -\frac{e^2 g_2}{2\cos\theta_W}\sum_q g^Z_{A,q}Q_q^2\,\epsilon^{\nu\mu\alpha\beta}p_{1\alpha}p_{2\beta}\left[\frac{1}{\pi^2} + \frac{m_q^2}{\pi^2}\int_0^1 dx_1\int_0^{1-x_1} dx_2\,\frac{1}{\Delta_q}\right] \end{aligned}\tag{3.55}$$

with

$$\Delta_q = -xyk^2 + m_q^2, \tag{3.56}$$

where the constant term $(1/\pi^2)$ vanishes in an anomaly-free theory. It is convenient to define the function

$$\mathcal{G}_q(k^2, m_q) = \epsilon\left[\varepsilon_{1g}, \varepsilon_{2g}, p_1, p_2\right] m_q^2 \mathcal{I}_q(m_q) \tag{3.57}$$

with

$$\mathcal{I}_q(m_q) = \frac{1}{\pi^2}\int_0^1 dx_1\int_0^{1-x_1} dx_2\,\frac{1}{\Delta_q}, \tag{3.58}$$

where ε is the polarization of the gluon, which allows one to express the squared amplitude as

$$\langle|\mathcal{M}_{gg\to\gamma\gamma}|^2\rangle = \left(\frac{e^2 g_2}{2\cos\theta_W}\right)^4 \frac{s^6}{4M_Z^4}\left(\sum_q g_A^q Q_q^2 \mathcal{G}_q(m_q)\right)^2\left(\sum_f g_A^f Q_f^2 \mathcal{G}_f(m_f)\right)^2, \tag{3.59}$$

with $s \equiv k^2$. Notice that in the large energy limit $\mathcal{I}_q \sim \mathcal{J}_f \sim 1/s^2$ [103]. This shows that double prompt photon production, in the SM, is non-resonant and is proportional to the quark masses, neglecting the contributions coming from the masses of the leptons.

3.6 Gauge parameter dependence in the physical basis

When this analysis is extended to a complete anomalous model such as the mLSOM [1, 12, 91, 92] even the direct proof of the cancellation of the gauge dependence in the Z' exchange is quite complex and not obvious, although it is expected at a formal level. We recall that we are working with a broken phase and the axion has been decomposed into its physical component (χ, which is the axi-Higgs) and the Goldstone modes. In [92] it has been shown that the counterterms of the theory can be fixed in the Stückelberg phase and then re-expressed, in the Higgs-Stückelberg phase, in the physical base, which confirm the correctness of the approach followed in Chap. 2 for the determination of the effective Lagrangian of the model after electroweak symmetry breaking.

The matrix O^χ, needed to rotate into the mass eigenstates of the CP-odd sector, relating the axion χ and the two neutral Goldstones of this sector to the Stückelberg field b and the CP-odd phases of the two Higgs doublets satisfies the following relation

$$\begin{pmatrix} ImH_u^0 \\ ImH_d^0 \\ b \end{pmatrix} = O^\chi \begin{pmatrix} \chi \\ G_1^0 \\ G_2^0 \end{pmatrix},$$

where the Goldstones in the physical basis are obtained by the following combination

$$\begin{aligned} G^Z &= G_1^0 \left[f_u \frac{v_u}{M_Z} O^\chi_{12} + f_d \frac{v_d}{M_Z} O^\chi_{22} + g_B \frac{M_1}{M_Z} O^A_{ZB} O^\chi_{32} \right] \\ &+ G_2^0 \left[f_u \frac{v_u}{M_Z} O^\chi_{13} + f_d \frac{v_d}{M_Z} O^\chi_{23} + g_B \frac{M_1}{M_Z} O^A_{ZB} O^\chi_{33} \right] \\ &= c_1 G_1^0 + c_2 G_2^0 \\ G^{Z'} &= G_1^0 \left[f_{u,B} \frac{v_u}{M'_Z} O^\chi_{12} + f_{d,B} \frac{v_d}{M'_Z} O^\chi_{22} + g_B \frac{M_1}{M'_Z} O^A_{Z'B} O^\chi_{32} \right] \\ &+ G_2^0 \left[f_{u,B} \frac{v_u}{M'_Z} O^\chi_{13} + f_{d,B} \frac{v_d}{M'_Z} O^\chi_{23} + g_B \frac{M_1}{M'_Z} O^A_{Z'B} O^\chi_{33} \right] \\ &= c'_1 G_1^0 + c'_2 G_2^0 \,. \end{aligned} \tag{3.60}$$

Here we have defined the following coefficients

$$\begin{aligned} f_u &= g_2 O^A_{ZW_3} - g_Y O^A_{ZY} - q_u^B g_B O^A_{ZB} \qquad & f_d &= g_2 O^A_{ZW_3} - g_Y O^A_{ZY} - q_d^B g_B O^A_{ZB} \\ f_{u,B} &= g_2 O^A_{Z'W_3} - g_Y O^A_{Z'Y} - q_u^B g_B O^A_{Z'B} \qquad & f_{d,B} &= g_2 O^A_{Z'W_3} - g_Y O^A_{Z'Y} - q_d^B g_B O^A_{Z'B} \,, \end{aligned} \tag{3.61}$$

and the $q^B_{u,d}$ charges are defined in Tab. 3.2. The relations containing the physical Goldstones can be inverted so we obtain

$$\begin{aligned} G_1^0 &= C_1 G^Z + C_2 G^{Z'} \\ G_2^0 &= C'_1 G^Z + C'_2 G^{Z'} \,, \end{aligned} \tag{3.62}$$

where we give the explicit expression only for the coefficient C'_1, since this is the one relevant for our

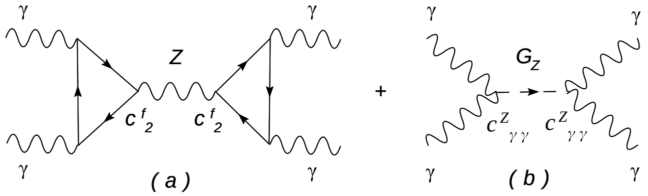

Figure 3.11: Cancellation of the spurious poles in the physical basis, $m_f = 0$.

purposes. Then, after the orthonormalization procedure, we obtain

$$C_1' = \frac{c_2}{\sqrt{c_2^2 + c_2'^2}} \,. \tag{3.63}$$

We illustrate the proof of gauge independence from the Z gauge parameter of the amplitudes in Fig. 3.11. In this case the cancellation of the spurious poles takes place via the combined exchange of the Z propagator and of the corresponding Goldstone mode G_Z. If we isolate the gauge-dependent part in the Z boson propagator we obtain

$$\begin{aligned}
& \mathcal{M}_{A\xi} + \mathcal{M}_{B\xi} \\
= \; & \left(-\frac{1}{2} c_2^f \Delta_{AVV}^{\lambda\mu\nu}(p_1,p_2)\right) \frac{-i}{k^2 - \xi_Z M_Z^2} \left(\frac{k^\lambda k^{\lambda'}}{M_Z^2}\right) \left(\frac{1}{2} c_2^f \Delta_{AVV}^{\lambda'\mu'\nu'}(k_1,k_2)\right) \\
& +4 \times \left(4 c_{\gamma\gamma}^Z \epsilon[p_1,p_2,\mu,\nu]\right) \frac{i}{k^2 - \xi_Z M_Z^2} \left(4 c_{\gamma\gamma}^Z \epsilon[k_1,k_2,\mu',\nu']\right) \\
= \; & \left(-\frac{a_n}{2} c_2^f \epsilon[p_1,p_2,\mu,\nu]\right) \frac{-i}{k^2 - \xi_Z M_Z^2} \left(\frac{1}{M_Z^2}\right) \left(\frac{a_n}{2} c_2^f \epsilon[k_1,k_2,\mu',\nu']\right) \\
& +4 \times \left(4 c_{\gamma\gamma}^Z \epsilon[p_1,p_2,\mu,\nu]\right) \frac{i}{k^2 - \xi_Z M_Z^2} \left(4 c_{\gamma\gamma}^Z \epsilon[k_1,k_2,\mu',\nu']\right) \,,
\end{aligned} \tag{3.64}$$

where

$$c_{\gamma\gamma}^Z = \left[\frac{F}{M_1}(O_{W\gamma}^A)^2 + \frac{C_{YY}}{M_1}(O_{Y\gamma}^A)^2\right] O_{33}^\chi C_1'. \tag{3.65}$$

The coefficient $c_{\gamma\gamma}^Z$ in the $\mathcal{M}_{B\xi}$ amplitude (G_Z exchange) must be compared with the massless coefficients c_2^f of the $\mathcal{M}_{A\xi}$ amplitude (Z boson exchange) and the explicit expressions of the coefficients C_{YY} and F have been already computed in Sec. 2.5. Adding the contributions of the two diagrams we obtain

$$\begin{aligned}
& \mathcal{M}_{A\xi} + \mathcal{M}_{B\xi} \\
= \; & \left\{\frac{a_n}{2}\left[g_B g_Y^2 \theta_f^{BYY} R_{Z\gamma\gamma}^{BYY} + g_B g_2^2 \theta_f^{BWW} R_{Z\gamma\gamma}^{BWW}\right] \epsilon[p_1,p_2,\mu,\nu]\right\} \frac{i}{k^2 - \xi_Z M_Z^2} \left(\frac{1}{M_Z^2}\right) \\
& \left\{\frac{a_n}{2}\left[g_B g_Y^2 \theta_f^{BYY} R_{Z\gamma\gamma}^{BYY} + g_B g_2^2 \theta_f^{BWW} R_{Z\gamma\gamma}^{BWW}\right] \epsilon[k_1,k_2,\mu',\nu']\right\} \\
& +4 \times \left\{4\left[\frac{F}{M_1}(O_{W\gamma}^A)^2 + \frac{C_{YY}}{M_1}(O_{Y\gamma}^A)^2\right] O_{33}^\chi C_1' \epsilon[p_1,p_2,\mu,\nu]\right\} \frac{i}{k^2 - \xi_Z M_Z^2} \\
& \left\{4\left[\frac{F}{M_1}(O_{W\gamma}^A)^2 + \frac{C_{YY}}{M_1}(O_{Y\gamma}^A)^2\right] O_{33}^\chi C_1' \epsilon[k_1,k_2,\mu',\nu']\right\} .
\end{aligned} \tag{3.66}$$

At this point, the pattern of cancellation can be separated in three different sectors, a pure BYY sector, a pure BWW and mixed BYY-BWW sectors, and it requires the validity of the relations

$$\left(\frac{a_n}{2} g_B g_Y^2 \theta_f^{BYY} R_{Z\gamma\gamma}^{BYY}\right)^2 \frac{1}{M_Z^2} + 4\left(4\frac{C_{YY}}{M_1}(O_{Y\gamma}^A)^2 O_{33}^\chi C_1'\right)^2 = 0, \tag{3.67}$$

$$\left(\frac{a_n}{2} g_B g_2^2 \theta_f^{BWW} R_{Z\gamma\gamma}^{BWW}\right)^2 \frac{1}{M_Z^2} + 4\left(4\frac{F}{M_1}(O_{W\gamma}^A)^2 O_{33}^\chi C_1'\right)^2 = 0, \tag{3.68}$$

$$\left(a_n\, g_B g_Y^2 \theta_f^{BYY} R_{Z\gamma\gamma}^{BYY}\, a_n\, g_B g_2^2 \theta_f^{BWW} R_{Z\gamma\gamma}^{BWW}\right) \frac{1}{M_Z^2} + 4\left(8\frac{F}{M_1}(O_{W\gamma}^A)^2 \frac{C_{YY}}{M_1}(O_{Y\gamma}^A)^2 O_{33}^\chi C_1'\right) = 0. \tag{3.69}$$

We have been able to verify that these relations are automatically satisfied because of the following identity, which connects the rotation matrix of the interaction to the mass eigenstates O^A to a component of the matrix O^χ. This matrix appears in the rotation from the basis of Stückelberg axions to the basis of the Goldstones G_Z and $G_{Z'}$ and of the axi-Higgs χ. The relation is

$$O_{BZ}^A \frac{1}{M_Z} = 2 O_{33}^\chi C_1' \frac{1}{M_1}\,, \tag{3.70}$$

with

$$O_{33}^\chi = \frac{1}{\sqrt{\frac{(q_u^B - q_d^B)^2}{M_1^2} \frac{v_u^2 v_d^2}{v_u^2 + v_d^2} + 1}}, \tag{3.71}$$

with M_1 the Stückelberg mass. The origin of this connection has to be found in the Yukawa sector and the condition of gauge invariance of the Yukawa couplings.

3.7 Unitarity bounds: the partonic contribution $gg \to \gamma\gamma$

In this section we compute the $gg \to \gamma\gamma$ cross section with two on-shell gluons and two on-shell photons in the final state. The same computation is carried out both in the SM and in the mLSOM, where the charge assignments have been determined as in [93, 60], to determine the different behavior of these amplitudes in the two cases. The list of contributions that we have included are all shown in Fig. 3.12. We report some of the results of the graphs in order to clarify the notation. For instance we obtain for

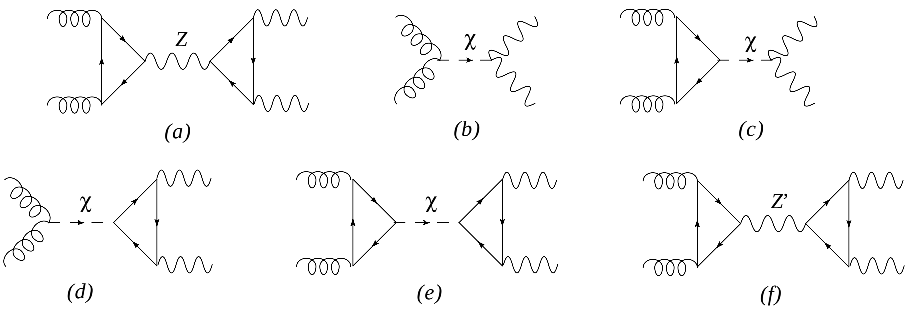

(a) (b) (c)
(d) (e) (f)

Figure 3.12: Anomalous contributions to $gg \to \gamma\gamma$ in the mLSOM.

diagram (a)

$$\sigma_A(s) = \frac{1}{2048\pi} \left[\sum_q \frac{1}{2} c_1^q A_{6,q} \right]^2 \left[\sum_f \frac{1}{2} c_2^f A_{6,f} \right]^2 \frac{s^5}{M_Z^4}, \tag{3.72}$$

where we have defined the coefficients

$$\begin{aligned} c_1^q &= g_3^2 \left[g_Y \theta_q^Y O^A_{YZ} + g_2 \theta_q^W O^A_{WZ} + g_B \theta_q^B O^A_{BZ} \right], \\ c_2^f &= \left[g_Y^3 \theta_f^{YYY} \bar{R}^{YYY}_{Z\gamma\gamma} + g_Y^3 \theta_f^{WWW} \bar{R}^{WWW}_{Z\gamma\gamma} + g_Y g_2^2 \theta_f^{YWW} R^{YWW}_{Z\gamma\gamma} + g_Y^2 g_2 \theta_f^{YYW} R^{YYW}_{Z\gamma\gamma} \right. \\ &\left. + g_B g_Y^2 \theta_f^{BYY} R^{BYY}_{Z\gamma\gamma} + g_B g_2^2 \theta_f^{BWW} R^{BWW}_{Z\gamma\gamma} + g_B g_Y g_2 \theta_f^{BYW} R^{BYW}_{Z\gamma\gamma} \right], \end{aligned} \tag{3.73}$$

and the mass $M_{Z'}$ of the extra Z' is given by Eq. (2.181). We recall that $A_6^f(s)$ is approximately

$$A_6^f(s) \approx \frac{1}{2\pi^2 s} - \frac{m_f^2}{2s^2} + O\left(\frac{m_f^2}{s^2} \log\left(\frac{m_f^2}{s^2} \right) \right), \tag{3.74}$$

at large values of s. We have seen that the SM contribution, in the presence of a massive fermion circulating in the loop is suppressed by a factor that is $O\left(m_f^2/s^2\right)$. In the case of an anomalous model this contribution becomes subleading, the dominant one coming from the anomalous parts, proportional to the chiral asymmetries θ_f of the anomalous charge assignments between left-handed and right-handed fermion modes. The amplitude in diagram (b) is given by

$$\sigma_B(s) = \frac{2}{\pi} \left(g^\chi_{gg}\right)^2 \left(g^\chi_{\gamma\gamma}\right)^2 \frac{s^3}{(s - M_\chi^2)^2}. \tag{3.75}$$

where, for convenience, we have defined

$$g^\chi_{gg} = \frac{D}{M} O^\chi_{31}, \tag{3.76}$$

$$g^\chi_{\gamma\gamma} = \left[\frac{F}{M} (O^A_{W\gamma})^2 + \frac{C_{YY}}{M} (O^A_{Y\gamma})^2 \right] O^\chi_{31}. \tag{3.77}$$

Here we have used the model-dependent WZ coefficients D, F and C_{YY} already computed in Sec. 2.5. Proceeding in a similar way, graph c) gives

$$\sigma_C(s) = \frac{1}{32\pi} \frac{s^3}{(s - M_\chi^2)^2} (g^\chi_{gg})^2 \left[\sum_q C_0(s, m_q) c^{\chi,q}_{gg} \right]^2 \tag{3.78}$$

where we have used Eq. (3.31) and we have set

$$C_0(s, m_f) = -\frac{m_f}{4\pi^2 s} \log^2 \frac{\rho_f + 1}{\rho_f - 1}. \tag{3.79}$$

Starting from the Yukawa couplings shown in Lagrangian (2.1) it is convenient to define the following coefficients, which will be used below

$$\begin{aligned} c^{\chi,q}_{gg} &= g_3^2 c^{\chi,q}, \qquad q = u, d \\ c^{\chi,f}_{\gamma\gamma} &= e^2 c^{\chi,f}, \qquad q = u, d, \nu, e. \end{aligned} \tag{3.80}$$

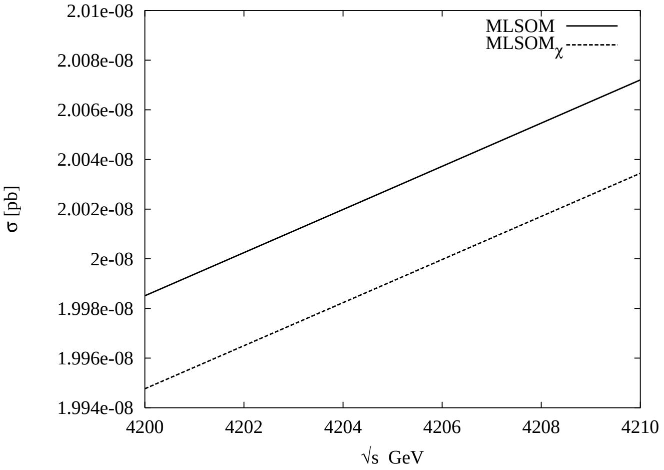

Figure 3.13: Partonic cross section for the anomalous process $gg \to \gamma\gamma$ with $m_f = 0$, $\tan\beta = 40$, $g_B = 0.1$, $M_\chi = 10$ GeV and $M_1 = 800$ GeV. The solid line refers only to the exchange of the Z and the Z', while the dashed line refers to the complete cross section including the χ exchange.

We have used a condensed notation for the flavors, with u = {u, c, t}, d = {d, s, b}, $\nu = \{\nu_e, \nu_\mu, \nu_\tau\}$ and e = {e, μ, τ}. The couplings of the physical axion to the fermions are given by

$$\begin{aligned} c^{\chi,u} &= \Gamma^u \frac{i}{\sqrt{2}} O^\chi_{11} = \frac{m_u}{v_u} i O^\chi_{11}, \qquad c^{\chi,d} = -\Gamma^d \frac{i}{\sqrt{2}} O^\chi_{21} = -\frac{m_d}{v_d} i O^\chi_{21}, \\ c^{\chi,\nu} &= \Gamma^\nu \frac{i}{\sqrt{2}} O^\chi_{11} = \frac{m_\nu}{v_u} i O^\chi_{11}, \qquad c^{\chi,e} = -\Gamma^e \frac{i}{\sqrt{2}} O^\chi_{21} = -\frac{m_e}{v_d} i O^\chi_{21}. \end{aligned} \tag{3.81}$$

We have also relied on the O^χ matrix elements introduced in Sec. 2.9. The fermion masses have been expressed in terms of the Yukawa couplings by the relations

$$m_u = \frac{v_u \Gamma_u}{\sqrt{2}}, \quad m_d = \frac{v_d \Gamma_d}{\sqrt{2}}, \quad m_\nu = \frac{v_u \Gamma_\nu}{\sqrt{2}}, \quad m_e = \frac{v_d \Gamma_e}{\sqrt{2}}. \tag{3.82}$$

The cross section for the amplitude (d) in Fig. 3.12 is given by

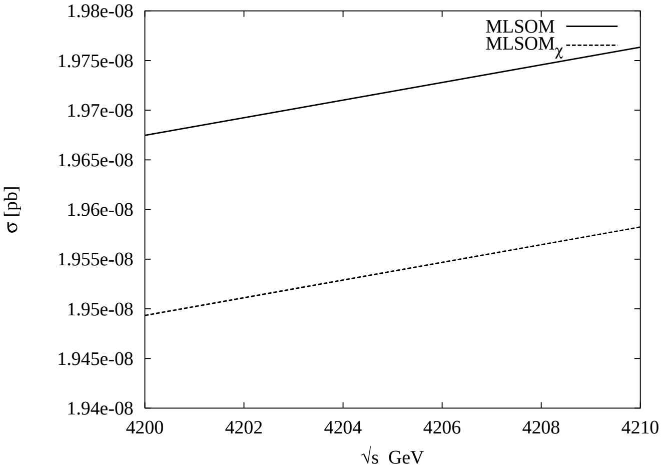

Figure 3.14: The same as in Fig. 3.13 but with $m_f \neq 0$.

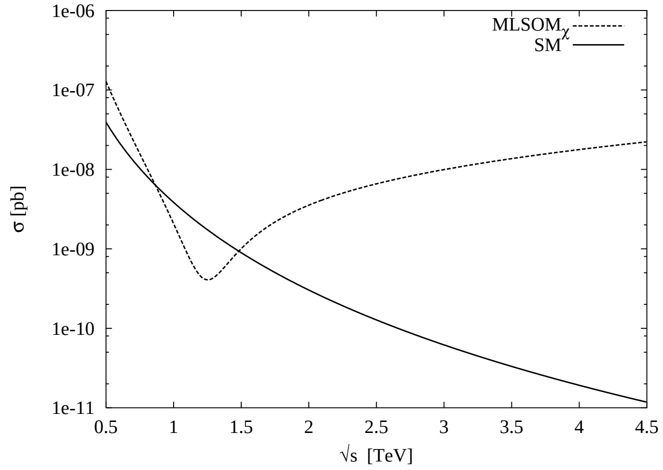

Figure 3.15: Partonic cross section for the anomalous process $gg \to \gamma\gamma$, with $\tan\beta = 40$, $g_B = 0.1$, $M_\chi = 10$ GeV and $M_1 = 800$ GeV. The solid line refers to the SM with the exchange of the Z boson. The dashed line refers to the mLSOM case. The point of minimum divides the anomaly-free region from the region where the anomalous contributions dominate.

$$\sigma_D(s) = \frac{s^3}{32\pi(s - M_\chi^2)^2}(g^\chi_{\gamma\gamma})^2 \left[\sum_f C_0(s, m_f) c^{\chi,f}_{\gamma\gamma}\right]^2 , \tag{3.83}$$

With these notations, we are now ready to express the cross section for graph e) as

$$\sigma_E(s) \quad = \quad \frac{s^3}{2048\pi(s - M_\chi^2)^2} \left[\sum_q C_0(s, m_q) c^{\chi,q}_{gg}\right]^2 \left[\sum_f C_0(s, m_f) c^{\chi,f}_{\gamma\gamma}\right]^2 . \tag{3.84}$$

Finally, the cross section for the Z' exchange is given by

$$\sigma_F(s) = \frac{1}{2048\pi} \left[\sum_q \frac{1}{2} d_1^q A_{6,q}\right]^2 \left[\sum_f \frac{1}{2} d_2^f A_{6,f}\right]^2 \frac{s^5}{M_{Z'}^4} , \tag{3.85}$$

where, again, in order to simplify the notation we have defined the coefficients

$$\begin{aligned} d_1^q &= g_3^2 \left[g_Y \theta_q^Y O^A_{YZ'} + g_2 \theta_q^W O^A_{WZ'} + g_B \theta_q^B O^A_{BZ'}\right] , \\ d_2^f &= \left[g_Y^3 \theta_f^{YYY} \bar{R}^{YYY}_{Z'\gamma\gamma} + g_2^3 \theta_f^{WWW} \bar{R}^{WWW}_{Z'\gamma\gamma} + g_Y g_2^2 \theta_f^{YWW} R^{YWW}_{Z'\gamma\gamma} + g_Y^2 g_2 \theta_f^{YYW} R^{YYW}_{Z'\gamma\gamma}\right. \\ &\quad \left. + g_B g_Y^2 \theta_f^{BYY} R^{BYY}_{Z'\gamma\gamma} + g_B g_2^2 \theta_f^{BWW} R^{BWW}_{Z'\gamma\gamma} + g_B g_Y g_2 \theta_f^{BYW} R^{BYW}_{Z'\gamma\gamma}\right] . \end{aligned} \tag{3.86}$$

In the SM case we work in the unitary gauge, being a tree-level Z exchange, and we have only one contribution whose explicit expression is given by

$$\begin{aligned} \sigma^{SM}(s) \quad &= \quad \frac{1}{32768\pi^9} \frac{1}{s^3 M_Z^4} \left[\sum_q c^{SM}_{1,q} m_q^2 \log^2\left(\frac{\rho_q + 1}{\rho_q - 1}\right)\right]^2 \\ &\quad \times \left[\sum_f c^{SM}_{2,f} m_f^2 \log^2\left(\frac{\rho_f + 1}{\rho_f - 1}\right)\right]^2 , \end{aligned} \tag{3.87}$$

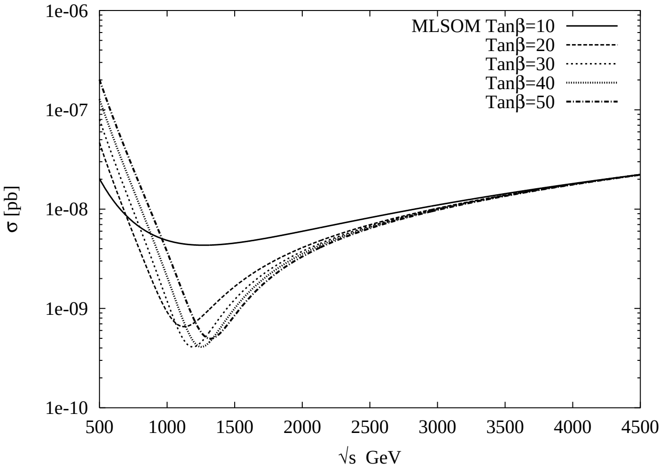

Figure 3.16: Partonic cross section for the anomalous process $gg \to \gamma\gamma$ with $g_B = 0.1$, $M_\chi = 10$ GeV and $M_1 = 800$ GeV. The lines refer to the cross section evaluated for different values of $\tan\beta$.

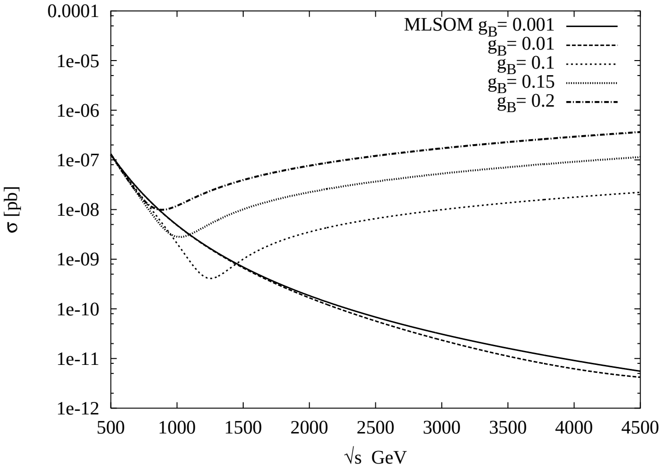

Figure 3.17: Partonic cross section for the anomalous process $gg \to \gamma\gamma$ with $\tan\beta = 40$, $M_\chi = 10$ GeV and $M_1 = 800$ GeV. The lines refer to the cross section evaluated for different values of the coupling constant g_B.

where we have defined the SM coefficients

$$\begin{aligned} c^{SM}_{1,q} &= g_3^2 \left[g_Y \theta^Y_q O^A_{YZ} + g_2 \theta^W_q O^A_{WZ} \right] \\ c^{SM}_{2,f} &= \left[g_Y^3 \theta^{YYY}_f \bar{R}^{YYY} + g_2^3 \theta^{WWW}_f \bar{R}^{WWW} + g_Y g_2^2 \theta^{YWW}_f R^{YWW} + g_Y^2 g_2 \theta^{YYW}_f R^{YYW} \right] . \end{aligned} \tag{3.88}$$

The partonic SM cross section is in agreement with unitarity in its asymptotic behavior, which is given by

$$\sigma^{SM}(s \to \infty) \approx \frac{\left[\sum_q c^{SM}_{1,q} m_q^2\right]^2 \left[\sum_f c^{SM}_{2,f} m_f^2\right]^2}{s^3 M_Z^4} . \tag{3.89}$$

In our anomalous model the complete expression of the same cross section is given by

$$\sigma^{mLSOM}(s)$$

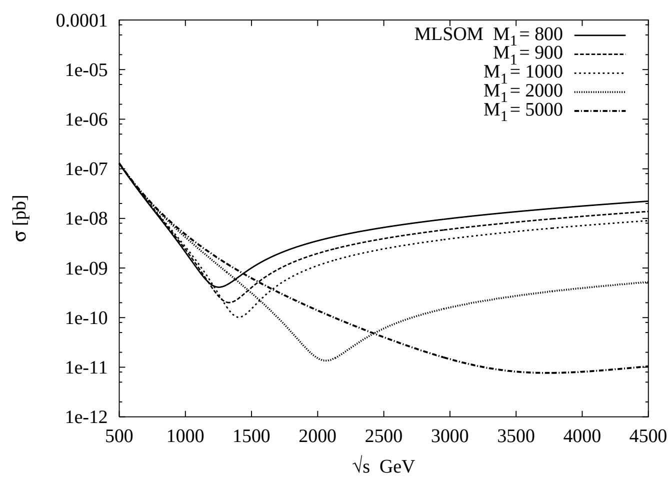

Figure 3.18: Partonic cross section for the anomalous process $gg \to \gamma\gamma$, with $\tan\beta = 40$, $g_B = 0.1$ and $M_\chi = 10$ GeV. The lines refer to the cross section evaluated for different values of the Stückelberg mass M_1.

$$
\begin{aligned}
= \Bigg\{ & \frac{1}{2048\pi}\frac{s^5}{M_Z^4}\left[\frac{1}{2}\sum_q c_1^q\frac{\mathcal{A}(s,m_q)}{2\pi^2 s}\right]^2\left[\frac{1}{2}\sum_f c_2^f\frac{\mathcal{A}(s,m_f)}{2\pi^2 s}\right]^2 + \frac{2}{\pi}\frac{\left(g_{gg}^\chi\right)^2\left(g_{\gamma\gamma}^\chi\right)^2 s^3}{(s-M_\chi^2)^2} \\
& + \frac{1}{32\pi}\frac{(g_{gg}^\chi)^2\, s^3}{(s-M_\chi^2)^2}\left[\sum_q C_0(s,m_q)c_{gg}^{\chi,q}\right]^2 + \frac{(g_{\gamma\gamma}^\chi)^2 s^3}{32\pi(s-M_\chi^2)^2}\left[\sum_f C_0(s,m_f)c_{\gamma\gamma}^{\chi,f}\right]^2 \\
& + \frac{s^3}{2048\pi(s-M_\chi^2)^2}\left[\sum_q C_0(s,m_q)c_{gg}^{\chi,q}\right]^2\left[\sum_f C_0(s,m_f)c_{\gamma\gamma}^{\chi,f}\right]^2 \\
& + \frac{1}{2048\pi}\frac{s^5}{M_{Z'}^4}\left[\frac{1}{2}\sum_q d_1^q\frac{\mathcal{A}(s,m_q)}{2\pi^2 s}\right]^2\left[\frac{1}{2}\sum_f d_2^f\frac{\mathcal{A}(s,m_f)}{2\pi^2 s}\right]^2 \\
& + \frac{g_{gg}^\chi g_{\gamma\gamma}^\chi s^4}{16\pi M_Z^2(s-M_\chi^2)}\left[\frac{1}{2}\sum_q c_1^q\frac{\mathcal{A}(s,m_q)}{2\pi^2 s}\right]\left[\frac{1}{2}\sum_f c_2^f\frac{\mathcal{A}(s,m_f)}{2\pi^2 s}\right] \\
& + \frac{s^4}{1024 M_Z^2\pi(s-M_\chi^2)}\left[\frac{1}{2}\sum_q c_1^q\frac{\mathcal{A}(s,m_q)}{2\pi^2 s}\right]\left[\frac{1}{2}\sum_f c_2^f\frac{\mathcal{A}(s,m_f)}{2\pi^2 s}\right]\times \\
& \times\left[\sum_{f'} C_0(s,m_{f'})c_{\gamma\gamma}^{\chi,f'}\right]\left[\sum_{q'} C_0(s,m_{q'})c_{gg}^{\chi,q'}\right] \\
& + \frac{1}{1024\pi}\frac{s^5}{M_Z^2\, M_{Z'}^2}\left[\frac{1}{2}\sum_q d_1^q\frac{\mathcal{A}(s,m_q)}{2\pi^2 s}\right]\left[\frac{1}{2}\sum_f d_2^f\frac{\mathcal{A}(s,m_f)}{2\pi^2 s}\right]\times \\
& \times\left[\frac{1}{2}\sum_{q'} c_1^{q'}\frac{\mathcal{A}(s,m_{q'})}{2\pi^2 s}\right]\left[\frac{1}{2}\sum_{f'} c_2^{f'}\frac{\mathcal{A}(s,m_{f'})}{2\pi^2 s}\right] \\
& + \frac{s^4}{1024\, M_{Z'}^2\,\pi\,(s-M_\chi^2)}\left[\frac{1}{2}\sum_q d_1^q\frac{\mathcal{A}(s,m_q)}{2\pi^2 s}\right]\left[\frac{1}{2}\sum_f d_2^f\frac{\mathcal{A}(s,m_f)}{2\pi^2 s}\right]\times \\
& \times\left[\sum_{f'} C_0(s,m_{f'})c_{\gamma\gamma}^{\chi,f'}\right]\left[\sum_{q'} C_0(s,m_{q'})c_{gg}^{\chi,q'}\right]
\end{aligned}
$$

$$+\frac{1}{16\pi}\frac{g^{\chi}_{gg}g^{\chi}_{\gamma\gamma}\,s^4}{M^2_{Z'}(s-M^2_{\chi})}\left[\frac{1}{2}\sum_q d_1^q\frac{\mathcal{A}(s,m_q)}{2\pi^2 s}\right]\left[\frac{1}{2}\sum_f d_2^f\frac{\mathcal{A}(s,m_f)}{2\pi^2 s}\right]\Bigg\}, \tag{3.90}$$

where we have introduced the notation

$$\mathcal{A}(s,m_f) \equiv \left[1-\frac{m_f^2}{s}\log^2\left(\frac{\rho_f+1}{\rho_f-1}\right)\right]. \tag{3.91}$$

At high energy we can neglect the mass of the axion ($s - M^2_{\chi} \approx s$) and from the limits

$$\mathcal{A}(s\to\infty,m_f)=1, \qquad C_0(s\to\infty,m_f)=0, \tag{3.92}$$

we obtain that the total cross section reduces to

$$\sigma^{mLSOM}(s\to\infty)=\frac{\mathcal{K}^2}{\pi}s, \tag{3.93}$$

which is linearly divergent and has a unitarity bound. $\mathcal{K}\equiv\mathcal{K}(s_b,g_B,\alpha_S(s),\tan\beta)$ is defined by

$$\begin{aligned}
\mathcal{K}^2 = \quad & \frac{1}{2048M_Z^4}\left(\sum_q\frac{c_{1,q}}{4\pi^2}\right)^2\left(\sum_f\frac{c_{2,f}}{4\pi^2}\right)^2+2(g^{\chi}_{gg})^2(g^{\chi}_{\gamma\gamma})^2\\
&+\frac{1}{16M_Z^2}\left(\sum_q\frac{c_{1,q}}{4\pi^2}\right)\left(\sum_f\frac{c_{2,f}}{4\pi^2}\right)g^{\chi}_{gg}g^{\chi}_{\gamma\gamma}+\frac{1}{16M_{Z'}^2}\left(\sum_q\frac{d_{1,q}}{4\pi^2}\right)\left(\sum_f\frac{d_{2,f}}{4\pi^2}\right)g^{\chi}_{gg}g^{\chi}_{\gamma\gamma}\\
&+\frac{1}{1024M_Z^2M_{Z'}^2}\left(\sum_q\frac{c_{1,q}}{4\pi^2}\right)\left(\sum_f\frac{c_{2,f}}{4\pi^2}\right)\left(\sum_{q'}\frac{d_{1,q'}}{4\pi^2}\right)\left(\sum_{f'}\frac{d_{2,f'}}{4\pi^2}\right)\\
&+\frac{1}{2048M_{Z'}^4}\left(\sum_q\frac{d_{1,q}}{4\pi^2}\right)^2\left(\sum_f\frac{d_{2,f}}{4\pi^2}\right)^2.
\end{aligned} \tag{3.94}$$

The derivation of the unitarity bound for this cross section is based, in analogy with Fermi theory, on the partial wave expansion

$$\frac{d\sigma}{d\Omega}=|f(\theta)|^2=|\frac{1}{2ik}\sum_{l=0}^{\infty}(2l+1)f_lP_l(\cos\theta)|^2, \tag{3.95}$$

with an s-wave contribution given by

$$\frac{d\sigma}{d\Omega}=\frac{1}{s}|f_0|^2+\ldots \tag{3.96}$$

Since unitarity requires that $|f_l|\leq 1$ we obtain the bound

$$\frac{d\sigma}{d\Omega}\leq\frac{1}{s}, \tag{3.97}$$

or, equivalently,

$$\sigma\leq\frac{4\pi}{s} \tag{3.98}$$

$$\sqrt{s} \geq \sqrt{\frac{2\pi}{\mathcal{K}}}. \tag{3.99}$$

The bound is computed numerically by looking for values s_b at which

$$s_b^2 = \frac{2\pi}{\mathcal{K}(s_b, g_B, \alpha_S(s_b), \tan\beta)} \tag{3.100}$$

where in the total parametric dependence of the factor $\mathcal{K}$, $\mathcal{K}(s_b, g_B, \alpha_S(s_b), \tan\beta)$, we have included the whole energy dependence, including that coming from running of the coupling (up to three-loop level). We will analyze below the bound numerically in the context of the specific brane model of [93, 60, 64].

3.8 Couplings and Parameters in the Madrid Model

We now turn to a brief illustration of the specific charge assignments of the class of models that we have implemented in our numerical analysis. These are defined by a set of free parameters, which can be useful in order to discern between different scenarios. In our implementation we rotate the fields from the D-brane basis to the hypercharge basis and at the same time we redefine the Abelian charges and couplings. The four $U(1)$ in the hypercharge basis are denoted $U(1)_{X_i}$ with $i = A, B, C$ and U_Y, where the last is the hypercharge $U(1)$, which is demanded to be anomaly-free. This fixes the hypercharge generator in the hypercharge basis in terms of the generator q_α ($\alpha = a, b, c, d$) in the D-brane basis. The $U(1)_a$ and $U(1)_d$ symmetries can be identified with (three times) the baryon number and (minus) the lepton number respectively. The $U(1)_c$ symmetry can be identified with the third component of right-handed weak isospin and finally the $U(1)_b$ is a PQ-like symmetry. Specifically the hypercharge generator is given by

$$Y = \frac{1}{6}(q_a + 3q_d) - \frac{1}{2}q_c, \tag{3.101}$$

which in fact is a linear combination of the two anomaly-free generators $(q_a + 3q_d)$ and q_c, while the orthogonal combinations

$$X_A = 3q_a - q_d, \qquad X_B = q_b, \tag{3.102}$$

represent anomalous generators in the hypercharge basis. Note that relation (3.101) must be imposed in these models in order to obtain a correct massless hypercharge generator as in the SM. The set (Y, A, B) does not depend on the model, while the fourth generator X_C is model-dependent and is given by

$$X_C = \left(\frac{3\,\beta_2\, n_{a2}}{\beta_1}\, q_a \;+\; 6\,\rho\, n_{b1}\, q_b \;+\; 2\, n_{c1}\, q_c \;+\; \frac{3\,\rho\,\beta_2\, n_{d2}}{\beta_1}\, q_d \right). \tag{3.103}$$

As can be seen in the detailed analysis performed in [93, 60, 64], the general solutions are parametrized by a phase $\epsilon = \pm 1$, the Neveu-Schwarz background on the first two tori $\beta_i = 1 - b_i = 1, 1/2$, the four integers n_{a2}, n_{b1}, n_{c1} and n_{d2}, which are the wrapping numbers of the branes around the extra (toroidal) manifolds of the compactification, and a parameter $\rho = 1, 1/3$, with an additional constraint in order to obtain the correct massless hypercharge

$$n_{c1} \;=\; \frac{\beta_2}{2\beta_1}(n_{a2} + 3\,\rho\, n_{d2}). \tag{3.104}$$

This choice of the parameters identifies a particular class of models which are called Class A Models [64] and all the parameters are listed in Tabs. 3.1, 3.2, 3.3. Whether anomalous or not, the Abelian fields

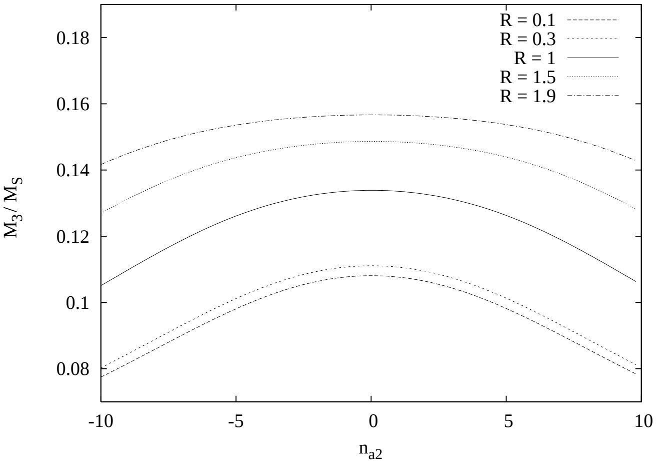

Figure 3.19: Lightest eigenvalue related to the generator X_B for a model of Class A. We have chosen the couplings g_c and g_d such that their ratio $\mathcal{R} = g_d/g_c$.

have mass terms induced by the Stückelberg mechanism, the mass matrix of the $U(1)$ gauge bosons in the D-brane basis is given by the following expression

$$(\mathcal{M}^2)_{\alpha\beta} = g_\alpha g_\beta M_S^2 \sum_{i=1}^{3} c_i^\alpha c_i^\beta, \tag{3.105}$$

where M_S is some string scale to be tuned. Greek indices run over the D-brane basis $\{a, b, c, d\}$, the Latin index i runs over the three additional Abelian gauge groups, while the g_α and g_β are the couplings of the four $U(1)$. The eigenvectors $w_{i=Y,A,B,C}$ and their eigenvalues λ_i for the matrix $(\mathcal{M}^2)_{\alpha\beta}$ have been computed in terms of the various classes of models in reference [93, 60]

$$\begin{aligned} w_Y &= \frac{1}{|w_Y|}\left\{\frac{g_d}{3g_a}, 0, -\frac{g_d}{g_c}, 1\right\}_\alpha & (3.106)\\ w_i &= \frac{1}{|w_i|}\{w_{ia}, w_{ib}, w_{ic}, 1\} & (3.107)\end{aligned}$$

where the $w_{i=A,B,C}$ are the components of the eigenvectors. On the basis of the analysis of the mass matrix one can derive a plot of the lightest eigenvalue M_3, which corresponds to the X_B generator in the hypercharge basis [64]. We have reproduced independently the result for the lightest eigenvalue M_3, which is in agreement with the predictions of [64]. We have implemented numerically the diagonalization of the mass matrix and shown in Fig. 3.19 the behavior of the ratio M_3/M_S as a function of the wrapping number n_{a_2} and for several values of the ratio $\mathcal{R} = g_d/g_c$. This ratio, which characterizes the couplings of $U(1)_c$ and $U(1)_d$, appears as a free parameter in the gauge boson mass matrix. M_S, the string scale, is arbitrary and can be tuned at low values in the region of a few TeV. We have selected a Stückelberg mass M_3 (which is essentially the mass of the extra Z') of 800 GeV. From Fig. 3.19, if we choose the curve with $\mathcal{R} = 1$ at the peak value, then this value is 13% of the string scale, which in this case is lowered to approximately 6.1 TeV. It is quite obvious that the mass of the extra Z' can be reasonably assumed to be a free parameter for all practical purposes. The matrix $E_{i\alpha} \equiv (w_i)_\alpha$ constructed with the eigenvectors of the mass matrix defines the rotation matrix $U_{i\alpha}$ for the $U(1)$ charges from the D-brane basis $\{a, b, c, d\}$

ν	β_1	β_2	n_{a2}	n_{b1}	n_{c1}	n_{d2}
1/3	1/2	1	n_{a2}	-1	1	1 - n_{a2}

Table 3.1: Parameters for a Class A Model with a $D6$-brane .

	Y	X_A	X_B
H_u	1/2	0	2
H_d	1/2	0	-2

Table 3.2: Higgs charges in the Madrid Model.

into the hypercharge basis $\{Y, A, B, C\}$ as follows

$$q_i = \sum_{\alpha=a,b,c,d} U_{i\alpha} q_\alpha \, , \quad U_{i\alpha} = \frac{g_\alpha}{g_i} E_{i\alpha}, \qquad (i = Y, A, B, C). \tag{3.108}$$

So for the hypercharge we find that

$$q_Y = \frac{g_d}{3 g_Y |w_Y|}(q_a - 3q_c + 3q_d) \equiv \frac{1}{6}(q_a + 3q_d) - \frac{1}{2} q_c, \tag{3.109}$$

to be identified with the correct hypercharge assignment given in expression (3.101). This identification gives a relation between the gauge couplings

$$\frac{1}{g_Y^2} = \frac{|w_Y|^2}{4 g_d^2} = \frac{1}{36 g_a^2} + \frac{1}{4 g_c^2} + \frac{1}{4 g_d^2}. \tag{3.110}$$

For the third generator a similar argument gives

$$q_B = \frac{g_a}{g_B} w_{Ba} \, q_a + \frac{g_b}{g_B} w_{Bb} \, q_b + \frac{g_c}{g_B} w_{Bc} \, q_c + \frac{g_d}{g_B} w_{Bd} \, q_d \equiv q_b, \tag{3.111}$$

where we identify the gauge symmetry $U(1)_B$ corresponding to the lightest mass eigenvalue as an anomalous generator q_B. The charges q_B of the SM spectrum are given in Tab. 3.4. We recall that given a particular non-Abelian $SU(N)$ gauge group, with coupling g_N, arising from a stack of N parallel branes and the corresponding $U(1)$ field living in the same stack, the two coupling constants are related by $g_1 = g_N/\sqrt{2N}$. Therefore, in particular the couplings g_a and g_b are determined using the SM values of the couplings of the non-Abelian gauge groups

$$g_a^2 = \frac{g_{QCD}^2}{6}, \qquad g_b^2 = \frac{g_L^2}{4}, \tag{3.112}$$

where g_L is the $SU(2)_L$ gauge coupling, while g_c and g_d are constrained by relation (3.110). Imposing gauge invariance for the Yukawa couplings [91] we obtain the assignments for the Higgs doublets shown in Tab. 3.2.

3.8.1 Anomalous and anomaly-free regions: numerical results

We have implemented in CANDIA 1.0 [104] a numerical program that will provide full support for the experimental collaborations for their analysis of the main signals in this class of models at the LHC, with the charge assignments discussed in the previous section. CANDIA 1.0 has been planned to deal

	q_a	q_b	q_c	q_d
Q_L	1	-1	0	0
u_R	-1	0	1	0
d_R	-1	0	-1	0
L	0	-1	0	-1
e_R	0	0	-1	1
N_R	0	0	1	1

Table 3.3: SM spectrum charges in the D-brane basis for the Madrid Model.

	Q_L	u_R	d_R	L	e_R	N_R
q_Y	1/6	- 2/3	1/3	-1/2	1	0
q_B	-1	0	0	-1	0	0

Table 3.4: Fermion spectrum charges in the Y-basis for the Madrid Model.

with the analysis of extra neutral interactions at hadron colliders in specific channels, such as Drell-Yan processes and double prompt photon processes with the highest precision. The program is entirely based on the theory developed in [1, 12, 40, 91, 13, 105] and is tailored to determine the basic processes, which provide the signal for the anomalous and anomaly-free extra Z' both from string and GUT models. The QCD corrections, including the parton evolution, is treated with extreme accuracy using the theory of the logarithmic expansions, developed in the last several years. Here we provide only parton level results for the anomalous processes that we have discussed in the previous sections, which clarify the role played by the WZ Lagrangian in the restoration of unitarity at high energy. A complete analysis for the LHC is presented in Chap. 5.

- **σ reduction by the exchange of χ**

  We show in Fig. 3.13 a plot of the (small) but increasing partonic cross section for double prompt photon production from anomalous gluon fusion. We have chosen a typical SM-like value for the coupling constant of the extra Z' included in the analysis and varied the center of mass energy of a few GeV around 4.2 TeV. We show two plots, both in the brane model, one with the inclusion of the axi-Higgs χ and one without it, with only the exchange of the Z and Z'. Notice that the exchange of the χ is a separate gauge invariant contribution. We have chosen a Stückelberg mass of 800 GeV. The plots show the theoretically expected reduction of the linear growth of the cross section, but the improvement is tiny, for these values of the external parameters. In these two plots, the fermion masses have been removed, as we worked in the chiral limit. The inclusion of all the mass effects in the amplitude has an irrelevant effect on the growth of the cross section. This is shown in Fig. 3.14 where, again, the inclusion of the axi-Higgs lowers the growth, but not in a significantly way. We have analyzed the behavior of the cross sections in the presence of a light axi-Higgs (ten or more GeV), but also in this case the effects are negligible. This feature can be easily checked from Eq. (3.90); in fact, the mass term M_χ is contained in the denominator of the propagator for the scalar, and in the TeV region we have $(s - M_\chi^2) \approx s$. The numerical value of the unitarity bound remains essentially unchanged.

- **Anomaly-free and anomalous regions**

  An interesting behavior shows up in Fig. 3.15, where we compare the results in the SM and in the mLSOM for the same cross section, starting at a lower energy. It is clear that the SM result,

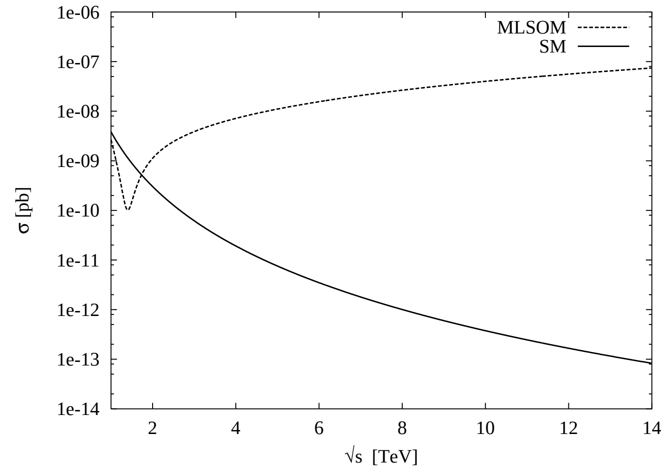

Figure 3.20: Partonic cross section for the anomalous process $gg \to \gamma\gamma$ with $\tan\beta = 40$, $g_B = 0.1$, $M_\chi = 10$ GeV and $M_1 = 1$ TeV. The lines refer to the cross section evaluated for different values of the center of mass energy $\sqrt{s}$.

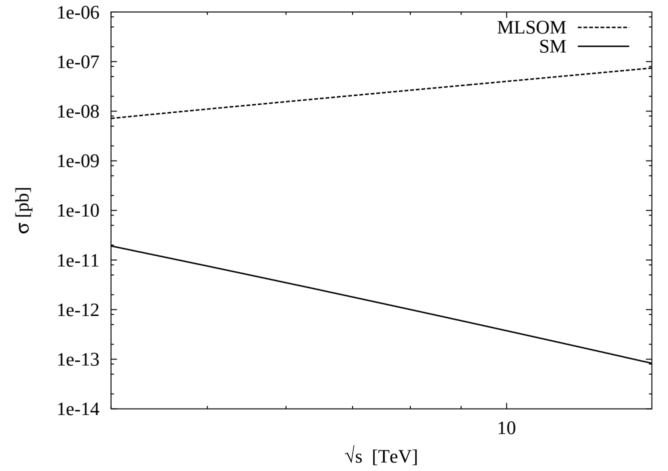

Figure 3.21: The partonic cross section with a parameter choice as in Fig. 3.20. The dashed upper lines refer to mLSOM cross sections evaluated with and without the χ exchange, while the decreasing solid line refers to the SM.

being anomaly-free, is characterized by a fast-falling cross section, while the mLSOM result is very different. In particular, one finds a region of lower energy, where essentially the Model follows the SM behavior (below 1 TeV) - but smaller by a factor of 10 - the growth of the anomalous contributions still being not large, and a region of higher energy, where the anomalous contributions take over (at about 2 TeV) and which drive the growth of the cross section, as in the previous two plots. There is a minimum at about 1.2 TeV, which is the point at which the anomalous subcomponent becomes sizeable.

- **$\tan\beta$, g_b and M_1 variations**

The variation of the same behavior shown in the previous plot with $\tan\beta$ is shown in Fig. 3.16, where we have varied this parameter from small to larger values (10÷50). The depth of the minimum increases as we increase this value. At the same time, the cross section tends to fall much steeper, starting from larger values in the anomaly-free region.

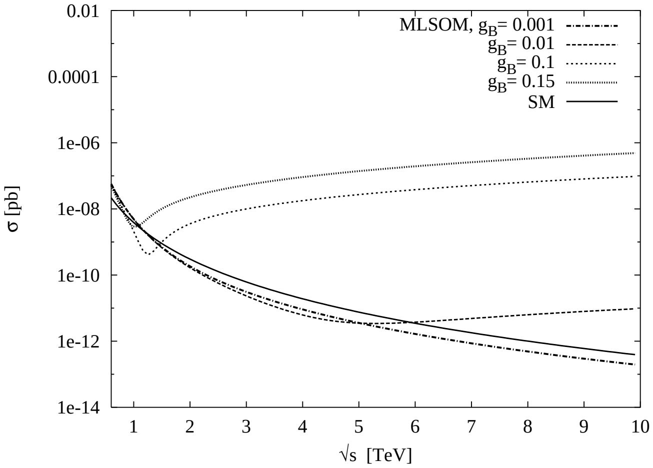

Figure 3.22: Partonic cross section plotted for different values of the coupling constant g_B. The parameters are chosen as before.

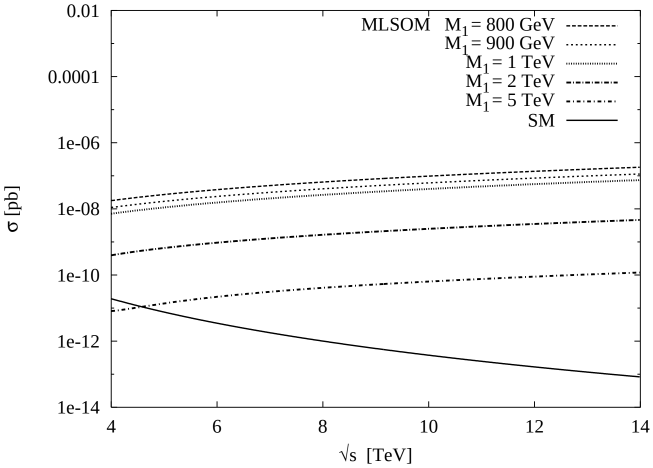

Figure 3.23: Partonic cross section for the anomalous process $gg \to \gamma\gamma$, $\tan\beta = 40$, $g_B = 0.1$, and $M_\chi = 10$ GeV plotted for different values of the Stückelberg mass M_1.

In Fig. 3.17 we study the variation of σ as we tune the coupling g_B of the anomalous $U(1)_B$. A very small value of the coupling tends to erase the anomalous behavior, rendering the anomalous components subleading. The cross section then falls quite fast before increasing reaching the bound. The falling region is quite visible for the two values of $g_B = 0.001$ and 0.01, showing that the set of minimum points, or the anomaly-free region, is pushed up to several TeV, in this case above 4.5 TeV. The unitarity bound is weaker, being pushed up significantly. The situation is opposite for stronger values of g_B.

A similar study is performed in Fig. 3.18, but for different Stückelberg masses M_1. As this mass parameters increase, the anomaly-free region tends to grow wider and the cross section stabilizes. For instance, for a value of the Stückelberg mass around 5 TeV, the region in which σ has a normal behavior moves up to 3.5 TeV. The explanation of this result has to be found in the fact that the anomalous growth is controlled by the mass of the anomalous Z' in the s-channel, appearing in the denominator of the cross section. This suppression is seen both in the direct diagram and in the counterterm diagram, which describes the exchange of the axi-Higgs. Obviously, it is expected that as we reduce the coupling of the anomalous gauge boson, the anomalous behavior is reduced as

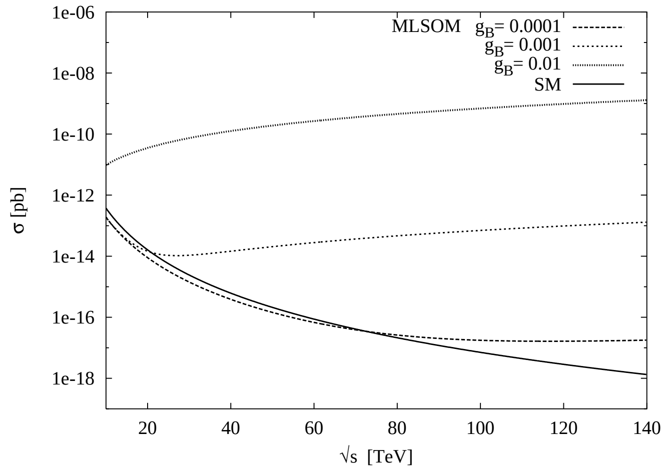

Figure 3.24: Partonic cross section for the anomalous process $gg \rightarrow \gamma\gamma$, $\tan\beta = 40$ $M_1 = 800$ GeV and $M_\chi = 10$ GeV. The different plots show a comparison between the SM and the mLSOM cross sections, at very high energies, for small value of the coupling constant g_B.

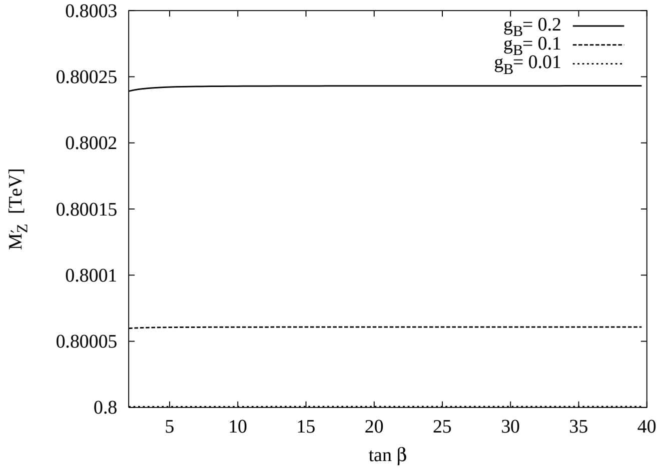

Figure 3.25: Behavior of the mass of the additional anomalous Z' as a function of $\tan\beta$ for different values of g_B. The variations are very small.

well. The different behavior of the cross section in the SM and mLSOM cases can easily be inferred from Fig. 3.20 having chosen a Stückelberg mass of the order of 1 TeV. A similar behavior is quite evident also from Fig. 3.21, from which it appears that in the mLSOM the deviations compared to the SM partonic predictions get sizeable at parton level already at an energy of 4-6 TeV. Notice also from Fig. 3.14 that the presence of the axi-Higgs seems to be irrelevant for the chosen values of the couplings and parameters of the model. We show in Fig. 3.22 a plot of the dependence of the predictions on g_B at larger energy values, which appears to be quite significant.

Furthermore, in the TeV region the mLSOM predictions for small values of the coupling constant ($g_B = 0.001$) go below the SM prediction and this is due to the axi-Higgs exchange, which is negative in this kinematical domain. Moving below to 1 TeV the axi-Higgs interference has an opposite sign and the mLSOM predictions are above the SM. A similar analysis, this time for a varying Stückelberg mass, is shown in Fig. 3.23, and also in this case, as in the previous one, the results confirm that this dependence is very relevant.

Finally, in Fig. 3.24 we plot the SM and mLSOM results on a larger interval, from 10 to 140 TeV,

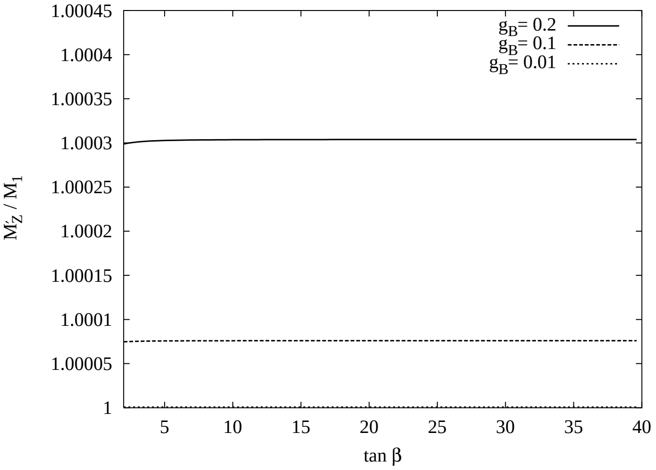

Figure 3.26: Mass of the extra Z' gauge boson for different values of the Stückelberg mass.

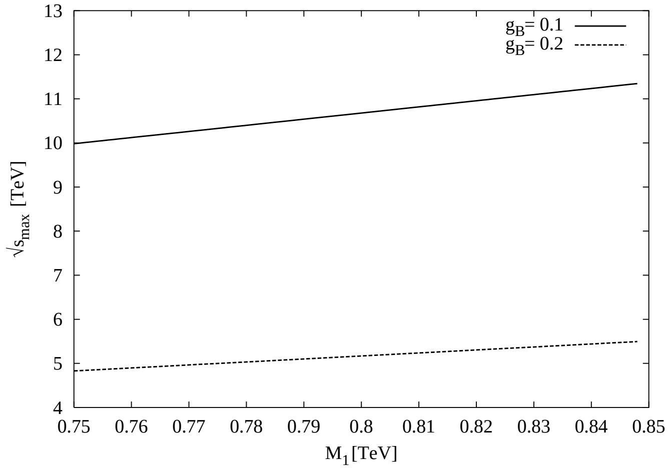

Figure 3.27: Bound for different values of the Stückelberg mass and $\tan\beta = 40$. The bound grows as we reduce the anomalous coupling, and approaches the Standard Model behavior. For $g_B = 0.01$ the model exhibits a bound around $\sqrt{s}_{max} = 100$ TeV (not shown).

from which the drastically different behavior of the two cross sections are quite clear. Notice that as we lower g_B, for instance down to 10^{-4}, the anomaly-free region extends up to energy values that are of the order of 200 TeV or so. We conclude that the enhancement of the anomalous contributions with respect to the SM prediction are in general quite large and very sensitive to the mass of the extra Z' and to the strength of the anomalous coupling. Interestingly, a very weakly coupled Z' gives a cross section that has a faster fall-off compared to the SM case in the anomaly-free region. The mLSOM and SM predictions intersect at a very large energy scale (140 TeV), when the anomalous contribution starts to increase.

Before drawing conclusions, it is necessary to comment on the other dependence, that on $\tan\beta$, which appears to be far less significant compared to that on M_1 (or M'_Z) and g_B. This third parameter essentially has a (very limited) influence on the mass of the extra Z' and on the overall predictions. This is clearly shown in Figs. 3.25 and 3.26, where we have varied both $\tan\beta$ and g_B. Therefore, the mass of the extra Z' and the Stückelberg mass may be taken to be essentially coincident, to a first approximation.

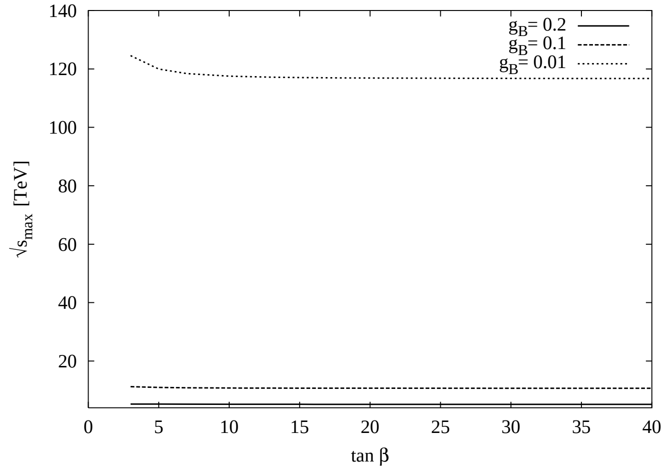

Figure 3.28: Bound for different values of $\tan\beta$, for $M_1 = 800$ GeV.

- **The bounds**

  We conclude our analysis with two plots, depicted in Figs. 3.27 and 3.28, which show the variations of the bounds with the parameters g_B and M_1. In the first plots, shown in Fig. 3.27, we choose a large value of $\tan\beta$ and we have varied both the Stückelberg mass and the strength of the anomalous coupling. For a Stückelberg mass around 1 TeV, the bound is around 5 TeV, for an anomalous coupling $g_B = 0.2$. For a smaller value of $g_B = 0.1$ the bound grows to 10 TeV. For a smaller value of $g_B = 10^{-2}$, the bound is around $100 \div 120$ TeV. This result is particularly interesting, because it should allow one to set limits on the Stückelberg mass and the value of the anomalous couplings at the LHC in the near future. Smaller values of g_B are tested in Fig. 3.28, where the bound is shown to increase significantly as g_B gets smaller.

3.9 Conclusions

We have analyzed the connection between the WZ term and the GS mechanism in the context first of simple models and then in a complete brane model, containing three extra anomalous $U(1)$. We have shown that the WZ method of cancellation of the anomaly does not protect the theory from an excessive growth, which is bound to violate unitarity beyond a certain scale. We have also studied the connection between the two mechanisms, illustrating the corresponding differences.

We have quantified the unitarity bound for several choices of the parameters of the theory. The significant dependences are those on the Stückelberg mass M_1 and the coupling constant g_B of the anomalous generator. We have also shown that the exchange of a physical axion χ lowers the cross section, but not significantly, whose growth remains essentially untamed at high energy. We have shown that in these models one can identify a region that is SM-like, where some anomalous processes have a fast fall-off, from a second region, where the anomaly dominates.

The analysis in this chapter has been confined to the parton level, but we postpone more definitive predictions for the detection of anomalous interactions at the LHC to Chap. 5.

The approach that we have suggested, the use of BIM amplitudes to search for unitarity violations at future colliders, can be a way in the search to differentiate between non-anomalous [106] and anomalous extra Z' [107]. Our objective here has been to show that there is a systematic way to analyze the two mechanisms for canceling the anomalies at the phenomenological level and that unitarity issues are important in order to characterize the region in which a certain theory starts to be dominated by the chiral anomaly.

3.10 Appendix. The cross section

The total cross section is given by the sum of all the contributions shown in Fig. 3.12

$$\begin{aligned} \sigma^{mLSOM}(s) &= \sigma_A(s) + \sigma_B(s) + \sigma_C(s) + \sigma_D(s) + \sigma_E(s) + \sigma_F(s) \\ &\quad + \sigma_{AB}(s) + \sigma_{AE}(s) + \sigma_{AF}(s) + \sigma_{BF}(s) + \sigma_{EF}(s). \end{aligned} \tag{3.113}$$

The interference term between Z exchange and χ exchange, diagram (b) in Fig. 3.12, is given by

$$\sigma_{AB}(s) = \frac{1}{16\pi}\left[\sum_q \frac{1}{2} c_1^q A_{6,q}\right]\left[\sum_f \frac{1}{2} c_2^f A_{6,f}\right] g_{gg}^{\chi} g_{\gamma\gamma}^{\chi} \frac{s^4}{M_Z^2(s - M_\chi^2)}. \tag{3.114}$$

The following interference terms are vanishing

$$\begin{aligned} &\mathcal{M}_A\mathcal{M}_C^\dagger + \mathcal{M}_C\mathcal{M}_A^\dagger = 0, \qquad \mathcal{M}_A\mathcal{M}_D^\dagger + \mathcal{M}_D\mathcal{M}_A^\dagger = 0, \\ &\mathcal{M}_B\mathcal{M}_C^\dagger + \mathcal{M}_C\mathcal{M}_B^\dagger = 0, \qquad \mathcal{M}_B\mathcal{M}_D^\dagger + \mathcal{M}_D\mathcal{M}_B^\dagger = 0. \end{aligned} \tag{3.115}$$

The interference term between the exchange of the Z boson and χ exchange, diagram (e) in Fig. 3.12, gives

$$\begin{aligned} \sigma_{AE}(s) &= \frac{s^4}{1024 M_Z^2 \pi (s - M_\chi^2)} \left[\sum_q \frac{1}{2} c_1^q A_{6,q}\right]\left[\sum_f \frac{1}{2} c_2^f A_{6,f}\right] \\ &\quad \times \left[\sum_{f'} C_0(s, m_{f'}) c_{\gamma\gamma}^{\chi,f'}\right]\left[\sum_{q'} C_0(s, m_{q'}) c_{gg}^{\chi,q'}\right], \end{aligned} \tag{3.116}$$

while the interference term between χ exchange and Z' boson exchange contributes with

$$\sigma_{BE}(s) = -\frac{s^3}{16\pi(s - M_\chi^2)^2} g_{\gamma\gamma}^{\chi} g_{gg}^{\chi} \left[\sum_f C_0(s, m_f) c_{\gamma\gamma}^{\chi,f}\right]\left[\sum_q C_0(s, m_q) c_{gg}^{\chi,q}\right]. \tag{3.117}$$

The other interference term in the cross section is given by

$$\sigma_{CD}(s) = \frac{s^3}{16\pi(s - M_\chi^2)^2} g_{\gamma\gamma}^{\chi} g_{gg}^{\chi} \left[\sum_q C_0(s, m_q) c_{gg}^{\chi,q}\right]\left[\sum_f C_0(s, m_f) c_{\gamma\gamma}^{\chi,f}\right], \tag{3.118}$$

so we obtain

$$\sigma_{CD}(s) + \sigma_{BE}(s) = 0. \tag{3.119}$$

Other interference terms also vanish; in fact, we get

$$\mathcal{M}_C\mathcal{M}_E^\dagger + \mathcal{M}_E\mathcal{M}_C^\dagger = 0, \qquad \mathcal{M}_D\mathcal{M}_E^\dagger + \mathcal{M}_E\mathcal{M}_D^\dagger = 0, \tag{3.120}$$

$$\mathcal{M}_C \mathcal{M}_F^\dagger + \mathcal{M}_F \mathcal{M}_C^\dagger = 0, \qquad \mathcal{M}_D \mathcal{M}_F^\dagger + \mathcal{M}_F \mathcal{M}_D^\dagger = 0. \tag{3.121}$$

The interference term between Z exchange and Z' exchange takes the form

$$\sigma_{AF} = \frac{1}{1024\pi} \left[\sum_q \frac{1}{2} d_1^q A_{6,q} \right] \left[\sum_f \frac{1}{2} d_2^f A_{6,f} \right] \left[\sum_{q'} \frac{1}{2} c_1^{q'} A_{6,q'} \right] \left[\sum_{f'} \frac{1}{2} c_2^{f'} A_{6,f'} \right] \frac{s^5}{M_Z^2 \, M_{Z'}^2} \,. \tag{3.122}$$

The interference term between Z' exchange and χ exchange of diagram (b) in Fig. 3.12 is given by

$$\sigma_{BF}(s) = \frac{1}{16\pi} \left[\sum_q \frac{1}{2} d_1^q A_{6,q} \right] \left[\sum_f \frac{1}{2} d_2^f A_{6,f} \right] g_{gg}^\chi g_{\gamma\gamma}^\chi \frac{s^4}{M_{Z'}^2 (s - M_\chi^2)} \,. \tag{3.123}$$

Finaly, the interference between Z' exchange and χ exchange, diagram (e) in Fig. 3.12, gives

$$\begin{aligned} \sigma_{EF}(s) \quad = \quad & \frac{s^4}{1024 \, M_{Z'}^2 \, \pi \, (s - M_\chi^2)} \left[\sum_q \frac{1}{2} d_1^q A_{6,q} \right] \left[\sum_f \frac{1}{2} d_2^f A_{6,f} \right] \\ & \times \left[\sum_{f'} C_0(s, m_{f'}) c_{\gamma\gamma}^{\chi, f'} \right] \left[\sum_{q'} C_0(s, m_{q'}) c_{gg}^{\chi, q'} \right] . \end{aligned} \tag{3.124}$$

Chapter 4

Axions and Anomaly-Mediated Interactions: The Green-Schwarz and Wess-Zumino Vertices at Higher Orders and $g - 2$ of the muon

4.1 Introduction to the chapter

Understanding the role played by the Green-Schwarz (GS) and Wess-Zumino (WZ) mechanisms in quantum field theory is important in order to grasp the implications of the chiral gauge anomaly at the level of model building, especially in the search of extra trilinear gauge interactions at future colliders. In recent years several proposals coming either from string theory or from theories with extra dimensions have introduced new perspectives in regard to the various mechanisms of cancellation of the gauge anomalies in effective low energy Lagrangians, which require further investigation in order to be fully understood. These effective models are characterized by the presence of higher dimensional operators and interactions of axion-like particles. In a class of vacua of string theory this enterprise has some justification, for instance in orientifold models (see [26, 90, 93]), where deviations from the Standard Model may appear in the form of higher dimensional corrections which are not heavily suppressed and which could be accessible at the LHC.

In anomaly-free realizations of chiral gauge theories the trilinear anomalous gauge interactions vanish (identically) in the chiral limit, by a suitable distribution of charges among the fermions of each generation (or inter-generational), showing that residual interactions are proportional to the mass differences of the various fermions. In the GS realization this request is far more relaxed and the mechanism requires only the cancellation, in the presence of anomalous contributions, of the longitudinal component of the anomaly vertex rather than that of the entire triangle diagram. In the WZ case, the cancellation of the anomaly takes place at Lagrangian level, rather than at the vertex level, and requires an axion as an asymptotic state, which is a generalization of the Peccei-Quinn interaction.

The effective field theory of the WZ mechanism has been analyzed in [1, 40, 91, 13, 105, 92], together with its supersymmetric extensions [108] while a string derivation of the GS constructions has been outlined in [69]. Pseudoscalar fields (axion-like particles) - with a mass and a coupling to gauge fields which are left unrelated - have been the subject of several investigations and proposals for their detection either in ground-based experiments [109] or to explain some puzzling results on gamma ray propagation [110, 80], while new solutions of the strong CP-problem in more general scenarios have also received attention [111]. At the same time the search for extra Z' at the LHC from string models and extra dimensions, together with precision studies on the resonance to uncover new effects, has also received a new strength ([112, 113, 106, 114, 29, 115]).

If the GS and the WZ mechanisms are bound to play any role at future experiments (see for instance [116]) remains to be seen, given the very small numerical impact of the anomaly corrections in the cleanest processes that can be studied, for instance, at the LHC; nevertheless more analysis is needed in order to understand the theoretical implications of "anomaly mediation" and of its various realizations, in the form of GS and WZ interactions, in effective models.

Both mechanisms are quite tricky, since they show some unusual features which are not common to the rest of anomaly-free field theories and it is not hard to find in the literature several issues which have been debated for a long time, concerning the consistency of these approaches [94, 96, 97].

For instance, in the GS case, one of them concerns unitarity, due to the claimed presence of extra "double poles" [20] in a certain class of interactions which would render completely invalid a perturbative prescription; another one concerns the physical interpretation of the longitudinal subtraction, realized within the same mechanism, which is usually interpreted as due to the exchange of an axion, which, however, as pointed out in [105] is not an asymptotic state.

The first part of this chapter is a study of the organization of the perturbative expansion for anomalous theories in the presence of counterterms containing double poles in virtual corrections and, in principle, in $s/t/u-$channel exchanges. Our point of view and conclusions are in contradiction with those of [20], formulated within axial QED, where the analysis of the anomaly pole counterterm was not taking into account the fact that the subtracted term is an intrinsic part of the triangle (anomaly) diagram, corresponding to one of its invariant amplitudes, in a specific formulation.

The picture that emerges from our analysis is that of consistency -rather than of inconsistency- of the GS mechanism at the level of effective field theory. In other words, it should be possible to subtract the longitudinal pole of the anomaly diagram with no further consequences at perturbative level. The structure of the perturbative expansion in the presence of explicit GS counterterms is worked out and we detail the methods for the computations of graphs containing extra poles in the propagators and compare the general features of this expansion to an ordinary expansion.

In any case, in the absence of a direct check of the unitarity equations -which is hard to perform given the rather high order at which these anomalous corrections appear- the problems in perturbation theory can potentially appear in the form of double poles in some (*external*) propagators. A re-examination of several diagrams brings us to conclude that this situation is avoided.

Coming to a direct phenomenological application, we investigate the role of these vertices in the study of the anomalous magnetic moment of the muon. We stress that if the physical mechanism introduced for the cancellation of the anomaly is of WZ type, then a physical axion appears in the spectrum. This is the case if the anomalous extra Z' receives its mass both by the Higgs and the Stückelberg mechanisms. Both for the GS and the WZ case we outline the role of the anomalous extra Z' and of the pseudoscalar exchange up to two-loop level. A previous analysis of the leading contribution to $g-2$ for intersecting brane models can be found in [68].

More recently, the GS vertex has been used in the study of the coupling of the Kaluza-Klein (KK) [116, 117] excitations of gauge bosons to fermions, where it has been pointed out the possibility to detect these coupling at the LHC, for instance in $t\bar{t}$ production. We find that several of these results are based on a still unsatisfactory understanding of the GS mechanism at theoretical level, and our work is an attempt to clarify some of these points. From our analysis will emerge the correct structure of the broken Ward Identities for the GS vertex, which are specific of a non-local theory. These points will be carefully analyzed in the final section of this chapter.

4.2 The GS and WZ vertices

The field theory version of the GS mechanism, deprived of all its stringy features, appears in an attempt to cancel the anomaly by introducing a specific non-local counterterm added to the anomalous theory. This attempt had been the cause of serious debates which have questioned the consistency of the approach. The mechanism uses a ghost-like particle, which in string theory is generically identified as an axion - although there it does not appear as an asymptotic state - to restore the broken Ward Identities due to the anomaly. A paradigm for the GS mechanism in field theory is an anomalous version of axial QED in 4-dimensions defined by the Lagrangian

$$\mathcal{L}_{5\,QED} = \overline{\psi}\left(i\partial\!\!\!/ + eB\!\!\!/\gamma_5\right)\psi - \frac{1}{4}F_B^2 \tag{4.1}$$

plus the counterterm

$$\mathcal{S}_{ct} = \frac{1}{24\pi^2}\langle \partial B(x)\Box^{-1}(x-y)F(y)\wedge F(y)\rangle. \tag{4.2}$$

Federbush [100] proposed to reformulate this Lagrangian in terms of one axion and one ghost-like particle interacting via a Wess-Zumino (WZ) counterterm (see the discussion in Chap. 3). An equivalent formulation of the same subtraction counterterm is given in [94], where a transversality constraint ($\partial B = 0$) is directly imposed on the Lagrangian via a multiplier. Eq. (4.2) can be obtained by performing the functional integral over a and b of the following action

$$\begin{aligned}\mathcal{L} \;&=\; \overline{\psi}\left(i\;\partial\!\!\!/ + e\;B\!\!\!/\gamma_5\right)\psi - \frac{1}{4}F_B^2 + \frac{e^3}{48\pi^2 M}F_B\wedge F_B(a+b)\\ &\quad+\frac{1}{2}\left(\partial_\mu b - MB_\mu\right)^2 - \frac{1}{2}\left(\partial_\mu a - MB_\mu\right)^2.\end{aligned} \tag{4.3}$$

The integral on a and b are gaussians and one recovers the non-local contribution in (4.2) after partial integration. Notice that b has a positive kinetic term and a is ghost-like. Both a and b shift by the same amount under a gauge transformation of B

$$a \to a + M\theta, \quad b \to b + M\theta \tag{4.4}$$

where θ is the gauge parameter. This second (local) formulation of the pole counterterm contained in (4.2) shows the connection between this action and the WZ mechanism. Both actions, in fact, share some similarities, but describe different theories. In particular, the WZ action is obtained by removing the ghost term (b) and keeping only the axion. This second theory is characterized by a unitarity bound, as shown in Chap. 3. The bound is due to the fact that in effective models containing Wess-Zumino interactions, gauge invariance of the effective action requires a cancellation between different trilinear vertices: the anomalous vertices and the axion counterterm $\phi F\wedge F$, while for Green-Schwarz vertices the subtraction of the longitudinal component of the anomaly is sufficient to make the effective vertex gauge-invariant to all orders. In both cases the physical amplitudes are gauge-independent.

In the WZ case the proof of gauge independence is rather involved and has been discussed before in

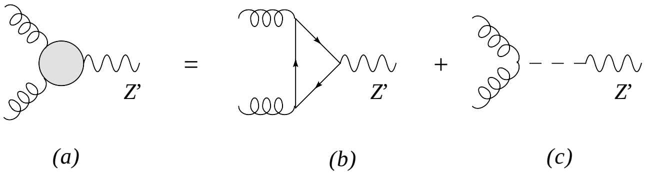

Figure 4.1: A gauge invariant GS vertex of the AVV type, composed of an AVV triangle and a single counterterm of Dolgov-Zakharov form. Each term is denoted by $\Delta^{\lambda\mu\nu\, GS}_{AVV}$ (a), $\Delta^{\lambda\mu\nu}_{AVV}$ (b) and $C^{\lambda\mu\nu}_{AVV}$ (c).

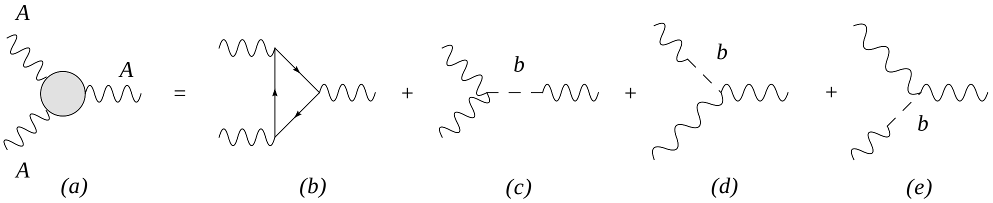

Figure 4.2: All the contributions to the GS gauge invariant vertex, for an AAA triangle. The single terms are denoted by $\Delta^{\lambda\mu\nu\, GS}_{AAA}$ (a), $\Delta^{\lambda\mu\nu}_{AAA}$ (b), $C^{\lambda\mu\nu}_{AVV}$ (c), $C^{\mu\nu\lambda}_{AVV}$ (d) and $C^{\nu\mu\lambda}_{AVV}$ (e).

Chaps. 1, 2. In the GS case, instead, this is trivial since the vertex is gauge-invariant by construction. Notice that a local counterterm in the form of a Peccei-Quinn term is not sufficient to remove the power-like growth with energy of a class of amplitude (BIM amplitudes) that are characterized by anomalous production and anomalous decay of massless gauge bosons in the initial and final states, mediated by the exchange of an anomalous Z' in the s-channel (see Chap. 3 for more details). These amplitudes are quite interesting since they evade the Landau-Yang theorem, triggering a $Z\gamma\gamma$ vertex. The phenomenological implications of these amplitudes are discussed in Chap. 5.

4.2.1 The GS vertex in the AAA and AVV cases

In our analysis, we denote with $T_{\mu\nu\lambda}$ the three-point function in momentum space, obtained from the Lagrangians (4.1) and (4.2). In the case of three axial-vector currents we define the correlator

$$(2\pi)^4\delta(k_1+k_2-k)\Delta^{\lambda\mu\nu}_{AAA}(k,k_1,k_2) = \int dx_1\, dx_2\, dx_3\, e^{i(k_1x_1+k_2x_2-kx_3)}\langle J^5_\mu(x_1)J^5_\nu(x_2)J^5_\lambda(x_3)\rangle. \tag{4.5}$$

and a symmetric distribution of the anomaly for the AAA vertex [1]

$$\begin{aligned} k_\lambda\Delta^{\lambda\mu\nu}_{AAA}(k,k_1,k_2) &= \frac{a_n}{3}\epsilon[\mu,\nu,k_1,k_2] \\ k_{1\mu}\Delta^{\lambda\mu\nu}_{AAA}(k,k_1,k_2) &= \frac{a_n}{3}\epsilon[\lambda,\nu,k,k_2] \\ k_{2\nu}\Delta^{\lambda\mu\nu}_{AAA}(k,k_1,k_2) &= \frac{a_n}{3}\epsilon[\lambda,\mu,k,k_1]. \end{aligned} \tag{4.6}$$

In the AVV case, a second vector-like gauge interaction (A_μ) is introduced in Eq. (4.3) for more generality and we have

$$(2\pi)^4\delta(k_1+k_2-k)\Delta^{\lambda\mu\nu}_{AVV}(k,k_1,k_2) = \int dx_1\, dx_2\, dx_3\, e^{i(k_1x_1+k_2x_2-kx_3)}\langle J_\mu(x_1)J_\nu(x_2)J^5_\lambda(x_3)\rangle, \tag{4.7}$$

---

[1] We have used the following notation $a_n = -\frac{i}{2\pi^2}$ and $\epsilon[\mu,\nu,k_1,k_2] = \epsilon^{\mu\nu\alpha\beta}k_{1\alpha}k_{2\beta}$

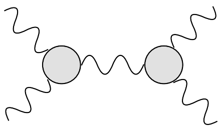

Figure 4.3: Amplitude with two full GS vertices and the exchange of an axial-vector current in the s-channel. For on-shell external lines the contributions from the extra poles disappear.

where the anomaly equations are

$$\begin{aligned}
&k_\lambda \Delta^{\lambda\mu\nu}_{AVV}(k,k_1,k_2) = a_n \epsilon^{\mu\nu\alpha\beta} k_{1\alpha} k_{2\beta} \\
&k_{1\mu} \Delta^{\lambda\mu\nu}_{AVV}(k,k_1,k_2) = 0 \\
&k_{2\nu} \Delta^{\lambda\mu\nu}_{AVV}(k,k_1,k_2) = 0. \qquad (4.8)
\end{aligned}$$

Below we will consider both the AVV and AAA cases. The GS counterterm that corresponds to the exchange of the massless pole of Eq. (4.2) takes the following form in momentum space in the AVV case

$$C^{\lambda\mu\nu}_{AVV}(k,k_1,k_2) = C^{\mu\nu}(k_1,k_2) k^\lambda = -\frac{a_n}{k^2} k^\lambda \epsilon[\mu,\nu,k_1,k_2]. \qquad (4.9)$$

Similarly, a GS counterterm in the AAA case, with incoming momentum k and outgoing momenta k_1, k_2, is defined as

$$\begin{aligned}
C^{\lambda\mu\nu}_{AAA}(k,k_1,k_2) &= \frac{1}{3}\left(C^{\lambda\mu\nu}_{AVV}(k,k_1,k_2) + C^{\mu\nu\lambda}_{AVV}(-k_1,k_2,-k) + C^{\nu\lambda\mu}_{AVV}(-k_2,-k,k_1)\right) \\
&= \frac{1}{3}\left(C^{\mu\nu}(k_1,k_2)k^\lambda - C^{\nu\lambda}(k_2,-k)k_1^\mu - C^{\lambda\mu}(-k,k_1)k_2^\nu\right) \\
&= -\frac{1}{3}\left(\frac{a_n}{k^2}k^\lambda\epsilon[\mu,\nu,k_1,k_2] + \frac{a_n}{k_1^2}k_1^\mu\epsilon[\lambda,\nu,k,k_2] + \frac{a_n}{k_2^2}k_2^\nu\epsilon[\lambda,\mu,k,k_1]\right), \qquad (4.10)
\end{aligned}$$

and corresponds to the Dolgov-Zakharov form (DZ) of the anomaly diagram [101] (modulo a minus sign). The re-defined vertex shown in Fig. 4.1 is written as

$$\Delta^{\lambda\mu\nu\, GS}_{AVV}(k,k_1,k_2) = \Delta^{\lambda\mu\nu}_{AVV}(k,k_1,k_2) + C^{\lambda\mu\nu}_{AVV}(k,k_1,k_2) \qquad (4.11)$$

and we obtain a similar expression for the AAA vertex (Fig. 4.2) just by replacing AVV with AAA in Eq. (4.11) and taking into account the different form of the counterterms. These gauge invariant vertices trivially satisfy the Ward Identities

$$k_\lambda \Delta^{\lambda\mu\nu\, GS}(k,k_1,k_2) = k_{1\mu}\Delta^{\lambda\mu\nu\, GS}(k,k_1,k_2) = k_{2\nu}\Delta^{\lambda\mu\nu\, GS}(k,k_1,k_2) = 0, \qquad (4.12)$$

where again $\Delta^{\lambda\mu\nu\, GS}$ refers either to an AVV or to an AAA correlator.

4.2.2 Implications of the GS vertex: vanishing of (real) light-by-light scattering at two-loop

To illustrate some of the properties of the GS vertex and its implications, we consider a two-loop process in which we have two massless vector bosons in the initial and in the final state with the exchange in the s-channel of an axial-vector current (Fig. 4.3). The example that we provide here comes from anomalous

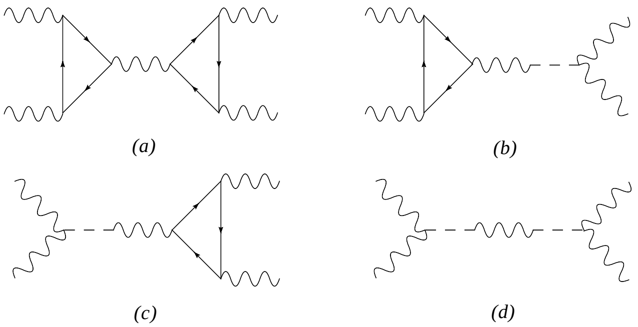

Figure 4.4: All the contributions from the GS gauge invariant vertex, in the AVV case, to the amplitude $VV \to VV$ via an axial-vector current.

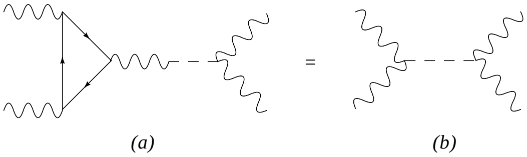

Figure 4.5: The sub-amplitude in Fig. 4.4b after the contraction $k^\lambda \Delta^{\lambda\mu\nu}_{AVV}$ which gives the anomaly equation.

axial QED, but it can be extended to more realistic models with no major variants. In Fig. 4.3 both the initial and the final state contain anomalous subdiagrams, but the two GS vertices are defined in such a way to absorb all the longitudinal subtractions terms inside each of the blobs. The amplitude of such a process is given by

$$\mathcal{M}^{\mu\nu\mu'\nu'} = \Delta^{\lambda\mu\nu\,GS}_{AVV}(-k,-k_1,-k_2)\left(-\frac{i g_{\lambda\lambda'}}{k^2}\right)\Delta^{\lambda'\mu'\nu'\,GS}_{AVV}(k,k_1',k_2'). \tag{4.13}$$

In the expression above, the propagator is deprived of its longitudinal momentum dependence due a WI. The amplitude in Eq. (4.13) can be decomposed into the four sub-amplitudes shown in Fig. 4.4 after expanding the two GS vertices with Eq. (4.11)

$$\mathcal{M}^{\mu\nu\mu'\nu'} = -\left(\Delta^{\lambda\mu\nu}_{AVV}(-k,-k_1,-k_2) - k^\lambda C^{\mu\nu}(-k_1,-k_2)\right)\frac{i g_{\lambda\lambda'}}{k^2}\left(\Delta^{\lambda'\mu'\nu'}_{AVV}(k,k_1',k_2') + C^{\lambda'\mu'\nu'}(k_1',k_2')\right), \tag{4.14}$$

but only two sub-amplitudes survive (Fig. 4.4a) and 4.4b)) because of the Ward Identities in Eq. (4.12). We are left with two contributions which cancel, for on-shell matrix elements. In fact, while off-shell the graph in Fig. 4.5 spoils unitarity, when instead the four external lines are on-shell the triangle contribution (the first term) reduces to the DZ form and the cancellation between the two terms is identical. In view of the structure of the anomaly vertex and of the GS vertex given before, this cancellation implies that the anomaly diagram, for on-shell (axial-vector) photons and in the chiral limit, is purely longitudinal (DZ form). A similar result holds also for the AAA case.

It is then natural to look at more general situations when these types of diagrams appear into higher-order contributions. In these more general cases, the anomaly diagram does not coincide with its DZ form, except for specific kinematical points ($k_1^2 = k_2^2 = k^2$, off-shell), and there is no identical cancellation of the anomalous trilinear gauge interactions. We conclude that compared to the identical cancellation

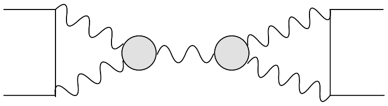

Figure 4.6: The embedding of the BIM amplitude with GS vertices in a fermion/antifermion scattering.

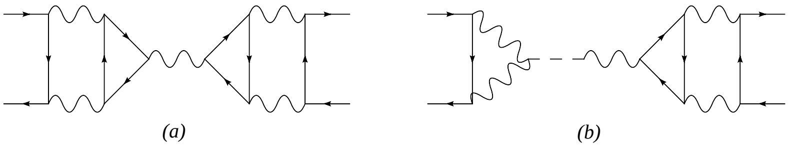

Figure 4.7: Contributions to the fermion-antifermion scattering with the GS mechanism.

of the anomaly by charge assignment on each generation, which eliminates all-together all the trilinear gauge interactions, the GS vertex can be either transversal or vanishing (in the chiral limit) for each given flavour.

As we have previously mentioned, an anomaly vertex with the addition of the pole counterterms (i.e. deprived of the anomaly pole) has been criticized in previous works in [20]. There the author brings in as an example a class of amplitudes which are affected by double poles, claiming a unitarity failure of the model. We will argue against this interpretation.

4.2.3 Embedding the GS vertex into higher-order diagrams

When we embed the amplitude into higher-order diagrams (see Fig. 4.6), and consider an on-shell fermion-antifermion scattering, according to [20], we are forced to move away from a symmetric configurations of the loop momenta and the identical vanishing of the anomaly is not ensured any longer, for the reasons that we have just raised above. In particular, according to [20], the s-channel exchange is affected by a double pole.

There is no better way to check the correctness of these conclusions than going through an explicit computation of this amplitude.

Expanding the two GS vertices, which are clearly non-zero in this case, we end up with several contributions, such as a graph with two triangle diagrams, and a specific set of counterterms. The two contributions involved in the study of fermion-antifermion scattering are shown in Fig. 4.7. Notice the presence of the box-triangle diagram ($\mathcal{BT}$) in the first graph, which remains non-trivial to compute even in the chiral limit. The second graph is the only contribution which does not disappear, according to [20], and therefore describes a spurious s-channel exchange characterized by a double pole.

The conclusions of [20] are erroneous for two reasons: 1) in this specific case the double pole cancels in the explicit computation, so it is not a good counter example; 2) the cancellation or the presence of double poles should be analyzed together with the anomalous vertex and not separately. This second point will be addressed in the next sections.

To prove point 1) we need the two-loop structure of the $\mathcal{BT}$ graph, which is just proportional to its tree-level axial-vector form times a form factor $\mathbf{G}(s)$, function of $s = (p_1 + p_2)^2$,

$$\bar{v}(p_2)\gamma^\lambda\gamma^5 u(p_1)\mathbf{G}(s). \tag{4.15}$$

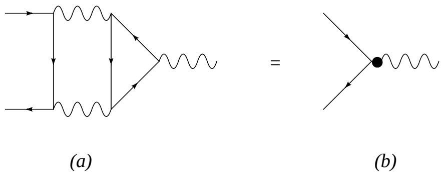

Figure 4.8: The axial-vector form factor for the $\mathcal{BT}$ diagram.

Explicit expressions of the $\mathbf{G}(s)$ coefficient in the massless case are obtained from [118] and are given by

$$\begin{aligned} \mathcal{R}e\mathbf{G}(s, m_i = 0, m_q = 0) &= 3\log\left(\frac{s}{\mu^2}\right) - 9 + 2\zeta(2) \\ \mathcal{I}m\mathbf{G}(s, m_i = 0, m_q = 0) &= -3, \end{aligned} \tag{4.16}$$

where m_i is the mass of the internal fermion with flavor i circulating in the triangle diagram while m_q is the mass of the fermionic external leg with flavor q.

We have for the two sub-amplitudes in Fig. 4.7

$$\begin{aligned} \mathcal{M}_a &= -\mathbf{G}^2(s)\bar{v}(p_2)\gamma^\lambda\gamma^5 u(p_1)\frac{i}{k^2}\bar{u}(p_1')\gamma_\lambda\gamma^5 v(p_2') \\ \mathcal{M}_b &= i\int\frac{d^4k_1}{(2\pi)^4}\left[\bar{v}(p_2)\gamma^\nu\frac{\not{p}_1 - \not{k}_1}{(p_1-k_1)^2}\gamma^\mu u(p_1)\frac{1}{k_1^2}\frac{1}{k_2^2}a_n\epsilon[\mu,\nu,k_1,k_2]\right]\frac{1}{(k^2)^2}\bar{u}(p_1')\not{k}\gamma^5\mathbf{G}(s)v(p_2') = 0\,, \end{aligned} \tag{4.17}$$

where $\mathcal{M}_b$ is identically zero, because of the equations of motion satisfied by the external fermion lines $(k = p_1' + p_2')$.

We can easily generalize our analysis to an AAA case. When an AAA triangle is embedded in the two-loop fermion-antifermion scattering process we can formally write the amplitude as follows

$$\mathcal{S} = \int\frac{d^4k_1}{(2\pi)^4}\frac{d^4k_1'}{(2\pi)^4}\bar{v}(p_2)\gamma^\nu\frac{1}{\not{p}_1-\not{k}_1}\gamma^\mu u(p_1)\frac{1}{k_1^2}\frac{1}{k_2^2}\mathcal{S}^{\,\mu\nu\mu'\nu'}\bar{u}(p_1')\gamma^{\mu'}\frac{1}{\not{k}_1'-\not{p}_1'}\gamma^{\nu'}v(p_2')\frac{1}{{k_1'}^2}\frac{1}{{k_2'}^2} \tag{4.18}$$

where the tensor sub-amplitude is defined as

$$\begin{aligned} \mathcal{S}^{\,\mu\nu\mu'\nu'} &= -\Delta_{AAA}^{\lambda\mu\nu\,GS}(-k,-k_1,-k_2)\frac{ig^{\lambda\lambda'}}{k^2}\Delta_{AAA}^{\lambda'\mu'\nu'\,GS}(k,k_1',k_2') \\ &= -[\Delta_{AAA}^{\lambda\mu\nu}(-k,-k_1,-k_2) + C_{AAA}^{\lambda\mu\nu}(-k,-k_1,-k_2)]\frac{i}{k^2}[\Delta_{AAA}^{\lambda\mu'\nu'}(k,k_1',k_2') + C_{AAA}^{\lambda\mu'\nu'}(k,k_1',k_2')]. \end{aligned} \tag{4.19}$$

Using the WI $k^\lambda\Delta_{AAA}^{\lambda\mu\nu\,GS}(-k,-k_1,-k_2) = 0$, we can drop the GS counterterm $C_{AAA}^{\lambda\mu'\nu'}(k,k_1',k_2')$. In this way the sixteen terms which contribute to the sub-amplitude $\mathcal{S}^{\,\mu\nu\mu'\nu'}$ given in Eq. (4.19) reduce to the four terms shown in Fig. 4.10. Therefore the total femion-antifermion scattering amplitude is given by the sum of four terms $\mathcal{S}_a$, $\mathcal{S}_b$, $\mathcal{S}_c$ and $\mathcal{S}_d$ which are defined below

$$\begin{aligned} \mathcal{S}_a &= -\,\mathcal{BT}^\lambda_{AAA}\frac{i}{k^2}\mathcal{BT}^\lambda_{AAA} \\ \mathcal{S}_b &= i\int\frac{d^4k_1}{(2\pi)^4}\left(\bar{v}(p_2)\gamma_\nu\frac{1}{\not{p}_1-\not{k}_1}\gamma_\mu u(p_1)\frac{1}{k_1^2}\frac{1}{k_2^2}\right)\frac{a_n}{3}\frac{k^\lambda}{k^2}\epsilon[\mu,\nu,k_1,k_2]\frac{1}{k^2}\mathcal{BT}^\lambda_{AAA} \end{aligned}$$

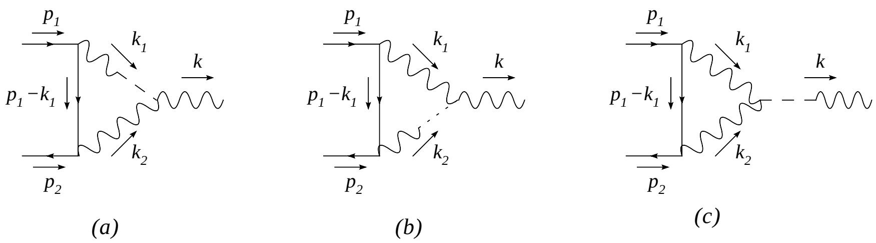

Figure 4.9: The one-loop GS counterterms included in the $\mathcal{BT}$ as its longitudinal part.

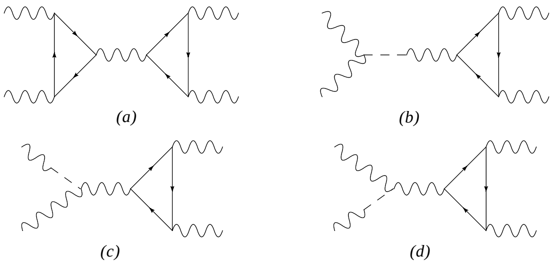

Figure 4.10: All the contributions in the symmetric GS vertex.

$$
\begin{aligned}
\mathcal{S}_c &= i\int \frac{d^4k_1}{(2\pi)^4}\left(\bar{v}(p_2)\gamma_\nu\frac{1}{\not p_1-\not k_1}\gamma_\mu u(p_1)\frac{1}{k_2^2}\frac{1}{k_1^2}\frac{a_n}{3}\frac{k_1^\mu}{k_1^2}\epsilon[\nu,\lambda,k_2,k]\right)\frac{1}{k^2}\mathcal{BT}^\lambda_{AAA}\\
\mathcal{S}_d &= i\int \frac{d^4k_1}{(2\pi)^4}\left(\bar{v}(p_2)\gamma_\nu\frac{1}{\not p_1-\not k_1}\gamma_\mu u(p_1)\frac{1}{k_1^2}\frac{1}{k_2^2}\frac{a_n}{3}\frac{k_2^\nu}{k_2^2}\epsilon[\lambda,\mu,k,k_1]\right)\frac{1}{k^2}\mathcal{BT}^\lambda_{AAA}\,, \qquad (4.20)
\end{aligned}
$$

where we have defined

$$
\mathcal{BT}^\lambda_{AAA}(k,p_1',p_2') = -\int \frac{d^4k_1'}{(2\pi^4)}\Delta^{\lambda\mu'\nu'}_{AAA}(k,k_1',k_2')\bar{u}(p_1')\gamma^{\mu'}\frac{1}{\not k_1'-\not p_1'}\gamma^{\nu'}v(p_2')\frac{1}{k_1'^2}\frac{1}{k_2'^2} \qquad (4.21)
$$

and the total amplitude is given by

$$
\mathcal{S} = \mathcal{S}_a + \mathcal{S}_b + \mathcal{S}_c + \mathcal{S}_d. \qquad (4.22)
$$

In the $\mathcal{S}_b$ sub-amplitude we distribute the anomaly symmetrically on each vertex and using the following Ward Identities on the vector currents we obtain

$$
k^\lambda \mathcal{BT}^\lambda_{VAV} = k^\lambda \mathcal{BT}^\lambda_{VVA} = 0. \qquad (4.23)
$$

This allows us to simplify the $\mathcal{S}_b$ expression as follows

$$
\mathcal{S}_b = i\int \frac{d^4k_1}{(2\pi)^4}\left(\bar{v}(p_2)\gamma_\nu\frac{1}{\not p_1-\not k_1}\gamma_\mu u(p_1)\frac{1}{k_1^2}\frac{1}{k_2^2}\right)\frac{a_n}{3}\frac{1}{(k^2)^2}\epsilon[\mu,\nu,k_1,k_2]\bar{u}(p_1')\not k\gamma^5 G(s)v(p_2') = 0\,, \qquad (4.24)
$$

where we have used the result shown in [118].

Also the third amplitude $\mathcal{S}_c$ does not contribute to $\mathcal{S}$, in fact we have

$$\mathcal{S}_c = i\,\bar{v}(p_2)\gamma_\nu u(p_1)\frac{a_n}{3}\epsilon[\nu,\lambda,\rho,\sigma]k^\sigma \int \frac{d^4k_1}{(2\pi)^4}\left(\frac{k_1^\rho}{(k-k_1)^2 k_1^4}\right)\frac{1}{k^2}\mathcal{B}\mathcal{T}^\lambda_{AAA} = 0, \tag{4.25}$$

which vanishes by symmetry due to the structure of the tensor integral, which is proportional to k^ρ. In the same way also the fourth contribution vanishes, $\mathcal{S}_d = 0$. This explicit computations contradicts the conclusions of [20] where the same amplitude was conjectured to be affected by double poles in the s-channel.

There are some conclusions to be drawn. The first is that the replacement of the two anomaly vertices in the amplitude with two GS vertices, in this case, is irrelevant as far as the fermions are massless. Equivalently, the longitudinal components of the two anomaly vertices decouple in the graph and the only invariant amplitudes coming from the anomaly vertices that survive - after the integration on the second loop momentum - are the transverse ones. This is one special case in which the anomaly diagram is transverse in the virtual corrections just by itself. In other cases this does not happen and the extra poles introduced by the counterterm are sufficient to cancel those generated by the anomaly. For this reason the presence of extra poles in a partial amplitude is not necessarily the sign of an inconsistency.

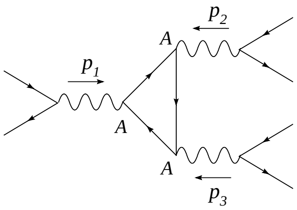

Figure 4.11: Typical graph in which the longitudinal anomalous component vanishes.

4.2.4 The vertex in the longitudinal/transverse (L/T) formulation

The analysis presented above becomes more transparent if we use a special parameterization of the anomaly diagram in which the longitudinal part of the vertex is separated from the transverse one, as done in recent studies of radiative corrections to the anomalous magnetic moment of the gluon [119]. This parameterization is more convenient than the usual Rosenberg form [42].

While the longitudinal component of the anomaly diagram is given by its DZ form, once this component is subtracted from the general triangle diagram, it leaves behind an anomaly-free vertex which is purely transverse and corresponds to the GS trilinear interaction. The Ward Identities restrict the general covariant decomposition of ${\Delta^{GS}}_{\lambda\mu\nu}(k_3,k_1,k_2)$ into invariant functions to three terms (with all incoming momenta)

$$\begin{aligned} {\Delta^{GS}}_{\lambda\mu\nu}(k_1,k_2) \quad = \quad & -\frac{1}{8\pi^2}\Big(w_T^{(+)}\left(k_1^2,k_2^2,k_3^2\right)\, t^{(+)}_{\lambda\mu\nu}(k_1,k_2) + w_T^{(-)}\left(k_1^2,k_2^2,k_3^2\right)\, t^{(-)}_{\mu\nu\rho}(k_1,k_2) \\ & +\widetilde{w}_T^{(-)}\left(k_1^2,k_2^2,k_3^2\right)\, \widetilde{t}^{(-)}_{\mu\nu\rho}(k_1,k_2)\Big)\,, \end{aligned} \tag{4.26}$$

with the transverse tensors given by

$$t^{(+)}_{\mu\nu\rho}(k_1,k_2) \quad = \quad k_{1\nu}\,\epsilon_{\mu\rho\alpha\beta}\; k_1^\alpha k_2^\beta \;-\; k_{2\mu}\,\epsilon_{\nu\rho\alpha\beta}\; k_1^\alpha k_2^\beta \;-\; (k_1\cdot k_2)\,\epsilon_{\mu\nu\rho\alpha}\;(k_1-k_2)^\alpha$$

$$\begin{aligned}
&+ \frac{k_1^2 + k_2^2 - k_3^2}{k_3^2}\, \epsilon_{\mu\nu\alpha\beta}\, k_1^\alpha k_2^\beta (k_1 + k_2)_\rho \ , \\
t^{(-)}_{\mu\nu\rho}(k_1, k_2) \ &= \ \left[(k_1 - k_2)_\rho - \frac{k_1^2 - k_2^2}{(k_1 + k_2)^2}\, (k_1 + k_2)_\rho \right] \varepsilon_{\mu\nu\alpha\beta}\, k_1^\alpha k_2^\beta \\
\widetilde{t}^{(-)}_{\mu\nu\rho}(k_1, k_2) \ &= \ k_{1\nu}\, \epsilon_{\mu\rho\alpha\beta}\, k_1^\alpha k_2^\beta + k_{2\mu}\, \epsilon_{\nu\rho\alpha\beta}\, k_1^\alpha k_2^\beta - (k_1 \cdot k_2)\, \epsilon_{\mu\nu\rho\alpha}\, (k_1 + k_2)^\alpha \ , \qquad (4.27)
\end{aligned}$$

where, due to Bose symmetry $(k_1, \mu \leftrightarrow k_2, \nu)$ we have

$$\begin{aligned}
w_T^{(+)}\left(k_2^2, k_1^2, k_3^2\right) \ &= \ +w_T^{(+)}\left(k_1^2, k_2^2, k_3^2\right) , \\
w_T^{(-)}\left(k_2^2, k_1^2, k_3^2\right) \ &= \ -w_T^{(-)}\left(k_1^2, k_2^2, k_3^2\right) , \quad \widetilde{w}_T^{(-)}\left(k_2^2, k_1^2, k_3^2\right) = -\widetilde{w}_T^{(-)}\left(k_1^2, k_2^2, k_3^2\right) . \qquad (4.28)
\end{aligned}$$

This version of the GS-corrected AVV vertex satisfies the Ward Identities on all the three external lines. The explicit expression of these invariant amplitudes can be obtained from [120]

$$\begin{aligned}
\widetilde{w}_T^{(-)}(k_1^2, k_2^2, k_3^2) \ &= \ -w_T^{(-)}(k_1^2, k_2^2, k_3^2), \qquad (4.29) \\
k_3^2 \Delta^2 w_T^{(-)}(k_1^2, k_2^2, k_3^2) \ &= \ 8(x-y)\Delta + 8(x-y)(6xy + \Delta)\Phi^{(1)}(x,y) \\
&- \ 4[18xy + 6x^2 - 6x + (1 + x + y)\Delta)]L_x \\
&+ \ 4[18xy + 6y^2 - 6y + (1 + x + y)\Delta)]L_y \ , \qquad (4.30)
\end{aligned}$$

$$\begin{aligned}
k_3^2 \Delta^2 w_T^{(+)}(k_1^2, k_2^2, k_3^2) \ &= \ 8[6xy + (x+y)\Delta]\Phi^{(1)}(x,y) + 8\Delta \\
&- \ 4[6x + \Delta](x - y - 1)L_x \\
&+ \ 4[6y + \Delta](x - y + 1)L_y \qquad (4.31)
\end{aligned}$$

with

$$L_x = \ln x, \qquad L_y = \ln y, \quad x = \frac{k_1^2}{k_3^2} \quad y = \frac{k_2^2}{k_3^2} \qquad (4.32)$$

which involves the scalar triangle diagram for general off-shell lines and determines the function $\Phi^{(1)}$ [121] as

$$\Phi^{(1)}(x,y) = \frac{1}{\lambda} \left\{ 2\left(\mathrm{Li}_2\left(-\rho x\right) + \mathrm{Li}_2\left(-\rho y\right)\right) + \ln\frac{y}{x} \ln\frac{1 + \rho y}{1 + \rho x} + \ln(\rho x)\ln(\rho y) + \frac{\pi^2}{3} \right\} , \qquad (4.33)$$

where

$$\lambda(x,y) \equiv \sqrt{\Delta} \quad , \quad \rho(x,y) \equiv 2\,(1 - x - y + \lambda)^{-1}, \quad \Delta \equiv (1 - x - y)^2 - 4xy \ . \qquad (4.34)$$

The full anomaly amplitude is simply obtained by adding the anomaly pole to this expression

$$\Delta^{\lambda\mu\nu} = w_L k^\lambda \epsilon[\mu, \nu, k_1, k_2] + \Delta^{GS\,\lambda\mu\nu} \qquad (4.35)$$

with $w_L = 1/(8\pi^2 k^2)$.

In a non-anomalous theory a specific charge assignment -in the chiral limit- sets to zero the entire trilinear gauge interaction (identically), while in theories characterized by the GS vertex we require the vanishing of the anomalous part (the anomaly pole). The pole is part of the expression of the triangle diagram, which may or may not contribute in certain graphs. A typical example is shown in Fig. 4.11 which is not sensitive (in the massless fermion limit) to the longitudinal component of the anomaly, due to the Ward Identities satisfied by the fermion antifermion currents on each external photon line (we

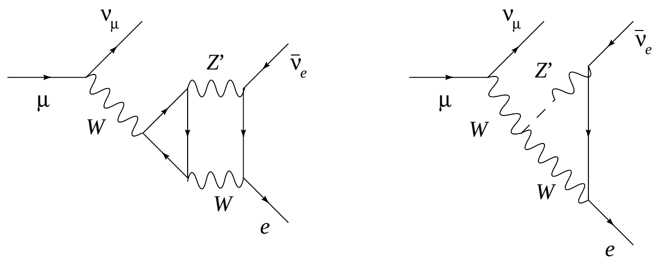

Figure 4.12: The muon decay process via a BT diagram.

are considering axial-vector interactions for each photon). In fact, this is a case in which a GS vertex or a complete anomaly vertex give the same contributions. In this sense, the anomaly, for this graph, is harmless since the external fermion current is conserved, but this situation is not general. In fact, we will analyze cases in which a similar situation occurs, and others in which the decoupling of the longitudinal part requires the subtraction of w_L from the anomaly diagram. As we have seen above, there are other cases in which the GS vertex is identically vanishing, and this happens in graphs in which the transverse part of the anomaly diagram is zero, as in light-by-light scattering. The anomaly diagrams are purely longitudinal, and their replacement with the GS vertex has to give necessarily zero. We come therefore to discuss point 2) which has been raised in the previous section. We cannot address the issue of double poles *only* in the DZ counterterms and forget that the same poles are also present in the triangle anomaly. In other words: the cancellation of the counterterms in specific graphs takes place if and only if the anomaly diagram is harmless.

4.2.5 Examples of explicit GS counterterms: anomaly in muon decay

In general, a given amplitude containing an anomalous extra Z' can be harmless if we neglect all the fermion masses and harmful in the opposite case. An interesting example is shown in Fig. 4.12 which describes a special decay of the muon, mediated by a WWZ vertex. In general, in anomalous extensions of the SM, this amplitude requires a longitudinal subtractions either with the inclusion of a GS or a WZ counterterm. For massless fermions, for instance, the process is anomaly-free. To show this point consider the amplitude for the second diagram in Fig. 4.12 which is given by

$$\begin{aligned}
\mathcal{P} &= i\int \frac{d^4k_2}{(2\pi)^4}\bar{u}(p_1')\gamma^\mu \frac{1}{\not{p}_1' + \not{k}_1}\gamma^\nu v(p_2')\,\frac{1}{k_1^2}\left(g^{\beta\nu} - \frac{k_2^\beta k_2^\nu}{M_W^2}\right)\frac{1}{k_2^2 - M_W^2} \\
&\quad \frac{a_n}{3}\frac{k_2^\beta}{k_2^2}\epsilon[\alpha,\mu,k,k_1]\frac{1}{k^2}\bar{u}(p_2)\gamma^\alpha u(p_1) \\
&= i\,\bar{u}(p_1')\gamma^\mu v(p_2')\frac{1}{k^2}\bar{u}(p_2)\gamma^\alpha u(p_1)\epsilon[\alpha,\mu,p_{12}',\tau]\int \frac{d^4k_2}{(2\pi)^4}\frac{k_2^\tau}{k_2^2\,(-p_{12}' - k_2)^2}. \qquad (4.36)
\end{aligned}$$

After using the equations of motion for on-shell spinors with $p_1' + p_2' + k_1 + k_2 = 0$ and the tensor integral decomposition in terms of the only momentum in the loop, $p_{12}' = p_1' + p_2'$, it is trivial to verify that the expression vanishes. If we switch-on the external fermion masses, violation of the Ward Identities will induce a longitudinal coupling of the anomaly pole on the neutral current, which need an explicit GS subtraction. We will come back to address the structure of the anomalous contributions away from the chiral limit below, when we will analyze the contribution of similar diagrams to $g-2$ of the muon.

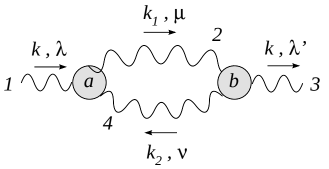

Figure 4.13: Self-energy amplitude.

4.2.6 Self-energy and gauge invariance

Anomalous contributions, in these models, appear also in the running of the coupling, though at a rather large order. Also in this case transversality of the self-energy is ensured by construction, being the GS vertex transverse by definition, however, the separation of the vertex into anomaly graph and GS counterterms illustrates how the cancellation of all the double poles takes place.

The corrections appear at three-loop level and are shown in Fig. 4.13. We denote with a, b the GS vertices and assign a number on each line of all the vertices. For instance, in Fig. 4.13 vertex a shares lines 2 and 4 with vertex b. The anomaly diagrams are denoted by Δ_a and Δ_b, respectively, and are separated into the linear combinations AVV, VAV and VVA as in the previous example, carrying partial anomalies. The pole counterterm can be "emitted" by the vertex either toward the initial or the final state of the diagram along the numbered line. For instance C_{a2} denotes the DZ counterterm that is generated by vertex a with a mixing/ double pole term generated on line 2. Other trivial cancellations are obtained due to the orthogonality relations between DZ counterterms associated to different lines when they are contracted together.

The expression of the integrand in the amplitude is given by

$$\begin{aligned}\mathcal{M}^{\lambda\lambda'}_{self} &= -\Delta^{\lambda\mu\nu\,GS}_{AAA,a}(k,k_1,-k_2)\frac{g^{\mu\mu'}}{k_1^2}\frac{g^{\nu\nu'}}{(k_1-k)^2}\Delta^{\lambda'\mu'\nu'\,GS}_{AAA,b}(-k,-k_1,k_2)\\ &= -\left[\Delta_{AAA,a}+C_{AAA,a}\right]^{\lambda\mu\nu}\frac{1}{k_1^2(k_1-k)^2}\left[\Delta_{AAA,b}+C_{AAA,b}\right]^{\lambda'\mu\nu}, \end{aligned} \tag{4.37}$$

which is given explicitly by

$$\begin{aligned}C^{\lambda'\mu\nu}_{AAA,b}(-k,-k_1,k_2) &= \frac{1}{3}\Big(C^{\lambda'\mu\nu}_{b3}(-k,-k_1,k_2)+C^{\mu\nu\lambda'}_{b2}(k_1,k_2,k)+C^{\nu\lambda'\mu}_{b4}(-k_2,k,-k_1)\Big)\\ &= C^{\mu\nu}_{b3}(-k_1,k_2)k^{\lambda'}+C^{\nu\lambda'}_{b2}(k_2,k)k_1^{\mu}+C^{\lambda'\mu}_{b4}(k,-k_1)k_2^{\nu}. \end{aligned} \tag{4.38}$$

$$\begin{aligned}C^{\lambda\mu\nu}_{AAA,a}(k,k_1,-k_2) &= \frac{1}{3}\Big(C^{\lambda\mu\nu}_{a1}(k,k_1,-k_2)+C^{\mu\nu\lambda}_{a2}(-k_1,-k_2,-k)+C^{\nu\lambda\mu}_{a4}(k_2,-k,k_1)\Big)\\ &= C^{\mu\nu}_{a1}(k_1,-k_2)k^{\lambda}+C^{\nu\lambda}_{a2}(-k_2,-k)k_1^{\mu}+C^{\lambda\mu}_{a4}(-k,k_1)k_2^{\nu} \end{aligned} \tag{4.39}$$

so using the Ward Identities

$$k_1^{\mu}\Delta^{\lambda'\mu\nu\,GS}_{AAA,b}(-k,-k_1,k_2)=k_2^{\nu}\Delta^{\lambda'\mu\nu\,GS}_{AAA,b}(-k,-k_1,k_2)=0 \tag{4.40}$$

we can reduce the sixteen contributions of the amplitude $\mathcal{M}^{\lambda\lambda'}_{self}$ to eight terms.

The GS counterterms C_{a1} and C_{b3} are non-zero for off-shell external photons and are needed to remove the longitudinal poles from the anomaly diagram, while the remaining counterterm contributions are those shown in Fig. 4.14. The latter are transverse just by themselves, as we are going to show. They

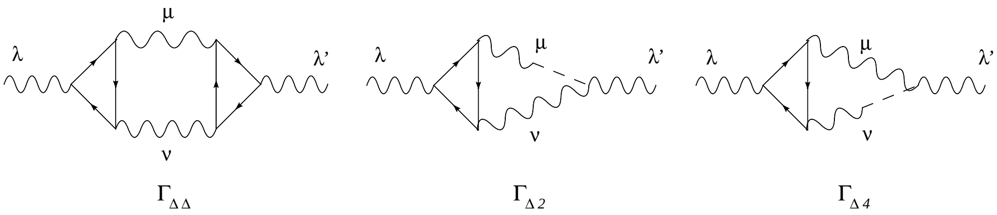

Figure 4.14: Contributions to the self-energy amplitude.

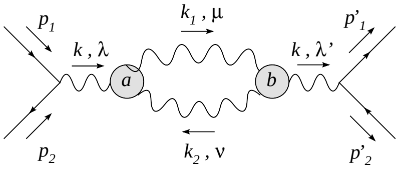

Figure 4.15: A self-energy amplitude embedded in a physical process of fermion-antifermion scattering with on-shell external lines.

are given by

$$
\begin{aligned}
\mathcal{M}^{\lambda\lambda'}_{self} &= -\Delta^{\lambda\mu\nu}_{AAA,a}\frac{1}{k_1^2(k_1-k)^2}\left[\Delta_{AAA,b}+C_{b2}+C_{b4}\right]^{\lambda'\mu\nu} \\
&= -\left(\Delta^{\lambda\mu\nu}_{AAA,a}\frac{1}{k_1^2(k_1-k)^2}\Delta^{\lambda'\mu\nu}_{AAA,b}+\Delta^{\lambda\mu\nu}_{AAA,a}\frac{1}{k_1^2(k_1-k)^2}C^{\mu\nu\lambda'}_{b2}+\Delta^{\lambda\mu\nu}_{AAA,a}\frac{1}{k_1^2(k_1-k)^2}C^{\nu\lambda'\mu}_{b4}\right) \\
&= \Gamma^{\lambda\lambda'}_{\Delta\Delta}+\Gamma^{\lambda\lambda'}_{\Delta 2}+\Gamma^{\lambda\lambda'}_{\Delta 4}.
\end{aligned}
\tag{4.41}
$$

The amplitude $\Gamma_{\Delta 2}$ can be cast in this form using dimensional regularization in D dimensions

$$
\begin{aligned}
\Gamma^{\lambda\lambda'}_{\Delta 2} &= -\int\frac{d^4k_1}{(2\pi)^4}\Delta^{\lambda\mu\nu}_{AAA,a}(k,k_1,-k_2)\frac{1}{k_1^2(k_1-k)^2}C^{\mu\nu\lambda'}_{b2}(k_1,k_2,k) \\
&= \frac{a_n}{3}\epsilon[\lambda,\nu,\alpha,k]\frac{a_n}{3}\epsilon[\nu,\lambda',\beta,k]\int\frac{d^4k_1}{(2\pi)^4}\frac{k_1^\alpha k_1^\beta}{k_1^4(k_1-k)^2} \\
&= -\frac{1}{2}\left(\frac{a_n}{3}\right)^2\epsilon[\lambda,\nu,\alpha,k]\epsilon[\nu,\lambda',\beta,k]g^{\alpha\beta}\frac{1-D}{s}Bub^{D+2}(s) \\
&= \left(\frac{a_n}{3}\right)^2(k^\lambda k^{\lambda'}-k^2g^{\lambda\lambda'})(1-D)\frac{Bub^D(s)}{8\pi(3-2\epsilon)} \\
&= C\,(k^\lambda k^{\lambda'}-k^2g^{\lambda\lambda'})Bub^D(s),
\end{aligned}
\tag{4.42}
$$

where the explicit expressions of the two master integrals $Bub^D(s)$ and $Bub^{D+2}(s)$ can be found in [98] and

$$
C=\left(\frac{a_n}{3}\right)^2\frac{1-D}{8\pi(3-2\epsilon)}. \tag{4.43}
$$

If we include the same amplitude in a fermion-antifermion scattering, see Fig. 4.15, we obtain

$$
\begin{aligned}
\mathcal{S}_{\Delta 2} &= -\bar{v}(p_2)\gamma^\lambda u(p_1)\frac{1}{k^2}\left(\frac{k^\lambda k^{\lambda'}}{k^2}-g^{\lambda\lambda'}\right)k^2C\,Bub^D(s)\,\frac{1}{k^2}\bar{u}(p_1')\gamma^{\lambda'}v(p_2') \\
&= \bar{v}(p_2)\gamma^\lambda u(p_1)\frac{1}{k^2}C\,Bub^D(s)\,\bar{u}(p_1')\gamma^\lambda v(p_2'),
\end{aligned}
\tag{4.44}
$$

with

$$Bub^D(s) = \frac{i\pi^{D/2}}{(2\pi)^D}\,\mu^{2\epsilon}\left(\frac{e^\gamma}{4\pi}\right)^\epsilon \frac{c_\Gamma}{\epsilon(1-2\epsilon)}(s)^{-\epsilon}(-1)^\epsilon, \tag{4.45}$$

where we have used the equations of motion for the on-shell spinors ($k = p_1 + p_2 = p_1' + p_2'$). The transversality of the pole counterterm comes as a surprise, since while the total amplitude with GS vertices is transverse by construction, the anomalous contribution, in principle, is not expected separately to be so. The computation shows that internal double poles, those due to the GS counterterms, give contributions which are also transversal. This shows once more that there are no apparent inconsistencies in the perturbative expansion of the theory.

4.3 Higher-order diagrams

Having worked out several examples in which either the extra poles appear explicitly or cancel by themselves, signalling a harmless anomaly, we now move to discuss more complex cases, where these techniques will be systematized.

We have two ways to apply the GS vertex at higher-order. We could use its explicit form -in terms of its transverse invariant amplitudes- or we could use it in the form "anomaly diagrams plus counterterms". This second form is the most useful one. The presence of higher poles in the counterterms, which balance those -not explicit- in the anomaly diagrams, can be treated perturbatively as a field theory of a higher perturbative order. We will illustrate below one case from which we can easily infer the general features of the perturbative expansion with these types of graphs. It should be clear that the cancellation of all the poles from the external lines takes place only on-shell, but this is not a problem since we are interested in S-matrix elements.

4.3.1 Three-point functions

For this reason we consider the four-loop diagram shown in Fig. 4.16 with three symmetric GS vertices of the AAA type connected together, which is given by

$$\mathcal{M}^{\lambda\rho\tau} = i\,(\Delta + C_1 + C_2 + C_6)_a^{\lambda\mu\nu}\frac{1}{k_2^2}\,(\Delta + C_2 + C_3 + C_4)_b^{\mu\rho\sigma}\,\frac{1}{k_4^2}(\Delta + C_4 + C_5 + C_6)_c^{\sigma\tau\nu}\frac{1}{k_6^2}, \tag{4.46}$$

where, as done in the previous sections, Δ denotes an AAA triangle amplitude with a symmetric anomaly distribution on each vertex and C_i a single GS counterterm with the derivative coupling on the i-th line. At this stage we start simplifying the term $(\Delta + C_2 + C_3 + C_4)_b$ as $(GS)_b$ and in a similar way the c blob

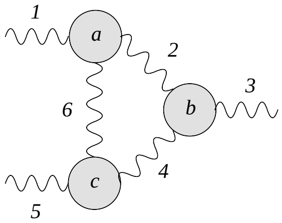

Figure 4.16: A four-loop amplitude given by three GS vertices with on-shell external lines.

using the Ward Identities

$$C_{a2}(GS)_b = C_{a6}(GS)_c = C_{b4}(GS)_c = 0, \tag{4.47}$$

and then omit the GS counterterms C_{a1}, C_{b3}, C_{c5} in which the transversality conditions

$$\epsilon_{1\lambda}k_1^\lambda = \epsilon_{5\tau}k_5^\tau = \epsilon_{3\rho}k_3^\rho = 0 \tag{4.48}$$

act on the derivative coupling, which allow to reduce the $\mathcal{M}$ amplitude to the six contributions

$$\begin{aligned}
\mathcal{M}^{\lambda\rho\tau} &= i\,(\Delta)_a^{\lambda\mu\nu}\frac{1}{k_2^2}\,(\Delta + C_2)_b^{\mu\rho\sigma}\frac{1}{k_4^2}\,(\Delta + C_4 + C_6)_c^{\sigma\tau\nu}\frac{1}{k_6^2} \\
&= \frac{i}{k_2^2\,k_4^2\,k_6^2}\left(\Delta_a\Delta_b\Delta_c + \Delta_a\Delta_b C_{c4} + \Delta_a\Delta_b C_{c6} + \Delta_a C_{b2}\Delta_c + \Delta_a C_{b2}C_{c4} + \Delta_a C_{b2}C_{c6}\right)^{\lambda\rho\tau} \\
&= \left(\Delta_a\Delta_b\Delta_c + \Gamma_4 + \Gamma_6 + \Gamma_2 + \Gamma_{24} + \Gamma_{26}\right)^{\lambda\rho\tau},
\end{aligned} \tag{4.49}$$

where the notation Γ_i and Γ_{ij} refers to the line corresponding to the counterterm in Fig. 4.16. At this point we consider the $\Delta_a\Delta_b C_{c4}$ contribution represented in Fig. 4.17 with a counterterm on the line 4 denoted by $\Gamma_4^{\lambda\rho\tau}$

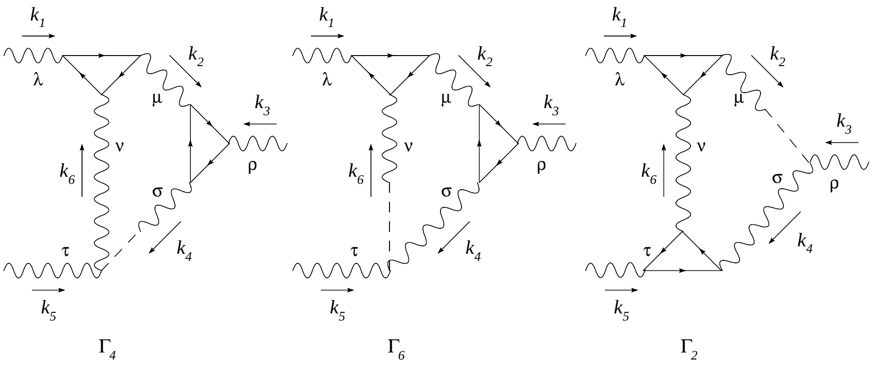

Figure 4.17: The Γ_4, Γ_6 and Γ_2 contributions taken from $\mathcal{M}$ at four-loop level.

$$\Gamma_4^{\lambda\rho\tau} = i\int\frac{d^4k_4}{(2\pi)^4}\left[\Delta_a^{\lambda\mu\nu}(k_1,k_2,-k_6)\frac{1}{k_2^2}\Delta_b^{\mu\rho\sigma}(k_2,-k_3,k_4)\frac{1}{k_4^2}\frac{a_n}{3\,k_4^2}k_4^\sigma\,\epsilon[\tau,\nu,k_5,k_6]\frac{1}{k_6^2}\right], \tag{4.50}$$

in which we substitute the Rosenberg parametrization for the triangle amplitude $\Delta_a^{\lambda\mu\nu}(k_1,k_2,-k_6)$ given by

$$\begin{aligned}
\Delta_a^{\lambda\mu\nu}(k_1,k_2,-k_6) &= A_1\,\epsilon[k_2,\mu,\nu,\lambda] - A_2\,\epsilon[k_6,\mu,\nu,\lambda] - A_3\,k_2^\nu\,\epsilon[k_2,k_6,\mu,\lambda] \\
&+ A_4\,k_6^\nu\,\epsilon[k_2,k_6,\mu,\lambda] - A_5\,k_2^\mu\,\epsilon[k_2,k_6,\nu,\lambda] + A_6\,k_6^\mu\,\epsilon[k_2,k_6,\nu,\lambda],
\end{aligned} \tag{4.51}$$

and the anomaly equation

$$k_4^\sigma\Delta_b^{\mu\rho\sigma}(k_2,-k_3,k_4) = -\frac{a_n}{3}\epsilon[\mu,\rho,k_2,k_3]. \tag{4.52}$$

We choose k_1 and k_5 as independent momenta, so we have

$$k_3 = -(k_1 + k_5), \qquad k_2 = k_1 + k_4 + k_5, \qquad k_6 = k_4 + k_5, \tag{4.53}$$

with the on-shell conditions $k_1^2 = k_5^2 = k_3^2 = 0$. A direct computation of the $\Gamma_4^{\lambda\rho\tau}$ amplitude shows the complete cancellation of the spurious double pole relative to the k_4 momentum.

In an analogous way we can consider the $\Delta_a \Delta_b C_{c6}$ term or Γ_6 in Eq. (4.49), that is

$$\Gamma_6^{\lambda\rho\tau} = i\int \frac{d^4k_6}{(2\pi)^4}\left[\Delta_a^{\lambda\mu\nu}(k_1,k_2,-k_6)\frac{1}{k_2^2}\Delta_b^{\mu\rho\sigma}(k_2,-k_3,k_4)\frac{1}{k_4^2}\frac{a_n}{3\,k_6^2}\,k_6^{\nu}\epsilon[\sigma,\tau,k_4,k_5]\frac{1}{k_6^2}\right] \tag{4.54}$$

and the $\Delta_a C_{b2} \Delta_c$ term or Γ_2

$$\Gamma_2^{\lambda\rho\tau} = i\int \frac{d^4k_2}{(2\pi)^4}\left[\Delta_a^{\lambda\mu\nu}(k_1,k_2,-k_6)\frac{1}{k_2^2}\frac{a_n}{3\,k_2^2}k_2^{\mu}\epsilon[\rho,\sigma,k_3,k_4]\frac{1}{k_4^2}\Delta_c^{\sigma\tau\nu}(k_4,-k_5,k_6)\frac{1}{k_6^2}\right], \tag{4.55}$$

for which the conditions in Eqs. (4.51) and (4.52) have to be modified in a suitable form. After the expansion of the tensor integrals in terms of the two external momenta k_1 and k_5 we can conclude that also in this case the double poles don't contribute to the physical on-shell amplitude.

In a similar way we can show the vanishing of the last contributions $\Delta_a\, C_{b2}\, C_{c4}$ (Γ_{24}) and $\Delta_a\, C_{b2}\, C_{c6}$ (Γ_{26}) shown in Fig. 4.18 due to antisymmetry

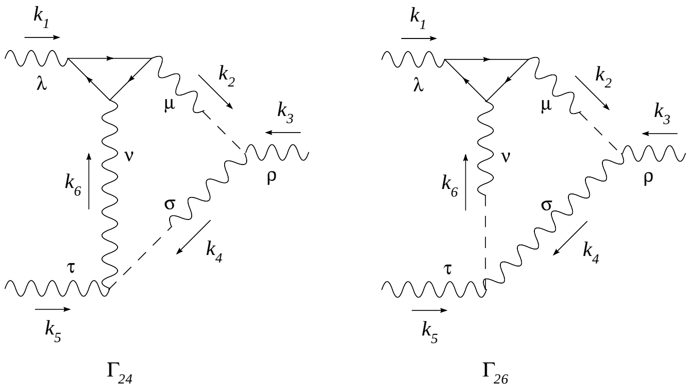

Figure 4.18: Representation of Γ_{24} and Γ_{26}, the two terms with double poles on the internal lines.

$$\Gamma_{24}^{\lambda\rho\tau} = i\int \frac{d^4k_2}{(2\pi)^4}\left[\Delta_a^{\lambda\mu\nu}(k_1,k_2,-k_6)\frac{1}{k_2^2}\frac{a_n}{3\,k_2^2}k_2^{\mu}\epsilon[\rho,\sigma,k_3,k_4]\frac{1}{k_4^2}\frac{a_n}{3\,k_4^2}k_4^{\sigma}\epsilon[\tau,\nu,k_5,k_6]\frac{1}{k_6^2}\right] = 0. \tag{4.56}$$

In the $\Delta_a C_{b2} C_{c6}$ case one obtains the same result after using the anomaly equation, so that

$$\Gamma_{26}^{\lambda\rho\tau} = i\int \frac{d^4k_2}{(2\pi)^4}\left[\Delta_a^{\lambda\mu\nu}(k_1,k_2,-k_6)\frac{1}{k_2^2}\frac{a_n}{3\,k_2^2}k_2^{\mu}\epsilon[\rho,\sigma,k_3,k_4]\frac{1}{k_4^2}\frac{a_n}{3\,k_6^2}\,k_6^{\nu}\,\epsilon[\sigma,\tau,k_4,k_5]\frac{1}{k_6^2}\right], \tag{4.57}$$

where the contraction

$$k_2^{\mu}\Delta_a^{\lambda\mu\nu}(k_1,k_2,-k_6) = -\frac{a_n}{3}\epsilon[\nu,\lambda,k_6,k_1] \tag{4.58}$$

gives $\Gamma_{26} = 0$ for antisymmetry. In conclusion, the amplitude $\mathcal{M}$ at four-loop level, composed by three GS symmetric vertices, is not affected by unphysical massless poles arising from the derivative coupling

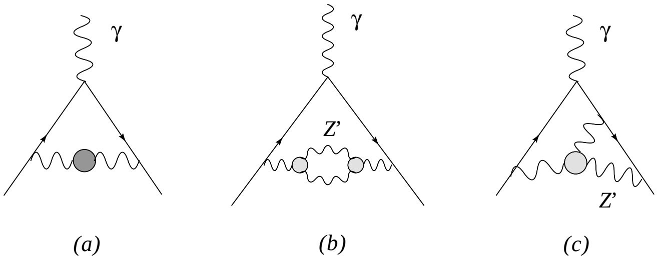

Figure 4.19: Higher-order contributions to the muon magnetic moment in the GS case.

present on some internal lines. As a result of this analysis it is clear that there are far more cancellations than expected in some of these complex diagrams, due to the structure of the pole counterterms. In fact each DZ counterterm induces a WI on an attached triangle diagram and brings in antisymmetric ϵ-tensors into the integrand. This is enough, in many cases, to cause a diagram to vanish by symmetry/antisymmetry of the integrand.

4.4 WZ and GS interactions, anomalous magnetic moment of the muon and muonium

In this section we move to discuss the role played by the GS and the WZ mechanism in $g-2$ of the muon and in muonium. This is the case where the L/T decomposition of the anomaly amplitude shows its direct relevance and the role of the GS and WZ vertices can be easily worked out.

Our aim is not to proceed with a complete study of these corrections, some of which require a separate study, but to highlight the role played by the two mechanisms in the context of specific processes which can be accurately quantified in future studies. The possibility of searching for anomalous extra Z' and axions in precision measurements of several observables is challenging but realistic.

4.4.1 The GS case

We show in Figs. 4.19 and 4.23 some of the lowest order GS contributions to the anomalous magnetic moment of the muon and to the hyperfine splitting of muonium. Some of the recent theoretical attention to $a_\mu \equiv g-2$ has been focused on the study of effects at two-loop level and higher, such as those shown in Fig. 4.19a and 4.19d. The first indicates generically the hadronic contributions coming from self-energy insertions in the lowest order vertex. Of these types are also the corrections coming from the self-energy graphs involving GS vertices. The corrections are tiny, being of order g^8 and their computation involves a 4-loop graph with ordinary propagators (the two-triangle diagram of Fig. 4.14) and two-loop graphs related to the pole counterterms that we have studied in the analysis of the self-energy. Clearly, the underlying Lagrangian should allow an anomalous extra Z' in the spectrum. Working models of this type have been studied previously, and include several anomalous $U(1)'s$, such as in the case of intersecting branes. The presence of a physical axion that mixes with the Higgs sector (the axi-Higgs) via a kinetic Stückelberg term (and eventually a Peccei-Quinn breaking term) makes these models quite attractive. The axi-Higgs is massless in the first case and massive in the second case. Models with an axi-Higgs are constructed using only WZ interactions and not GS interactions.

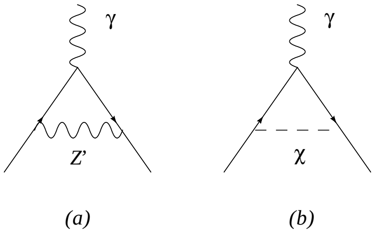

Figure 4.20: Leading order corrections to the anomalous magnetic moment of the muon.

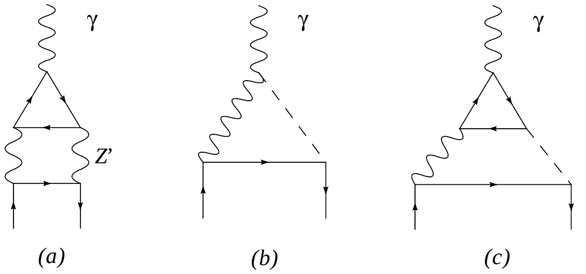

Figure 4.21: Higher-order corrections to the anomalous magnetic moment of the muon with a WZ vertex.

4.4.2 Anomalous corrections to a_μ

The evaluation of the anomalous corrections to a_μ in the GS and WZ cases are quite different. In the WZ case there is a larger set of contributing graphs due to the interaction of the axion with the fermions and involve the exchange of an axi-Higgs (massless or massive), which is proportional to the fermion mass. The simplest corrections due to the presence of an anomalous extra Z' are shown in Fig. 4.20. These do not involve the anomaly diagram and are the leading ones. They have been computed in [68]. Higher-order corrections are those shown in Fig. 4.21, also involving a physical axi-Higgs.

It is convenient to describe in some detail the structure of the perturbative expansion at higher orders to emphasize the differences between the two mechanisms.

The structure of the expansion can be grasped more easily if we work in the chiral limit (all the fermions are taken to be massless) and focus our attention, for example, on graph (b) in Fig. 4.19 since in this case there is no direct point-like interaction of the axion with the fermion. If we decide to cancel the anomaly with WZ counterterms, we know that we can draw a counterterm diagram in which the axion is emitted and absorbed by the gauge line. In this case it is clear that the anomaly is potentially harmful and only a direct computation is able to show if the counterterm is zero or not. In this specific diagrams we know that explicit pole counterterms are needed, as we have shown in the previous sections. If we consider diagram (c), however, the application of this argument shows immediately that the anomaly, in this case, is harmless, since there is no axion counterterm of WZ type that we can draw. A similar result is obtained for diagram (a) in Fig. 4.21. Also in this case we are unable to draw a WZ counterterm in which the axion is attached only to gauge lines. Therefore this diagram is also well defined even in the presence of an anomaly diagram, since its longitudinal part cancels automatically due to the topology of the graph. In these last two diagrams the gauge lines have to be attached in all possible ways to the muon lines for this to happen. Diagram (c) appears in the massive case, but it is not a counterterm.

Coming to the GS case in the massive fermion case, the anomaly diagram developes a mass-dependence in the residue of the anomaly pole, shown in graphs (c) of Fig. 4.22. As we are going to show in the next

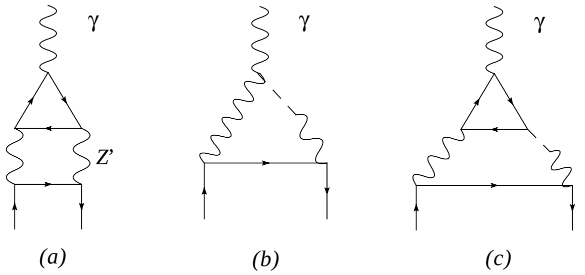

Figure 4.22: As in Fig. 4.21 for a GS vertex.

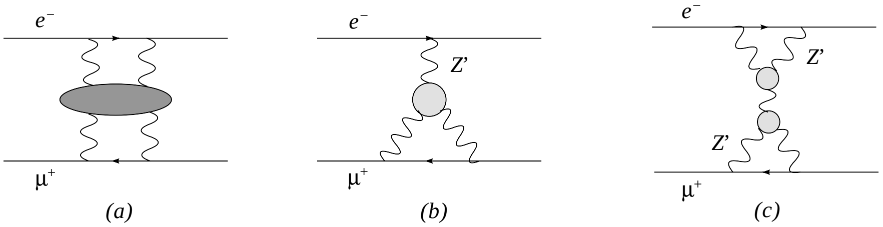

Figure 4.23: Hadronic contributions (a), higher-order anomalous contributions (b) and light-by-light contributions (c) to the hyperfine splitting in muonium.

section, this is not an anomaly counterterm. The only counterterm is still given only by diagram (b). More details will be given below and in the final section.

4.5 Two-loop Contributions to $g-2$: Anomalous Diagrams

In this section we briefly analyze the general structure of these corrections for both mechanisms when anomaly diagrams are present. The analysis that we follow is close to the discussions for $g-2$ presented in [122, 123, 124], adapted to our case. Most of the physical discussion carried out in these papers, in the case of the muon anomalous magnetic moment, has to do with the identification of the effects due to chiral symmetry breaking in the computation of the anomaly diagrams, which are related both to perturbative and to non-perturbative effects, treated within the operator product expansion. In our case we will be interested only in the perturbative contributions with the GS and WZ vertices. We will point out the differences compared to those previous studies while reviewing their derivation in order to be self-contained. In the GS case the anomaly diagram, corrected by the pole subtraction, does not satisfy any longer the Vainshstein relation [125] between the longitudinal ($w_L(q^2)$) and transverse ($w_T(q^2)$) component of the anomaly vertex

$$w_L(q^2) = 2w_T(q^2), \tag{4.59}$$

which is obtained in a specific kinematical limit of the anomaly diagram. In particular, in the chiral limit, the longitudinal component w_L of the GS vertex is zero. Away from the chiral limit a pole $O(1/q^4)$ reappears, multiplied by additional contributions proportional to the fermion mass squared (m_f^2), but it is not an anomaly pole. The separation between L and T components, away from the chiral limit, for $m_f \neq 0$, can be done in several ways. In [123] this is obtained by isolating the anomalous pole contribution from the rest. After the subtraction of the pole term, the new anomaly-free vertex is still not transverse and satisfies a broken WI. The truly transverse component ($\tilde{w}^T$) is isolated by acting

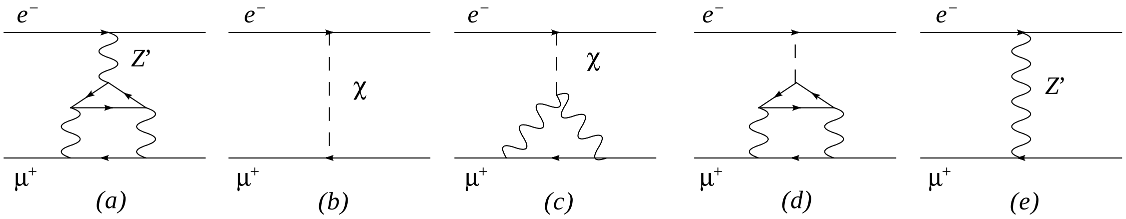

Figure 4.24: Leading contributions to the hyperfine splitting in muonium and denoted as $\mathcal{N}_i$, with i=a,b,c,d in the WZ case.

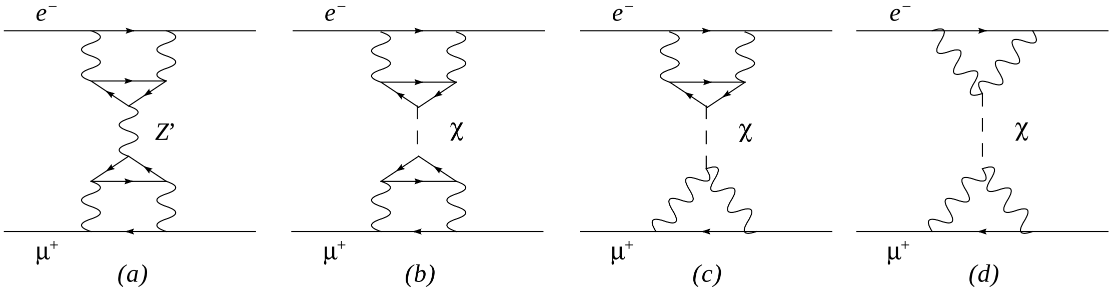

Figure 4.25: Explicit (higher-order) expansion of the diagram in Fig. 4.23c for a trilinear WZ vertex. Each amplitude is denoted as $\mathcal{M}_i$ with i=a,b,c,d in the text with p_1, p_1' as incoming momenta and p_2, p_2' as outcoming ones.

with a specific projection on the vertex, as we shall see below. This assumes a special form in the limit in which one of the photons is on-shell ($k^2 \to 0$) and soft ($k \to 0$). It can be expressed in terms of a set of scalar diagrams which come from the rank-2 tensor decomposition of the fermionic triangle (C_{ij}), and which are well-known in the literature. The explicit expressions of these integrals, which are for instance given in [86], are singular in the soft/on-shell photon limit that is needed in order to extract their contribution to $g-2$. This is the reason for the re-analysis of these contributions using the operator product expansion (OPE), which in this case follows the approach of [122, 123]. In our case, both for the GS and WZ vertices, the OPE analysis would be similar, and can be performed on the two currents carrying large momentum ($q^2 \to \infty$), therefore we omit it. In the WZ case the pseudoscalar exchanges involve a Goldstone and of a physical axion, this second one being not present in the SM.

We start our analysis by stating our conventions. The coupling of the extra neutral current to the fermions is given by

$$-\frac{i g_2}{4\cos\theta_W}\bar{\psi}_i\left(g_V^{Z,Z'}\gamma^\mu + g_A^{Z,Z'}\gamma^\mu\gamma^5\right)\psi_i V_\mu \tag{4.60}$$

where the vector boson V_μ stays for the Z or the Z' and the vector and the axial-vector couplings can be written as

$$\begin{aligned}
\frac{-ig_2}{4c_w}\gamma^\mu {g_V}^{Z',j} &= \frac{-ig_2}{c_w}\frac{1}{2}\left[-\varepsilon c_w^2 T_3^{L,j} + \varepsilon s_w^2 (\frac{\hat{Y}_L^j}{2} + \frac{\hat{Y}_R^j}{2}) + \frac{g_z}{g_2} c_w (\frac{\hat{z}_{L,j}}{2} + \frac{\hat{z}_{R,j}}{2})\right]\gamma^\mu \\
\frac{-ig_2}{4c_w}\gamma^\mu\gamma^5 {g_A}^{Z',j} &= \frac{-ig_2}{c_w}\frac{1}{2}\left[\varepsilon c_w^2 T_3^{L,j} + \varepsilon s_w^2 (\frac{\hat{Y}_R^j}{2} - \frac{\hat{Y}_L^j}{2}) + \frac{g_z}{g_2} c_w (\frac{\hat{z}_{R,j}}{2} - \frac{\hat{z}_{L,j}}{2})\right]\gamma^\mu\gamma^5.
\end{aligned} \tag{4.61}$$

Here j is an index which represents the quark or the lepton and we have set $\sin\theta_W = s_w, \cos\theta_W = c_w$ for brevity. We denote with $\hat{z}_{R,L}$ the charges of the fermions under the extra anomalous $U(1)$ and with

g_z the coupling constant of the anomalous gauge interaction.

The electroweak vertex that we need to compute in order to take into account the corrections to the anomalous magnetic moment of the muon, due to the exchange of an extra anomalous Z', in analogy with the discussion presented in [123], is given by

$$\begin{aligned}
&\langle \bar{\mu}(p')|V^{em}_\rho(0)|\mu(p)\rangle = \bar{u}(p')\Gamma_\rho(p',p)u(p) = \\
&\int \frac{d^4q}{(2\pi)^4}\frac{-i}{q^2}\frac{-i}{(p'-p-q)^2-M_Z^2}(-ie)(-ie)\left(\frac{ig_2}{4\cos\theta_W}\right)\left(\frac{-ig_2}{4\cos\theta_W}\right)\times \\
&\bar{u}(p')\left[\gamma^\mu\frac{i}{\not{p}'-\not{q}-m_\mu}g^{Z'}_{A,\mu}\gamma^\nu\gamma_5+g^{Z'}_{A,\mu}\gamma^\nu\gamma_5\frac{i}{\not{p}+\not{q}-m_\mu}\gamma^\mu\right]u(p)\times \\
&\int dx\, e^{iq\cdot x}\int dy\, e^{i(p'-p-q)\cdot y}\langle 0|T\{A^\gamma_\mu(x)Z'_\nu(y)A^\gamma_\rho(0)\}|0\rangle\,, \qquad (4.62)
\end{aligned}$$

where

$$A^\gamma_\mu(x)=\bar{q}(x)\gamma_\mu\, Q_f\, q(x)\,, \qquad Z'_\nu(y)=\bar{q}(y)\gamma_\nu\gamma_5\, g^{Z'}_{A,f}\, q(y) \qquad (4.63)$$

are the fermion currents of quarks, and $g^{Z'}_{A,f}$ refers to a quark of flavor f. The most general CP invariant expression for a vertex function satisfying the current conservation is defined by

$$\Gamma^\mu=-ie\bar{u}(p_2)\left[F_1(q^2)\gamma^\mu+F_2(q^2)\frac{q_\alpha}{4m_\mu}\sigma^{\alpha\mu}+F_3(q^2)\frac{\left(q^\mu\not{q}-\gamma^\mu q^2\right)\gamma^5}{4M_W^2}\right]u(p_1) \qquad (4.64)$$

where the coefficients $F_i(q^2)$ are the form-factors and $q=p_2-p_1$, M_W and m_μ denote the mass of the W and of the muon, respectively. Taking the limit $q^2\to 0$ in the Pauli form-factor we obtain the value of the anomalous magnetic moment

$$a=\frac{g-2}{2}=F_2(0), \qquad (4.65)$$

and using the equation of motion we obtain [124]

$$\Gamma_\mu=aa_\mu \qquad a_\mu=ie\bar{u}(p_2)\frac{1}{2m_\mu}(p_1+p_2)_\mu u(p_1). \qquad (4.66)$$

We can use a project operator to extract $F_2(0)$

$$F_2(0)=\lim_{k^2\to 0}\mathrm{Tr}\left\{(\not{p}+m_\mu)\Lambda_2^\rho(p',p)(\not{p}'+m_\mu)\Gamma_\rho(p',p)\right\}\,, \qquad (4.67)$$

where $(p'=p+k)$

$$\Lambda_2^\rho(p',p)=\frac{m_\mu^2}{k^2}\frac{1}{4m_\mu^2-k^2}\gamma^\rho-\frac{m_\mu}{k^2}\frac{2m_\mu^2+k^2}{(4m_\mu^2-k^2)^2}(p+p')^\rho \qquad (4.68)$$

is the projector on the Pauli form factor. The triangle contribution is obtained from the one-loop correlator of the electroweak currents

$$(2\pi)^4\delta(p'-p-q)\Delta^{\mu\nu\rho}_{VAV}(q,k)=\int dx\, e^{iq\cdot x}\int dy\, e^{i(p'-p-q)\cdot y}\langle 0|T\{A^\gamma_\mu(x)Z'_\nu(y)A^\gamma_\rho(0)\}|0\rangle \qquad (4.69)$$

with p' the incoming photon four-momentum. The corresponding tensor structure of the triangle in the $k^2\to 0$ limit for a fermion of flavor f is given by [124], obtained from the Rosenberg representation [42]

$$\Delta^{\mu\nu\rho}_{VAV}(q,k)\longrightarrow\frac{g}{\pi^2\cos\theta_W}g^{Z'}_{A,f}\; e^2Q_f^2\; q^\alpha q^\beta S^{\mu\nu\rho}_{\alpha\beta}(k)\int_0^1 dx\frac{x(1-x)}{x(1-x)q^2-m_f^2}$$

$$S^{\mu\nu\rho}_{\alpha\beta}(k) = -2k_\tau \epsilon^{\tau\lambda\mu\rho}\left(g_{\alpha\lambda}g^{\nu}_{\beta} - g_{\alpha\beta}g^{\nu}_{\lambda}\right) + g_{\alpha\lambda}\epsilon^{\lambda\tau\nu\rho}\left(k_\beta g^{\mu}_{\tau} - g^{\mu}_{\beta}k_\tau\right), \tag{4.70}$$

where $k = p' - p$. This expression, in the GS case, is simply modified by the subtraction of the longitudinal pole due to the anomaly. The tensor $\Delta^{\mu\nu\rho}_{VAV}(q,k)$ in momentum space is affected by the longitudinal (anomaly) pole, similarly to the case of axial QED discussed above, in the form of a longitudinal $w_L(q^2)$ contribution [120]. In fact the asymptotic behavior at large $Q^2 = -q^2$ is given by [122]

$$w^f_L(Q^2) = \frac{g_2}{\cos\theta_W} g^{Z'}_{A,f} e^2 Q^2_f \left[\frac{1}{2\pi^2 Q^2} - 2\frac{m^2_f}{\pi^2 Q^4}\log\frac{Q^2}{m^2_f} + O\left(\frac{1}{Q^6}\right)\right]. \tag{4.71}$$

and in the GS case it becomes

$${w_L}^f(Q^2)|_{GS} = -\frac{g_2}{\pi^2\cos\theta_W} g^{Z'}_{A,f} e^2 Q^2_f \left[2\frac{m^2_f}{Q^4}\log\frac{Q^2}{m^2_f} + O\left(\frac{1}{Q^6}\right)\right]. \tag{4.72}$$

Following [123] we can always write

$$\Delta^f_{\mu\nu\rho}(q,k) = \Delta_{\mu\nu\rho}(q,k)_{\text{anomaly}} + \tilde{\Delta}^f_{\mu\nu\rho}(q,k)\,, \tag{4.73}$$

where

$$\Delta_{\mu\nu\rho}(q,k)_{\text{anomaly}} = \sum_f g^{Z'}_{A,f} e^2 Q^2_f a_n \frac{(q-k)_\nu}{(q-k)^2}\epsilon_{\mu\rho\alpha\beta}q^\alpha k^\beta\,, \tag{4.74}$$

with $a_n = -i/(2\pi^2)$. The function $\tilde{\Delta}^f_{\mu\nu\rho}(q,k)$ is transverse with respect to the momenta q^μ and k^ρ

$$q^\mu \tilde{\Delta}^f_{\mu\nu\rho}(q,k) = 0\,,\ k^\rho \tilde{\Delta}^f_{\mu\nu\rho}(q,k) = 0\,, \tag{4.75}$$

but in the presence of massive fermions we isolate the longitudinal components of the corresponding broken WI

$$\tilde{\Delta}^f_{\mu\nu\rho}(q,k) = \tilde{\Delta}^{f,\text{long}}_{\mu\nu\rho}(q,k) + \tilde{\Delta}^{f,\text{trans}}_{\mu\nu\rho}(q,k)\,. \tag{4.76}$$

Differentiating the 2nd expression in Eq. (4.75) with respect to k_ρ we obtain

$$\tilde{\Delta}_{\mu\nu\rho}(q,k) = -k^\sigma \frac{\partial}{\partial k^\rho}\tilde{\Delta}_{\mu\nu\sigma}(q,k) \tag{4.77}$$

where we have suppressed the flavor index f for simplicity. Since we are interested in the soft photon limit, the relevant contributions are those linear in k. In [123] these are extracted in the form

$$\tilde{\Delta}^{\text{trans}}_{\mu\nu\rho}(q,k) = k^\sigma \Delta_{\mu\nu\rho\sigma}(q) + \ldots \tag{4.78}$$

where the tensor $\Delta_{\mu\nu\rho\sigma}(q)$ is obtained by using the projection operator $\Pi^{\nu\nu'}$ as follows

$$\begin{aligned}
\Pi^{\nu\nu'}(q,k) &= \left(g^{\nu\nu'} - \frac{(q-k)^\nu}{(q-k)^2}(q-k)^{\nu'}\right), \\
\Delta_{\mu\nu\rho\sigma}(q) &= -\frac{\partial}{\partial k^\rho}\left(\Pi^{\nu\nu'}\Delta_{\mu\nu'\rho}\right)|_{\lim k\to 0}.
\end{aligned} \tag{4.79}$$

It is not difficult to notice that

$$\Pi^{\nu\nu'}\Delta_{\mu\nu'\rho} = \Pi^{\nu\nu'}\tilde{\Delta}_{\mu\nu'\rho}. \tag{4.80}$$

As we have already mentioned, the action of $\Pi^{\nu\nu'}$ is to remove all the longitudinal parts from the $\Delta_{\mu\nu\rho}$ tensor, including the anomalous term. $\Delta_{\mu\nu\rho\sigma}(q)$ in (4.78) has the form

$$\Delta_{\mu\nu\rho\sigma}(q) = i\Delta(Q^2)\left[q_\rho\epsilon_{\mu\nu\alpha\sigma}q^\alpha - q_\sigma\epsilon_{\mu\nu\alpha\rho}q^\alpha\right], \tag{4.81}$$

where $q^2 = -Q^2$. We can now try to apply this formalism to the anomalous triangle diagrams. We use the generic parametrization of a AVV triangle given in [86],

$$\begin{aligned}\Delta^f_{\mu\nu\rho}(q,k) = &-\frac{g_2}{\pi^2\cos\theta_W}g^{Z'}_{A,f}e^2Q_f^2\left[A(k,-q,m_f)(k_\rho\epsilon_{\nu\mu\beta\sigma}k^\beta - k^2\epsilon_{\nu\mu\rho\sigma})(-q)^\sigma\right.\\ &+A(-q,k,m_f)(q_\mu\epsilon_{\nu\rho\beta\sigma}q^\beta - q^2\epsilon_{\nu\rho\mu\sigma})k^\sigma\\ &\left.-B(k,-q,m_f)(q-k)_\nu\epsilon_{\rho\mu\alpha\beta}k^\alpha(-q)^\beta\right],\end{aligned} \tag{4.82}$$

where the functions $A(k,-q,m_f)$ and $B(k,-q,m_f)$ are given by in terms of the tensor-reduction coefficients C_{ij} as follows

$$\begin{aligned}A(k,-q,m_f) &= (C_{11} - C_{12} + C_{21} - C_{23})(k,-q,m_f)\\ B(k,-q,m_f) &= (C_{12} + C_{23})(k,-q,m_f),\end{aligned} \tag{4.83}$$

and are defined in Eqs. (A.2), (A.3) of Ref. [86]. The WI on the axial-vector current is given by

$$(q-k)^\nu\Delta^f_{\mu\nu\rho}(q,k) = -\frac{g_2}{\pi^2\cos\theta_W}g^{Z'}_{A,f}e^2Q_f^2\left[\frac{1}{2} - 2m_f^2C_0\right]\epsilon_{\rho\mu\alpha\beta}\,k^\alpha(-q)^\beta \tag{4.84}$$

and the most general expression of the coefficient C_0 is given in Eq. (A.8) of ref. [86]. C_0 is the scalar three-point function with a fermion of mass m_f circulating in the loop. In the soft photon limit the invariant amplitude defined by the right-hand-side of (4.84) reduces to (4.71). The purely transverse part (for $m_f \neq 0$) is obtained by applying the projection operator given in (4.79)

$$\begin{aligned}\Delta^{trans}_{\mu\nu\rho}(q,k) &= -k^\sigma\frac{\partial}{\partial k^\rho}\left(\Pi^{\nu\nu'}(q,k)\Delta^f_{\mu\nu\sigma}(q,k)\right)|_{\lim k\to 0}\\ &= -k^\sigma\frac{\partial}{\partial k^\rho}\Delta^T_{\mu\nu\sigma}(q,k)|_{\lim k\to 0},\end{aligned} \tag{4.85}$$

where

$$\begin{aligned}\Delta^T_{\mu\nu\sigma}(q,k) = &A(k,-q,m_f)\left[q^\alpha\epsilon_{\alpha\mu\nu\sigma}k^2 - \frac{k_\nu\,k^2}{(q-k)^2}\epsilon_{\mu\sigma\alpha\beta}k^\alpha q^\beta + \frac{q_\nu\,k^2}{(q-k)^2}\epsilon_{\mu\sigma\alpha\beta}k^\alpha q^\beta + k_\sigma\epsilon_{\mu\nu\alpha\beta}k^\alpha q^\beta\right]\\ &+A(-q,k,m_f)\left[k^\alpha\epsilon_{\alpha\mu\nu\sigma}q^2 - \frac{k_\nu\,q^2}{(q-k)^2}\epsilon_{\mu\sigma\alpha\beta}k^\alpha q^\beta + \frac{q_\nu\,q^2}{(q-k)^2}\epsilon_{\mu\sigma\alpha\beta}k^\alpha q^\beta - q_\mu\epsilon_{\nu\sigma\alpha\beta}k^\alpha q^\beta\right],\end{aligned} \tag{4.86}$$

Differentiating with respect to k_ρ and taking the $\lim k\to 0$ we obtain

$$\begin{aligned}\frac{\partial}{\partial k^\rho}\Delta^T_{\mu\nu\sigma}(q,k)|_{\lim k\to 0} &= A(Q^2)\left[\epsilon_{\rho\mu\nu\sigma}q^2 + q_\nu\epsilon_{\mu\sigma\rho\beta}q^\beta - q_\mu\epsilon_{\nu\sigma\rho\beta}q^\beta\right]\\ &= A(Q^2)\left[q_\rho\epsilon_{\mu\nu\alpha\sigma}q^\alpha - q_\sigma\epsilon_{\mu\nu\alpha\rho}q^\alpha\right].\end{aligned} \tag{4.87}$$

where $A(Q^2)$ denotes the soft limit of the $A(-q,k,m_f)$ amplitude. The intermediate steps to simplify the contribution to a_μ are those of [126]. In our case, with the modifications discussed above, the Pauli form-factor for a circulating fermion of flavor f we obtain

$$\begin{aligned} F_2(0)|_{Z'} = (-e^2)\frac{g_2^2}{16\cos^2\theta_W}\frac{1}{M_{Z'}^2}\lim_{k^2\to 0}\int\frac{d^4q}{(2\pi)^4}\frac{1}{q^2}\left(\frac{M_{Z'}^2}{q^2-M_{Z'}^2}\right)\times \\ \frac{1}{4k^2}\,\mathrm{Tr}\left\{(\not{p}+m_\mu)\left[\gamma^\rho\ \not{k}-\left(k^\rho+\frac{p^\rho}{m_\mu}\ \not{k}\right)\right]\right. \\ \left.\left[\gamma^\mu\frac{(\not{p}-\ \not{q}+m_\mu)}{q^2-2q\cdot p}g_{A,\mu}^{Z'}\gamma^\nu\gamma_5+g_{A,\mu}^{Z'}\gamma^\nu\gamma_5\frac{(\not{p}+\not{q}+m_\mu)}{q^2+2q\cdot p}\gamma^\mu\right]\right\}\times \\ g_{A,f}^{Z'}Q_f\left[-i\tilde{\Delta}_{\mu\nu\rho}^{f,\mathrm{long}}\,(q,k)+k^\sigma\left[q_\rho\epsilon_{\mu\nu\alpha\sigma}q^\alpha-q_\sigma\epsilon_{\mu\nu\alpha\rho}q^\alpha\right]A(Q^2)\right], \end{aligned} \tag{4.88}$$

where $\tilde{\Delta}_{\mu\nu\rho}^{\mathrm{f,long}}$ is not anomalous and in the soft photon limit it is given by

$$\tilde{\Delta}_{\mu\nu\rho}^{\mathrm{f,long}}(q,k)=\frac{q_\nu}{q^2}\tilde{w}_L^f\epsilon_{\mu\rho\alpha\sigma}q^\alpha k^\sigma \tag{4.89}$$

where

$$\tilde{w}_L^f=-\left[-\frac{2}{\pi^2}\frac{m_f^2}{q^4}\log\frac{(-q)^2}{m_f^2}+O\left(\frac{1}{q^6}\right)\right]. \tag{4.90}$$

It is obvious from this analysis that in presence of the GS mechanism there is a two-loop counterterm which removes the pure anomalous contribution in Eq. (4.88) and is given by see Fig. 4.22b. Diagram c) in the same figure is the longitudinal part of the diagram and appears in the broken WI that we will discuss in the last section. Finally, after some manipulations, similar to those performed in [119, 123, 127, 122], the final result for the anomalous contributions to a_μ takes the form

$$F_2(0)|_{Z'}=(-e^2Q_f)\frac{g_2^2g_{A,\mu}^{Z'}g_{A,f}^{Z'}}{16\cos^2\theta_W}\left(\frac{m_\mu^2}{M_{Z'}^2}\right)\frac{1}{4\pi^2}\int_{m_\mu}^\infty dQ^2\left(\tilde{w}_L^f(Q^2)+\frac{M_{Z'}^2}{Q^2+M_{Z'}^2}A(Q^2)\right), \tag{4.91}$$

where $-q^2=Q^2$ and $\tilde{w}_L^f(Q^2)$ vanishes in the chiral limit.

4.5.0.1 The Wess-Zumino Counterterm

A similar analysis can be performed in the case of the WZ mechanism. The leading non anomalous one-loop contributions Fig. 4.20 have been calculated in [68] for a specific D-brane model. These are due to the coupling of the axi-Higgs to the fermions. The organization of the perturbative expansion for a theory with an axion-like particle has been discussed in [40, 13], where the explicit cancellation of the gauge dependence has been discussed on general grounds. We show in Fig. 4.21 the contribution coming from the Z' propagator (graph a) in the anomalous exchange, the additional graphs b) and c) represent the axion counterterm due to the WZ interaction (b) and the correction due to the coupling of the axion to the massive fermions (c). We have omitted a graph similar to (c) in which the exchanged pseudoscalar is a Goldstone and cancels the gauge dependence of the Z' propagator.

The computation of graph a) follows exactly the analysis of [123] and can be performed in dimensional regularization in the unitary gauge, to give

$$\begin{aligned} \lambda_{\overline{\mathrm{MS}}} &\equiv \frac{\mu^{d-4}}{16\pi^2}\left[\frac{1}{d-4}-\frac{1}{2}\left(\log 4\pi+2+\Gamma'(1)\right)\right], \\ F_2(0)\Big|_{\mathrm{anom}}^{(f)} &= \frac{g_2^2}{16\pi^2\cos^2\theta_W}\frac{m_\mu^2}{M_{Z'}^2}\frac{1}{4\pi^2}Q_f^2g_A^{Z',f}\times\left[\log\left(\frac{\mu_R^2}{M_{Z'}^2}\right)-32\pi^2\lambda_{\overline{\mathrm{MS}}}+\log\left(\frac{M_{Z'}^2}{m_\mu^2}\right)+\frac{1}{2}\right]. \end{aligned}$$

$$\tag{4.92}$$

The expression of the extra contributions when a physical axion is exchanged are given by

$$\begin{aligned}
F_2(k^2)\big|_{(c)_{\rm long}} &= eQ_\mu c^\chi_\mu \lim_{k^2\to 0}\int \frac{d^4q}{(2\pi)^4}\,\frac{1}{q^2}\,\frac{1}{(p'-p-q)^2-M^2_{Z'}}\times\\
&\bar{u}(p')\left[\gamma^\mu\frac{1}{\slashed{p}'-\slashed{q}-m_\mu}\gamma_5+\gamma_5\frac{1}{\slashed{p}+\slashed{q}-m_\mu}\gamma^\mu\right]u(p)\times\\
&\left[2\frac{m_\mu}{M^2_{Z'}}\sum_f eQ_f c^\chi_f\frac{1}{(q-k)^2-M^2_\chi}\right]\Delta_{\mu\rho}(m_f,q,k,q-k),
\end{aligned}\tag{4.93}$$

where c^χ_f is coupling of the axi-Higgs to the fermions and

$$\begin{aligned}
\Delta_{\mu\rho}(m_f,q,k,q-k) &= \epsilon_{\mu\rho\alpha\beta}q^\alpha k^\beta\left(-\frac{1}{2\pi^2}\right)I(m_f)\\
I(m_f) &\equiv -\int_0^1\int_0^{1-x}dx\,dy\,\frac{1}{m^2_f+(x-1)xq^2+(y-1)yk^2-2xyq\cdot k}\,.
\end{aligned}\tag{4.94}$$

Using the projection operator we get

$$\begin{aligned}
F_2(0)\big|_{(c)_{\rm long}} &= eQ_\mu c^\chi_\mu \lim_{k^2\to 0}\int \frac{d^4q}{(2\pi)^4}\,\frac{1}{q^2}\,\frac{1}{(p'-p-q)^2-M^2_{Z'}}\times\\
&\frac{1}{4k^2}\,\mathrm{Tr}\left\{(\slashed{p}+m_\mu)\left[\gamma^\rho\,\slashed{k}-\left(k^\rho+\frac{p^\rho}{m_\mu}\,\slashed{k}\right)\right]\times\right.\\
&\left.\left[\gamma^\mu\frac{1}{\slashed{p}'-\slashed{q}-m_\mu}\gamma_5+\gamma_5\frac{1}{\slashed{p}+\slashed{q}-m_\mu}\gamma^\mu\right]\right\}\times\\
&\left[2\frac{m_\mu}{M^2_{Z'}}\sum_f eQ_f c^\chi_f\frac{1}{(q-k)^2-M^2_\chi}\right]\Delta_{\mu\rho}(m_f,q,k,q-k).
\end{aligned}\tag{4.95}$$

The contribution coming from the diagram in Fig. 4.21b is similar to Fig. 4.21c and we obtain

$$\begin{aligned}
F_2(0)\big|_{(b)_{\rm long}} &= eQ_\mu c^\chi_\mu \lim_{k^2\to 0}\int \frac{d^4q}{(2\pi)^4}\,\frac{1}{q^2}\,\frac{1}{(p'-p-q)^2-M^2_{Z'}}\times\\
&\frac{1}{4k^2}\,\mathrm{Tr}\left\{(\slashed{p}+m_\mu)\left[\gamma^\rho\,\slashed{k}-\left(k^\rho+\frac{p^\rho}{m_\mu}\,\slashed{k}\right)\right]\times\right.\\
&\left.\left[\gamma^\mu\frac{1}{\slashed{p}'-\slashed{q}-m_\mu}\gamma_5+\gamma_5\frac{1}{\slashed{p}+\slashed{q}-m_\mu}\gamma^\mu\right]\right\}\times\\
&\left[-2\frac{m_\mu}{M^2_{Z'}}g^\chi_{\gamma\gamma}\frac{1}{(q-k)^2-M^2_\chi}\right]\epsilon_{\mu\rho\alpha\beta}q^\alpha k^\beta.
\end{aligned}\tag{4.96}$$

where the coefficient $g^\chi_{\gamma\gamma}$ is the coupling of the axi-Higgs to the photons and it will be given explicitly in the next section together with the coefficient c^χ.

4.5.1 Corrections to muonium

A similar analysis of the role played by both mechanisms in anomalous processes at higher orders can be done in the case of muonium. A recent analysis of the hadronic effects in this type of systems can be found in [128]. One of the typical contributions is given by virtual light-by-light scattering, shown in Fig. 4.23. In the presence of anomalous gauge interactions a dominant contribution for the GS case is given by diagram (b). Diagram (c) is subdominant. This is expanded in terms single and double counterterms, typically given in Fig. 4.26. In the WZ case we report some of the corresponding contributions in Figs. 4.24 and 4.25, where we allow a coupling of the axi-Higgs to the fermions. The leading contribution are diagrams (b) and (e) of Fig. 4.24, which are the analogue of (a) and (b) of Fig. 4.20. The diagrams involving light-by-light scattering in the presence of a WZ vertex with a physical axi-Higgs χ coupled to fermions are shown in Fig. 4.25; their expression can be easily obtained by taking into account some recent results on two-loop QCD corrections [118] and a specific choice of parameters for an anomalous model developed and fully described in Chaps. 1, 2. So we have

$$\begin{aligned}\mathcal{M}_a &= \bar{u}(p_2)\left[e^4\sum_f g_{Z'}a^f_{Z'}Q_f^2\,\Lambda_\mu(s,m_f,m_e)\right]u(p_1)\frac{-i}{k^2-M_{Z'}^2}\left(g^{\mu\nu}-\frac{k^\mu k^\nu}{M_{Z'}^2}\right)\\ &\quad \bar{v}(p_1')\left[e^4\sum_{f'} g_{Z'}a^{f'}_{Z'}Q_{f'}^2\Lambda_\nu(s,m_{f'},m_\mu)\right]v(p_2'),\end{aligned} \tag{4.97}$$

where the axial-vector vertex function $\Lambda_\mu(s,m_f,m_{ext})$ is given [118] in terms of some coefficients named G_1 and G_2 as

$$\Lambda_\mu(s,m_f,m_{ext}) = \gamma_\mu\gamma_5 G_1(s,m_f,m_{ext}) + \frac{1}{2m_{ext}}k_\mu\gamma_5 G_2(s,m_f,m_{ext}) \tag{4.98}$$

and m_{ext} refers to the electron or the muon. Their explicit expression can be found in [118]. For $\mathcal{M}_b$, with an axi-Higgs exchanged in the t-channel we obtain

$$\mathcal{M}_b = \bar{u}(p_2)\left[e^2\sum_f c^{\chi,f}_{\gamma\gamma}\Lambda(s,m_f,m_e)\right]u(p_1)\frac{i}{k^2-m_\chi^2}\bar{v}(p_1')\left[e^2\sum_{f'} c^{\chi,f'}_{\gamma\gamma}\Lambda(s,m_{f'},m_\mu)\right]v(p_2') \tag{4.99}$$

with the general coupling of the physical axion

$$c^{\chi,f}_{\gamma\gamma} = e^2 Q_f^2 c^{\chi,f}, \qquad (f=u,d,\nu,e) \tag{4.100}$$

and the pseudoscalar vertex function $\Lambda(s,m_f,m_{ext})$ (see [118])

$$\Lambda(s,m_f,m_{ext}) = \gamma_5 A(s,m_f,m_{ext}). \tag{4.101}$$

We have used a condensed notation for the flavors in Eq. 4.100 with u = {u, c, t}, d = {d, s, b}, ν = {ν_e, ν_μ, ν_τ} and e = {e, μ, τ}, whose expansion yields

$$\begin{aligned} c^{\chi,u} &= \Gamma^u\frac{i}{\sqrt{2}}O^\chi_{11} = \frac{m_u}{v_u}iO^\chi_{11}, \qquad c^{\chi,d} = -\Gamma^d\frac{i}{\sqrt{2}}O^\chi_{21} = -\frac{m_d}{v_d}iO^\chi_{21},\\ c^{\chi,\nu} &= \Gamma^\nu\frac{i}{\sqrt{2}}O^\chi_{11} = \frac{m_\nu}{v_u}iO^\chi_{11}, \qquad c^{\chi,e} = -\Gamma^e\frac{i}{\sqrt{2}}O^\chi_{21} = -\frac{m_e}{v_d}iO^\chi_{21},\end{aligned} \tag{4.102}$$

where the elements of the O^χ rotation matrix from the interaction to the mass eigenstate basis are given in App. 2.9.

The most difficult to analyze are those of higher order, shown in Fig. 4.25

$$\mathcal{M}_c = \bar{u}(p_2)\left[e^2\sum_f c^{\chi,f}_{\gamma\gamma}\Lambda(s,m_f,m_e)\right]u(p_1)\frac{i}{k^2-m_\chi^2}\bar{v}(p_1')F(s,m_\mu)g^\chi_{\gamma\gamma}e^2v(p_2') \tag{4.103}$$

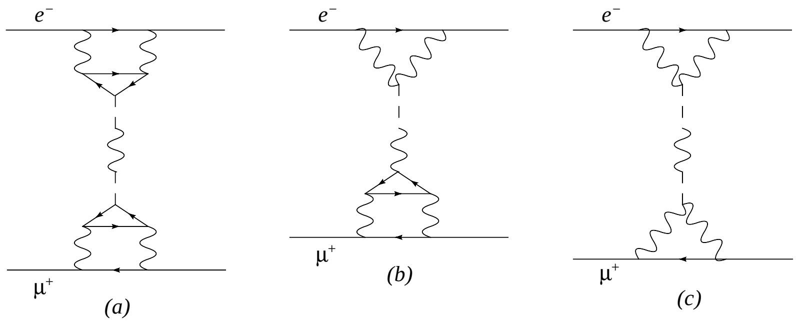

Figure 4.26: As in Fig. 4.25 for a GS vertex.

$$\mathcal{M}_d = \bar{u}(p_2)F(s,m_e)g^{\chi}_{\gamma\gamma}e^2u(p_1)\frac{i}{k^2-m_\chi^2}\bar{v}(p_1')F(s,m_\mu)g^{\chi}_{\gamma\gamma}e^2v(p_2'), \tag{4.104}$$

with the one-loop anomalous vertex function $F(s,m_{ext})$ [118]

$$F(s,m_{ext}) = 2i\,m_{ext}\,f(s,m_{ext})\,\gamma_5 \tag{4.105}$$

where m_{ext} is the mass of the external fermion, in this case the muon mass, and the specific choice of coupling given by

$$g^{\chi}_{\gamma\gamma} = \left[\frac{F}{M_1}(O^A_{W\gamma})^2 + \frac{C_{YY}}{M_1}(O^A_{Y\gamma})^2\right]O^{\chi}_{31} \tag{4.106}$$

in terms of model dependent parameters defined in Chap. 2.
The simplest corrections are those of Fig. 4.24 and can be written as

$$\mathcal{N}_a = \bar{u}(p_2)(g_{Z'}a^e_{Z'})\gamma^\mu\gamma^5u(p_1)\frac{-i}{k^2-M_{Z'}^2}\left(g^{\mu\nu}-\frac{k^\mu k^\nu}{M_{Z'}^2}\right)\bar{v}(p_1')\left[e^4\sum_f g_{Z'}a^f_{Z'}Q_f^2\Lambda_\nu(s,m_f,m_\mu)\right]v(p_2'), \tag{4.107}$$

$$\mathcal{N}_b = \bar{u}(p_2)c^{\chi,e}\gamma^5u(p_1)\frac{i}{k^2-m_\chi^2}\bar{v}(p_1')c^{\chi,\mu}\gamma^5v(p_2'), \tag{4.108}$$

$$\mathcal{N}_c = \bar{u}(p_2)c^{\chi,e}\gamma^5u(p_1)\frac{i}{k^2-m_\chi^2}\bar{v}(p_1')F(s,m_\mu)g^{\chi}_{\gamma\gamma}e^2v(p_2'), \tag{4.109}$$

$$\mathcal{N}_d = \bar{u}(p_2)c^{\chi,e}\gamma^5u(p_1)\frac{i}{k^2-m_\chi^2}\bar{v}(p_1')\left[e^2\sum_f c^{\chi,f}_{\gamma\gamma}\Lambda(s,m_f,m_\mu)\right]v(p_2'), \tag{4.110}$$

where the one-loop functions Λ_ν, F and Λ have been given above and can be found in the literature.

4.6 The longitudinal subtraction and the broken Ward Identities of the GS vertex

There is one last important point that we will address in this final section which concerns the correct interpretation of the anomaly counterterm in both (chiral) phases of theory. The GS vertex satisfies a broken WI, which is easy to derive diagrammatically. The identity is similar to that of the ordinary triangle diagram, but with a subtraction of the (massless) anomaly pole. In the massless fermion case, the GS counterterm restores the WI on the anomaly vertex; in the massive case the mass-dependent terms are a signal of chiral symmetry breaking, but are not counterterms. The only counterterm is the anomaly pole. We briefly clarify this point.

We recall that, for on-shell photons (analogously for gluons) in an anomalous theory, the pole contribution to the AVV triangle is given by

$$T^{\lambda\mu\nu} = g_{V_{KK}}\theta_f^{KK} g_s^2 Tr[t^a t^b] k^\lambda \epsilon[k_1,k_2,\mu,\nu] \left[\frac{1}{2\pi^2 s} - \frac{m_f^2}{2\pi^2 s^2}\log^2\left(\frac{\rho_f+1}{\rho_f-1}\right)\right]$$
$$\rho_f = \sqrt{1-\frac{4m_f^2}{s}} \tag{4.111}$$

and the anomalous WI on the axial-vector line gives

$$k_\lambda T^{\lambda\mu\nu} = g_{V_{KK}}\theta_f^{KK} g_s^2 Tr[t^a t^b] \left(\epsilon[k_1,k_2,\mu,\nu]\frac{1}{2\pi^2} + 2m_f T^{\mu\nu}\right)$$
$$T^{\mu\nu} = \frac{m_f}{2\pi^2}\int_0^1\int_0^{1-x} dx\, dy\, \frac{\epsilon[k_1,k_2,\mu,\nu]}{m_f^2 - 2xyk_1\cdot k_2}. \tag{4.112}$$

The second term in the WI above, or $T_{\mu\nu}$, in a local gauge theory with spontaneous symmetry breaking (in an anomaly-free theory), is determined by the BRS invariance of the correlator. In an anomalous theory the first term is the anomaly, while the second term comes from chiral symmetry breaking. If we use a WZ counterterm to restore the gauge symmetry, the WI is modified with the addition of the $bF\tilde{F}$ graph, and the analysis can be found in [92]. Eq. (4.112) takes a more general form for off-shell gauge lines. The general corrections to the anomaly pole are of the form

$$\Delta^{\lambda\mu\nu} = g_{V_{KK}}\theta_f^{KK} g_s^2 Tr[t^a t^b] k^\lambda \epsilon[k_1,k_2,\mu,\nu]\left[\frac{1}{2\pi^2 s} - 2m_f^2 C_0(t,k_1^2,k_2^2,m_f)\right] \tag{4.113}$$

where $C_0(t,k_1^2,k_2^2,m_f)$ is the scalar triangle diagram. Also in this case the C_0 terms are not counterterms. We don't need to add any mass-dependent term to the GS vertex to restore the WI of the non-local theory. These longitudinal contributions, following the analysis of $g-2$ in [123] and the discussion of the previous sections, are easily interpreted as the longitudinal parts of the non-anomalous components of the vertex, generated by the breaking of the chiral symmetry. There are two ways to write the broken WI in GS case. The first form is given by

$$k_\lambda\left(\Delta^{\lambda\mu\nu} + \Gamma_{GS}^{\lambda\mu\nu}\right) + T^{\mu\nu} = 0, \tag{4.114}$$

in which the $T_{\mu\nu}$ term, which is of the form (4.113), is derived simply by acting with the WI on the GS vertex (anomaly plus massless pole term) and bringing the result to the first member. The chiral symmetry breaking corrections to the pole term are then obtained from the decomposition

$$\Delta^{GS\,\lambda\mu\nu} = \tilde{\Delta}_{long}^{\lambda\mu\nu} + \tilde{\Delta}_{trans}^{\lambda\mu\nu} \tag{4.115}$$

where

$$k_\lambda\tilde{\Delta}_{long}^{\lambda\mu\nu} = \frac{1}{4\pi^2}m_f^2 C_0(t,k_1^2,k_2^2,m_f)\epsilon[\mu,\nu,k_1,k_2] \equiv -T^{\mu\nu} \tag{4.116}$$

and

$$k_\lambda\tilde{\Delta}_{trans}^{\lambda\mu\nu} = 0. \tag{4.117}$$

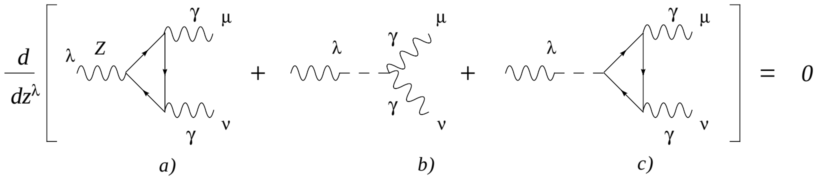

Figure 4.27: Broken WI in the presence of a GS interaction.

A second form of the same equation is obtained by extracting a massless pole from $T_{\mu\nu}$

$$k_\lambda \left(\Delta^{\lambda\mu\nu} + \Gamma^{\lambda\mu\nu}_{GS} + \frac{k^\lambda}{k^2} T^{\mu\nu} \right) = 0, \tag{4.118}$$

whose explicit form is shown in Fig. 4.27. This result is in disagreement with [117], where the authors write down an *exact* WI for the GS vertex in the chirally broken phase, identity which clearly does not exist, since the pole counterterm and the effects due to chiral symmetry breaking should be kept separate.

There are other issues concerning the use of this vertex to describe the mixing of the Kaluza-Klein excitations of gauge bosons to an axion, claimed to be relevant in $t\bar{t}$ production, which also point toward an inconsistency of these types of formulations in theories with extra dimensions and chiral delocalization on the brane. These quietly assume that the GS vertex is generated by sewing together local-interactions ($bF\tilde{F}$ vertex and $B\,b$ mixing), which are claimed to be obtained from extra dimensional theories [117]. The bilinear mixing is assumed to be physical (i.e. no gauge-fixing condition can remove it). If these constructions were consistent, this would imply that the anomaly can be removed by adding a finite number of local interactions. Instead, the anomaly pole can be removed, but at the expense of building a non-local theory. This result does not contradict the use of the WZ mechanism for the "cancellation" of the anomaly, since the WZ theory, being local, generates an effective theory which is unitary only below a certain scale, while remaining gauge invariant at all scales. The theory, in fact, needs to be amended by higher dimensional operators for the restoration of unitarity, and therefore the description of axion-like particle, involving Stückelberg axions and PQ interactions, are not unitary at all scales. In fact, the number of local interactions needed to obtain an anomaly-free theory is infinite, which is the price to pay for not having a pole counterterm as in the GS case. The presence of BIM amplitudes for the WZ mechanism provides a clear example of processes with a non-unitary growth at high energy, as clearly shown in Chap. 3.

4.7 Conclusions

We have investigated the consistency of the subtraction of pole counterterm in an anomalous theory, re-analysing the problem of the generation of double poles in the perturbative expansion due to the extra subtractions, and in particular, in some s-channel exchanges. Having the anomaly diagram a natural separation into longitudinal and transverse contributions, the subtraction of the longitudinal component can be viewed simply as the remotion of one of its *independent* invariant amplitudes. If the structure of a given graph does not render the anomaly vertex harmless, the longitudinal subtraction is explicit, otherwise the subtraction vanishes by itself, as does the longitudinal component of the anomaly in that case.

In principle, the perturbative expansion for the GS vertex can be formulated directly in terms of its transverse components. Away from the chiral limit there is still no anomaly pole, and the decoupling of the anomaly should hold at all orders and also in the broken chiral phase.

We have argued by explicit examples that the organization of the perturbative expansion in terms of anomaly diagrams and pole counterterms (or DZ counterterms) is just a matter of convenience, especially if a given computation has to be carried out to higher orders. In this case, the double poles due to the counterterms have to be interpreted as genuine contributions which are embedded in two-loop graphs. We have pointed out that the emergence of double poles is not an isolated case, but a standard result, common to a specific way to address the tensor decomposition of a Feynman graph.

In this approach the computation of tensor integrals is performed using scalar integrals with higher power of the denominators and then re-formulated in terms of suitable sets of master integrals. Therefore, an ordinary perturbative expansion at two-loop level - after integration on one of the loop momenta - gives -with no surprise- a theory with propagators of second order and higher.

A final comment goes to the high energy behavior od the GS vertex. The good high energy behavior of the vertex is related to its gauge invariance, with BIM amplitudes which are identically vanishing in the chiral limit. A similar feature is absent in the WZ case, which violates unitarity at high energy. Finally, we have investigated the emergence of GS and of WZ vertices in $g-2$ of the muon and in muonium, describing the differences between the SM case and its anomalous extensions, involving one axion-like particle and an extra anomalous Z', concentrating our attention, in particular, on the anomalous contributions, which can be studied accurately in the future in view of the planned experiments on $g-2$ at BNL. In general, in the WZ case, the leading contributions to $g-2$ come from the exchange of an axi-Higgs and an anomalous Z', while in the GS case they involve directly the transverse components of the GS vertex.

4.8 Appendix. Some features of the GS and WZ vertices

We comment on the relation between the WZ and GS formulation.

There are several ways to parameterize an anomaly vertex (AVV), the most well known being the one due to Rosenberg [42] which involves six invariant amplitudes ($A_1, A_2, ...A_6$), two of which are ill-defined and determined by the Ward Identities of the theory in terms of the finite ones. The presence of an anomaly pole is not obvious in this formulation, although its structure was clearly established by Dolgov and Zakharov in their work [101] using dispersion relations. The basic interpretation of this result is that the anomaly is not just an ultraviolet but also an infrared effect.

The extraction of the anomaly pole from the rest of the amplitude is not so evident from the Rosenberg parameterization, but is quite obvious from the L/T formulation of this vertex, discussed in Sec. 4.2.4. As we have discussed in the same section, the GS mechanism corresponds to a redefinition of the anomaly vertex. It means that whenever we encounter an anomaly diagram we replace it with another vertex in which the DZ pole has been explicitly removed. In a Lagrangian formulation this operation is equivalent to the addition of the counterterm shown in diagram c) of Fig. 4.1. We stress once more that there is no direct coupling of the axion to the fermion, since in this approach the axion is not an asymptotic state. As we have extensively discussed in the previous sections this subtraction can be understood in a local version of the effective action by using Federbush's formulation of the GS mechanism with two pseudoscalars, Eq. (4.3), one of them being actually a ghost, with negative kinetic energy. This formulation could, in principle, be extended so to describe a coupling of one of these two axions to the fermions.

In the WZ case the local counterterm $bF \wedge F$ introduces the axion as an asymptotic state of the corresponding S-matrix. Therefore, the axion takes an important role in the mechanisms of symmetry breaking, being this due either to a Higgs sector or to the Stückelberg mechanism, or to both. For this reason, in the presence of electroweak symmetry breaking, there is a direct coupling of the axion to the fermions via the corresponding Yukawa couplings. One point which is worth to stress is that the WZ mechanism guarantees the gauge invariance of the one-loop effective action but not of the trilinear gauge vertex. The differences between the two mechanisms can be seen rather clearly, for instance, by comparing Fig. 4.25 and 4.26. Notice that fermion mass effects, in the WZ case, induced either by chiral symmetry breaking and/or electroweak symmetry breaking cause a direct interaction of the axion to the fermion. If they are both absent, then those diagrams in which the axion couples to the fermions are trivially vanishing.

4.8.1 Gauge choices

The cancellation of the gauge dependence in the perturbative expansion is rather trivial in the GS case while it is less straightforward in the WZ case. In the first case, the redefinition of the trilinear gauge vertex is sufficient to obtain from the beginning a gauge invariant result. For this purpose we may work directly in the R_ξ gauge, denoting with ξ_B the gauge-fixing parameter. The gauge dependent propagator for the gauge field is given by

$$\frac{-i}{k^2}\left[g^{\lambda\lambda'}-\frac{k^\lambda k^{\lambda'}}{k^2}(1-\xi_B)\right] \tag{4.119}$$

and the longitudinal components disappear whenever they are attached to a GS vertex, due to the Ward Identities satisfied on all the gauge lines. In the WZ case the cancellation of the gauge dependence is more subtle and has been discussed extensively in Chap. 1.

4.9 Appendix. Simplifications in some of the integrands on higher-point functions

4.9.1 Computation of the diagrams in Fig. 4.9

We show the vanishing of the counterterms in Fig. 4.9. We have

$$\begin{aligned} C_1^\lambda &= \int \frac{d^4k_1}{(2\pi)^4}\bar{v}(p_2)\gamma_\nu\frac{1}{\not{p}_1-\not{k}_1}\gamma_\mu u(p_1)\frac{1}{k_1^2}\frac{1}{k_2^2}\,C^{\mu\nu\lambda}_{AVV}(k_1,-k_2,k) \\ &= \int \frac{d^4k_1}{(2\pi)^4}\bar{v}(p_2)\gamma_\nu\frac{1}{\not{p}_1-\not{k}_1}\gamma_\mu u(p_1)\frac{1}{k_2^2}\frac{k_1^\mu}{k_1^4}\frac{a_n}{3}\epsilon[\lambda,\nu,k,k_2], \end{aligned} \tag{4.120}$$

with $k_2 = k - k_1$ so that

$$C_1^\lambda = \bar{v}(p_2)\gamma_\nu u(p_1)\frac{a_n}{3}\epsilon[\lambda,\nu,k,\rho]\int\frac{d^4k_1}{(2\pi)^4}\frac{k_1^\rho}{(k-k_1)^2k_1^4}, \tag{4.121}$$

where the expansion of the integrand function yields a result proportional to the independent momentum k^ρ and finally $C_1^\lambda = 0$. The C_2 counterterm vanishes in an analogous way as C_1^λ, so we take into account the last diagram in Fig. 4.9

$$C_3^\lambda = \int\frac{d^4k_1}{(2\pi)^4}\bar{v}(p_2)\gamma_\nu\frac{\not{p}_1-\not{k}_1}{(p_1-k_1)^2}\gamma_\mu u(p_1)\frac{1}{k_1^2}\frac{1}{k_2^2}C^{\lambda\mu\nu}_{AVV}(-k,-k_1,-k_2), \tag{4.122}$$

with $k_2 = k - k_1$ and $C^{\lambda\mu\nu}_{AVV}(-k,-k_1,-k_2) = \frac{a_n}{3}\frac{k^\lambda}{k^2}\epsilon[\mu,\nu,k_1,k_2]$. C_3^λ is given by the sum of a first-rank and a second-rank tensor integral which can be further reduced with the well-known tensor-reduction technique. The general expansion for the two integrands is

$$\begin{aligned}
\int \frac{d^4k_1}{(2\pi)^4}\frac{k_1^\alpha}{(p_1-k_1)^2 k_1^2 (k-k_1)^2} &= C_1\, p_1^\alpha + C_2\, k^\alpha, &(4.123)\\
\int \frac{d^4k_1}{(2\pi)^4}\frac{k_1^\alpha k_1^\beta}{(p_1-k_1)^2 k_1^2 (k-k_1)^2} &= C_{00}\, g^{\alpha\beta} + C_{12}\,(p_1^\alpha k^\beta + p_1^\beta k^\alpha) + C_{11}\, p_1^\alpha p_1^\beta + C_{22}\, k^\alpha k^\beta, &(4.124)
\end{aligned}$$

first we notice that all the terms proportional to k^α trivially vanish after the contraction with the anti-symmetric Levi-Civita tensor in Eq. (4.122) and then we conclude $C_3^\lambda = 0$ by using the following relations in Eq. (4.122)

$$\begin{aligned}
\bar{v}(p_2)\gamma_\nu \not{p}_1 \gamma_\mu \epsilon[\mu,\nu,p_1,k]u(p_1) &= 2i\,\bar{v}(p_2)(p_1^2 \not{k} - k\cdot p_1 \not{p}_1)\,\gamma^5 u(p_1) = 0, &(4.125)\\
\bar{v}(p_2)\gamma_\nu \gamma_\beta \gamma_\mu \epsilon[\mu,\nu,\beta,k]u(p_1) &= 6i\,\bar{v}(p_2)\not{k}\,\gamma^5 u(p_1) = 0. &(4.126)
\end{aligned}$$

for massless external fermions with momenta p_1 and p_2 and $k = p_1 + p_2$.

4.9.2 Simplifications of the integrands in Sec. 4.2.3

The third amplitude $\mathcal{S}_c$ does not contribute to $\mathcal{S}$, in fact we have

$$\begin{aligned}
\mathcal{S}_c &= \int \frac{d^4k_1}{(2\pi)^4}\left(\bar{v}(p_2)\gamma_\nu \frac{1}{\not{p}_1 - \not{k}_1}\not{k}_1 u(p_1)\frac{1}{k_2^2}\frac{1}{k_1^2}\frac{a_n}{3}\frac{1}{k_1^2}\epsilon[\nu,\lambda,k_2,k]\right)\frac{1}{k^2}\mathcal{B}\mathcal{T}^\lambda_{AAA}\\
&= -\bar{v}(p_2)\gamma_\nu u(p_1)\frac{a_n}{3}\int \frac{d^4k_1}{(2\pi)^4}\left(\frac{1}{(k-k_1)^2}\frac{1}{k_1^4}\epsilon[\nu,\lambda,k-k_1,k]\right)\frac{1}{k^2}\mathcal{B}\mathcal{T}^\lambda_{AAA}\\
&= \bar{v}(p_2)\gamma_\nu u(p_1)\frac{a_n}{3}\epsilon[\nu,\lambda,\rho,\sigma]k^\sigma \int \frac{d^4k_1}{(2\pi)^4}\left(\frac{k_1^\rho}{(k-k_1)^2 k_1^4}\right)\frac{1}{k^2}\mathcal{B}\mathcal{T}^\lambda_{AAA}\\
&\propto \bar{v}(p_2)\gamma_\nu u(p_1)\frac{a_n}{3}\epsilon[\nu,\lambda,k,k]\frac{1}{k^2}\mathcal{B}\mathcal{T}^\lambda_{AAA} = 0, \qquad (4.127)
\end{aligned}$$

where by the tensor integral decomposition we obtain the following result

$$\epsilon[\nu,\lambda,\rho,\sigma]k^\sigma \int \frac{d^4k_1}{(2\pi)^4}\left(\frac{k_1^\rho}{(k-k_1)^2 k_1^4}\right) = \epsilon[\nu,\lambda,\rho,\sigma]k^\sigma B k_\rho = 0. \qquad (4.128)$$

Here we omit the explicit form of the coefficient of the rank-1 tensor decomposition B, since it is not essential for the calculation. We can apply the same arguments to prove that $\mathcal{S}_d = 0$.

Chapter 5

An Anomalous Extra Z' from Intersecting Branes with Drell-Yan and Direct Photons at the LHC

5.1 Introduction to the chapter

The study of anomalous gauge interactions at the LHC and at future linear colliders is for sure a difficult topic, but also an open possibility that deserves close theoretical and experimental attention. Hopefully, these studies will be able to establish if an additional anomalous extra Z' is present in the spectrum, introduced by an Abelian extension of the gauge structure of the Standard Model (SM), assuming that extra neutral currents will be found in the next several years of running of the LHC [106]. The interactions that we discuss are characterized by *anomalous vertices* in which gauge anomalies cancel in some non trivial way, not by a suitable (anomaly-free) charge assignment of the chiral fermion spectrum for each generation.

The phenomenological investigation of this topic is rather new, while various mechanisms of cancellation of the gauge anomalies involving axions have been around for quite some time. Global anomalies, for instance, introduced for the solution of the strong CP-problem, such as the Peccei-Quinn solution [129, 22, 130, 131, 132, 133, 134, 135] (reviewed in [136]) require an axion, while local anomalies, cancelled by a Wess-Zumino counterterm, allow an axion-like particle in the spectrum, whose mass and gauge coupling - differently from PQ axions - are independent. Similar constructions hold also in the supersymmetric case and a generalization of the WZ mechanism is the Green-Schwarz mechanism (GS) of string theory. The two mechanisms are related but not identical, the first of them being characterized by a unitarity bound [105]. Details on the relation between the two at the level of effective field theory can be found in [105, 98].

Intersecting brane models, in which several anomalous $U(1)$'s and Stückelberg mass terms are present, may offer a realization of these constructions [137, 93, 26, 56], which can also be investigated in a bottom-up approach by using effective Lagrangians built out of the requirements of gauge invariance of the one-loop effective action [1]. In our analysis we will consider the simplest extension of these anomalous Abelian gauge factors, which involves a single anomalous $U(1)$, denoted as $U(1)_B$. The corresponding anomalous gauge boson B gets its mass via a combination of the Higgs and of Stückelberg mechanisms. Axions play a key role in the cancellation of the anomalies in these theories although they may appear in other constructions as well, due to the decoupling of a chiral fermion in anomaly-free theories [13].

The presence of an anomalous $U(1)$ in effective models derived from string theory is quite common, although in all the previous literature before [1] and [13, 40, 91] the phenomenological relevance of the anomalous $U(1)$ had not been worked out in any detail. In particular, the dynamics of the anomalous extra gauge interaction had been neglected, by invoking a decoupling of the anomalous sector on the assumption of a large mass of the extra gauge boson. In [1] it was shown that only one physical axion appears in the spectrum of these models, independently of the number of Abelian factors, which is the most important feature of these realizations. In our case, the axion can be massless or massive, depending on the structure of the scalar potential. Recent developements in the study of these models include their supersymmetric extensions [108] and their derivations as symplectic forms of supergravity [138, 139]. Other interesting variants include the Stückelberg extensions considered in [29, 30, 74] which depart significantly from the Minimal Low Scale Orientifold Model (mLSOM) introduced in [1] and discussed below. Specifically these models are also characterized by the presence of two mechanisms of symmetry breaking (Higgs and Stückelberg) but do not share the anomalous structure. As such they do not describe the anomalous $U(1)$'s of these special vacua of string theory.

Axion-like particles, beside being a natural candidate for dark matter, may play a role in explaining some puzzling results regarding the propagation of high energy gamma rays [80, 110] due to the oscillations of photons into axions in the presence of intergalactic magnetic field. In general, the presence of independent mass/coupling relations for these particles allows to evade most of the experimental bounds coming from CAST and other experiments on the detection of PQ axions, characterized by a suppression of both mass and gauge couplings of this particle by the same large scale ($10^{10} \div 10^{12}$ GeV), (see [109, 140]). Here we focus our attention on the gauge sector, quantifying the rates for the detection of anomalous neutral currents at the LHC in some specific and very important channels.

- **Drell-Yan**

Being leptoproduction the best way to search for extra neutral interactions, it is then obvious that the study of the anomalous vertices and of possible anomalous extra Z' should seriously consider the investigation of this process. We describe the modifications induced on Drell-Yan computed in the Standard Model (SM) starting from the description of some of the properties of the new anomalous vertices and of the corresponding one-loop counterterms, before moving to the analysis of the corrections. These appear - both in the WZ and GS cases in the relevant partonic channels at NNLO in the strong coupling constant ($O(\alpha_s^2)$). We perform several comparisons between anomalous and non-anomalous extra Z' models and quantify the differences with high accuracy.

- **Direct Photons (Di-photon, DP)**

Double prompt (direct) photons offer an interesting signal which is deprived of the fragmentation contributions especially at large values of their invariant mass Q, due to the steep falling of the photon fragmentation functions. In addition, photon isolation may provide an additional help in selecting those events coming from channels in which the contribution of the anomaly is more sizeable, such as gluon fusion. Also in this case we perform a detailed investigation of this sector. For direct photons, the anomaly appears in gluon fusion - at parton level - in a class of amplitudes which are characterized by two-triangles graphs - or BIM amplitudes - using the definitions of Chap. 3.

In both cases the quantification of the background needs extreme care, due to the small signal, and the investigation of the renormalization/factorization scale dependence of the predictions is of outmost importance. In particular, we consider all the sources of scale-dependence in the analysis, including those coming from the evolution of the parton densities (PDF's) which are just by themeselves enough to overshadow the anomalous corrections. For this reason we have used the program CANDIA 1.0 in the evolution of the PDF's, which has been documented in [104]. The implementation of DY and DP processes is part of two programs CANDIA$_{DY}$ and CANDIA$_{Axion}$ for the study of the QCD background with the modifications induced by the anomalous signal. The QCD background in DP is computed using DIPHOX [141] and GAMMA2MC based on Ref. [142]. The NLO corrections to DP before the implementation of DIPHOX have been computed by Gordon and Corianò back in 1995 [43] and implemented in a Monte Carlo based on the phase space slicing method.

In the numerical analysis that we present we have included all the contributions coming from the two mechanisms as separate cases, corrections that are implemented in DY and DP processes. We will start analyzing the contributions to these processes in more detail in the next sections, discussing the specific features of the anomalous contributions and of the corresponding counterterms at a phenomenological level.

The chapter is organized as follows. After a brief description of the anomalous interactions and the counterterms that appear either at Lagrangian level (WZ case) or at the level of the trilinear gauge vertex (GS case), we discuss the main properties of these vertices and we address the structure of the corrections in DY and in DP. Our study is mainly focused on the invariant mass distributions in the two cases. The need for performing these types of analysis in parallel will be explained below, and there is the hope that it may be extended to other processes and observables in the future, such as rapidity distributions and rapidity correlations [143]. We present high precision estimates of the QCD background at NNLO, which is the order where, in these processes, the anomalous corrections start to appear. Other analysis, of course, are also possible, such as those involving four-fermion decays in trilinear gauge interactions which could, in principle, be sensitive to Chern-Simons terms [1, 69] if at least two anomalous $U(1)$'s are present in the spectrum. These additional interactions are allowed, as discussed in [92], whenever the distribution of the partial anomalies on a diagram is not fixed by symmetry requirements. A complete description of these vertices has been carried out in [92], useful for direct phenomenological studies.

As we are going to show, the search for effects due to anomalous $U(1)$ at the LHC in pp collisions cannot avoid an analysis of the QCD background at NNLO. DY and DP are the only two cases where this level of precision has been obtained in perturbation theory. As we are going to show, the anomalous effects at the LHC in these two key processes are tiny, since the invariant mass distributions are down by a factor of $10^3 \div 10^4$ compared to the NNLO (QCD) background. The accuracy required at the LHC to identify these effects on these observables should be of a fraction of a percent (0.1% and below), which is beyond reach at a hadron collider due to the larger indetermination intrinsic in QCD factorization and the parton model.

5.2 Anomaly-free versus an anomalous extra Z' in Drell-Yan

As we have already mentioned, the best mode to search for extra Z' at the LHC is in the production of a lepton pair via the Drell-Yan mechanism ($q\bar{q}$ annihilation) mediated by neutral currents. The final state is easily tagged and resonant due to the s-channel exchange of the extra gauge boson. In particular, a new heavier gauge boson modifies the invariant mass distribution also on the Z peak due to the small modifications induced on the couplings and to the $Z - Z'$ interference. In the anomalous model that we have investigated, though based on a specific charge assignment, we find larger rates for these distributions both on the peak of the Z and of the Z' compared to the other models investigated, if the extra resonance is around 1 TeV. This correlation is expected to drop as the mass of the extra Z' increases. In our case, as we will specify below, the mass of the extra resonance is given by the Stückelberg (M_1) mass, which appears also (as a suppression scale) in the interaction of the physical axion to the gluons and it is essentially a free parameter.

In DY, the investigation of the NNLO hard scatterings goes back to [144], with a complete computation of the invariant mass distributions, made before that the NNLO corrections to the DGLAP evolution had been fully completed. In our analysis we will compare three anomaly-free models against a model of intersecting brane with a single anomalous $U(1)$. The anomaly-free charge assignments come from a gauged $B-L$ Abelian symmetry, a "$q+u$" Model -both described in [145] - and the Free Fermionic Model analyzed in [107]. We start by summarizing our definitions and conventions.

In the anomaly-free case we address Abelian extensions of the gauge structure of the form $SU(3) \times SU(2) \times U(1)_Y \times U(1)_z$, with a covariant derivative in the $W^3_\mu, B^\mu_Y, B^\mu_z$ (interaction) basis defined as

$$\hat{D}_\mu = \left[\partial_\mu - ig_2\left(W^1_\mu T^1 + W^2_\mu T^2 + W^3_\mu T^3\right) - i\frac{g_Y}{2}\hat{Y}B^\mu_Y - i\frac{g_z}{2}\hat{z}B^\mu_z\right] \tag{5.1}$$

where we denote with g_2, g_Y, g_z the couplings of $SU(2)$, $U(1)_Y$ and $U(1)_z$, with $\tan\theta_W = g_Y/g_2$. After the diagonalization of the mass matrix we have

$$\begin{pmatrix} A_\mu \\ Z_\mu \\ Z'_\mu \end{pmatrix} = \begin{pmatrix} \sin\theta_W & \cos\theta_W & 0 \\ \cos\theta_W & -\sin\theta_W & \varepsilon \\ -\varepsilon\sin\theta_W & \varepsilon\sin\theta_W & 1 \end{pmatrix} \begin{pmatrix} W^3_\mu \\ B^Y_\mu \\ B^z_\mu \end{pmatrix} \tag{5.2}$$

where ε is a perturbative parameter which is around 10^{-3} for the models analyzed, introduced in [145] and [107]. It is defined as

$$\varepsilon = \frac{\delta M^2_{ZZ'}}{M^2_{Z'} - M^2_Z} \tag{5.3}$$

while the mass of the Z boson and of the extra Z' are

$$\begin{aligned} M^2_Z &= \frac{g^2_2}{4\cos^2\theta_W}(v^2_{H_1} + v^2_{H_2})\left[1 + O(\varepsilon^2)\right] \\ M^2_{Z'} &= \frac{g^2_z}{4}(z^2_{H_1}v^2_{H_1} + z^2_{H_2}v^2_{H_2} + z^2_\phi v^2_\phi)\left[1 + O(\varepsilon^2)\right] \\ \delta M^2_{ZZ'} &= -\frac{g_2 g_z}{4\cos\theta_W}(z^2_{H_1}v^2_{H_1} + z^2_{H_2}v^2_{H_2}). \end{aligned} \tag{5.4}$$

In this class of models we have two Higgs doublets H_1 and H_2, whose v.e.v.'s are v_{H_1} and v_{H_2} and an extra $SU(2)_W$ singlet ϕ whose v.e.v. is v_ϕ. The extra $U(1)_z$ charges of the Higgs doublets are respectively z_{H_1} and z_{H_2}, while for the singlet this is denoted as z_ϕ. Taking the value of v_{H_2} of the order of the electroweak scale ($\approx$ 246 GeV), we fix v_{H_1} with $\tan\beta = v_{H_2}/v_{H_1}$, and we still have one free parameter, v_ϕ, which enters in the calculation of the mass of the extra Z'. Then it is obvious that we can take the mass $M_{Z'}$ and the coupling constant g_z as free parameters. We choose $\tan\beta \approx 40$ in order to reproduce the mass of the Z boson at 91.187 GeV, choice that is performed, for consistency, also in the anomalous model. In this last case the Higgs sector is characterized only by 2 Higgs doublets, with the v.e.v. of the extra singlet being replaced by the Stückelberg mass. We define $g_2\sin\theta_W = g_Y\cos\theta_W = e$ and construct the $W^\pm$ charge eigenstates and the corresponding generators $T^\pm$ as usual

$$W^\pm = \frac{W_1 \mp iW_2}{\sqrt{2}} \qquad T^\pm = \frac{T_1 \pm iT_2}{\sqrt{2}},$$

while in the neutral sector we introduce the rotation matrix

$$\begin{pmatrix} W^3_\mu \\ B^Y_\mu \\ B^z_\mu \end{pmatrix} = \begin{pmatrix} \frac{\sin\theta_W(1+\varepsilon^2)}{1+\varepsilon^2} & \frac{\cos\theta_W}{1+\varepsilon^2} & \varepsilon\frac{\cos\theta_W}{1+\varepsilon^2} \\ \frac{\cos\theta_W(1+\varepsilon^2)}{1+\varepsilon^2} & -\frac{\sin\theta_W}{1+\varepsilon^2} & \varepsilon\frac{\sin\theta_W}{1+\varepsilon^2} \\ 0 & \frac{\varepsilon}{1+\varepsilon^2} & \frac{1}{1+\varepsilon^2} \end{pmatrix} \begin{pmatrix} A_\mu \\ Z_\mu \\ Z'_\mu \end{pmatrix} \tag{5.5}$$

which relates the interaction and the mass eigenstates. Substituting these expression in the covariant derivative we obtain

$$\begin{aligned} \hat{D}_\mu = \Bigg[& \partial_\mu - iA_\mu\left(g_2 T_3 \sin\theta_W + g_Y\cos\theta_W\frac{\hat{Y}}{2}\right) - ig_2\left(W^-_\mu T^- + W^+_\mu T^+\right) \\ & -iZ_\mu\left(g_2\cos\theta_W T_3 - g_Y\sin\theta_W\frac{\hat{Y}}{2} + g_z\varepsilon\frac{\hat{z}}{2}\right) \\ & -iZ'_\mu\left(-g_2\cos\theta_W T_3\varepsilon + g_Y\sin\theta_W\frac{\hat{Y}}{2}\varepsilon + g_z\frac{\hat{z}}{2}\right)\Bigg] \end{aligned} \tag{5.6}$$

where we have neglected all the $O(\varepsilon^2)$ terms. In the limit $g_z \to 0$ and $\varepsilon \to 0$ we obtain the SM expression. The vector and the axial-vector couplings of the Z and Z' to the fermions are expressed equivalently in terms of the left - (z_L) and right - (z_R) $U(1)_z$ chiral charges and hypercharges (Y_R, Y_L) of the models that we have implemented. These can be found in [107] for the free fermionic case and in [145] for the remaining models with a V-A structure given by

$$\begin{aligned} \frac{-ig_2}{4c_w}\gamma^\mu g_V{}^{Z,j} &= \frac{-ig_2}{c_w}\frac{1}{2}\left[c_w^2 T_3^{L,j} - s_w^2\left(\frac{\hat{Y}^j_L}{2} + \frac{\hat{Y}^j_R}{2}\right) + \varepsilon\frac{g_z}{g_2}c_w\left(\frac{\hat{z}_{L,j}}{2} + \frac{\hat{z}_{R,j}}{2}\right)\right]\gamma^\mu \\ \frac{-ig_2}{4c_w}\gamma^\mu\gamma^5 g_A{}^{Z,j} &= \frac{-ig_2}{c_w}\frac{1}{2}\left[-c_w^2 T_3^{L,j} - s_w^2\left(\frac{\hat{Y}^j_R}{2} - \frac{\hat{Y}^j_L}{2}\right) + \varepsilon\frac{g_z}{g_2}c_w\left(\frac{\hat{z}_{R,j}}{2} - \frac{\hat{z}_{L,j}}{2}\right)\right]\gamma^\mu\gamma^5 \\ \frac{-ig_2}{4c_w}\gamma^\mu g_V{}^{Z',j} &= \frac{-ig_2}{c_w}\frac{1}{2}\left[-\varepsilon c_w^2 T_3^{L,j} + \varepsilon s_w^2\left(\frac{\hat{Y}^j_L}{2} + \frac{\hat{Y}^j_R}{2}\right) + \frac{g_z}{g_2}c_w\left(\frac{\hat{z}_{L,j}}{2} + \frac{\hat{z}_{R,j}}{2}\right)\right]\gamma^\mu \\ \frac{-ig_2}{4c_w}\gamma^\mu\gamma^5 g_A{}^{Z',j} &= \frac{-ig_2}{c_w}\frac{1}{2}\left[\varepsilon c_w^2 T_3^{L,j} + \varepsilon s_w^2\left(\frac{\hat{Y}^j_R}{2} - \frac{\hat{Y}^j_L}{2}\right) + \frac{g_z}{g_2}c_w\left(\frac{\hat{z}_{R,j}}{2} - \frac{\hat{z}_{L,j}}{2}\right)\right]\gamma^\mu\gamma^5, \end{aligned} \tag{5.7}$$

where j is an index which represents the quark or the lepton and we have set $\sin\theta_W = s_w, \cos\theta_W = c_w$ for brevity.

5.2.1 An anomalous extra Z'

In the presence of anomalous interactions we can use the same formalism developed so far for anomaly-free models with some appropriate changes. Since the effective Lagrangian of the class of the anomalous models that we are investigating includes both a Stückelberg and a two-Higgs doublet sector, the masses of the neutral gauge bosons are provided by a combination of these two mechanisms, as can be clearly understood from the expressions of M_Z and $M_{Z'}$ in Eqs. (2.181). In this case we have as free parameters the Stüeckelberg mass M_1 and the anomalous coupling constant g_B, with $\tan\beta$ as in the remaining anomaly-free models. As we have already stressed, the analysis does not depend significantly on the choice of this parameter. The value of the Stückelberg mass M_1 is loosely constrained by the D-brane model in terms of suitable wrapping numbers (n) of the 4-branes which define the charge embedding

	Q_L	u_R	d_R	L	e_R	N_R
q_Y	1/6	- 2/3	1/3	-1/2	1	0
q_B	-1	0	0	-1	0	0

Table 5.1: Fermion spectrum charges in the Y-basis for the Madrid Model [64].

[64, 93] reported in Tabs. 3.1, 3.2, 3.3 of Sec. 3.8 and Tab. 5.1. As shown in Sec. 2.9, the physical gauge fields are obtained from the hypercharge basis by means of the rotation matrix O^A which can be approximated at the first order as

$$O^A \simeq \begin{pmatrix} \frac{g_Y}{g} & \frac{g_2}{g} & 0 \\ \frac{g_2}{g} + O(\epsilon_1^2) & -\frac{g_Y}{g} + O(\epsilon_1^2) & \frac{g}{2}\epsilon_1 \\ -\frac{g_2}{2}\epsilon_1 & \frac{g_Y}{2}\epsilon_1 & 1 + O(\epsilon_1^2) \end{pmatrix} \tag{5.8}$$

which is the analogue of the matrix in Eq. (5.2) for the anomaly-free models, but here the role of the mixing parameter ϵ_1 is taken by the expression

$$\epsilon_1 = \frac{x_B}{M_1^2}. \tag{5.9}$$

A relation between the two expansion parameters can be easily obtained in an approximate way by a direct comparison. For simplicity we take all the charges to be O(1) in all the models obtaining

$$\begin{aligned} &M_Z^2 \sim g_2^2 v^2 \\ &M_{Z'}^2 - M_Z^2 \sim g_z^2 v_\phi^2 \\ &\delta M_{ZZ'}^2 \sim g_2 g_z v^2 \end{aligned} \tag{5.10}$$

giving

$$\epsilon_1 \sim \frac{v^2}{M_1^2}, \tag{5.11}$$

which is the analogue of Eq. (5.9), having identified the Stückelberg mass with the v.e.v. of the extra singlet Higgs, $M_1 \sim g_z v_\phi$. This is natural since the Stückelberg mechanism can be thought of as the low energy remnant of an extra Higgs whose radial fluctuations have been frozen and with the imaginary phase surviving at low energy as a CP-odd scalar [13]. Concerning the charge assignments, the corresponding model is obtained form the intersection of four branes (a, b, c, d) with generators (q_a, q_b, q_c, q_d) which are rotated to the hypercharge basis, with an anomaly free hypercharge. The identification of the generators involve the solution of some constraint equations, solutions which for a T^6 compactification are parametrized by a phase $\epsilon = \pm 1$; the Neveu-Schwarz background on the first two tori $\beta_i = 1 - b_i = 1, 1/2$, four integers $n_{a2}, n_{b1}, n_{c1}, n_{d2}$, which are the wrapping numbers of the branes around the extra (toroidal) manifolds of the compactification, and a parameter $\rho = 1, 1/3$, with an additional constraint in order to obtain the correct massless hypercharge. One of the choice for these parameters is reported in Tab. 3.1 of Sec. 3.8.

5.3 The GS and WZ vertices and gluon fusion

As we have mentioned above in the previous sections, the two available mechanisms that enforce at the level of the effective Lagrangian the cancellation of the anomalies involve either PQ-like (axion-like)

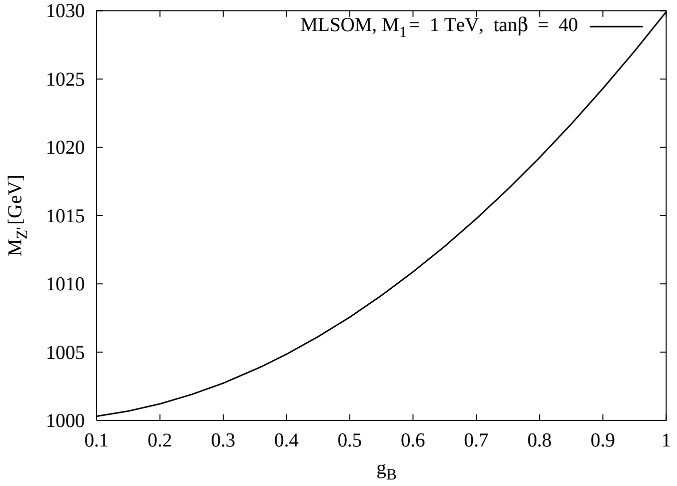

Figure 5.1: Anomalous $M_{Z'}$ as a function of the coupling g_B.

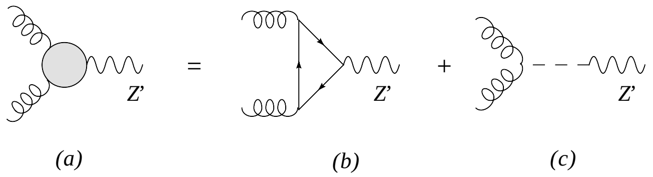

Figure 5.2: A gauge invariant GS vertex of the AVV type, composed of an AVV triangle and a single counterterm of the Dolgov-Zakharov form.

interactions - in the WZ case - or the subtraction of the anomaly pole (for the GS case). In the GS case, the anomaly of a given diagram is removed by subtracting the longitudinal pole of the triangle amplitude in the chiral limit. We have stressed that the counterterm (the pole subtraction) amounts to the removal of one of the invariant amplitudes of the anomaly vertex (the longitudinal component) and corresponds to a vertex re-definition.

The procedure is exemplified in Fig. 5.2 where we show the triangle anomaly and the pole counterterm which is subtracted from the first amplitude. The combination of the two contributions defines the GS vertex, which is made of purely transverse components in the chiral limit [98] and satisfies an ordinary WI. Notice that the vertex does not require an axion as an asymptotic state in the related S-matrix; for a non-zero fermion mass in the triangle diagram, the vertex satisfies a broken WI. We now proceed and summarize some of these properties, working in the chiral limit.

Processes such as $gg \to \gamma\gamma$, mediated by an anomalous gauge boson Z', can be expressed in a simplified form in which only the longitudinal component of the anomaly appears. We therefore set $k_1^2 = k_2^2 = 0$ and $m_f = 0$, which are the correct kinematical conditions to obtain the anomaly pole, necessary for a parton model (factorized) description of the cross section in a pp collision at the LHC, where the initial state of the partonic hard-scatterings are on-shell.

We start from the Rosenberg form of the AVV amplitude, which is given by

$$\begin{aligned} T^{\lambda\mu\nu} &= A_1\epsilon[k_1,\lambda,\mu,\nu] + A_2\epsilon[k_2,\lambda,\mu,\nu] + A_3 k_1^{\mu}\epsilon[k_1,k_2,\nu,\lambda] \\ &+ A_4 k_2^{\mu}\epsilon[k_1,k_2,\nu,\lambda] + A_5 k_1^{\nu}\epsilon[k_1,k_2,\mu,\lambda] + A_6 k_2^{\nu}\epsilon[k_1,k_2,\mu,\lambda]\,, \end{aligned} \tag{5.12}$$

and imposing the Ward Identities to bring all the anomaly on the axial-vector vertex, we obtain the usual conditions

$$\begin{aligned}
A_1 &= k_2^2 A_4 + k_1 \cdot k_2 A_3 \\
A_2 &= k_1^2 A_5 + k_1 \cdot k_2 A_6 \\
A_3(k_1, k_2) &= -A_6(k_1, k_2) \\
A_4(k_1, k_2) &= -A_5(k_1, k_2),
\end{aligned} \tag{5.13}$$

where the invariant amplitudes $A_3, \ldots, A_6$ are free from kinematical singularities for off-shell external lines. We set $k^2 = (k_1 + k_2)^2 = s$. As we have mentioned, in the parton model we take the initial gluons to be on-shell, while the hadronic cross section is obtained by convoluting the hard scattering given above (corrected by a color factor) with the PDF's. The amplitude simplifies drastically in this case and takes the form

$$T^{\mu\nu\lambda} = A_6 k^\lambda \epsilon[k_1, k_2, \nu, \mu] + (A_4 + A_6) \left(k_2^\nu \epsilon[k_1, k_2, \mu, \lambda] - k_1^\mu \epsilon[k_1, k_2, \nu, \lambda]\right), \tag{5.14}$$

in which the second piece drops off for physical on-shell photon/gluon lines, leaving only a single invariant amplitude to contribute to the final result

$$T^{\mu\nu\lambda} = A_6^f(s)(k_1 + k_2)^\lambda \epsilon\left[k_1, k_2, \nu, \mu\right] \tag{5.15}$$

where

$$A_6^f(s) = \frac{1}{2\pi^2 s}\left(1 + \frac{m_f^2}{s}\log^2\frac{\rho_f + 1}{\rho_f - 1}\right), \qquad \rho_f = \sqrt{1 - 4\frac{m_f^2}{s}}, \quad s < 0. \tag{5.16}$$

The anomaly pole is given by the first term of Eq. (5.16)

$$T_c^{\mu\nu\lambda} \equiv \frac{1}{2\pi^2 s}(k_1 + k_2)^\lambda \epsilon\left[k_1, k_2, \nu, \mu\right]. \tag{5.17}$$

The logarithmic functions in the expression above are continued in the following way in the various region

$$\begin{aligned}
& 0 < s < 4m_f^2 : \\
& \rho_f \to i\sqrt{-\rho_f^2}; \qquad \frac{1}{2}\log\left(\frac{\rho_f + 1}{\rho_f - 1}\right) \to -i\arctan\frac{\sqrt{s}}{\sqrt{4m_f^2 - s}}, \\
& s > 4m_f^2 > 0 : \\
& \sqrt{-\rho_f^2} \to -i\rho_f; \qquad \arctan\frac{1}{\sqrt{-\rho_f^2}} \to \frac{\pi}{2} + \frac{i}{2}\log\left(\frac{\sqrt{s - 4m_f^2} + \sqrt{s}}{\sqrt{s} - \sqrt{s - 4m_f^2}}\right).
\end{aligned} \tag{5.18}$$

Notice that the surviving amplitude A_6 multiplies a longitudinal momentum exchange and, as discussed in the literature on the chiral anomaly in QCD [103, 101], is characterized by a massless pole in s, which is the anomaly pole, as one can clearly conclude from Eq. (5.16). This equation shows also how chiral symmetry breaking effects appear in this amplitude at this special kinematical point by the m_f terms.

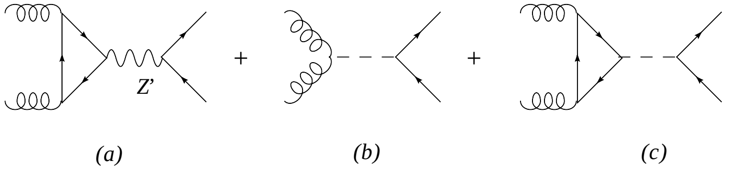

Figure 5.3: One loop vertices and counterterms for the WZ mechanism.

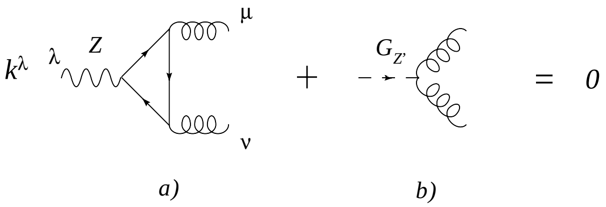

Figure 5.4: WI in the WZ case in the chiral limit.

The subtraction of the anomaly pole is shown in Fig. 5.2 and is represented by diagram c). The combination of diagrams b) and c) defines the GS vertex of the theory [98], with diagram c) described by Eq. (5.17) ($-T_c$). It is easily verified that in the massless fermion limit and for on-shell gluon lines, the GS vertex is trivially vanishing by construction. In general, for any asymmetric configuration of the external lines in the vertex, even in the massless limit, the vertex has non-zero transverse components [119, 120]. The expression is well known [123, 120] in the chiral limit and has been shown to satisfy the Adler-Bardeen theorem [120].

For a non-vanishing m_f the GS vertex, for generic virtualities, can be defined to be the general AVV vertex, for instance extracted from [86] or, in the longitudinal/transverse formulation, by the amplitudes given in [120], with the subtraction of the anomaly pole, as given in [98]. We will refer to the anomaly (subtraction) counterterm of diagram b) as to the Dolgov-Zakharov [101] (DZ) counterterm. The anomaly diagram reduces to its DZ form for two on-shell gauge lines (photons/gluons) and in this case the transverse components completely disappear. There are other cases in which, instead, the longitudinal components cancel. This occurs if, for instance, a conserved current is attached to the anomalous line, rendering the anomaly "harmless", as explained in [98].

The analogous interaction in the WZ case is shown in Fig. 5.3, where we have attached a fermion pair in the final state to better identify the contributions. In this case, beside the anomalous contribution of diagram a), the mechanism will require the exchange of a physical axion, shown in diagram b) and c). Diagram b) is the usual WZ counterterm (or generalized PQ interaction) while the third diagram is non-vanishing only in the presence of fermions of non-zero mass. This third contribution is numerically irrelevant and in DY is usually omitted. The WZ mechanism re-establish gauge invariance of the effective Lagrangian but is not based on a vertex re-definition and, furthermore, involves an asymptotic axion state. As shown in Chap. 3 the presence of a unitarity bound in this mechanism is a signal of its limitation as an effective theory (see also the discussion in [98]). We have summarized in an appendix the discussion of this point in a simple case.

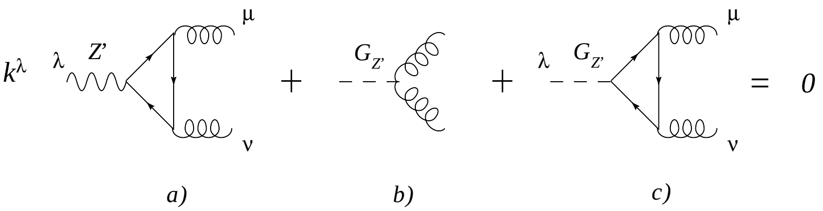

Figure 5.5: Generalized WI in the WZ case.

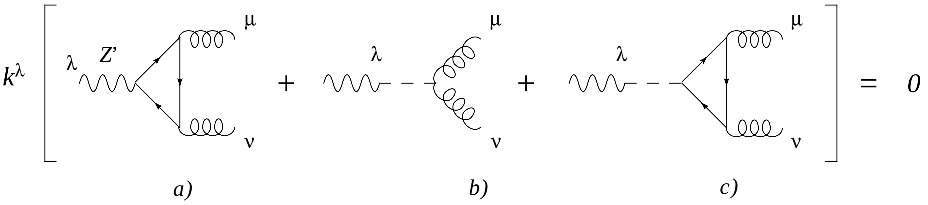

Figure 5.6: Generalized WI in the GS case.

5.3.1 Ward Identities

Both vertices satisfy ordinary Ward Identities in the chiral limit and generalized Ward Identities away from it. In the chiral limit, for instance, the WZ mechanism adds to the effective action of the anomalous theory an interaction of the Stückelberg field (b) with the gluons ($b\,G \wedge G$), shown in diagram b) of Fig. 5.4. In this figure we have shown a diagrammatic realization of the WI for this case.

In WZ, being the cancellation based on a local field theory, the derivation of the generalized WI can be formally obtained from the requirement of BRST invariance of the gauge-fixed effective action, as shown in [92]. This is illustrated in Fig. 5.5, in the case of an anomalous Z', where we show the coupling of the Goldstone - in the broken Higgs phase - to the gluons (diagram b)) and to the massive fermion (diagram c)) [92]. The normalization of the counterterm in b) can be chosen to remove the anomaly of diagram a) when a single fermion runs inside the anomaly loop. Alternatively, the same graphical representation holds if in the first and the last diagram we sum over the entire generation. In this case the counterterm is normalized to cancel the entire anomaly of the complete vertex. The analysis in the GS case is slightly more subtle. We show in Fig. 5.6 the generalized WI satisfied by the vertex in the massive case. In the massless case only diagrams a) and b) survive, while the contribution of diagram c) comes from a direct computation. It is obtained by multiplying typical pseudoscalar interaction - such as the one shown in Fig. 5.5, diagram c) - by a massless pole. If we denote by $T^{\mu\nu}$ the diagram describing the decay of a pseudoscalar into two gluons, diagram c) takes the form $k^\lambda/k^2 T_{\mu\nu}$, with a factorized pole on the anomalous external line. We refer to [98] for a detailed discussion of these points.

In our analysis we encounter a class of BIM amplitudes which are characterized by two anomaly vertices connected by an s-channel exchange of the anomalous gauge boson. These amplitudes grow quadratically with the energy and are not eliminated by fine tuning Fig. 5.7. The true BIM amplitude is the one shown in diagram b) and appears in the gluon fusion sector in the WZ case. In the SM a similar graph contributes only if heavy fermions run in the loop. They are comparable in size to the anomalous BIM amplitude. Obviously, this contribution would be identically vanishing if all the fermions of a given generation would be mass-degenerate.

Diagram a) shown in the same figure, instead, is the GS version of the BIM amplitude and is identically

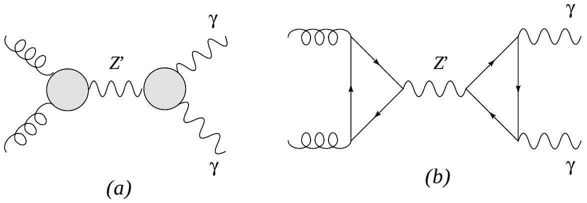

Figure 5.7: BIM amplitude with an anomalous Z' exchange.

zero in the chiral limit for on-shell gluon lines, as is the case in the parton model. For this reason the gluon fusion sector disappears completely for DP (in the GS mechanism), since the BIM amplitude in this case is obtained by replacing diagram b) of this figure with diagram a) which is indeed vanishing.

We can summarize the basic features of the anomalous sectors in anomaly free-models after QCD factorization, for generic virtualities of the external gauge lines, according to the following points:

1) In the SM the residual contributions coming from anomalous diagrams, such as in the VVZ, VVZ' vertices, where V is a gauge field, are proportional to the mass of the heavy quarks in the anomaly loop. In the chiral limit, instead, both the anomaly pole contribution and the transverse component of the anomaly cancel by charge assignment.

2) In the GS case, as we have just discussed, the anomaly pole is absent by definition, while the transverse contributions are allowed. This separation between longitudinal and transverse components is less transparent for a heavy fermion mass, which induce a longitudinal component, proportional to m_f^2/s^2 times a small logarithmic correction of the ratio of the same variables, away from the chiral limit. This longitudinal component, however, should not be confused with the anomaly pole and *is not shifted or corrected* perturbatively in any way. It can couple, for instance, to a $t\bar{t}$ (top) quark current because of a broken WI and can be interpreted as a manifestation of the GS mechanism at the LHC, but can be easily overshadowed by SM contributions. This point will be re-addressed more formally below in Eq. (5.27).

At some special kinematical points (two massless gauge lines, or three massless gauge lines of the same virtualities) where the anomalous vertex takes its DZ form, the GS vertex is identically vanishing in the massless case. In the presence of a heavy fermion the logarithmic correction shown in Eq. (5.16) reappears.

3) In the WZ case the anomaly pole is not cancelled. A second sector (the exchange of the axion) is needed to restore the gauge invariance of the effective action. In a hadronic collision the BIM amplitudes induce very small deviations from the SM behavior after the convolution with the gluon density. They are absent in DY at NNLO. In DP they affect the invariant mass distributions - at large Q - of the photon pair, for a given center of mass energy of the two colliding protons. As such they are sensitive to large (Bjorken) x-values of the gluon PDF's, region where the gluon density is rapidly decreasing. In particular, in DP their contribution becomes more sizeable via intereference with some box-like amplitudes ($gg \to \gamma\gamma$). In previous NLO study of this process [43] they had been included even though they exceed the NLO accuracy, being truly NNLO contributions. These amplitudes and vertices are the basic building blocks of our numerical analysis and are responsible for all the anomalous signal both in DY and in DP. We will quantify their impact in the invariant mass distributions in both cases.

5.4 Invariant mass distributions in Drell-Yan

Our NNLO analysis of the invariant mass distributions for lepton pair production, for the computation of the QCD sectors, is based on the hard scatterings of Ref. [144], and the NNLO evolution of the parton distributions (PDF's) has been obtained with CANDIA 1.0 [104]. The anomalous corrections to the invariant mass distributions have been evaluated separately, since at NNLO they appear in DY in the interference with the lowest order graph, and added to the standard QCD background. It is important to recall that lepton pair production at low Q via Drell-Yan is sensitive to the PDF's at small-x values, while in the high mass region this process is essential in the search of additional neutral currents. In our analysis we have selected a mass of 1 TeV for the extra gauge boson and analyzed the signal and the background both on the peaks of the Z and of the of the new resonance.

At hadron level the colour-averaged inclusive differential cross section for the reaction $H_1 + H_2 \to l_1 + l_2 + X$, is given by the expression [144]

$$\frac{d\sigma}{dQ^2} = \tau\sigma_{\mathcal{Z}}(Q^2, M^2_{\mathcal{Z}})W_{\mathcal{Z}}(\tau, Q^2) \qquad \tau = \frac{Q^2}{S}, \tag{5.19}$$

where $\mathcal{Z} \equiv Z, Z'$ is the point-like cross section and all the information from the hadronic initial state is contained in the PDF's. The hadronic structure function $W_{\mathcal{Z}}(\tau, Q^2)$ is given by a convolution product between the parton luminosities $\Phi_{ij}(x, \mu_R^2, \mu_F^2)$ and the Wilson coefficients $\Delta_{ij}(x, Q^2, \mu_R^2, \mu_F^2)$

$$W_{\mathcal{Z}}(\tau, Q^2, \mu_R^2, \mu_F^2) = \sum_{i,j}\int_\tau^1 \frac{dx}{x}\Phi_{ij}(x, \mu_R^2, \mu_F^2)\Delta_{ij}(\frac{\tau}{x}, Q^2, \mu_F^2), \tag{5.20}$$

where the luminosities are given by

$$\Phi_{ij}(x, \mu_R^2, \mu_F^2) = \int_x^1 \frac{dy}{y} f_i(y, \mu_R^2, \mu_F^2) f_j\left(\frac{x}{y}, \mu_R^2, \mu_F^2\right) \equiv [f_i \otimes f_j](x, \mu_R^2, \mu_F^2) \tag{5.21}$$

and the Wilson coefficients (hard scatterings) depend on both the factorization (μ_F) and renormalization scales (μ_R), formally expanded in the strong coupling α_s as

$$\Delta_{ij}(x, Q^2, \mu_F^2) = \sum_{n=0}^{\infty} \alpha_s^n(\mu_R^2)\Delta_{ij}^{(n)}(x, Q^2, \mu_F^2, \mu_R^2). \tag{5.22}$$

We will vary μ_F and μ_R independently in order to determine the sensitivity of the prediciton on their variations and their optimal choice.

The anomalous corrections to the hard scatterings computed in the SM will be discussed below. We just recall that the relevant point-like cross sections appearing in the factorization formula (5.19) and which are part of our analysis include, beside the Z and the Z' resonance, also the contributions due to the photon and the $\gamma - Z$, $\gamma - Z'$ interferences. For instance in the Z' case we have

$$\sigma_\gamma(Q^2) = \frac{4\pi\alpha_{em}^2}{3Q^4}\frac{1}{N_c}$$

$$\sigma_{Z'}(Q^2) = \frac{\pi\alpha_{em}}{4M_{Z'}\sin^2\theta_W\cos^2\theta_W N_c}\frac{\Gamma_{Z'\to\bar{l}l}}{(Q^2 - M_{Z'}^2)^2 + M_{Z'}^2\Gamma_{Z'}^2}$$

$$\sigma_{Z',\gamma}(Q^2) = \frac{\pi\alpha_{em}^2}{6N_c}\frac{g_V^{Z',l}g_V^{\gamma,l}}{\sin^2\theta_W\cos^2\theta_W}\frac{(Q^2 - M_{Z'}^2)}{Q^2(Q^2 - M_{Z'}^2)^2 + M_{Z'}^2\Gamma_{Z'}^2},$$

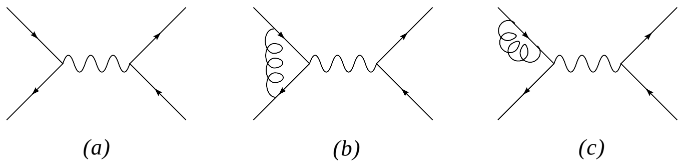

Figure 5.8: $q\bar{q} \to Z, Z'$ at LO and NLO (virtual corrections).

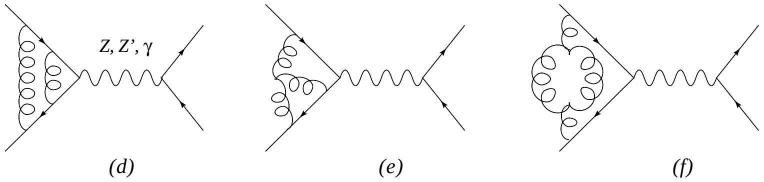

Figure 5.9: $q\bar{q} \to Z, Z'$ at NNLO (virtual corrections).

$$\sigma_{Z',Z}(Q^2) = \frac{\pi \alpha_{em}^2}{96} \frac{\left[g_V^{Z',l} g_V^{Z,l} + g_A^{Z',l} g_A^{Z,l}\right]}{\sin^4\theta_W \cos^4\theta_W N_c} \frac{(Q^2 - M_Z^2)(Q^2 - M_{Z'}^2) + M_Z \Gamma_Z M_{Z'} \Gamma_{Z'}}{\left[(Q^2 - M_{Z'}^2)^2 + M_{Z'}^2 \Gamma_{Z'}^2\right]\left[(Q^2 - M_Z^2)^2 + M_Z^2 \Gamma_Z^2\right]}. \tag{5.23}$$

where N_C is the number of colours, $\Gamma_{Z' \to \bar{l}l}$ is the partial decay width of the gauge boson and the total hadronic widths are defined by

$$\begin{aligned} \Gamma_Z &\equiv \Gamma(Z \to hadrons) = \sum_i \Gamma(Z \to \psi_i \bar{\psi}_i), \\ \Gamma_{Z'} &\equiv \Gamma(Z' \to hadrons) = \sum_i \Gamma(Z' \to \psi_i \bar{\psi}_i), \end{aligned} \tag{5.24}$$

where we refer to hadrons not containing bottom and top quarks (i.e. $i = u, d, c, s$). We also ignore electroweak corrections of higher-order and we have included the top-quark mass and QCD corrections. We have included only tree level decays into SM fermions, with a total decay rate for the Z and Z' which is given by

$$\Gamma_Z = \sum_{i=u,d,c,s} \Gamma(Z \to \psi_i \bar{\psi}_i) + \Gamma(Z \to b\bar{b}) + 3\Gamma(Z \to l\bar{l}) + 3\Gamma(Z \to \nu_l \bar{\nu}_l), \tag{5.25}$$

$$\Gamma_{Z'} = \sum_{i=u,d,c,s} \Gamma(Z' \to \psi_i \bar{\psi}_i) + \Gamma(Z' \to b\bar{b}) + \Gamma(Z' \to t\bar{t}) + 3\Gamma(Z' \to l\bar{l}) + 3\Gamma(Z' \to \nu_l \bar{\nu}_l). \tag{5.26}$$

Coming to illustrate the contributions included in our analysis, these are shown in some representative graphs. The complete NNLO expressions of the hard scatterings and the corresponding Feynman diagrams can be found in [144].

- **SM QCD contributions**

We show in Fig. 5.8 the leading $O(\alpha_w)$ and some typical next-to-leading order $O(\alpha_w \alpha_s)$ (LO, NLO) contributions to the process in the annihilation channel (virtual corrections). Examples of higher-order virtual corrections included in the hard scatterings are shown in Fig. 5.9, which are of $O(\alpha_s^2 \alpha_w)$, while the corresponding real emissions, integrated over the final state gluons, are shown in Fig. 5.10 at NLO (graph g)) and NNLO (graphs h) and i)).

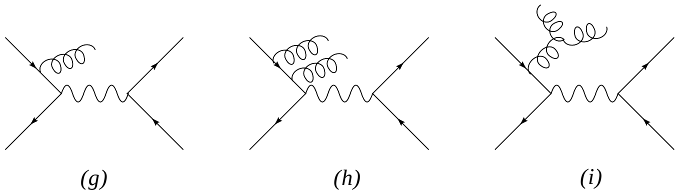

Figure 5.10: $q\bar{q} \to Z, Z'$ with real corrections at NLO (g) and at NNLO (h), (i).

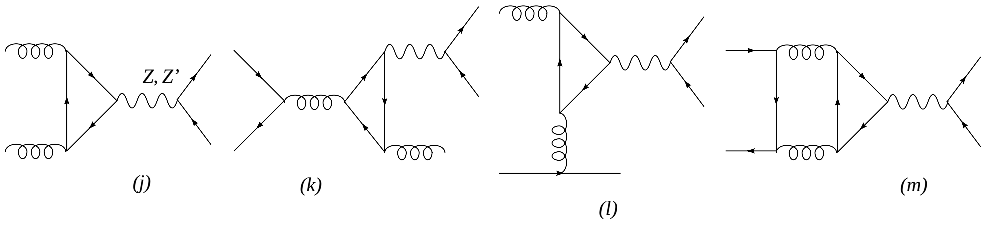

Figure 5.11: Anomalous contributions for Z' production in the gg, $q\bar{q}$ and qg sectors at lower orders.

- **Anomalous corrections**

We show in Fig. 5.11 the leading anomalous corrections to leptoproduction. At $O(\alpha_s\alpha_w)$ there is a first contribution coming from the interference between graph j) and the leading order $q\bar{q}$ annihilation vertex (graph a) of Fig. 5.8. The square of the same graph appears in the anomalous corrections at $O(\alpha_s^2\alpha_w)$. Other contributions that we have included are those due to the exchange of a physical axion and Goldstone modes, which can be removed in the unitary gauge. Of higher order are the contributions shown in diagram k), l) and n), which contribute via their interference with NLO tree level graphs. For instance k) interferes with diagram g) of Fig. 5.10, while m) interferes with the LO annihilation graph. The analogous contributions in the WZ and GS cases are obtained by replacing the triangle graph with the GS vertex, as in Fig. 5.2, or, for the WZ case, with Fig. 5.3. Notice that in Fig. 5.3, in the WZ case the anomaly pole is automatically cancelled by the WI on the lepton pair of the final state, if the two leptons are taken to be massless at high energy, as is the case. Then, the only new contributions from the anomaly vertex that survive are those related to the transverse component of this vertex. This is an example, as we have discussed in [98], of a "harmless" anomaly vertex. A similar situation occurs whenever there is no coupling of the longitudinal component of the anomaly to the (transverse) external leptonic current. This property continues to hold also away from the chiral limit, since the corrections due to the fermion mass in the anomaly have the typical structure

$$\Delta_{\mu\nu\rho}(q,k)_{\text{anomaly}} = \sum_f g^{Z'}_{A,f} e^2 Q_f^2 a_n \frac{(q-k)_\nu}{(q-k)^2}\left(\frac{1}{2} - 2m_f^2 C_0\right)\epsilon_{\mu\rho\alpha\beta}q^\alpha k^\beta + \tilde{\Delta}^{trans}\,, \tag{5.27}$$

where $\tilde{\Delta}^{trans}$ is the truly transversal component away from the chiral limit. The most general expression of the coefficient C_0 is given in Eq. (A.8) of ref. [86]. C_0 is the scalar three-point function with a fermion of mass m_f circulating in the loop. In both mechanisms anomaly (strictly massless) effects are comparable with the corresponding contributions coming from the SM for massive fermions. It should be clear by now that in the WZ case the anomaly pole is not cancelled, rather an additional exchange is necessary to re-establish the gauge independence of the S-matrix (the axion). In DY this sector does not play a significant role due to the small mass of the lepton pair. As we have discussed above, the cancellation of

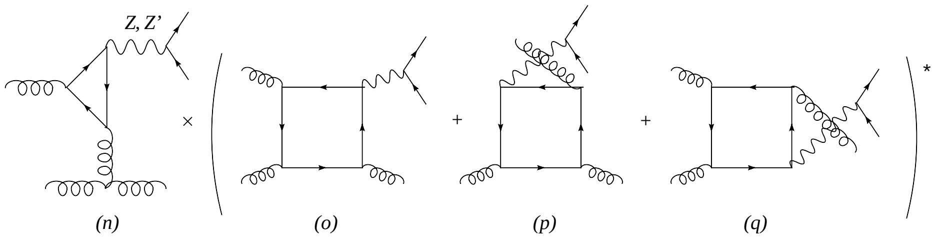

Figure 5.12: Anomalous contributions for the $gg \to gg$ process mediated by an anomalous Z' at higher perturbative orders.

the anomaly is due, in this case, to the WI of the leptonic current and there is no axion exchanged in the s-channel.

5.4.1 Precision studies on the Z resonance

The quantification of the corrections due to anomalous Abelian gauge structures in DY requires very high precision, being these of a rather high order. For this reason we have to identify all the sources of indeterminations in QCD which come from the factorization/renormalization scale dependence of the cross section, keeping into account the dependence on μ_F and μ_R *both* in the DGLAP evolution *and* in the hard scatterings. The set-up of our analysis is similar to that used for a study of the NNLO DGLAP evolution in Refs. [85, 146], where the study has covered every source of theoretical error, including the one related to the various possible resummations of the DGLAP solution, which is about $2-3\%$ in DY and would be sufficient to swamp away any measurable deviation due to new physics at the LHC.

These previous studies have been focused on the DY distributions on the resonance peaks, in particular on the peak of the Z, where the accuracy at the LHC is of outmost importance for QCD partonometry. The presence of anomalous corrections on the Z peak is due both to the anomalous components of the Z in the anomalous models and to the interference between the Z' and the Z, that we have taken into account. Notice that in DY the treatment of the anomalous corrections to the Z is drastically simplified if we neglect the (small) mass of the lepton pair, as usual. In fact, these are due to trilinear (anomaly) vertices which involve the BBB, BYY, BW_3W_3 and BGG gauge fields - in the interaction basis - all of them involving interactions of the Stückelberg field with the corresponding field-strengths of the gauge fields, such as $bF_B \wedge F_B$, $bF_Y \wedge F_Y$, $bF_W \wedge F_W$ and $bF_G \wedge F_G$, where G denotes the gluon field. The only contribution that is relevant for the LHC is then one obtained by projecting the $bF_G \wedge F_G$ vertex on the physical axion χ, whose mass is, in principle, a free parameter of the anomalous models. It is then clear that the axion channel plays a more important role in the production of the *top*, due to its large mass, than in leptoproduction. We will now briefly summarize the results for the new contributions in DY, starting from the non-anomalous ones.

In the $q\bar{q}$ sector we have two contributions involving triangle fermion loops see Fig. 5.11 k,m. The one depicted in Fig. 5.11m is a two-loop virtual correction with a Z or a Z' boson in the final state, while in Fig. 5.11k we have a real emission of a gluon in the final state which is integrated out. The first contribution has been calculated in [118, 147, 148, 149],

$$\begin{aligned}\Delta^{V}_{q\bar{q}}(x, Q^2, \mu_F^2, m^2) = \delta(1-x) a_q^{Z'} a_Q^{Z'} C_F T_f \frac{1}{2}\left(\frac{\alpha_s}{\pi}\right)^2 \times \\ \big[\theta(Q^2-4m^2) G_1(m^2/Q^2) + \theta(4m^2-Q^2) G_2(m^2/Q^2)\big)\end{aligned} \tag{5.28}$$

where C_F and T_f are the color factors, $q = u, d, c, s$, $Q = t, b$ and m the mass of the heavy flavors, while in the massless limit the functions G_1 and G_2 are given by

$$\begin{aligned} G_1(m=0) &= 3\log\left(\frac{Q^2}{\mu_R^2}\right) - 9 + 2\zeta(2) \\ G_2(m=0) &= 0 \end{aligned} \qquad (5.29)$$

and Q represents the invariant mass of the system. The contribution of Fig. 5.11k in the massless limit is given by

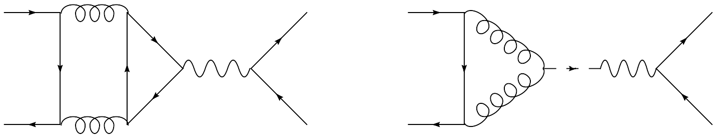
(a) (b)

Figure 5.13: GS mechanism: anomalous contribution and counterterm for the $q\bar{q}$ scattering sector.

$$\Delta^R_{q\bar{q}}(x, Q^2, \mu_F^2, m=0) = a_q^{Z'} a_Q^{Z'} C_F T_f \frac{1}{2}\left(\frac{\alpha_s}{\pi}\right)^2 \times \left\{\frac{(1+x)}{(1-x)_+}\left[-2 + 2x(1-\log(x))\right]\right\}, \qquad (5.30)$$

while in the qg sector we have the contribution shown in Fig. 5.11l which is given by

$$\begin{aligned} &\Delta_{qg}(x, Q^2, \mu_F^2, m^2) \\ &= a_q^{Z'} a_Q^{Z'} T_f^2 \frac{1}{2}\left(\frac{\alpha_s}{\pi}\right)^2 \times \left[\theta(Q^2 - 4m^2) H_1(x, Q^2, m^2) + \theta(4m^2 - Q^2) H_2(x, Q^2, m^2)\right] \end{aligned} \qquad (5.31)$$

with the massless limit of $H_1(x, Q^2, m^2)$ given by

$$\begin{aligned} &H_1(x, Q^2, m=0) \\ &= 2x\left[\log\left(\frac{1}{x}\right)\log\left(\frac{1}{x} - 1\right) + Li_2\left(1 - \frac{1}{x}\right)\right] + 2\left(1 - \frac{1}{x}\right)\left[1 - 2x\log\left(\frac{1}{x}\right)\right]. \end{aligned} \qquad (5.32)$$

Separating the anomaly-free from the anomalous contributions, the factorization formula for the invariant mass distribution in DY is given by

$$\frac{d\sigma}{dQ^2} = \tau\sigma_{\mathcal{Z}}(Q^2, M_{\mathcal{Z}}^2)\left\{W_{\mathcal{Z}}(\tau, Q^2) + W_{\mathcal{Z}}^{anom}(\tau, Q^2)\right\} \qquad (5.33)$$

$$W_{\mathcal{Z}}^{anom}(\tau, Q^2) = \sum_{i,j}\int_\tau^1 \frac{dx}{x}\Phi_{ij}(x, \mu_R^2, \mu_F^2)\Delta_{ij}^{anom}(\frac{\tau}{x}, Q^2, \mu_F^2) \qquad (5.34)$$

$$\begin{aligned} &\Delta_{ij}^{anom}(x, Q^2, \mu_F^2) \\ &= \Delta^V_{q\bar{q}}(x, Q^2, \mu_F^2, m=0) + \Delta^R_{q\bar{q}}(x, Q^2, \mu_F^2, m=0) + \Delta_{qg}(x, Q^2, \mu_F^2, m=0) \end{aligned} \qquad (5.35)$$

that we will be using in our numerical analysis below.

5.4.2 Di-lepton production: numerical results

We have used the MRST-2001 set of PDF's given in Refs. [150] and [151]. We start by showing in Fig. 5.14 various zooms of the differential cross section on the peak of the Z - for all the models - both at NLO and

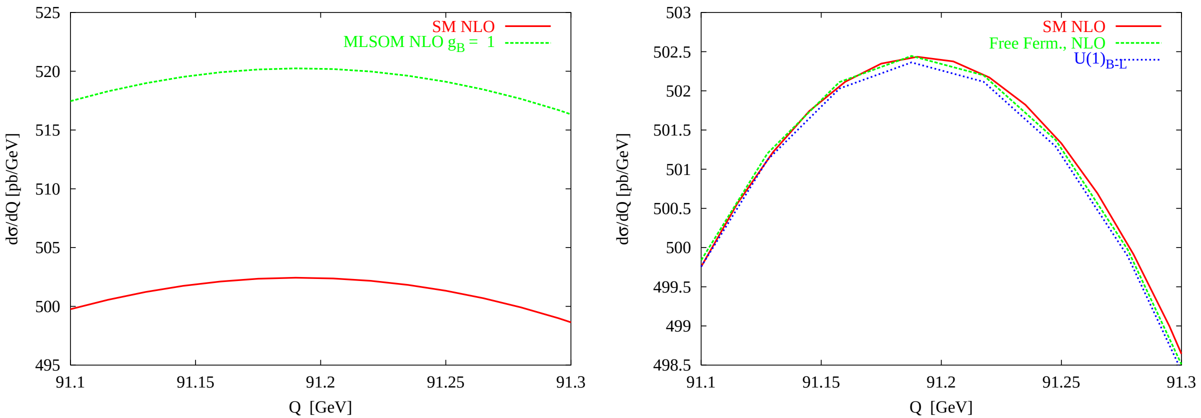

(a) SM vs mLSOM at NLO (b) SM vs Anomaly free models at NLO

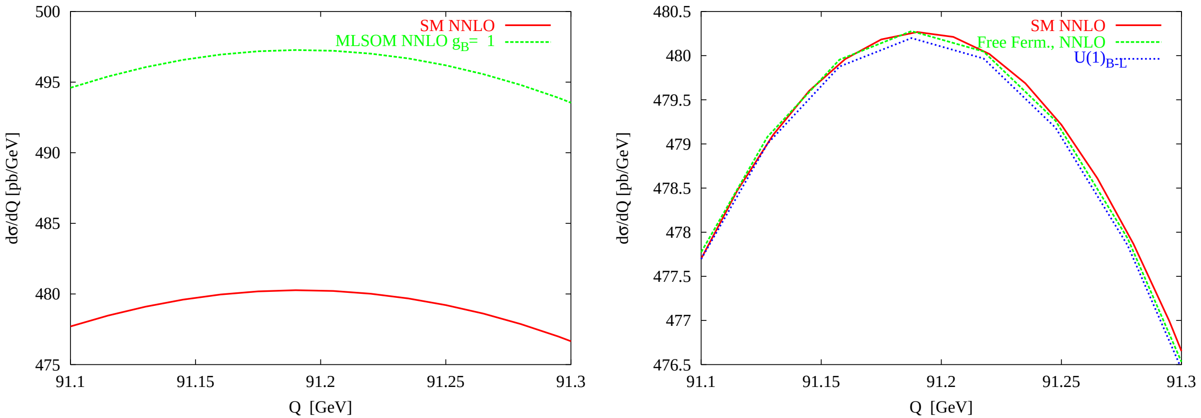

(c) SM vs mLSOM at NNLO (d) SM vs Anomaly free models at NNLO

Figure 5.14: Zoom on the Z resonance for anomalous Drell-Yan in the $\mu_F = \mu_R = Q$ at NLO/NNLO for all the models.

at NNLO. We have kept the factorization and renormalization scales coincident and equal to Q, while the mass of the extra Z' has been chosen around 1 TeV. The anomaly-free models, from the SM to the three Abelian extensions that we have considered (Free Fermionic [107] and $U(1)_{B-L}$ [145] in Fig. 5.14, while $U(1)_{q+u}$ appears in Tab. 5.4) show that the cross section is more enhanced for the mLSOM, illustrated in Fig. 5.14a, c. The plots show a sizeable difference (at a 3.5 % level) between the anomalous and all the remaining anomaly-free models. A comparison between (a) and (c) indicates, however, that this difference has to be attributed to the specific charge assignment of the anomalous model and not to the anomalous partonic sector, which is present in (c) but not in (a). The anomalous corrections in DY appear at NNLO and not at NLO, while in both figures the difference between the SM and the mLSOM remains almost unchanged.

Moving from NLO to NNLO the cross section is reduced. Defining the K-factor

$$\frac{\sigma_{NNLO} - \sigma_{NLO}}{\sigma_{NLO}} \equiv K_{NLO} \tag{5.36}$$

in the case of the mLSOM this factor indicates a reduction of about 4% on the peak and can be attributed to the NNLO terms in the DGLAP evolution, rather than to the NNLO corrections to the hard scatterings. This point can be explored numerically by the (order) variation [152, 85]

$$\Delta\sigma \quad \sim \quad \Delta\hat{\sigma} \otimes \phi + \hat{\sigma} \otimes \Delta\phi$$

$d\sigma^{nlo}/dQ$ [pb/GeV] for the mLSOM with $M_1 = 1$ TeV, $\tan\beta = 40$, Candia 1.0 evol.					
Q [GeV]	$g_B = 0.1$	$g_B = 0.36$	$g_B = 0.65$	$g_B = 1$	$\sigma^{SM}_{nlo}(Q)$
90.50	$3.8551 \cdot 10^{+2}$	$3.8711 \cdot 10^{+2}$	$3.9106 \cdot 10^{+2}$	$3.9902 \cdot 10^{+2}$	$3.8543 \cdot 10^{+2}$
90.54	$3.9712 \cdot 10^{+2}$	$3.9877 \cdot 10^{+2}$	$4.0284 \cdot 10^{+2}$	$4.1105 \cdot 10^{+2}$	$3.9704 \cdot 10^{+2}$
90.59	$4.0861 \cdot 10^{+2}$	$4.1030 \cdot 10^{+2}$	$4.1449 \cdot 10^{+2}$	$4.2294 \cdot 10^{+2}$	$4.0852 \cdot 10^{+2}$
90.63	$4.1988 \cdot 10^{+2}$	$4.2162 \cdot 10^{+2}$	$4.2592 \cdot 10^{+2}$	$4.3461 \cdot 10^{+2}$	$4.1979 \cdot 10^{+2}$
90.68	$4.3084 \cdot 10^{+2}$	$4.3263 \cdot 10^{+2}$	$4.3705 \cdot 10^{+2}$	$4.4596 \cdot 10^{+2}$	$4.3075 \cdot 10^{+2}$
90.99	$4.9041 \cdot 10^{+2}$	$4.9245 \cdot 10^{+2}$	$4.9749 \cdot 10^{+2}$	$5.0766 \cdot 10^{+2}$	$4.9031 \cdot 10^{+2}$
91.187	$5.0254 \cdot 10^{+2}$	$5.0463 \cdot 10^{+2}$	$5.0981 \cdot 10^{+2}$	$5.2024 \cdot 10^{+2}$	$5.0243 \cdot 10^{+2}$
91.25	$5.0143 \cdot 10^{+2}$	$5.0352 \cdot 10^{+2}$	$5.0869 \cdot 10^{+2}$	$5.1911 \cdot 10^{+2}$	$5.0133 \cdot 10^{+2}$
91.56	$4.6103 \cdot 10^{+2}$	$4.6296 \cdot 10^{+2}$	$4.6772 \cdot 10^{+2}$	$4.7732 \cdot 10^{+2}$	$4.6094 \cdot 10^{+2}$
91.77	$4.1178 \cdot 10^{+2}$	$4.1350 \cdot 10^{+2}$	$4.1776 \cdot 10^{+2}$	$4.2635 \cdot 10^{+2}$	$4.1170 \cdot 10^{+2}$
92.0	$3.5297 \cdot 10^{+2}$	$3.5444 \cdot 10^{+2}$	$3.5810 \cdot 10^{+2}$	$3.6547 \cdot 10^{+2}$	$3.5289 \cdot 10^{+2}$

Table 5.2: Invariant mass distributions at NLO for the mLSOM and the SM around the peak of the Z. The mass of the anomalous extra Z' is taken to be 1 TeV with $\mu_F = \mu_R = Q$.

$d\sigma^{nnlo}/dQ$ [pb/GeV] for the mLSOM with $M_1 = 1$ TeV, $\tan\beta = 40$, Candia 1.0 evol.					
Q [GeV]	$g_B = 0.1$	$g_B = 0.36$	$g_B = 0.65$	$g_B = 1$	$\sigma^{SM}_{nnlo}(Q)$
90.50	$3.6845 \cdot 10^{+2}$	$3.6997 \cdot 10^{+2}$	$3.7374 \cdot 10^{+2}$	$3.8132 \cdot 10^{+2}$	$3.6835 \cdot 10^{+2}$
90.54	$3.7956 \cdot 10^{+2}$	$3.8112 \cdot 10^{+2}$	$3.8500 \cdot 10^{+2}$	$3.9282 \cdot 10^{+2}$	$3.7945 \cdot 10^{+2}$
90.59	$3.9054 \cdot 10^{+2}$	$3.9215 \cdot 10^{+2}$	$3.9615 \cdot 10^{+2}$	$4.0419 \cdot 10^{+2}$	$3.9043 \cdot 10^{+2}$
90.63	$4.0132 \cdot 10^{+2}$	$4.0298 \cdot 10^{+2}$	$4.0708 \cdot 10^{+2}$	$4.1535 \cdot 10^{+2}$	$4.0121 \cdot 10^{+2}$
90.68	$4.1180 \cdot 10^{+2}$	$4.1351 \cdot 10^{+2}$	$4.1772 \cdot 10^{+2}$	$4.2621 \cdot 10^{+2}$	$4.1169 \cdot 10^{+2}$
90.99	$4.6879 \cdot 10^{+2}$	$4.7073 \cdot 10^{+2}$	$4.7554 \cdot 10^{+2}$	$4.8523 \cdot 10^{+2}$	$4.6866 \cdot 10^{+2}$
91.187	$4.8040 \cdot 10^{+2}$	$4.8239 \cdot 10^{+2}$	$4.8733 \cdot 10^{+2}$	$4.9727 \cdot 10^{+2}$	$4.8027 \cdot 10^{+2}$
91.25	$4.7935 \cdot 10^{+2}$	$4.8134 \cdot 10^{+2}$	$4.8627 \cdot 10^{+2}$	$4.9619 \cdot 10^{+2}$	$4.7922 \cdot 10^{+2}$
91.56	$4.4076 \cdot 10^{+2}$	$4.4259 \cdot 10^{+2}$	$4.4713 \cdot 10^{+2}$	$4.5628 \cdot 10^{+2}$	$4.4064 \cdot 10^{+2}$
91.77	$3.9371 \cdot 10^{+2}$	$3.9535 \cdot 10^{+2}$	$3.9941 \cdot 10^{+2}$	$4.0759 \cdot 10^{+2}$	$3.9360 \cdot 10^{+2}$
92.0	$3.3750 \cdot 10^{+2}$	$3.3891 \cdot 10^{+2}$	$3.4239 \cdot 10^{+2}$	$3.4942 \cdot 10^{+2}$	$3.3741 \cdot 10^{+2}$

Table 5.3: Invariant mass distributions at NNLO for the mLSOM and the SM around the peak of the Z. The mass of the anomalous extra Z' is taken to be 1 TeV with $\mu_F = \mu_R = Q$.

$$\Delta\sigma \equiv |\sigma_{NNLO} - \sigma_{NLO}| \tag{5.37}$$

which measures the "error" change in the hadronic cross section σ going from NLO to NNLO ($\Delta\sigma$) in terms of the analogous changes in the hard scatterings ($\Delta\hat{\sigma}$) and parton luminosities $\Delta\phi$). The dominance of the first or the second term on the rhs of Eq. (5.36) is an indication of the dominance of the hard scatterings or of the evolution in moving from lower to higher order. The same differences emerge also from Tabs. 5.2, 5.3. Differences in the resonance region of this size can be considered marginally relevant for the identification of anomalous components in this observables. In fact, in [85] a high precision study of this distributions on the same peak (in the SM case) shows that the total theoretical error is reasonably below the 4 % level and can decrease at 1.5-2 % level when enough statistics will allow to reduce the experimental errors on the Pdf's. It is then obvious that the isolation/identification of a specific model - whether anomalous or not - appears to be rather difficult from the measurement of a single observable even with very high statistics, such as the Z resonance. The evolution of the Pdf's has been performed with Candia 1.0 [104] which allows independent variations of μ_F and μ_R in the initial state. This analysis is shown in Fig. 5.15, where we vary μ_F up to $2Q$, while we have taken $1/2\mu_F \leq \mu_R \leq 2\mu_F$. We observe that by increasing both scales there is an enhancement in the result and this is due to the logarithms $\ln \mu_R^2/\mu_F^2$ and $\ln Q^2/\mu_F^2$, contained in the hard scatterings. The scale variations induce changes of about 4% in the SM case at NNLO and about 3.5% in the mLSOM on the peak of the Z. Notice that the variations are not symmetric as we vary the scales and the percentual changes refer to the maximum variability. This typical scale dependence is universal for all the studies presented so far on the peak of

σ_{tot}^{nnlo} [fb], $\sqrt{S} = 14$ TeV, $M_1 = 1$ TeV, $\tan\beta = 40$				
g_z	mLSOM	$U(1)_{B-L}$	$U(1)_{q+u}$	$FreeFerm.$
0.1	5.982	3.575	2.701	1.274
	0.173	0.133	0.177	0.122
	0.277	0.445	0.252	0.017
0.36	106.674	105.567	53.410	42.872
	2.248	1.733	2.308	1.583
	4.937	13.138	4.991	0.586
0.65	240.484	143.455	108.344	51.155
	7.396	5.700	7.592	5.205
	11.127	17.853	10.124	0.699
1	532.719	317.328	239.401	113.453
	17.810	13.720	18.274	12.530
	24.639	39.491	22.370	1.550

Table 5.4: Total cross sections, widths and $\sigma_{tot} \times BR(Z \to l\bar{l})$, where $BR(Z \to l\bar{l}) = \Gamma_{Z' \to l\bar{l}}/\Gamma_{Z'}$, for the mLSOM and three anomaly-free extensions of the SM; they are all shown as functions of the coupling constant.

the Z and is a limitation of the parton model prediction. After a large data taking, optimal choices for the PDF's and for μ_R and μ_F will allow a considerable reduction of this indetermination. In Fig. 5.15b we repeat the same analysis, for the same c.m. energy, this time for $Q \sim 1$ TeV, on the Z' resonance in the mLSOM, for a sizeable coupling of the anomalous gauge boson, $g_B = 1$. Compared to the value on the Z peak, the reduction of the cross section is by a factor of 2×10^4. Also in this interval the variation of the differential cross section with the two scales is around 3%. We have added Tab. 5.4 in which we show results for the total cross sections for the various models at the Z peak. In the first line of each column we show the results for the total cross section in $[fb]$, in the 2nd line the total width $\Gamma_{Z'}$, expressed in GeV and in the 3rd line the observable $\sigma_{tot} \times BR(Z \to l\bar{l})$, where $BR(Z \to l\bar{l}) = \Gamma_{Z' \to l\bar{l}}/\Gamma_{Z'}$. These quantities refer to the value of the coupling constant g_z listed in the first column. [1]

We show in Fig. 5.16a,b two plots of the results for the mLSOM of the DY cross section on the peak of the Z and of the extra Z', where we vary the scales both in the hard scatterings and in the parton luminosities. We have added and subtracted the anomalous sector in order to estimate their size respect to the remaining contributions. As we have already pointed out, the scale variability at NNLO is larger than the changes induced on the result by the anomalous graphs. The anomalous effects are more visible at large Q (subfig. (b)), on the resonance of the extra Z', and are due to the behavior of the anomalous components at large-x due to a growing Q. In Fig. 5.17a we show a plot of the mLSOM for different values of g_B and for different values of μ_R and μ_F. The first peak (purple line) corresponds to $g_B = 0.1$ the 2nd (blue line) to $g_B = g_Y$ and so on. As g_B grows the width of each peak gets larger but the peak-value of the cross section decreases. Different choices of g_B correspond to slightly different values of the mass of the extra Z' because of the relation between the Stückelberg mass M_1 and $M_{Z'}$ given in Eq. (2.181). For a fixed value of the coupling, the effects due to the variations of the scales become visible only for $g_B = 1$ and in this case they are around 2-3%. In the case $g_B = 1$ (red line), the uppermost lines correspond to the choice $\mu_F = 2Q$, $\mu_R = 1/2\mu_F$ and $\mu_R = 2\mu_F$, while the lowermost lines correspond to the choice $\mu_F = Q$, $\mu_R = 1/2\mu_F$ and $\mu_R = 2\mu_F$. Again, we notice that if we increase μ_F and μ_R the cross section grows.

In Fig. 5.17b we show the result of a comparison between the mLSOM and the anomaly-free extensions. We have also included the μ_R/μ_F scale dependence, which appears as a band, and the variations with respect to g_B. As shown in this figure, the red lines correspond to the mLSOM, the blue lines to the $U(1)_{B-L}$ model, the green lines to the free fermionic model and the purple lines to $U(1)_{q+u}$. Right as

---

[1] Notice that we have chosen $g_z = g_B$ for the mLSOM.

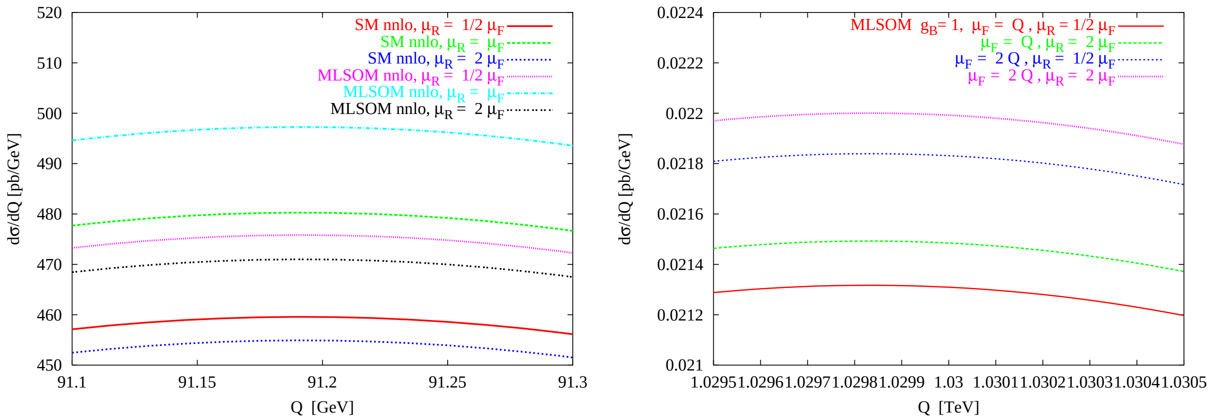

(a) (b)

Figure 5.15: Zoom on the Z resonance for anomalous Drell-Yan for varying factorization and renormalization scales at NNLO for the SM and the mLSOM. Results are shown for $Q \sim 91$ GeV (a) and 1 TeV (b) both for $\sqrt{S} = 14$ TeV.

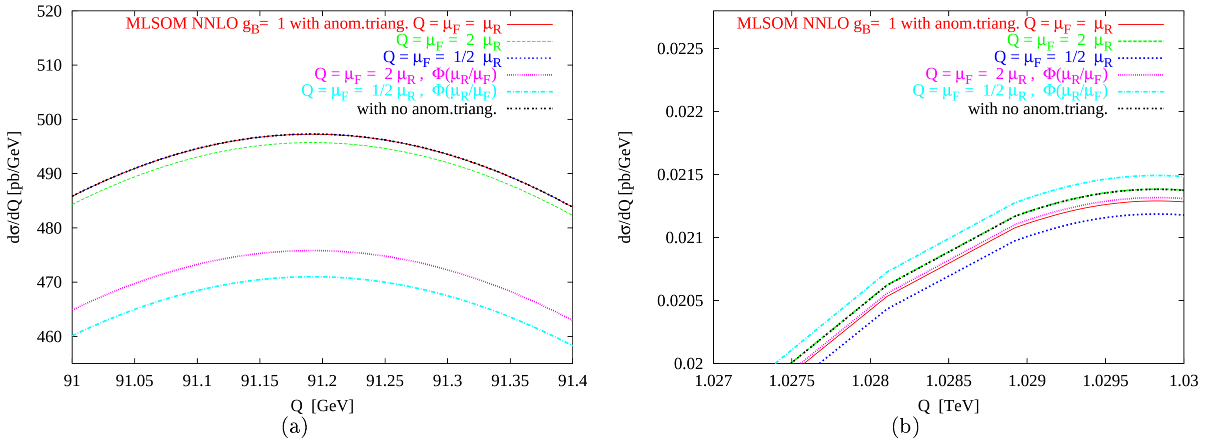

(a) (b)

Figure 5.16: Plot of the DY invariant mass distributions on the peak of the Z (a) and of the Z' (b). Shown are the total contributions of the mLSOM and those in which the anomalous terms have been removed. The variation of the result on μ_F and μ_R is included both in the hard scatterings and in the luminosities ($\Phi(\mu_F/\mu_R)$).

before, the first peak corresponds to $g_B = 0.1$, the 2nd to $g_B = g_Y$ etc. The peak-value of the anomalous model is the largest of all, with a cross section which is around 0.022 [pb/GeV], the free fermionic appears to be the smallest with a value around 0.006 [pb/GeV].

5.5 Direct Photons with GS and WZ interactions

The analysis of $pp \to \gamma\gamma$ proceeds similarly to the DY case, with a numerical investigation of the background and of the anomalous signal at parton level.

We start classifying the strong/weak interference effects that control the various sectors of the process and then identify the leading contributions due to the presence of anomaly diagrams. Direct photons are one of the possible channels to detect anomalous gauge interactions, although, as we are going to see, also in this case the anomalous signal remains rather small. Direct photons are produced by partonic interactions rather than as a result of the electromagnetic decay of hadronic states. At leading order (LO) they carry the transverse momentum of the hard scatterers, offering a direct probe of the underlying

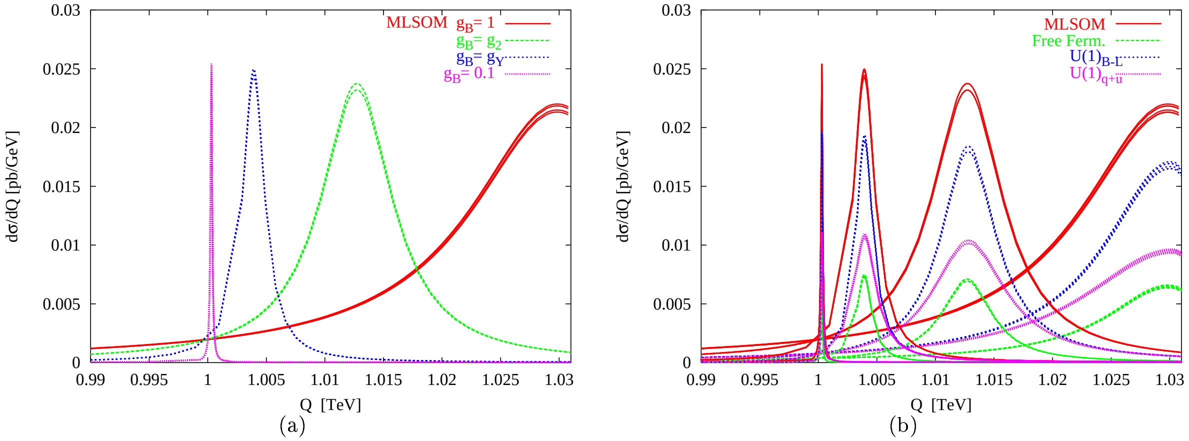

(a) (b)

Figure 5.17: (a) Anomalous Z' resonances obtained by varying g_B. (b) Comparisons among anomalous Drell-Yan in the mLSOM versus several anomaly-free models.

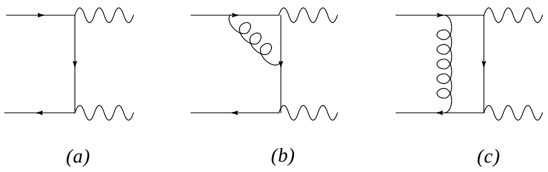

Figure 5.18: $q\bar{q}$ sector for the process $q\bar{q} \rightarrow \gamma\gamma$ including virtual corrections at LO (a) and NLO (b,c).

quark-gluon dynamics. The two main channels in pp collisions are the annihilation $q\bar{q}$ and Compton (qg), the second one being roughly 80% of the entire signal at large p_T (from $p_T = 4$ GeV on). The annihilation channel is subleading, due to the small antiquark densities in the proton. The cross section is also strongly suppressed (by a factor of approximately 10^{-3}) compared to the jet cross section. For this reason the electromagnetic decay of the produced hadrons is a significant source of background, coming mostly from the $\pi^0 \rightarrow \gamma\gamma$ decay. In this case the angular opening of the two photons is in general rather small, due to the small pion mass, and proportional to their energy asymmetry $((E_1 - E_2)/(E_1 + E_2))$. A limitation in the granularity of the detector, therefore, may cause the two photons to be unresolved experimentally, giving a spurious signal for direct photons. Even in the presence of enough granularity in the detector, very asymmetric decays can also cause the failure of the experimental apparatus to resolve the low energy photon. A second source of background is due to $\eta \rightarrow \gamma\gamma$ decay, which is about 20% of the pion contribution. These two contributions account for almost all the background to direct photons. The overall signal to background, though small, is supposed to raise with an increasing p_T. This is due to the steepening of the π and η spectra -at higher Q^2- respect to the p_T spectra of the parent jet, so there are smaller fractions of these particles that can fragment into photons. The reduction of the background can be performed either using reconstruction of the contributions due to the pions by measurements of the invariant mass of the pair in the final state, or by imposing isolation cuts. In the isolation procedure one can eliminate events with more than 2 particle in the final state, considering that emissions from fragmentation are usually accompanied by a large multiparticle background. The selection of appropriate isolation cuts are one of the way to render the anomalous signal more significant, considering that the tagged photon signal, although being of higher-order in α_s (NNLO in QCD), is characterized by a two-photon-only final state. As we are going to see this signal is non-resonant, even in the presence of an

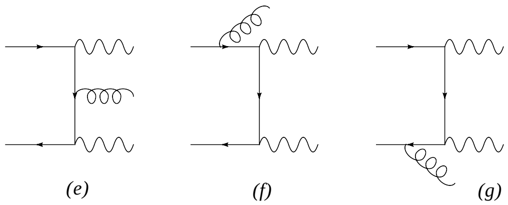

Figure 5.19: Real emissions for $q\bar{q} \rightarrow \gamma\gamma$ at NLO.

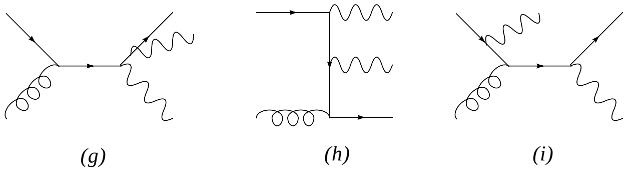

Figure 5.20: qg sector for the process $qg \rightarrow \gamma\gamma$.

s-channel exchange, due to the anomaly.

We show in Fig. 5.18 a partial list of the various background contributions to the DP channel in pp collisions. We show the leading order (LO) contribution in diagram (a) with some of the typical virtual corrections included in (b) and (c). These involve the $q\bar{q}$ sector giving a cross section of the form

$$\sigma_{q\bar{q}} = \alpha_{em}^2 (c_1 + c_2 \alpha_s). \tag{5.38}$$

These corrections are the NLO ones in this channel. The infrared safety of the process is guaranteed at the same perturbative order by the real emissions in Fig. 5.19 with an integrated gluon in the final state, which are also of $O(\alpha_{em}^2 \alpha_s)$.

A second sector is the qg one, which is shown in Fig. 5.20, also of the same order ($O(\alpha_s \alpha_{em})$). These corrections are diagrammatically the NLO ones. In general, the NLO prediction for this process are improved by adding a part of the NNLO (or $O(\alpha_{em}^2 \alpha_s^2)$) contributions, such as the box contribution (j) of the gg sector which is of higher order ($O(\alpha_{em}^2 \alpha_s^2)$) in α_s, the reason being that these contributions have been shown to be sizeable and comparable with the genuine NLO ones. All these corrections have been computed long ago [43] and implemented independently in a complete Monte Carlo in [141, 153] with a more general inclusion of the fragmentation. More recently, other NNLO contributions have been added to the process, such as those involving the gg sector through $O(\alpha_{em}^2 \alpha_s^3)$,

$$\sigma_{gg} = \alpha_{em}^2 (d_1 \alpha_s^2 + d_2 \alpha_s^3), \tag{5.39}$$

shown in graphs $(k), (l), (m)$. The other sectors have not yet been computed with the same accuracy, for instance in the qq and $q\bar{q}$ channels they involve 2 to 4 emission amplitudes which need to be integrated over 2 gluons. For instance, graph (m) is a real emission in σ_{gg} which is needed to cancel the infrared/collinear singularities of the virtual ones at the same order.

The anomalous contributions are shown in Figs. 5.22, 5.23, 5.24, 5.25 and 5.26.[2] One of the most important partonic process, in this case, is the BIM amplitude shown in diagram (n) which violates unitarity at very high energy. In the WZ case, where the axion b appears in trilinear interactions not as a

---

[2] As stated in the previous sections, the diagram in Fig. 5.25 vanish because of a WI.

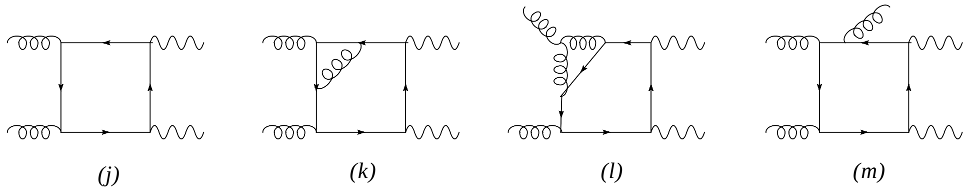

Figure 5.21: gg sector for the process $gg \to \gamma\gamma$ with virtual and real radiative corrections.

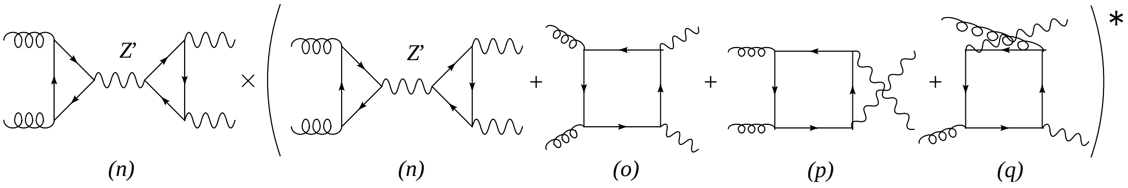

Figure 5.22: Anomalous contributions for $gg \to \gamma\gamma$ involving the BIM amplitude and its interference with the box graphs.

virtual state (such as in $(bF\wedge F)$) this amplitude has two main properties; 1) it is well defined and finite in the chiral limit even for on-shell physical gluons/photons and 2) it is non-resonant and can grow beyond the unitarity limit. Working in the chiral limit, its expression is given by the Dolgov-Zakharov limit of the anomaly amplitude (Eqs. (5.15) and (5.16), with $m_f = 0$), which appears both in the production mechanism of the extra Z', ($gg \to Z'$), where the Z' in the s-channel is virtual, and in its decay into two photons. We recall from Chap. 3 that the presence of an anomaly in the initial and in the final state cancels the resonance of a given channel. For simplicity we consider amplitude Fig. 5.22n, assuming to have photons both in the initial and in the final state. The amplitude is given by

$$\begin{aligned}
A^{\mu\nu\mu'\nu'}_{BIM} &= \frac{a_n}{k^2}k^\lambda\epsilon[\mu,\nu,k_1,k_2]\,\frac{-i}{k^2-M^2}\left(g^{\lambda\lambda'}-\frac{k^\lambda k^{\lambda'}}{M^2}\right)\frac{a_n}{k^2}(-k^{\lambda'})\epsilon[\mu',\nu',k_1',k_2'] \\
&= \frac{a_n}{k^2}\epsilon[\mu,\nu,k_1,k_2]\,\frac{-i}{k^2-M^2}\frac{k^{\lambda'}(M^2-k^2)}{M^2}\,\frac{a_n}{k^2}(-k^{\lambda'})\epsilon[\mu',\nu',k_1',k_2'] \\
&= \frac{a_n}{k^2}\epsilon[\mu,\nu,k_1,k_2]\left(\frac{-ik^2}{M^2}\right)\frac{a_n}{k^2}\epsilon[\mu',\nu',k_1',k_2'] \\
&= -\frac{a_n}{M}\epsilon[\mu,\nu,k_1,k_2]\,\frac{i}{k^2}\,\frac{a_n}{M}\epsilon[\mu',\nu',k_1',k_2']. \qquad (5.40)
\end{aligned}$$

where M denotes, generically, the mass of the anomalous gauge boson in the s-channel. If we multiply this amplitude by the external polarizators of the photons, square it and perform the usual averages, one finds that it grows quadratically with energy. The additional contributions in the s-channel for this amplitude are shown in Fig. 5.27. The exchange of a massive axion (Fig. 5.27b), due to a mismatch between the coupling and the parameteric dependence between Fig. 5.27a and b, does not erase the growth (see the discussion in the appendix). This mismatch is at the origin of the unitarity bound for this theory analyzed. The identification of this scale in the context of QCD is quite subtle, since the lack of unitarity in a partonic process implies a violation of unitarity also at hadron level, but at a different scale compared to the partonic one, which needs to be determined numerically directly from the total hadronic cross section σ_{pp}. Overall, the convolution of a BIM amplitude with the parton distributions will cause a suppression of the rising partonic contributions, due to the small gluon density at large

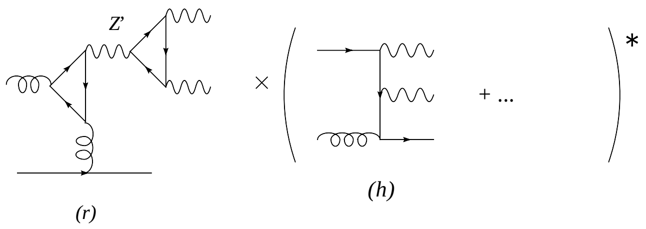

(r) (h)

Figure 5.23: Total amplitude for $qg \to \gamma\gamma$.

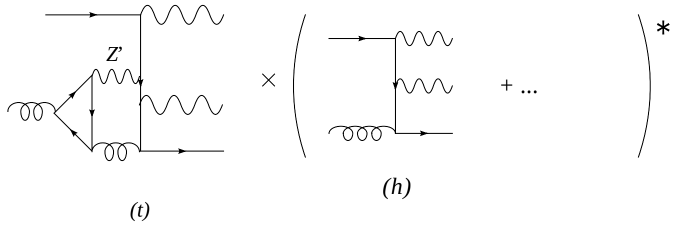

(t) (h)

Figure 5.24: Another configuration for the total amplitude of the $qg \to \gamma\gamma$ process.

Bjorken x. Therefore, the graphs do not generate a large anomalous signal in this channel. However, the problem of unitarizing the theory by the inclusion of higher dimensional operators beyond the minimal dimension-5 operator $bF \wedge F$ remains.

The anomalous terms, beside the (n)(n)* contribution with the exchange of an extra Z/Z' which carry an anomalous component, which is $O(\alpha_{em}^2 \alpha_s \alpha_w^2)$, include the interference between the $s/t/u$ box diagrams of $gg \to \gamma\gamma$ with the same BIM amplitude (n). In the gg sector the anomalous terms give, generically, an expression of the form

$$\sigma_{gg}^{an} = \alpha_{em}^2 (a_1 \alpha_s^2 \alpha_w + a_2 \alpha_s^2 \alpha_w^2), \tag{5.41}$$

with the first contribution coming from (n)(o)* and from the interference with the ($gg \to \gamma\gamma$) box diagram, while the second from (n)(n)*. Other contributions which appears at $O(\alpha_{em}^2 \alpha_s \alpha_w)$ are those shown in Fig. 5.23 which involve 2 anomaly diagrams (r) and their interference with the NLO real emission diagram of type (m). These contributions are phase-space suppressed. If we impose isolation cuts on the amplitude, we can limit our analysis, for the anomalous signal, only to 2-to-2 processes.

5.5.1 Helicity amplitudes: massless box diagrams and anomalous interferences

Moving to the computation of the anomalous contributions to $g(p_1, \pm) + g(p_2, \pm) \to \gamma(k_1, \pm) + \gamma(k_2, \pm)$, coming from the 2-to-2 sector we identify the following non-vanishing helicity amplitudes for the diagrams shown in Fig. 5.22, with the usual conventions

$$\begin{aligned} s &= (p_1 + p_2)^2 \\ t &= (p_1 - k_1)^2 = -s/2(1 - \cos\theta) \\ u &= (p_1 - k_2)^2 = -s/2(1 + \cos\theta), \end{aligned} \tag{5.42}$$

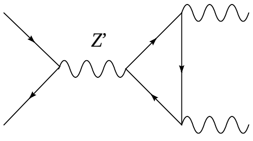

(s)

Figure 5.25: Single diagram with an exchanged Z' boson in the s-channel.

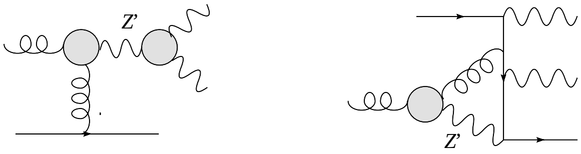

(u) (v)

Figure 5.26: Generic representation of the $qg \to \gamma\gamma$ process in the presence of a GS vertex of the AVV type.

where θ is the angle between $\vec{p}_1$ and $\vec{k}_1$, and we obtain

$$
\begin{aligned}
M^{\mathcal{Z}}_{++++} &= \frac{s}{(2\pi)^4 M^2_{\mathcal{Z}}}, \\
M^{\mathcal{Z}}_{----} &= \frac{s}{(2\pi)^4 M^2_{\mathcal{Z}}}, \\
M^{\mathcal{Z}}_{++--} &= i\,\epsilon[k_1,k_2,p_1,p_2]\frac{\left(t^2-u^2\right)^3 - s^2\,\left(t^4-u^4\right)}{8M^2_{\mathcal{Z}}\,\pi^4\,s^3\,t^2\,u^2} \\
&- \frac{\left(t^2-u^2\right)^4 - 2\,s^2\left(t^2-u^2\right)^2\,\left(t^2+u^2\right) + s^4\,\left(t^4+u^4\right)}{32\,M^2_{\mathcal{Z}}\,\pi^4\,s^3\,t^2\,u^2}, \\
M^{\mathcal{Z}}_{--++} &= -i\,\epsilon[k_1,k_2,p_1,p_2]\frac{\left(t^2-u^2\right)^3 - s^2\,\left(t^4-u^4\right)}{8M^2_{\mathcal{Z}}\,\pi^4\,s^3\,t^2\,u^2} \\
&- \frac{\left(t^2-u^2\right)^4 - 2\,s^2\left(t^2-u^2\right)^2\,\left(t^2+u^2\right) + s^4\,\left(t^4+u^4\right)}{32\,M^2_{\mathcal{Z}}\,\pi^4\,s^3\,t^2\,u^2}, \\
M^{\chi}_{++++} &= \frac{16s^2}{(s-M^2_{\chi})}, \\
M^{\chi}_{----} &= \frac{16s^2}{(s-M^2_{\chi})}, \\
M^{\chi}_{++--} &= -32\,i\epsilon[k_1,k_2,p_1,p_2]\frac{s^2\left(t^4-u^4\right) - \left(t^2-u^2\right)^3}{s^2\left(s-M^2_{\chi}\right)\,t^2\,u^2} \\
&- 8\,\frac{\left(t^2-u^2\right)^4 - 2\,s^2\,\left(t^2-u^2\right)^2\,\left(t^2+u^2\right) + s^4\,\left(t^4+u^4\right)}{s^2\,\left(s-M^2_{\chi}\right)\,t^2\,u^2}, \\
M^{\chi}_{--++} &= 32\,i\epsilon[k_1,k_2,p_1,p_2]\frac{s^2\left(t^4-u^4\right) - \left(t^2-u^2\right)^3}{s^2\left(s-M^2_{\chi}\right)\,t^2\,u^2} \\
&- 8\,\frac{\left(t^2-u^2\right)^4 - 2\,s^2\,\left(t^2-u^2\right)^2\,\left(t^2+u^2\right) + s^4\,\left(t^4+u^4\right)}{s^2\,\left(s-M^2_{\chi}\right)\,t^2\,u^2},
\end{aligned}
\tag{5.43}
$$

where again $\mathcal{Z}$ indicates either Z or Z' and the M_{χ} refers to the contributions with the exchange of a axi-Higgs. In the above formulas we have omitted all the coupling constants to obtain more compact

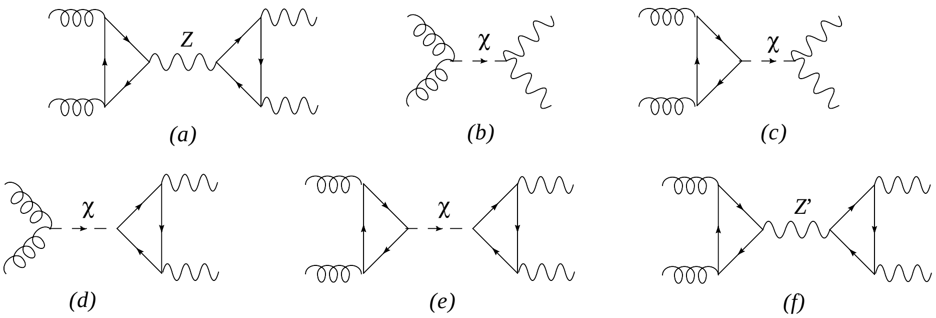

Figure 5.27: Complete list of amplitudes included in the type of graphs shown in Fig. 5.22. They also have the exchange of a physical axion and contributions proportional to the mass of the internal fermion.

results. The helicity amplitudes for the massless box contribution have been computed in [154] and are given by

$$\begin{aligned}
M^{box}_{--++} &= 1,\\
M^{box}_{-+++} &= 1,\\
M^{box}_{++++} &= -\frac{1}{2}\frac{t^2+u^2}{s^2}\left[\ln^2\left(\frac{t}{u}\right)+\pi^2\right]-\frac{t-u}{s}\ln\left(\frac{t}{u}\right)-1,\\
M^{box}_{+--+} &= -\frac{1}{2}\frac{t^2+s^2}{u^2}\ln^2\left(-\frac{t}{s}\right)-\frac{t-s}{u}\ln\left(-\frac{t}{s}\right)-1\\
&\quad -i\pi\left[\frac{t^2+s^2}{u^2}\ln\left(-\frac{t}{s}\right)+\frac{t-s}{u}\right],\\
M^{box}_{+-+-}(s,t,u) &= M^{box}_{+--+}(s,u,t), \qquad (5.44)
\end{aligned}$$

giving a differential cross section

$$\frac{d\sigma^{box}}{d\cos\theta}=\frac{\alpha_{em}^2\alpha_s^2N_c^2}{64\pi\, s}\left[\sum_f Q_f^2\right]^2\left\{|M^{box}_{--++}|^2+4\,|M^{box}_{-+++}|^2+|M^{box}_{++++}|^2+|M^{box}_{+--+}|^2+|M^{box}_{+-+-}|^2\right\}. \quad (5.45)$$

The interference terms are listed in Fig. 5.22 and the interference differential cross section is given by

$$\frac{d\sigma^{int}}{d\cos\theta}=\sum_{\mathcal{Z}=Z,Z'}\frac{d\sigma^{\mathcal{Z},box}}{d\cos\theta}+\frac{d\sigma^{\chi,box}}{d\cos\theta}, \quad (5.46)$$

where

$$\begin{aligned}
\frac{d\sigma^{\mathcal{Z},box}}{d\cos\theta} &= \frac{1}{256\pi s}\sum_q\frac{1}{2}c_1^q\sum_{q'}\frac{1}{2}c_2^{q'}\sum_f Q_f^2\alpha_{em}\alpha_s N_c \mathrm{Re}\left[2M^{\mathcal{Z}}_{++++}M^{*box}_{++++}+(M^{\mathcal{Z}}_{++--}+M^{\mathcal{Z}}_{--++})M^{*box}_{++--}\right]\\
&= -\frac{1}{8192\pi^5M_{\mathcal{Z}}^2}\sum_q\frac{1}{2}c_1^q\sum_{q'}\frac{1}{2}c_2^{q'}\sum_f Q_f^2\alpha_{em}\alpha_s N_c\left[\left(\cos^2\theta+1\right)\log^2\left(\frac{1-\cos\theta}{1+\cos\theta}\right)\right.\\
&\quad \left.+4\cos\theta\log\left(\frac{1-\cos\theta}{1+\cos\theta}\right)+\left(\cos^2\theta+1\right)\pi^2+8\right], \qquad (5.47)
\end{aligned}$$

$$\frac{d\sigma^{\chi,box}}{d\cos\theta} = \frac{g^{\chi}_{gg}g^{\chi}_{\gamma\gamma}}{256\pi s}\sum_f Q_f^2\alpha_{em}\alpha_s N_c\,\mathrm{Re}\left[2M^{\chi}_{++++}M^{*box}_{++++}+(M^{\chi}_{++--}+M^{\chi}_{--++})M^{*box}_{++--}\right]$$

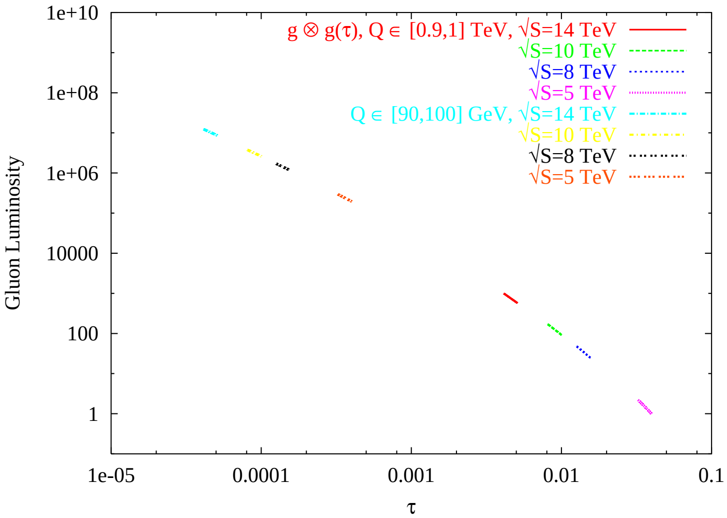

Figure 5.28: The NNLO gluon luminosity as a function of $\tau = Q^2/S$ for various value of the invariant mass of the photon pair (Q) and energy of the hadronic beam (S) at the LHC evolved with CANDIA 1.0.

$$
\begin{aligned}
= \quad & -\frac{s}{32\pi(s-M_\chi^2)} g_{gg}^{\chi} g_{\gamma\gamma}^{\chi} \sum_f Q_f^2 \alpha_{em} \alpha_s N_c \left[\left(\cos^2\theta + 1\right) \log^2\left(\frac{1-\cos\theta}{1+\cos\theta}\right) \right. \\
& \left. + 4\cos\theta \log\left(\frac{1-\cos\theta}{1+\cos\theta}\right) + \left(1+\cos^2\theta\right)\pi^2 + 8 \right], \qquad (5.48)
\end{aligned}
$$

where g_3 is the strong coupling constant while g_B is the anomalous coupling constant of the model. Here $M^{box}_{++--} = M^{box}_{--++}$ and we have used the parameters of the mLSOM, explicitly given in Chaps. 2, 3. The rotation matrix elements from the hypercharge basis to the physical basis after electroweak symmetry breaking of the neutral gauge sector (O^A) and rotation matrix elements of the CP-odd sector (O^χ) are defined in App. 2.9, while the couplings of the physical axion to the gluons and the photons, g^χ_{gg} and $g^\chi_{\gamma\gamma}$, are given in Eqs. 4.106. The axial-vector coupling $g^{\mathcal{Z}}_{A,q}$ of the neutral gauge bosons to a quark flavour q

$$
g^{\mathcal{Z}}_{A,q} = \frac{1}{2}(Q^{R,q}_{\mathcal{Z}} - Q^{L,q}_{\mathcal{Z}}), \qquad (\mathcal{Z} = Z, Z') \qquad (5.49)
$$

5.5.2 Numerical analysis for direct photons

In our numerical implementation of double prompt photon production we compare the size of the anomalous corrections respect to the SM background evaluated by a Monte Carlo [141, 142]. Since the anomalous signal is small compared to that of the SM, we have extracted both for the SM case and the anomalous case the gg sector and compared them at hadron level by convoluting the partonic contributions with the PDF's (see Fig. 5.28). In this comparison, the SM sector is given by the graphs shown in Fig. 5.21 plus the interference graphs shown in Fig. 5.22. In the SM case this second set of graphs contributes proportionally to the mass of the heavy quarks in the anomaly loop. At high energy the hard scatterings coming from this interference are essentially due to the mass of the top quark running inside a BIM amplitude and are, therefore, related to heavy quark effects. In the anomalous case the same set of graphs is considered, but now the anomaly contributions are explicitly included. The hadronic differential cross section due to the anomalous interactions for massless quarks is given by

$$
\begin{aligned}
\frac{d\sigma}{dQ} &= \int_0^{2\pi} d\phi \int_{-1}^{1} d\cos\theta \; \frac{\tau}{4Q} \int_\tau^1 \frac{dx}{x} \Phi_{gg}(\frac{\tau}{x}) \Delta(x,\theta), \\
\Phi_{gg}(y) &= \int_y^1 \frac{dz}{z} g(y/z) g(z), \\
\Delta(x) &= \delta(1-x) \left[\frac{d\sigma_Z}{d\cos\theta} + \frac{d\sigma_{Z'}}{d\cos\theta} + \frac{d\sigma_\chi}{d\cos\theta} + \frac{d\sigma_{int}}{d\cos\theta} \right] \\
\frac{d\sigma_{int}}{d\cos\theta} &= \frac{d\sigma^{Z,box}}{d\cos\theta} + \frac{d\sigma^{Z',box}}{d\cos\theta} + \frac{d\sigma^{\chi,box}}{d\cos\theta}.
\end{aligned}
\tag{5.50}
$$

The contributions which are part of this sector due to exchange of a Z or a Z' and a χ (see (a), (b) and (f) of the BIM set in Fig. 5.27) are those labelled above, while σ_{int} refers to the interferences shown in Fig. 5.22, with the inclusion of a Z' and a physical axion (such as Fig. 5.27b).

Defining

$$
\sigma_{gg\to\gamma\gamma} \equiv \int_0^{2\pi} d\phi \int d\cos\theta \; \Delta(x,\theta) \tag{5.51}
$$

the hadronic cross section takes the form of a product of the gluon luminosity and the partonic $gg \to \gamma\gamma$ cross section

$$
\frac{d\sigma}{dQ} = \frac{Q}{4S} \sigma_{gg\to\gamma\gamma} \Phi(\tau). \tag{5.52}
$$

5.5.3 The gg sector

Coming to the analysis of the gluon fusion sector, the result of this study is shown in Fig. 5.29 where

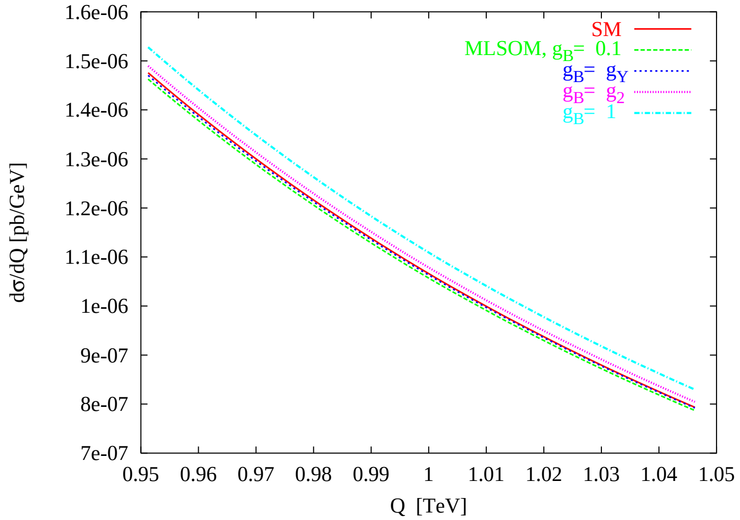

Figure 5.29: Comparison plots for the gluon sector in the SM and in the anomalous model for a resonance of 1 TeV. The box-like contributions are not included, while they appear in the interference with the BIM amplitudes.

we plot the gluon contribution to the hadronic cross section for both the SM and the mLSOM, having chosen $M_1 = 1$ TeV. We have used the MRST99 set of parton distributions to generate the NNLO gluon luminosity with $\alpha_s(M_Z) = 0.1175$, $Q = \frac{1}{2}\mu_R$ and $\sqrt{S} = 14$ TeV. We have chosen $\tan\beta = 40$ and different

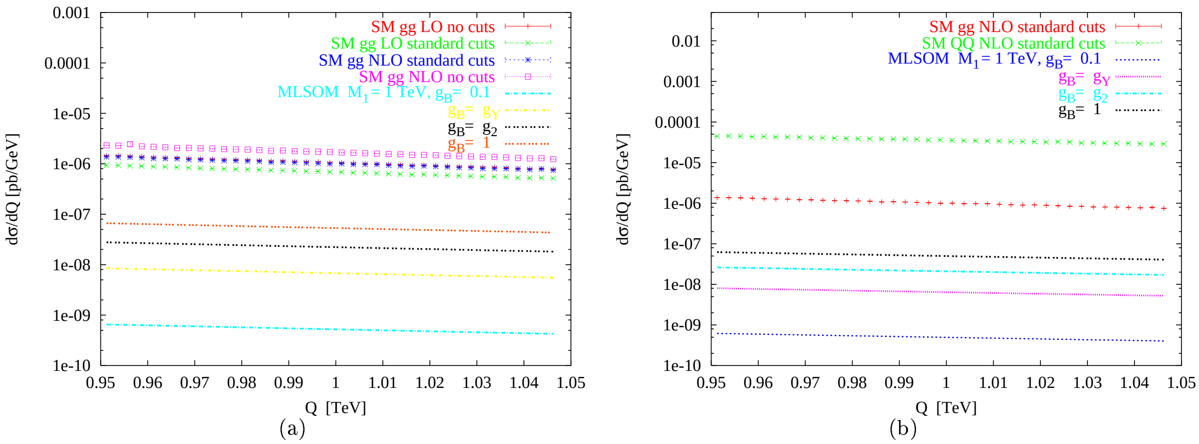

(a) (b)

Figure 5.30: (a): SM contributions for the gluon-gluon channel obtained with the Monte Carlo GAMMA2MC. These are indicated by dotted lines and include all the interferences and the box graphs. Shown are also the anomalous contributions of the mLSOM (no box). (b): as in (a) but we have included the Monte Carlo results for the SM qq channel at NLO.

values of g_B. The size of the cross section is around 10^{-6} [pb/GeV] - right on the mass of the resonance - for both models, with a difference that grows as we rise the coupling constant for the anomalous $U(1)$ (g_B). We have chosen four possible values for g_B: a small parametric value ($g_B = 0.1$); equal to the coupling of the hypercharge g_Y at the same scale ($g_B = g_Y$) or to the $SU(2)_w$ coupling g_2 ($g_B = g_2$) or, finally, parameterically sizeable, with $g_B = 1$. In the interference graphs used for this comparison between the anomalous signal of the mLSOM and the SM (in this second case the BIM amplitudes contribute via the heavy quark mass in the loops) we have included, beside the BIM amplitude, the entire set of contributions shown in Fig. 5.27, with the exchange of a Z, a Z' and the axi-Higgs χ. We have chosen a light Stückelberg axion with $m_\chi = 30$ GeV. For Q around m_χ the anomalous signal grows quite substantially, as we are going to show next. The overall flatness of the result in this region - the width of the interval is just 5 GeV in Fig. 5.29 - shows that the corrections are non-resonant and rather small. They are also overlapping for both models and the extraction of additional information concerning the anomalous sector appears to be very difficult. Before we get into a more detailed analysis of the various contributions to this sector, we mention that we have performed isolation cuts on the cross section of the SM background in DP with a choice of $R = 0.4$ for the radius of the cone of isolation of the photons. This is defined in terms of an azimuthal angle ϕ and pseudorapidity $\eta = \ln\tan\theta/2$, with a maximal value of transverse energy $E_{Tmax} = 15$ GeV in the cone, as implemented in [142]. We show a more detailed investigation of the results for the various contributions in the gg sector in Fig. 5.30a,b. The dotted lines are the results obtained by the Monte Carlo and include both 2-to-2 and 2-to-3 contributions (pure QCD) with and without cuts, computed at LO and at NLO. The size of these contributions is around 2×10^{-6} pb/GeV in the SM case. We show in the same subfigure the anomalous corrections in the mLSOM, which vary between 10^{-9} and 10^{-7} pb/GeV. Therefore, for $g_B \sim 1$, the anomalous sector of the mLSOM (the square of the box terms here are not included for the MSLOM) is suppressed by a factor of 10 respect to the signal from the same sector coming from the SM. In subfig. (b) we show the same contributions but we include in the SM also the quark channel (shown separately from the gluon channel), which is around 10^{-4} pb/GeV. Therefore, the quark sector overshadows the anomalous corrections by a factor of approximately 10^3, which are difficult to extract at this value of the invariant mass.

A comparison between the differential cross section obtained by the Monte Carlo and the anomalous

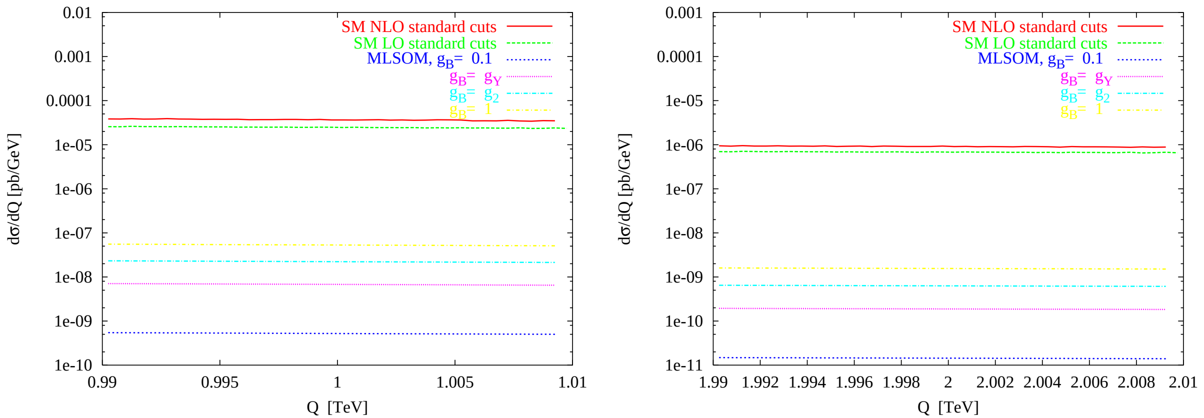

(a) (b)

Figure 5.31: (a) Plot of the invariant mass distribution for $Q \sim 1$TeV and for a Stückelberg mass of 1 TeV showing a comparison between the anomalous contributions (anomalous massless and massive BIM + interference with the box) and the SM contributions. All the sectors at one-loop and two-loop have been obtained with the Monte Carlo GAMMA2MC. (b) As in the previous figure but the invariant mass distribution has been chosen around 2 TeV.

contributions is shown in Fig. 5.31a, from which one can see that the anomalous components are down by a factor of $10^3 - 10^7$ respect to the background, depending on the value of the anomalous coupling g_B.

A similar comparison between anomalous signal and background for a 1 TeV extra gauge boson but at larger invariant mass (2 TeV) of the di-photon is shown in Fig. 5.31b. In both cases the ratio between the size of the anomalous signal and the background is 10^{-3}, showing the large suppression as in the other regions.

- **Anatomy of the gluon sector**

We show in Fig. 5.32a and b) two plots that illustrate the size of the various contributions to the gg sector in the SM and in the anomalous model. We have separated these contributions into several components in the mLSOM and SM cases.

In the anomalous model we have "pure BIM-like" amplitudes:

1) the square of the "BIM set" shown in Fig. 5.27, which contains the s-channel exchanges of the Z, of the Z' and of the χ. In Figs. 5.32a and b) these contributions are indicated as "BIM + χ".

Analogously, in the SM case we have that

1′) the BIM amplitudes contribute away from the chiral limit due to the exchange of the Z gauge boson and with top/bottom quarks running inside each of the two loops. In Figs. 5.32a and b the contributions in the SM are denoted by "SM: massive BIM", and are just obtained by squaring the single BIM amplitude of Fig. 5.27a. In the SM this component is sizeable around the threshold $s = 4m_t^2$, with m_t being the mass of the top quark, which explains the cusp in the figure around this energy value.

The interferences sets of the mLSOM ("BIM-Box") in which the BIM amplitudes interfere with the box graphs:

2) these are denoted as "Z-Box + Zp-Box + χ-Box". The three box diagrams are those shown in Fig. 5.22, corresponding to graphs (o), (p) and (q) in this figure.

In the SM we have similar contributions. These are generated by

2′) interfering the same box graphs mentioned above with the graph in Fig. 5.27a. In the SM case, as we have already mentioned, these contributions are due to heavy quarks, having neglected the mass

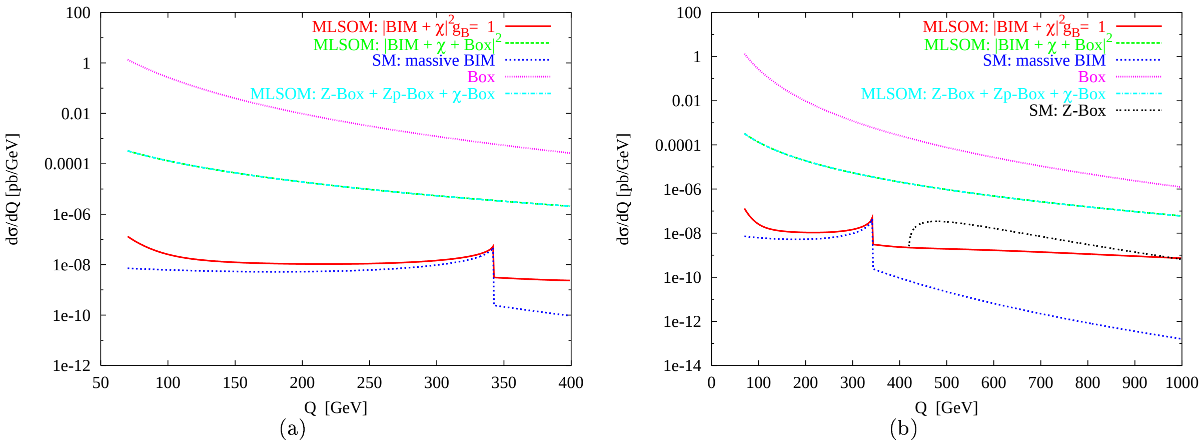

Figure 5.32: Plots of the various anomalous and box-like components in the SM and mLSOM sector at (a) lower Q and (b) higher Q.

of the leptons and of the light quarks. This interference is denoted as “Z-Box”.

Finally,

3) In both cases we have the squared “Box” contributions, which are just made from the o), p) and q) diagrams of Fig. 5.22.

From a look at Figs. 5.32a and b) it is quite evident that the contributions obtained by squaring the three box diagrams are by far the most important at $\sqrt{S} = 14$ TeV. We have tried to cover both the region $Q < 400$ GeV and the region 400 GeV $<$ Q $<$ 1 TeV. The second largest contributions, in these two plots, are those due to the interference between the BIM amplitudes and the box. These contributions are enhanced because of the presence of the box amplitude. Notice that in the SM case this interference is small and negative for $Q < 400$ GeV (see Fig. 5.32a) and is not reported. In the second region (400 GeV $<$ Q $<$ 1 TeV) this contribution gets sizeable around the two-particle cut of the scalar triangle diagram due to the top quark in the loop and shows up as a steepening in the line labeled as “Z-box” in Fig. 5.32b.

The “pure anomalous” contributions, due to the squared BIM amplitudes are down by a factor of about 10^5 respect to the dominant box contributions. A similar trend shows up also in the SM case. Around the 2-particle cut the BIM amplitudes both in the SM and in the mLSOM have a similar behavior, but differ substantially away from this point in the larger-Q and smaller-Q region. These are the two regions where the effects of the anomaly are more apparent. For instance, for $Q < 200$ GeV the steep rise of the anomalous contributions of the “BIM + χ” line is due to the fact that Q is getting closer to the resonance of the axion χ. In the SM the same region is characterized by a suppression by the ratio ${m_f}^2/Q^2$. At larger Q values, the growth of the anomalous contributions are due to the bad behavior of the anomaly, which grows quadratically with energy, as we have discussed above. This trend is more visible in Fig. 5.32b (red line) in the region $Q > 800$ GeV. The possibility of increasing the di-photon (gluon-fusion) signal is related to the possibility of imposing suitable kinematical constraints in the analysis of the final state - or phase-space cuts - in the experimental analysis. To achieve this goal there are several features of the process that should be kept into account. The first is the sharp decrease of the cross section at large invariant mass Q of the di-photon final state; the second is its increase with $\sqrt{S}$, the collision energy of the two colliding protons. In the first case we have an increase of the relevant parameter $\tau = Q^2/S$ characterizing the gluon density; in the second case this is reduced considerably, giving a fast enhancement of the gluon luminosity.

Since bounds on the coupling of the anomalous models may come both from a combined analysis of

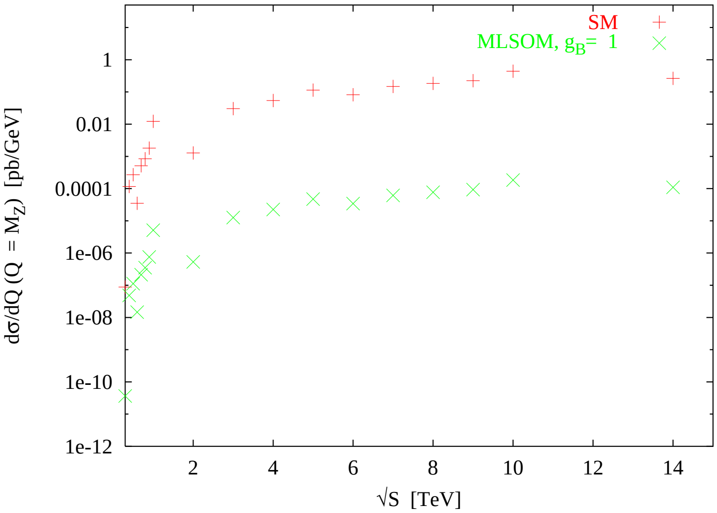

Figure 5.33: Double photon invariant mass cross section at $Q = M_Z$ plotted as a function of the energy. Here the SM contributions include the massive BIM + Box + interference, while the mLSOM contributions include the massless and massive BIM + interference.

both DY and of the di-photon cross section, we have chosen Q around the Z peak (small Q option) and the same luminosity evaluated on the peak of the extra Z' (large Q option), both as a function of the collisional energy S. This is shown in Fig. 5.33. The anomalous signal grows with $\sqrt{S}$ but the non-unitary growth is not apparent at LHC energies after convolution with the parton densities; on the other end, the growths in the SM and in the anomalous sector of the mLSOM appear to be, at LHC energies, quite similar.

If an extra Z' is found in DY, then the analysis of di-photon both on the peak of the Z and on the peak of the Z' could be used to set reasonable bounds on the coupling of the underlying model, trying to uncover the possible presence of an anomalous signal. A $\tau \sim 10^{-4}$ can be reached at the Z peak for a collision energy of 10 TeV, which causes an enhancement of the anomalous cross section by a factor of approximately 10^4 respect to the same anomalous contribution measured for $Q \sim 1$ TeV.

In a final figure we show the shapes of the distributions for the SM and the mLSOM using the Monte Carlo with a binning of the cross section in both cases. This is provided in Fig. 5.34, where the colored lines on top of each bin indicate the small anomalous signal in the cross section.

5.6 Conclusions

Both DY and DP have some special features, being characterized by a clean final state. In DY the identification of a new resonance in the neutral current sector would bring to the immediate conclusion that an extra Z' is present in the spectrum, but would give not specific indication concerning its true nature. Current experimental bounds constrain the mixing of a possible extra neutral component with the Z gauge boson, with a mass which should be larger than 800 GeV, rendering the future search of extra neutral interactions, at least for DY, quite delicate, being the allowed mass range at the tail of the invariant mass distribution of this process. For this reason, the identification of a restricted mass range for the extra gauge boson would be crucial for its discovery, but unfortunately, there is no extension of the SM that comes with a definite prediction for it.

In intersecting brane models one encounters a similar indetermination and for this reason in our

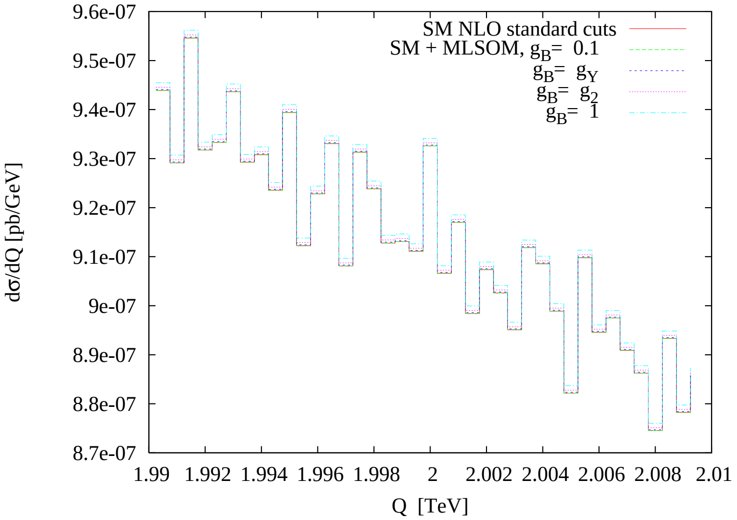

Figure 5.34: Binned cross sections for the SM and the mLSOM. The small anomalous corrections are the thick lines at the top of each bin.

construction the Stückelberg mass has been assumed to be a free parameter. If an extra s-channel resonance is found, then the investigation of its specific properties would require much more effort and several years of data collection at the LHC, especially for larger mass values (above 1.5 TeV or so) of the extra Z'. A sizeable width of the resonance could then allow to study the V-A structure of the coupling, though this study is quite complex. In most of the models studied so far the corresponding widths are expected to be quite small ($\ll 30 \div 40$ GeV) even for sizeable couplings ($g_B \sim O(1)$) [107], probably below or barely close to the limits of the effective resolution of the detector.

Under these conditions, deciding over the true nature of the extra Z', whether anomalous or not, would then be far more challenging and would require a parallel study of several independent channels. For this reason we have analyzed two processes which are both affected by anomalous contributions and could be used for correlated studies of the same interaction.

We have seen that changes in the factorization/renormalization scales both in the hard scatterings and in the evolution of the PDF's can easily overshadow the anomalous corrections, making a NLO/NNLO analysis truly necessary. We have focused our investigation on an extra Z' of mass 1 TeV and searched for anomalous effects in the invariant mass distributions on the Z peak, at 1 TeV and for large Q values (up to 2 TeV). From our analysis the large suppression of the anomalous signal compared to the QCD background is rather evident, although there are ways to improve on our results. In fact, our analysis has been based on the characterization of inclusive observables, which are not sensitive to the geometric structure of the final state. In principle, the shape of the final state event could be resolved at a finer level of detail, by analyzing, for instance, the rapidity correlations between the di-photon and a jet, or other similar less inclusive cross sections, as in other cases [143]. Obviously, these types of studies are theoretically challenging and require an excellent knowledge of the QCD background at NNLO for these observables.

5.7 Appendix

The decay rates into leptons for the Z and the Z' are universal and are given by

$$\begin{aligned}
\Gamma(\mathcal{Z} \to l\bar{l}) &= \frac{g^2}{192\pi c_w^2} M_{\mathcal{Z}} \left[(g_V^{\mathcal{Z},l})^2 + (g_A^{\mathcal{Z},l})^2 \right] = \frac{\alpha_{em}}{48 s_w^2 c_w^2} M_{\mathcal{Z}} \left[(g_V^{\mathcal{Z},l})^2 + (g_A^{\mathcal{Z},l})^2 \right], \\
\Gamma(\mathcal{Z} \to \psi_i \bar{\psi}_i) &= \frac{N_c \alpha_{em}}{48 s_w^2 c_w^2} M_{\mathcal{Z}} \left[(g_V^{\mathcal{Z},\psi_i})^2 + (g_A^{\mathcal{Z},\psi_i})^2 \right] \times \\
& \qquad \left[1 + \frac{\alpha_s(M_{\mathcal{Z}})}{\pi} + 1.409 \frac{\alpha_s^2(M_{\mathcal{Z}})}{\pi^2} - 12.77 \frac{\alpha_s^3(M_{\mathcal{Z}})}{\pi^3} \right],
\end{aligned} \tag{5.53}$$

where $i = u, d, c, s$ and $\mathcal{Z} = Z, Z'$.

For the Z' and Z decays into heavy quarks we obtain

$$\begin{aligned}
\Gamma(\mathcal{Z} \to b\bar{b}) &= \frac{N_c \alpha_{em}}{48 s_w^2 c_w^2} M_{\mathcal{Z}} \left[(g_V^{\mathcal{Z},b})^2 + (g_A^{\mathcal{Z},b})^2 \right] \times \\
& \qquad \left[1 + \frac{\alpha_s(M_{\mathcal{Z}})}{\pi} + 1.409 \frac{\alpha_s^2(M_{\mathcal{Z}})}{\pi^2} - 12.77 \frac{\alpha_s^3(M_{\mathcal{Z}})}{\pi^3} \right], \\
\Gamma(\mathcal{Z} \to t\bar{t}) &= \frac{N_c \alpha_{em}}{48 s_w^2 c_w^2} M_{\mathcal{Z}} \sqrt{1 - 4\frac{m_t^2}{M_{\mathcal{Z}}^2}} \times \\
& \qquad \left[(g_V^{\mathcal{Z},t})^2 \left(1 + 2\frac{m_t^2}{M_{\mathcal{Z}}^2} \right) + (g_A^{\mathcal{Z},t})^2 \left(1 - 4\frac{m_t^2}{M_{\mathcal{Z}}^2} \right) \right] \times \\
& \qquad \left[1 + \frac{\alpha_s(M_{\mathcal{Z}})}{\pi} + 1.409 \frac{\alpha_s^2(M_{\mathcal{Z}})}{\pi^2} - 12.77 \frac{\alpha_s^3(M_{\mathcal{Z}})}{\pi^3} \right].
\end{aligned} \tag{5.54}$$

5.8 Appendix. A comment on the unitarity breaking in WZ Lagrangians

In the framework of the Abelian A-B Model analyzed in Chap. 1, the presence of an untamed growth of the amplitude for a 2-to-2 process can be simplified as follows. In this simple model A is vector-like and B is axial-vector like. We also have a single chiral fermion, with an uncancelled BBB anomaly that requires an axion-like interaction $bF_B \wedge F_B$ of the Stückelberg (b) with the B gauge field for the restoration of gauge invariance. The two contributions to $BB \to BB$ are the BIM amplitude see Figs. 5.35, 5.36 for the process mediated by a B boson and a similar one mediated by a physical axion χ. If we neglect the Yukawa couplings (we take the fermion to be massless) the only contributions involved are those already shown in Fig. 5.27, diagrams (a) and (b), but with different couplings.

$$A_{BIM}^{\mu\nu\mu'\nu'} = (g_B)^3 \Delta^{\lambda\mu\nu}(-k_1, -k_2) \frac{-i}{k^2 - M_B^2} \left(g^{\lambda\lambda'} - \frac{k^\lambda k^{\lambda'}}{M_B^2} \right) (g_B)^3 \Delta^{\lambda'\mu'\nu'}(k_1, k_2) \tag{5.55}$$

where $M_B = \sqrt{M_1^2 + (2g_B v)^2}$ is the mass of the gauge boson in the s-channel after symmetry breaking. The exchange of the physical axion gives

$$B^{\mu\nu\mu'\nu'} = 4 \times \left(\frac{4}{M} \alpha_1 C_{BB} \right)^2 \epsilon[\mu, \nu, k_1, k_2] \frac{i}{k^2 - m_\chi^2} \epsilon[\mu', \nu', k_1', k_2'] \tag{5.56}$$

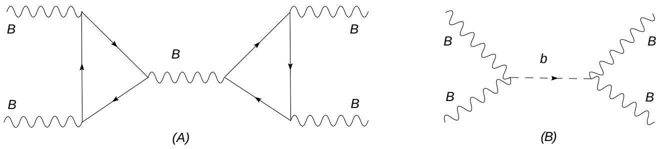

Figure 5.35: BIM amplitude for a toy model with a BBB anomaly and χ exchange diagram.

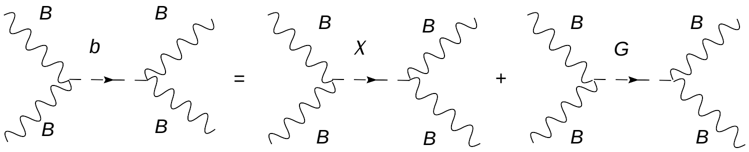

Figure 5.36: Decomposition of the Stückelberg axion in a Goldstone boson and a physical axion.

where the overall factor of 4 in front is a symmetry factor, the coefficient $\alpha_1 = \frac{2g_B v}{M_B}$ comes from the rotation of the b axion over the axi-Higgs χ, and the coefficient C_{BB} has been determined from the condition of gauge invariance of the anomalous effective action before symmetry breaking

$$C_{BB} = \frac{i g_B^3}{3!}\frac{1}{4} a_n \frac{M}{M_1}. \tag{5.57}$$

The anomaly diagrams are longitudinal, taking the DZ form

$$A_{BIM}^{\mu\nu\mu'\nu'}(a_n) = (g_B)^3 \frac{a_n}{k^2}(-k^\lambda)\epsilon[\mu,\nu,k_1,k_2] \frac{-i}{k^2 - M_B^2}\left(g^{\lambda\lambda'} - \frac{k^\lambda k^{\lambda'}}{M_B^2}\right)(g_B)^3 \frac{a_n}{k^2}(k^{\lambda'})\epsilon[\mu',\nu',k_1',k_2']. \tag{5.58}$$

It is easy to recognize in this anomalous amplitude the same structure of the amplitude for the axi-Higgs exchange in Eq. (5.56). If we add up these two amplitudes and impose the cancellation of the two amplitudes (which is a fine tuning) we obtain the condition

$$\frac{1}{M_B^2} + \frac{(2 g_B v)^2}{M_B^2 M_1^2} = 0 \tag{5.59}$$

in terms of the mass of the B and the Stückelberg mass M_1, which does not have a real solution. This is a simple example that conveys the issue of the presence of unitarity limit for (local) WZ interactions.

Bibliography

[1] C. Coriano', N. Irges and E. Kiritsis, Nucl. Phys. B746 (2006) 77, hep-ph/0510332.

[2] P. Langacker and M.x. Luo, Phys. Rev. D45 (1992) 278.

[3] F. Del Aguila, M. Cvetic and P. Langacker, Phys. Rev. D52 (1995) 37, hep-ph/9501390.

[4] M. Cvetic and S. Godfrey, (1995), hep-ph/9504216.

[5] S. Capstick and S. Godfrey, Phys. Rev. D37 (1988) 2466.

[6] A. Leike, Phys. Rept. 317 (1999) 143, hep-ph/9805494.

[7] A.E. Faraggi, (2002), hep-th/0208125.

[8] A.E. Faraggi and M. Thormeier, Nucl. Phys. B624 (2002) 163, hep-ph/0109162.

[9] C. Coriano and A.E. Faraggi, (2002), hep-ph/0201129.

[10] K. Hagiwara et al., Nucl. Phys. B282 (1987) 253.

[11] P. Binetruy et al., Phys. Lett. B403 (1997) 38, hep-ph/9612442.

[12] N. Irges, S. Lavignac and P. Ramond, Phys. Rev. D58 (1998) 035003, hep-ph/9802334.

[13] C. Coriano and N. Irges, Phys. Lett. B651 (2007) 298, hep-ph/0612140.

[14] C.T. Hill and C.K. Zachos, Phys. Rev. D71 (2005) 046002, hep-th/0411157.

[15] C.T. Hill, Phys. Rev. D73 (2006) 085001, hep-th/0601154.

[16] L.D. Faddeev and S.L. Shatashvili, Phys. Lett. B167 (1986) 225.

[17] N.V. Krasnikov, JETP Lett. 41 (1985) 586.

[18] R. Jackiw and R. Rajaraman, Phys. Rev. Lett. 54 (1985) 1219.

[19] P. Mitra, Annals Phys. 211 (1991) 158.

[20] C. Adam, Phys. Rev. D56 (1997) 5135, hep-th/9703130.

[21] J. Preskill, Ann. Phys. 210 (1991) 323.

[22] R.D. Peccei and H.R. Quinn, Phys. Rev. D16 (1977) 1791.

[23] L.F. Abbott and P. Sikivie, Phys. Lett. B120 (1983) 133.

[24] J.E. Kim, (1999), astro-ph/0002193.

[25] E.C.G. Stueckelberg, Helv. Phys. Acta 11 (1938) 225.

[26] E. Kiritsis, Fortsch. Phys. 52 (2004) 200, hep-th/0310001.

[27] B. Kors and P. Nath, Phys. Lett. B586 (2004) 366, hep-ph/0402047.

[28] B. Kors and P. Nath, JHEP 12 (2004) 005, hep-ph/0406167.

[29] D. Feldman, Z. Liu and P. Nath, JHEP 11 (2006) 007, hep-ph/0606294.

[30] D. Feldman, Z. Liu and P. Nath, Phys. Rev. Lett. 97 (2006) 021801, hep-ph/0603039.

[31] A. Salam and J.A. Strathdee, Phys. Rev. D2 (1970) 2869.

[32] R. Delbourgo, S. Twisk and G. Thompson, Int. J. Mod. Phys. A3 (1988) 435.

[33] H. Ruegg and M. Ruiz-Altaba, Int. J. Mod. Phys. A19 (2004) 3265, hep-th/0304245.

[34] D.J. Gross and R. Jackiw, Phys. Rev. D6 (1972) 477.

[35] C. Coriano and H. Yamagishi, Phys. Rev. D41 (1990) 3226.

[36] C. Coriano, Mod. Phys. Lett. A7 (1992) 1253, hep-th/9204021.

[37] J. Alfaro and P.H. Damgaard, Ann. Phys. 202 (1990) 398.

[38] C. Bouchiat, J. Iliopoulos and P. Meyer, Phys. Lett. B38 (1972) 519.

[39] R. Armillis et al., Nucl. Phys. B814 (2009) 15679, arXiv:0809.3772[hep-ph].

[40] C. Coriano, N. Irges and S. Morelli, JHEP 07 (2007) 008, hep-ph/0701010.

[41] A. Zee, Princeton, UK: Princeton Univ. Pr. (2003) 518 p.

[42] L. Rosenberg, Phys. Rev. 129 (1963) 2786.

[43] C. Coriano and L.E. Gordon, Nucl. Phys. B469 (1996) 202, hep-ph/9601350.

[44] S. Chang et al., Nucl. Phys. B512 (1998) 393, hep-ph/9705249.

[45] G. 't Hooft and M.J.G. Veltman, Nucl. Phys. B44 (1972) 189.

[46] P. Breitenlohner and D. Maison, Commun. Math. Phys. 52 (1977) 11.

[47] M. Dine, N. Seiberg and E. Witten, Nucl. Phys. B289 (1987) 589.

[48] J.J. Atick, L.J. Dixon and A. Sen, Nucl. Phys. B292 (1987) 109.

[49] C.D. Froggatt and H.B. Nielsen, Nucl. Phys. B147 (1979) 277.

[50] P. Binetruy and P. Ramond, Phys. Lett. B350 (1995) 49, hep-ph/9412385.

[51] P. Binetruy and E. Dudas, Phys. Lett. B389 (1996) 503, hep-th/9607172.

[52] G.R. Dvali and A. Pomarol, Phys. Rev. Lett. 77 (1996) 3728, hep-ph/9607383.

[53] P. Binetruy and G.R. Dvali, Phys. Lett. B388 (1996) 241, hep-ph/9606342.

[54] H. Georgi, J.E. Kim and H.P. Nilles, Phys. Lett. B437 (1998) 325, hep-ph/9805510.

[55] G. von Gersdorff and M. Quiros, Phys. Rev. D68 (2003) 105002, hep-th/0305024.

[56] R. Blumenhagen et al., Phys. Rept. 445 (2007) 1, hep-th/0610327.

[57] M. Bertolini et al., Nucl. Phys. B743 (2006) 1, hep-th/0512067.

[58] P. Anastasopoulos et al., Nucl. Phys. B759 (2006) 83, hep-th/0605226.

[59] A.E. Faraggi, S. Forste and C. Timirgaziu, JHEP 08 (2006) 057, hep-th/0605117.

[60] L.E. Ibanez, R. Rabadan and A.M. Uranga, Nucl. Phys. B542 (1999) 112, hep-th/9808139.

[61] I. Antoniadis, E. Kiritsis and J. Rizos, Nucl. Phys. B637 (2002) 92, hep-th/0204153.

[62] M.B. Green, J.H. Schwarz and E. Witten, Cambridge, Uk: Univ. Pr. (1987) 596 P. (Cambridge Monographs On Mathematical Physics).

[63] M.B. Green, J.H. Schwarz and E. Witten, Cambridge, Uk: Univ. Pr. (1987) 469 P. (Cambridge Monographs On Mathematical Physics).

[64] D.M. Ghilencea et al., JHEP 08 (2002) 016, hep-ph/0205083.

[65] D.M. Ghilencea, Nucl. Phys. B648 (2003) 215, hep-ph/0208205.

[66] P. Anastasopoulos, JHEP 08 (2003) 005, hep-th/0306042.

[67] P. Anastasopoulos, Phys. Lett. B588 (2004) 119, hep-th/0402105.

[68] E. Kiritsis and P. Anastasopoulos, JHEP 05 (2002) 054, hep-ph/0201295.

[69] P. Anastasopoulos et al., JHEP 11 (2006) 057, hep-th/0605225.

[70] P. Anastasopoulos, Fortsch. Phys. 55 (2007) 633, hep-th/0701114.

[71] I. Antoniadis et al., Nucl. Phys. B660 (2003) 81, hep-th/0210263.

[72] B. Kors and P. Nath, JHEP 07 (2005) 069, hep-ph/0503208.

[73] D. Feldman, Z. Liu and P. Nath, Phys. Lett. B662 (2008) 190, 0711.4591.

[74] D. Feldman, Z. Liu and P. Nath, Phys. Rev. D75 (2007) 115001, hep-ph/0702123.

[75] D.G.C. McKeon and T.J. Marshall, (2006), hep-th/0610034.

[76] S.A. Abel et al., Phys. Lett. B666 (2008) 66, hep-ph/0608248.

[77] H. Gies, J. Jaeckel and A. Ringwald, Phys. Rev. Lett. 97 (2006) 140402, hep-ph/0607118.

[78] A. Mirizzi, G.G. Raffelt and P.D. Serpico, Phys. Rev. D76 (2007) 023001, 0704.3044.

[79] E. Masso and J. Redondo, AIP Conf. Proc. 878 (2006) 387, hep-ph/0609275.

[80] A. De Angelis, O. Mansutti and M. Roncadelli, Phys. Rev. D76 (2007) 121301, 0707.4312.

[81] A. De Angelis, O. Mansutti and M. Roncadelli, Phys. Lett. B659 (2008) 847, 0707.2695.

[82] A. Dupays and M. Roncadelli, Nucl. Phys. Proc. Suppl. 168 (2007) 44, astro-ph/0612227.

[83] A. Barroso et al., Z. Phys. C28 (1985) 149.

[84] R.D. Carlitz, J.C. Collins and A.H. Mueller, Phys. Lett. B214 (1988) 229.

[85] A. Cafarella, C. Coriano and M. Guzzi, JHEP 08 (2007) 030, hep-ph/0702244.

[86] B.A. Kniehl and J.H. Kuhn, Nucl. Phys. B329 (1990) 547.

[87] K. Hagiwara, T. Kuruma and Y. Yamada, Nucl. Phys. B369 (1992) 171.

[88] J. Wess and B. Zumino, Phys. Lett. B37 (1971) 95.

[89] M.B. Green and J.H. Schwarz, Phys. Lett. B149 (1984) 117.

[90] I. Antoniadis, E. Kiritsis and T.N. Tomaras, Phys. Lett. B486 (2000) 186, hep-ph/0004214.

[91] C. Coriano, N. Irges and S. Morelli, Nucl. Phys. B789 (2008) 133, hep-ph/0703127.

[92] R. Armillis, C. Coriano and M. Guzzi, JHEP 05 (2008) 015, arXiv:0711.3424[hep-ph].

[93] L.E. Ibanez, F. Marchesano and R. Rabadan, JHEP 11 (2001) 002, hep-th/0105155.

[94] A.A. Andrianov, A. Bassetto and R. Soldati, Phys. Rev. Lett. 63 (1989) 1554.

[95] A.A. Andrianov, A. Bassetto and R. Soldati, Phys. Rev. D44 (1991) 2602.

[96] A.A. Andrianov, A. Bassetto and R. Soldati, Phys. Rev. D47 (1993) 4801.

[97] C. Fosco and R. Montemayor, Phys. Rev. D47 (1993) 4798.

[98] R. Armillis et al., JHEP 10 (2008) 034, arXiv:0808.1882[hep-ph].

[99] M. Srednicki, (2002), hep-th/0210172.

[100] P. Federbush, (1996), hep-th/9606110.

[101] A.D. Dolgov and V.I. Zakharov, Nucl. Phys. B27 (1971) 525.

[102] B.L. Ioffe, Int. J. Mod. Phys. A21 (2006) 6249, hep-ph/0611026.

[103] N.N. Achasov, Phys. Lett. B287 (1992) 213.

[104] A. Cafarella, C. Coriano and M. Guzzi, Comput. Phys. Commun. 179 (2008) 665, arXiv:0803.0462[hep-ph].

[105] C. Coriano, M. Guzzi and S. Morelli, Eur. Phys. J. C55 (2008) 629, arXiv:0801.2949[hep-ph].

[106] P. Langacker, (2008), 0801.1345.

[107] C. Coriano, A.E. Faraggi and M. Guzzi, Phys. Rev. D78 (2008) 015012, arXiv:0802.1792[hep-ph].

[108] P. Anastasopoulos et al., Phys. Rev. D78 (2008) 085014, 0804.1156.

[109] J. Jaeckel et al., Phys. Rev. D75 (2007) 013004, hep-ph/0610203.

[110] A. De Angelis et al., (2008), 0807.4246.

[111] Z. Berezhiani, L. Gianfagna and M. Giannotti, Phys. Lett. B500 (2001) 286, hep-ph/0009290.

[112] N.E. Adam, V. Halyo and S.A. Yost, JHEP 05 (2008) 062, 0802.3251.

[113] H.S. Lee, C. Luhn and K.T. Matchev, JHEP 07 (2008) 065, 0712.3505.

[114] B. Fuks, (2008), 0805.2004.

[115] B. Fuks et al., Nucl. Phys. B797 (2008) 322, 0711.0749.

[116] J. Kumar, A. Rajaraman and J.D. Wells, Phys. Rev. D77 (2008) 066011, 0707.3488.

[117] A. Djouadi, G. Moreau and R.K. Singh, Nucl. Phys. B797 (2008) 1, 0706.4191.

[118] W. Bernreuther et al., Nucl. Phys. B723 (2005) 91, hep-ph/0504190.

[119] M. Knecht et al., JHEP 03 (2004) 035, hep-ph/0311100.

[120] F. Jegerlehner and O.V. Tarasov, Phys. Lett. B639 (2006) 299, hep-ph/0510308.

[121] N.I. Usyukina and A.I. Davydychev, Phys. Lett. B298 (1993) 363.

[122] A. Czarnecki, W.J. Marciano and A. Vainshtein, Phys. Rev. D67 (2003) 073006, hep-ph/0212229.

[123] M. Knecht et al., JHEP 11 (2002) 003, hep-ph/0205102.

[124] T.V. Kukhto et al., Nucl. Phys. B371 (1992) 567.

[125] A. Vainshtein, Phys. Lett. B569 (2003) 187, hep-ph/0212231.

[126] E. de Rafael, Phys. Lett. B322 (1994) 239, hep-ph/9311316.

[127] S. Peris, M. Perrottet and E. de Rafael, Phys. Lett. B355 (1995) 523, hep-ph/9505405.

[128] A. Vainshtein, Nucl. Phys. Proc. Suppl. 169 (2007) 232.

[129] R.D. Peccei and H.R. Quinn, Phys. Rev. Lett. 38 (1977) 1440.

[130] S. Weinberg, Phys. Rev. Lett. 40 (1978) 223.

[131] F. Wilczek, Phys. Rev. Lett. 40 (1978) 279.

[132] J.E. Kim, Phys. Rev. Lett. 43 (1979) 103.

[133] M.A. Shifman, A.I. Vainshtein and V.I. Zakharov, Nucl. Phys. B166 (1980) 493.

[134] M. Dine, W. Fischler and M. Srednicki, Phys. Lett. B104 (1981) 199.

[135] A.R. Zhitnitsky, Sov. J. Nucl. Phys. 31 (1980) 260.

[136] R.D. Peccei, Lect. Notes Phys. 741 (2008) 3, hep-ph/0607268.

[137] I. Antoniadis, E. Kiritsis and T. Tomaras, Fortsch. Phys. 49 (2001) 573, hep-th/0111269.

[138] J. De Rydt et al., Class. Quant. Grav. 24 (2007) 5201, 0705.4216.

[139] J. De Rydt et al., (2008), 0808.2130.

[140] M. Ahlers et al., Phys. Rev. D77 (2008) 095001, 0711.4991.

[141] T. Binoth et al., Eur. Phys. J. C16 (2000) 311, hep-ph/9911340.

[142] Z. Bern, L.J. Dixon and C. Schmidt, Phys. Rev. D66 (2002) 074018, hep-ph/0206194.

[143] S. Chang, C. Coriano and L.E. Gordon, Phys. Rev. D58 (1998) 074002, hep-ph/9709496.

[144] R. Hamberg, W.L. van Neerven and T. Matsuura, Nucl. Phys. B359 (1991) 343.

[145] M.S. Carena et al., Phys. Rev. D70 (2004) 093009, hep-ph/0408098.

[146] A. Cafarella, C. Coriano' and M. Guzzi, Nucl. Phys. B748 (2006) 253, hep-ph/0512358.

[147] S.A. Larin, Phys. Lett. B303 (1993) 113, hep-ph/9302240.

[148] R.J. Gonsalves, C.M. Hung and J. Pawlowski, Phys. Rev. D46 (1992) 4930.

[149] P.J. Rijken and W.L. van Neerven, Phys. Rev. D52 (1995) 149, hep-ph/9501373.

[150] A.D. Martin et al., Eur. Phys. J. C23 (2002) 73, hep-ph/0110215.

[151] A.D. Martin et al., Phys. Lett. B531 (2002) 216, hep-ph/0201127.

[152] A. Cafarella, C. Coriano and M. Guzzi, AIP Conf. Proc. 964 (2007) 206, arXiv:0709.2115[hep-ph].

[153] T. Binoth et al., (2001), hep-ph/0111043.

[154] Z. Bern, A. De Freitas and L.J. Dixon, JHEP 09 (2001) 037, hep-ph/0109078.